Tectonic evolution of the Western Limassol Forest Complex, Cyprus

Thesis

DECLARATION

THE TECTONIC EVOLUTION OF THE WESTERN LIMASSOL FOREST COMPLEX, CYPRUS

A Thesis presented for the Degree
of Doctor of Philosophy

by

Bramley James Murton
B.Sc Hons., University of Edinburgh, 1982

Department of Earth Sciences
The Open University
November 1986

THE FOLLOWING APPENDICES HAVE BEEN EXCLUDED AT THE REQUEST OF THE UNIVERSITY

Frontispiece

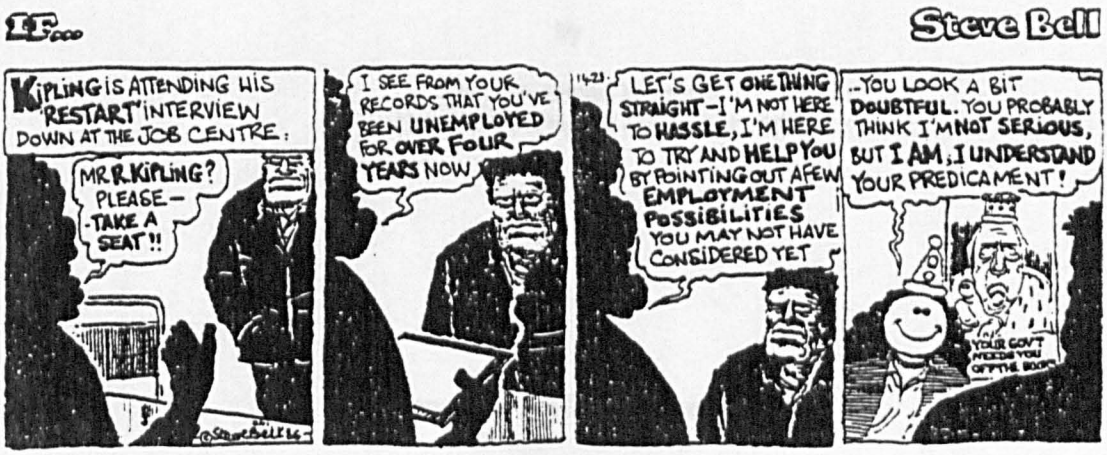

ABSTRACT

The Western Limassol Forest Complex (WLFC), Cyprus, forms an anomalous ophiolite terrain in the south of the Troodos Massif. Detailed studies have revealed magmatic and structural histories that differ markedly from the Penrose-type ophiolite of the Troodos Massif to the north. In the WLFC, a tectonised harzburgite of upper mantle origin has been intruded by multiple ultramafic and gabbroic plutons and swarms of mainly NE-SW trending dykes. The entire complex has been sheared along E-W trending serpentinite shear zones, the orientation of which indicate sinistral displacement. The various styles of deformation from ductile to brittle, and the progressive cooling history of the intrusive plutons and dykes indicate a history of about 4 km of uplift for the host upper mantle lithologies, while in a sea floor setting. The geochemistry of the intrusive plutons and dykes is similar to the lavas that crop out around the periphery of the WLFC, and indicate derivation from a depleted upper mantle source. Geochemical comparison with the Troodos massif basalts suggests a tectonic history involving rapid extension across the WLFC and adiabatic melting of the upper mantle producing boninitic magmas. The regional setting for the WLFC suggests a model of formation involving the development of a transtensional transform fault zone and an extensional relay zone that off-set to the south, sinistral transform movement along the Arakapas fault belt. Comparison of the WLFC with a transpressional palaeo-transform fault preserved in the Antalya complex of Turkey suggests that the Neo-Tethyan spreading system (within which the Troodos massif formed) was experiencing an anticlockwise rotational torque during the final stages of oceanic crustal formation.

ACKNOWLEDGEMENTS

I would like to thank the following:-

Prof. I G Gass, my supervisor, for recognising the significance of the project area, for his continuous encouragement and lively discussion throughout the period of study, for his extensive comments on earlier drafts of this thesis, and for the lobster meze at Paphos.

Costas Xenophontas and various members of the Cyprus Geological Survey, for many hours of interesting discussion over countless cups of coffee, for their help in organising vehicle logistics and for the supply of quality base maps.

Prof. John Malpas, Sherry Dunswater, Prof. P T Robinson and all the members of the Deep Crustal Drilling Project, Cyprus, for their comments, advice and company during the first field season of this study.

Andreas and Heleni at the Meteora Hotel, Agros, for sustaining me with excellent food, 'Krazi' and lodgings throughout the study. Also my many friends in Agros for their friendliness and good company, even on the celebration of the 30th anniversary of the first EOKA.

Chris Neary and Hazel Prichard for their visit to the field area, and their comments and company during the third field season. Kirsten Frazer, Frank McDermott and Nick Rogers for much patience while giving advice regarding the geochemistry of this study.

The technical staff of the Open University, and in particular Ian Chaplin, for their much needed assistance during sample preparation and for promptly producing so many thin sections. Also Ian Novell for slicing a very large rock into slabs.

John Watson for analysing major and trace element rock samples, some at a moments notice. Also for his invaluable help in discovering the source of the 'mysterious' Pb contamination. John Holbrook for his help in keeping the project financially viable. And Andy Tindle for his help and training on the electron microprobe, and advice on the Macintosh desktop publisher on which this thesis was compiled and produced.

John Taylor, whose help and cartographic advice was essential, and whose patience was stretched to the limit, during the drafting of the many diagrams.

Prof. Robert Shackleton for reading and commenting on the structural aspects of this study.

Eira Parker who began the typing of this manuscript and Carol Whale who finished it off and corrected much of the spelling, though all mistakes in this thesis are of course my own responsibility.

Mr and Mrs Bond for proof-reading the English; Richard Ash, Graham Ward and Fiona MacGibbon for checking the spelling, and help with photocopying. Terry Burgess for services beyond the call of friendship!

My mother and grandmother for their continuous support despite many financial crises and my forgetting to make their lunches during so many visits. My father for his continued hope that one day I may financially support him instead!

Finally, I am indebted to Jaqueline Bond for her support, interest and comment on all aspects of this work and her unceasing encouragement since its inception.

It is to her that this thesis is dedicated.

LIST OF CONTENTS

Appendix 5 Electron-micro Probe Analyses of Mineral Phases

Appendix 6 Instrumental Neutron Activation Analyses

List of Figures

CHAPTER 5

LIST OF PLATES

CHAPTER 5

LIST OF TABLES

CHAPTER 6

CHAPTER 7

LIST OF ENCLOSURES

CHAPTER 1

INTRODUCTION

List of contents

1.1 Regional Location and Tectonic Setting of the Troodos Ophiolite

The Troodos massif, Cyprus, is a coherent 'Penrose' ophiolite which forms part of a chain of Tethyan ophiolites that crop in and out around the northeastern Mediterranean (Figure 1.1). Palaeontological evidence (Allen, 1966; Mantis, 1971) indicates a minimum Late Cretaceous age for sediments directly overlying the massif, and this is supported by an 85 Ma, K^{40} Ar^{40} radiometric age for the igneous rocks of the massif (Vine *et al.*., 1973).

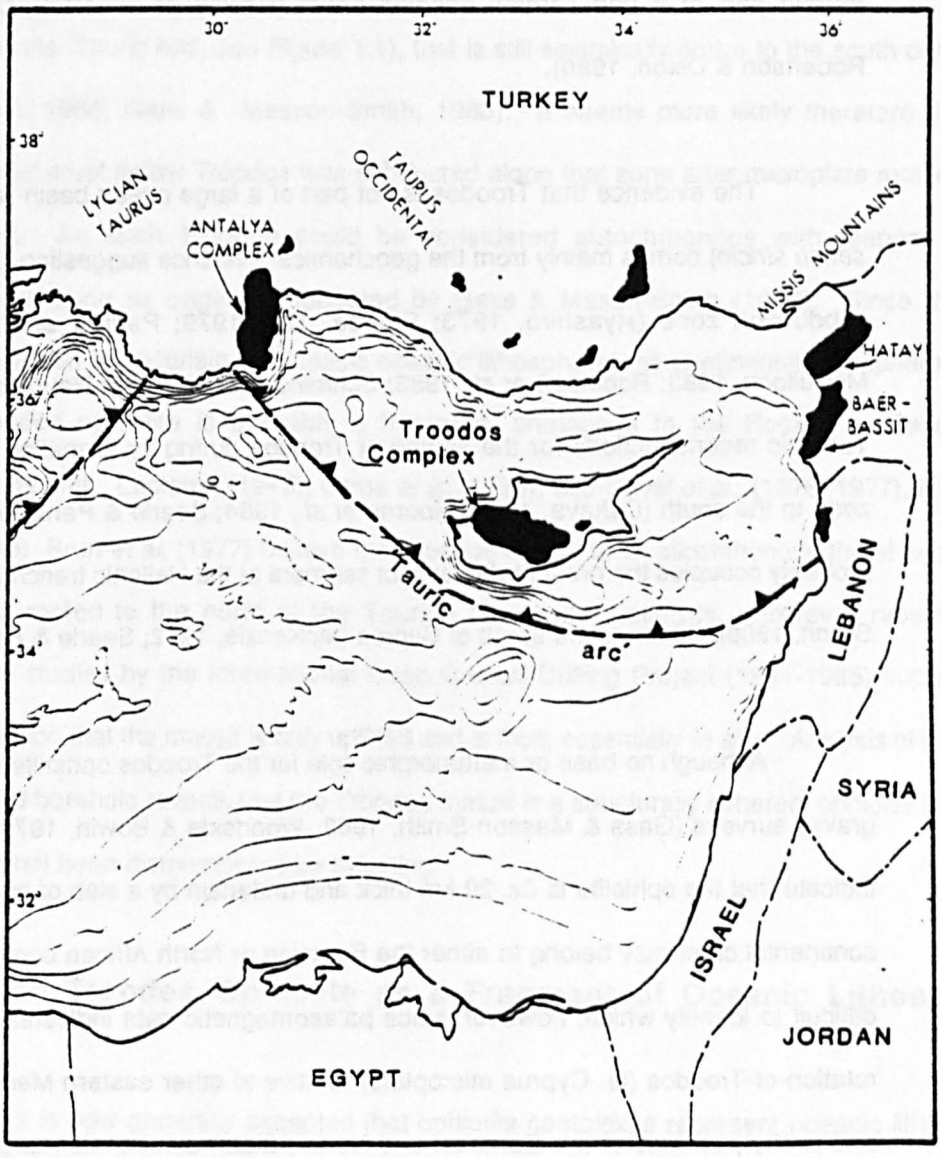

Figure 1.1 Regional location map of the eastern Mediterranean showing the position of the major ophiolite outcrops (in black), including the Troodos complex, Cyprus. A deep level earthquake belt (the 'Tauric Arc', after Brunn,1980) marks the position of a palaeo-subduction zone, with predominately continental crust to the north and Triassic oceanic lithosphere to the south. The bathymetric contours are at 300m intervals.

The regional tectonic setting of Cyprus within the eastern Mediterranean is complex (Dixon & Robertson, 1985) and involves the destruction of a major Palaeozoic oceanic plate which formed the floor of Tethys, that was subducted during the collision between Africa and Eurasia (Robertson & Woodcock, 1980; Smith, 1971). It is generally accepted, however, that the Troodos complex was formed at an oceanic spreading axis (Gass, 1968; Moores & Vine, 1971) in the Late Cretaceous. As such the Troodos complex and other eastern Mediterranean ophiolites (eg. the Antalya Complex; Juteau, 1975; Bear-Bassit, Lapierre & Parrot, 1972) formed part of a neo-Tethian oceanic basin (Dewey *et al.*, 1973; Dumont *et al.*, 1972; Robertson & Dixon, 1980).

The evidence that Troodos is not part of a large ocean basin (eg. not part of Tethys *sensu stricto*) comes mainly from the geochemical evidence suggesting it was formed above a subduction zone (Myashiro, 1973; Pearce, 1975,1979; Pearce *et al.*, 1984; Cameron & McCulloch, 1983; Robinson *et al.*, 1983; Schmincke *et al.*, 1983; Rautenschlein *et al.*, 1985). Tectonic reconstructions for the setting of Troodos during its formation favour a subduction zone to the south (Ozkaya, 1982; Moores *et al.*, 1984; Searle & Panayiotou, 1980), that now probably occupies the present day extinct segment at the Hellenic trench (ie. the 'Tauric Arc' of Brunn, 1980), 50 km to the south of Cyprus (McKenzie, 1972; Searle & Panayiotou, *op. cit.*).

Although no base or metamorphic sole for the Troodos ophiolite crops out on Cyprus, gravity surveys (Gass & Masson-Smith, 1963; Woodside & Bowin, 1970; Wong *et al.*, 1971) indicate that the ophiolite is Ca. 20 km thick and underlain by a slab of continental crust. This continental crust may belong to either the Eurasian or North African continental margins. It is difficult to identify which, however, since palaeomagnetic data indicates a 90^{o} anticlockwise rotation of Troodos (ie. Cyprus microplate) relative to other eastern Mediterranean ophiolites and to the positions of the Eurasian and North African continental margins (Moores & Vine, 1971; Lauer & Barry, 1976; Shelton & Gass, 1980; Clubb *et al.*, 1985). Rotation of the Cyprus micro-plate, the margins of which also have not been identified so far, began in the Late Cretaceous (Clubb *et al.*, *op. cit.*), probably during or shortly after the formation of the Troodos

ophiolite as oceanic lithosphere.

As the Troodos ophiolite, representing oceanic lithosphere, overlies continental crust, there must be some kind of structural dislocation between the two, with continental lithosphere being underthrust, or oceanic lithosphere being overthrust (ie. obducted). Whether ophiolite emplacement was before or after the 90^{o} anticlockwise rotation of the Cyprus microplate is uncertain. There is evidence for a northerly inclined palaeo-subduction zone (ie. the 'Tauric Arc', see Figure 1.1), that is still seismically active to the south of Cyprus (Harrison, 1955; Gass & Masson-Smith, 1963). It seems more likely therefore that the continental crust below Troodos was subducted along that zone after microplate rotation had occurred. As such Troodos could be considered autochthonous with respect to the subduction zone as originally suggeted by Gass & Mason-Smith (1963). Since the SW Mediterranean is underlain by Triassic oceanic lithosphere, the continental lithosphere below the Troodos ophiolite is probably a fragment, analogous to the Rockall or Seychelles microcontinents. Lapierre, (1975), Baroz *et al.* (1975), Biju-Duval *et al.*, (1976, 1977), Ricou *et al.*, (1975), Brun *et al.* (1977) believe the Troodos massif is an allochthonous thrust sequence which is rooted to the north of the Tauride carbonate platforms. However recent deep borehole studies by the International Deep Crustal Drilling Project (1981-1985) support the interpretation that the massif is only uplifted and is thus, essentially *in situ*. Analysis of the 6 km recovered borehole reveals that the Troodos massif is a structurally coherent ophiolite complex that has not been dismembered by thrusting.

1.2 The Troodos Ophiolite as a Fragment of Oceanic Lithosphere

It is now generally accepted that ophiolite complexes represent oceanic lithosphere formed at constructive ridge axes by sea-floor spreading (Gass 1982). Many of the currently accepted models of oceanic crustal formation have been based on the Troodos massif, which is arguably the most coherent and widely studied ophiolite in the world. The massif consists of an approximately stratiform sequence of mafic and ultramafic igneous rocks (Wilson, 1959)

capped by pelagic, manganoan clays, and deep oceanic, nannofossiliferous carbonates (Robertson & Hudson 1974) (Figure 1.2). Marine sediments overlie an igneous basement consisting of basaltic pillow lavas (Henson *et al.*, 1949) that pass downward into a north-south trending sheeted dyke complex, isotropic and layered gabbros, and cumulate dunites and wehrlites. The deepest structural levels exposed in the Troodos massif consist of tectonised harzburgite enclosing pods of dunite. The lithological association of marine sediments, mafic pillow lavas and (often serpentinised) ultramafics (usually found in young mountain belts), was first recognised by Steinmann (1927) and subsequently termed the 'Steinmann Trinity'. Although a marine origin for the 'Steinmann Trinity' was acknowledged, it was not until plate tectonics were generally accepted (Hess, 1962; Dietz, 1961; Vine & Matthews, 1963) that the full significance of ophiolite complexes was realised.

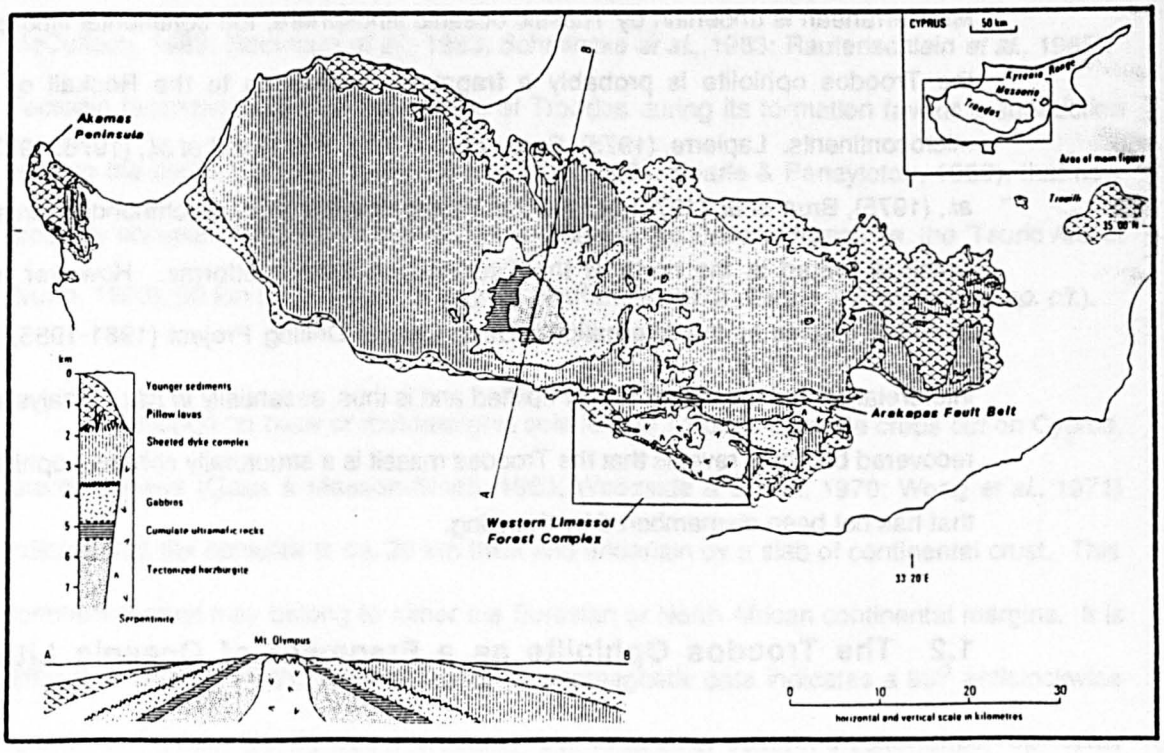

Figure 1.2 Simplified map showing the approximately annular outcrop pattern of the Troodos ophiolite complex and the position of the Western Limassol Forest Complex, the study area. A schematic cross section through the Troodos complex shows the coherent, generally layered petrologic structure of the ophiolite.

Based on its structure and especially the presence of a sheeted dyke complex, Gass (1968) and Moores & Vine (1971) concluded that the Troodos ophiolite "represents a volcanic edifice formed on the median ridge of Tethys..." during "sea-floor spreading". Figure 1.3 illustrates Greenbaum's (1972) model for the igneous layering of the Troodos ophiolite complex and attempts to relate it to the seismic crustal structure of most present day oceanic basins. Greenbaum's (1972) model involved a steady state magma chamber and a near continuous supply of magma to the surface through a vertical fracture, the walls of which form the sheeted dyke complex. Egress of the magma to the surface formed abundant, mafic pillow lavas (Figure 1.3). Although modified by the identification of multiple magma chambers by Moores & Vine (1971) and episodic influxes of melt into a high level magma chamber (Allen, 1975), the model has been applied to most present day oceanic spreading ridge axes (Cann, 1974; Smewing *et al.*, 1975; Kidd, 1977; Gass & Smewing, 1981).

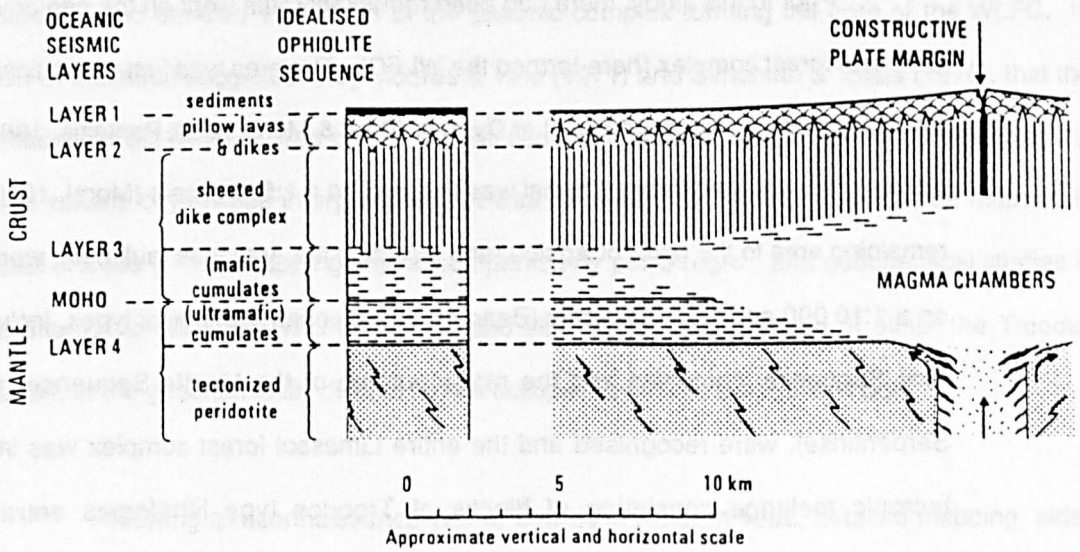

Figure 1.3 Greenbaum's model for a single magma chamber, spreading axis, at which the generally layered ophiolite sequence is generated. The various petrologic layers are correlated with oceanic seismic layers 1, 2, 3 and 4, (after Greenbaum, 1971).

1.3 Previous Work on the Arakapas Fault Belt and Limassol Forest Complex

The generally coherent, layered structure of the Troodos ophiolite (Figure 1.2) is applicable to almost the entire outcrop of the main massif. In the southeast of the massif, however, is a 360 km^2 area of anomalous ophiolite terrain separated from the more coherent northern complex by a 2 km wide, east-west trending fault belt. This linear structure, known as the Arakapas fault belt, was a bathymetric trough containing a sequence of intercalated lavas and breccias not found elsewhere in the Troodos massif (Moores & Vine, 1971; Simonian, 1975). Moores and Vine (*op. cit.*) suggested the Arakapas fault belt was part of a fossil oceanic fracture zone. This interpretation was upheld by Simonian and Gass (1978) who concluded that the fault belt was part of the northern margin of an east-west trending, fossil oceanic transform fault zone. Simonian and Gass (1978) also suggested that the area to the south of the fault belt, known as the Limassol forest complex was part of the same transform domain.

Prior to this study, there had been remarkably little work on the geology of the western Limassol forest complex (here termed the WLFC). The area was first geologically surveyed by the Geological Survey department of Cyprus, (Bear & Morel 1960; Pantazis, 1967). Most of the southern area of the Limassol forest was mapped on a 1:5000 scale (Morel, 1960), whereas the remaining area to the north of Apsiou (and including the Arakapas fault belt), were only mapped on a 1:10 000 and 1:50 000 scale (Bear, 1960). General lithological types, including disrupted Axis Sequence lithologies and the major outcrop of the Mantle Sequence (termed Bastite Serpentinite), were recognised and the entire Limassol forest complex was interpreted as a tectonic melange consisting of blocks of Troodos type lithologies entrained within a serpentinite diapir.

Following the completion of the initial geological survey of the Limassol forest (Pantazis, 1967), Lapierre & Rocci (1967) identified the major structural features in the area as NW-SE trending, southward transporting, low angle thrust faults. This they used to support their claim that the whole of the Troodos massif was a dismembered thrust imbricate. The

identification of Ni, Co, and Co sulphides, by the Cyprus Geological Survey in the mid-1970s, led Panayiotou (1977) to re-map the entire Limassol forest complex and work in detail on the mineralisation. In agreement with the conclusions made by the Cyprus Geological Survey department, Panayiotou (*op. cit.*) interpreted the entire complex, and especially the western Limassol forest area, as a tectonic melange in which major Axis Sequence crustal blocks were entrained within a serpentinite diapir of upper mantle origin. In contrast, however, with the proposition by Simonian & Gass (1978) that the Limassol forest complex is part of a fossil transform domain, Searle & Panayiotou (1980) interpreted the area as having undergone considerable synmagmatic compression, during the initiation of obduction of the Troodos ophiolite during the Late Cretaceous.

1.4 Objectives and Aims of the Present Study

The construction in 1980 of a road between Dheierona and Akrounda revealed abundant and detailed exposures of the plutonic complex forming the core of the WLFC. In view of the initial suggestions by Moores & Vine (1971) and Simonian & Gass (1978), that the Limassol forest complex was part of a fossil oceanic transform fault zone, and considering the wide variatiy of previous interpretations, it was decided that the WLFC should be mapped in detail (1:5000). The mapping was accompanied by petrologic and geochemical studies in an attempt to relate the WLFC basaltic and plutonic rocks with those of either the Troodos massif, or the geochemically distinct terrain occupied by the Arakapas fault belt.

Following a reconnaissance visit to Cyprus in Autumn 1982, detailed mapping, aided by 1:10 000 scale aerial photographic cover, of lithologies and structures in the WLFC required three field seasons (1983, 1984 and 1985) totalling nine months field work. Geochemical analysis of samples by E.D. XRF, electron microprobe and Instrumental Neutron Activation techniques were done in the laboratories of the Department of Earth Sciences at the Open University. Sample preparation and analytical techniques are briefly reviewed in Appendix 1.

1.5 Presentation of this study

The present study of the geology, structure and geochemistry of the WLFC is divided into seven chapters, the first being this introduction. The second chapter describes the geology and petrology of oceanic crustal blocks, termed the Axis Sequence, that are similar in structure to the ophiolitic sequence of the Troodos massif. The third chapter describes the geology and petrology of syntectonic ultramafic and mafic plutonic and hyperbyssal rocks (termed the Transform Sequence) that cut the Axis Sequence lithologies. Syntectonic eruption of the Transform Sequence magmas formed primative pillowed and massive lavas that are intercalated with breccia deposits, all of which are described in chapter four. Chapter five describes the structural evolution of the WLFC, from ductile to brittle deformation during Late Cretaceous sinistral, transtensional transform faulting, to brittle thrust faulting and Tertiary uplift of the Limassol forest complex. The geochemistry and petrogenesis of both the Axis Sequence and Transform Sequence is described and discussed in Chapter six. Chapter seven is mainly interpretative and seeks to test the hypothesis that the WLFC formed in the active domain of an oceanic, Late Cretaceous transform fault zone. Analytical techniques, geochemical analyses and petrographic descriptions are presented in the appendices. Geological and structural maps are enclosed inside the rear cover.

CHAPTER 2

THE AXIS SEQUENCE

List of Contents

2.1 Introduction

Two major stages of magmatic activity were involved in the formation of the western Limassol forest complex (WLFC). The initial stage generated a sequence with depleated mantle at the base that passes upwards through a palaeo-moho into a crustal sequence of cumulates, high level plutonics and finally into a Sheeted Dyke Complex. This lithostratigraphic succession is similar to that of other ophiolite complexes (Penrose, 1972) and is interpreted as having formed at a constructive plate margin. The Mantle Sequence consists mainly of tectonised harzburgite and is considered to be the depleted residue following partial melting of a plagioclase lherzolite from which the magmas forming the new oceanic lithosphere were derived (Moores & Vine, 1971; Gass & Smewing, 1973; Menzies & Allen, 1974).

Following Gass & Smewing (1973) the term Axis Sequence (A.S.) is given to the pseudostratigraphic ophiolite succession in the WLFC. This is consistent with the Troodos terminology of Allen (1975) and Smewing (1975) and that for the Arakapas fault belt lavas of Simonian (1975). It also allows the sequence to be differentiated from the later intrusive suite referred to below as the Transform Sequence (T.S.).

Field and petrological descriptions of two almost complete stratigraphic successions of the A.S. from the Argakin tis Kaloshis and Louveras areas are discussed and compared. Palinspastic reconstruction of the now disrupted A.S. has been made in Chapter 5, where it is shown to have been 3.7 km thick. Comparisons between the A.S. in the WLFC and that in the Troodos massif and Arakapas fault belt are discussed at the end of Chapter 2.

2.2 The Mantle Sequence

2.2.1 Introduction

Ninety-eight percent of the Mantle Sequence, the lowest structural unit of the A.S. exposed in the WLFC, is a serpentinised, tectonised harzburgite. Minor components of the Mantle Sequence include gabbroic and pyroxenite dykes and veins, dunite layers and pods, and massive chromite deposits. The deepest levels of the Mantle Sequence are exposed in the centre of the complex whereas in the Potimata [080550] and Vrysihou Laoudhi [070500] areas, the transition into dunite and layered wehrlite marks the petrological Moho.

The Mantle Sequence forms a range of mountains rising to 1200m, that has been deeply incised by a linear drainage pattern flowing mainly southward into Limassol Bay. On weathering the ultramafics oxidise to a characteristic buff colour which, despite moderate vegetation cover is readily identifiable on Landsat multispectral images (Plate 2.1).

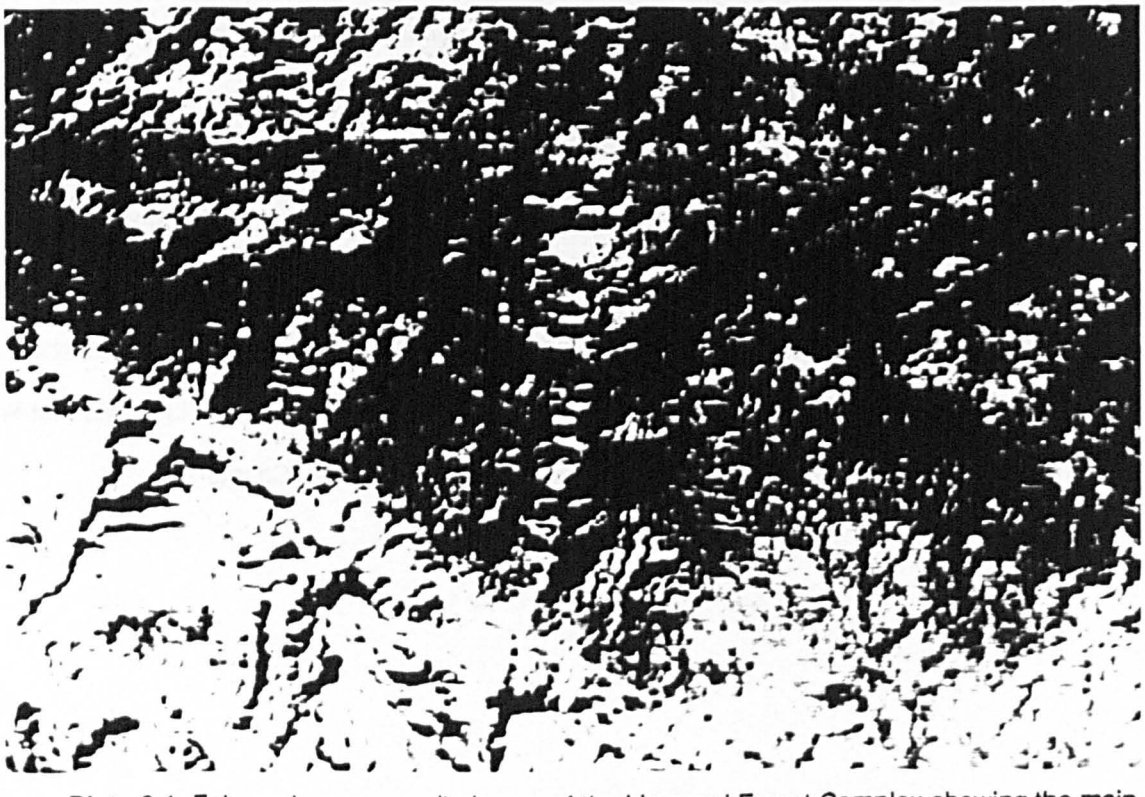

Plate 2.1 False colour composite image of the Limassol Forest Complex showing the main outcrop of the Mantle Sequence of serpentinised, tectonised harzburgite. Vegetation cover appears red, and covers most of the complex as sparse scrub.

2.2.2 Tectonised Harzburgite

The tectonised harzburgite was first described by Bear (1960) and later by Panayioutou (1977). Both previous studies deemed the entire Mantle Sequence to be of undifferentiated bastite serpentinite, similar in origin to the outcrop on the summit of Mt. Olympus in the Troodos massif. In the WLFC the tectonised harzburgite forms an outcrop of approximately 45 km^2. Weathered exposures are rounded and smooth with a characteristic red-brown oxidised surface that often obscures mineralogical textures and fabric. Sheared and disrupted exposures have a distinct blue-grey hue whereas fresh surfaces are dark green or black.

Vertical variation in the tectonised harzburgite has been studied by examination of sections from different structural levels within the Mantle Sequence. The deepest level, estimated at 800m below the petrological Moho is exposed in the centre of the complex along the Argakin tis Xerokiladhas river [040520] whereas the shallowest levels, estimated at just sub-Moho, form the majority of the outcrop of the Mantle Sequence in the WLFC.

In the Argakin tis Xerokiladhas river section a strongly developed foliation and a diffused layering of pyroxene and olivine-rich bands characterise the tectonised harzburgite. The foliation dips at 60^{o}E strike 005N and is produced by the elongation and flattening of orthopyroxene grains. Serpentinisation of the ultramafics in this region enhance the pyroxene foliation by antigorite veining parallel to the fabric giving the rock a striped appearance (Plate 2.2). Elongation, pullapart textures and stringers of chrome spinel define a linear fabric that is sub-parallel to the pyroxene foliation. Unlike the more readily identifiable pyroxene foliation this linear fabric is only rarely developed and hence has not been used in mantle fabric analysis. Lying within the foliation plane are diffuse, pyroxene-rich bands between 0.02 and 0.1m wide that are separated by Cpx-depleated layers. This banding is characterised by its 'lack of a consistent direction of compositional variation which, combined with its close structural

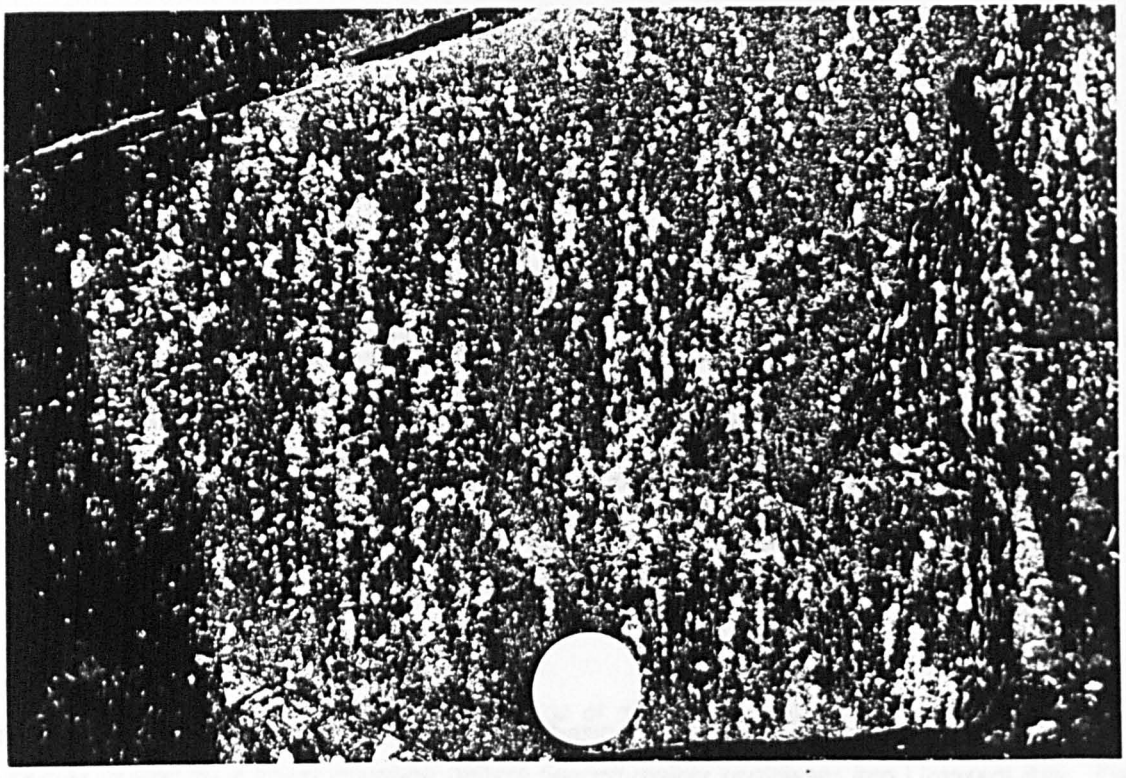

Plate 2.2 Tectonised harzburgite from the Mantle Sequence with a composition of $Ol_{88}Opx_{11}Spl_1$. Opx grains are elongated and form a pervasive, strong foliation that is enhanced by the growth of antigorite veins parallel to the tectonic fabric.

Plate 2.3 Photo-micrograph of serpentinised and tectonised harzburgite. The olivine has been totally hydrated forming a mesh texture. Orthopyroxene grains are elongated and show dislocation glide that is characteristic of deformation at upper mantle pressures and temperatures. Dumb-bell shaped chrome spinel grains are also the product of high P and T deformation.

relationship to the foliation and lineation, suggest a metamorphic origin' (George, 1975). Throughout the river section, the harzburgite is mineralogically variable with large areas that are relatively rich in pyroxene compared with others. The mineralogical composition of the harzburgite ranges from $Ol_{78}Opx_{18}Cpx_3Sp_1$ to $Ol_{89}Opx_8Cpx_2Sp_1$, reflecting areas of relatively fertile and depleted mantle respectively.

Petrographic analysis shows the harzburgite to be completely serpentinised with serpentine forming a micromesh texture that passively replaces all of the olivine. Fibrous antigorite forms 1mm wide cross-cutting veins. Orthopyroxene grains, although commonly replaced by fibrous uralite actinolite and bastite, retain their original morphology. These grains have suffered penetrative strain with kinking, dislocation glide, and occasionally dynamic recrystallisation forming polygonised grains (Plate 2.3). Flattening of orthopyroxene porphyroclasts defines the predominant foliation whereas the lineation is formed from chrome spinels that are elongated, have concave margins and occasionally form 'dumb-bell' shaped grains. In areas of high strain the chromite grains have pullapart textures forming stringers .

Outcrop, typical of higher structural levels in the Mantle Sequence, is exposed in the Makria Dhoxameni area [080490]. Here the tectonised harzburgite has a moderately strong foliation and a homogeneous composition. The pyroxene foliation is variable in both strength and orientation., although it generally strikes E-W to NE-SW. The harzburgite has a consistent composition of $Ol_{90}Opx_8Cpx_2Sp_{<1}$. Dunite pods and layers are characteristic of this level of outcrop and are described in detail in Section 2.2.3.

In thin section, the peridotite is strongly serpentinised with medium grained, porphyroclastic olivine only rarely preserved. Orthopyroxene grains are kinked and dislocated and chrome spinels are either equant or, where deformed, elongate and occasionally have pullapart textures. The tectonised peridotite in the Makria Dhoxameni area has relatively more olivine and less pyroxene and is therefore compositionally more refractory compared with that from deeper structural levels.

2.2.3 Pyroxenite and gabbroic veins and dykes

The tectonised harzburgite is host to a variety of gabbro and pyroxenite veins and dykes. These occur at all structural levels and are appparently randomly orientated. There are two generations of dykes and veins present: (i) early dykes and veins that are commonly rodingsitised, cut mantle fabrics and often have rather diffuse boundaries and (ii) later intrusive bodies that are related to the Transform Sequence; the former are described below.

The most abundant outcrop of pyroxenite dykes occurs in the Agakin tis Xerokiladhas river section, but are not restricted to this area. At their margins, the pyroxenite rapidly grades into harzburgite forming a diffuse contact. The dykes vary in width from 0.05 to 0.5m and are discontinuous along strike. Their grain size varies from coarse (3cm) to pegmatitic (11cm), and forms an equigranular texture. Although original textures are preserved the majority of pyroxenites have been altered to bastite pseudomorphing orthopyroxene and clinopyroxene. The pyroxenite dykes are rarely deformed and cut pre-existing mantle fabrics. The harzburgite in the immediate vicinity of the propagating tip of a dyke has been serpentinised, suggesting that the emplacement of the pyroxenite was related to high volatile activity. Indeed, it is unlikely that a siliceous melt of the composition of orthopyroxene would be available to form dykes and veins. Instead, a metasomatic formation is proposed in which silica-rich, hydrous fluids react with the ultramafic wall rock allowing generation of pegmatite orthopyroxene, i.e.

$$Mg_2SiO_4 + SiO_2 + H_2O = 2MgSiO_3 + H_2O$$

Forsterite *Silica* *Water* *Enstatite* *Water*

Although this is a simplified version of the reaction (after Wilson, 1959), it is more probable that siliceous hydrous fluids also contain Ca, Na and Al (Allen, 1975), that would produce small amounts of clinopyroxene in the orthopyroxenite veins.

Early gabbroic veins and dykes that occur through the Mantle Sequence are often irregular in shape, range from 1 to 50 cm wide and have sharp boundaries that cut mantle fabrics. Rodingsitation often obscures original textures which are medium grained to pegmatitic. The ubiquitous absence of chilled margins to the dykes indicates a relatively high temperature (500 - 800^{o}C) of the host peridotite during intrusion. Plate 2.4 illustrates a 50cm wide dyke that has a coarse (0.02m wide) margin of plagioclase, clinopyroxene and actinolite surrounding a fine grained core of microgabbro. At one location [07205410] a 1.5m wide, partly rodingsitised dyke cuts the harzburgite and has medium grained leucograbbro margins that surround a core of variable to coarse grained, pegmatitic (20-25 cm) actinolite, plagioclase and clinopyroxene megacrysts .

These gabbroic intrusions are similar to those described by Allen (1975) from the Troodos massif and by Browning (1982) from the Semail Nappe, Oman. In agreement with these authors, the gabbroic bodies are interpreted as basaltic liquids, derived by partial mantle melting beneath a spreading axis, that crystallised during their ascent though the Mantle Sequence .

2.2.4 Dunite layers and pods

In the Mantle Sequence, dunite is most abundant in the areas interpreted as just sub-Moho, (see enclosure 1). At deep structural levels [085515] the dunite forms discrete elongated pods (25 to 250m long) with diffuse margins that are sub-parallel to the mantle tectonite fabric. In the field the dunite weathers to a characteristic buff colour, its monomineralic composition producing smooth rounded exposures. Fresh surfaces are dark green or brown, reflecting a high degree of serpentinisation. In thin section the rock has a micromesh (0.5 - 1mm) replacement texture of antigorite after olivine, that obscures all original fabrics. Disseminated chrome spinel euhedra range from 0.01 to 0.08mm in diameter and vary in abundance from 0 to 0.5% of the mode.

In contrast and at the same structural level [08052], dunite forms narrow (0.5 to 2m) bands with sharp boundaries that interdigitate with the tectonised harzburgite, and are sub-parallel to the tectonite mantle foliation. This, combined with the presence of deformed, elongated grains and stringers of chrome spinel, suggest the dunite was originally discordant with the harzburgite but has since suffered similar mantle deformation. An identical relationship, noted by George (1975) for the Troodos massif was interpreted in terms of isoclinal folding during asthenospheric deformation.

Dunite at high structural levels within the Mantle Sequence crops out in the Potima [075555] area. The dunite forms a discontinuous, lensoidal body, 1.5 km long that is faulted against cumulate wehrlite to the north. The contact with the surrounding harzburgite is irregular, gradational over 10 to 30 m and discordant with the mantle tectonite fabric. Cutting both the harzburgite and dunite are small (1 - 10cm) pyroxenite veins and dykes. Like the Mantle Sequence, the dunite is pervasively serpentinised.

The generation of dunite as a refractory product would require unreasonably high degrees of partial mantle melting (in excess of 80% of a plagioclase lherzolite protolith). Therefore, Allen (1975) and Gass and Smewing (1981) argued in favour of Mantle Sequence dunite formation by olivine accumulation and segregation during ascent of basaltic melts beneath a constructive plate margin. The cumulative olivine is subsequently entrained within the surrounding tectonised harzburgite, while the liquid from which it precipitated continues to rise into the ridge magma chambers above.

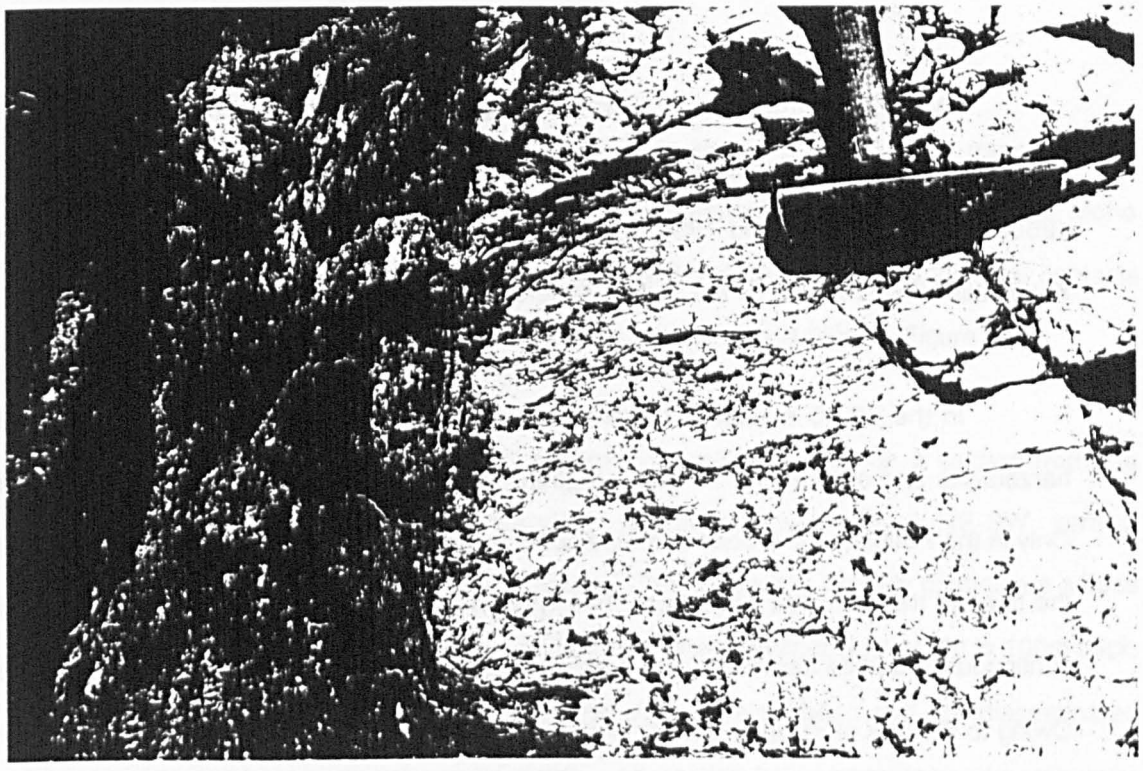

Plate 2.4 A coarse gabbroic dyke invades serpentinised harzburgite, cutting the high temperature deformation fabric. The dyke has a pegmatite margin suggesting a high volatile content when intruded.

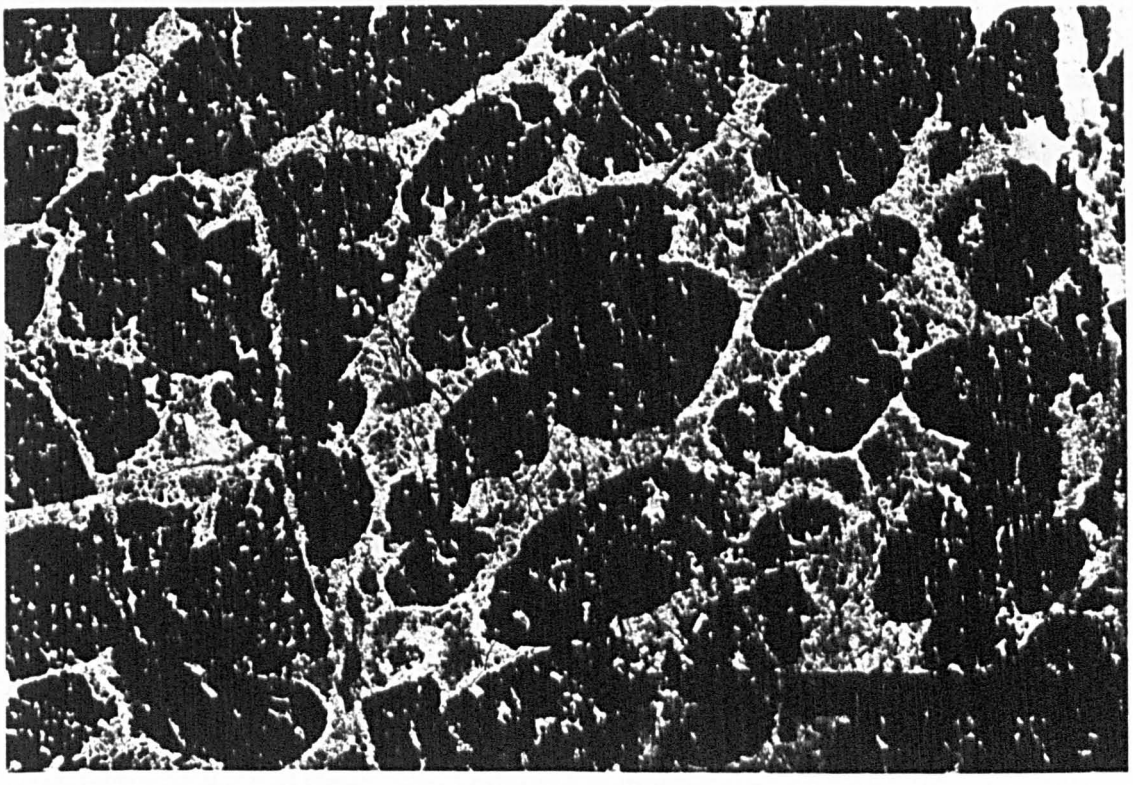

Plate 2.5 Orbicular chromite, known as '*leopard ore*', surrounded by a matrix of serpentinised olivine. The chromite forms ellipsoids indicating high P and T strain. The deformation has also fractured the ellipsoids perpendicular to their long axes.

2.2.5 Massive Chromites

Massive chromites crop out throughout the WLFC. Although not in large concentrations, these deposits were worked by small adits and larger mines until the mid 1950s. Between 1952 and 1954, up to 880 tons of massive ore were removed from the Kakomalis mine [040525] by the Cyprus Minerals Corporation.

In the WLFC massive chromites are predominantly associated with the tectonised harzburgite and often found as disaggregated lenses and pods in serpentinite shear zones. Only in the Potimata mine does chromite occur within a large dunite body that is interpreted as the base of the cumulate sequence. Two types of chromite are found, a massive ore with a continuous chromite framework and a disseminated ore with a continuous silicate framework. Owing to the lack of *in situ* exposure of chromite deposits, the relationship of the massive ore to its host silicates is unknown.

The disseminated ore commonly occurs as orbicular or leopard and grape ore (Plate 2.5). Leopard ore, found most abundantly in the Potimitsa Mine often forms ellipsoidal nodules 0.2 to 4cm in diameter. The percentage of silicate matrix varies from 20 to 70% and is of variably serpentinised olivine. Occasionally altered olivine forms a nucleus to the nodular overgrowths of chromite, which is then overgrown and surrounded by more olivine. A similar textural relationship, reported by Brown (1980) and Christiansen (1985) from the Semail Nappe, Oman, was interpreted as the product of magmatic segregation although melt immiscibility may also have been significant. Contacts between nodules show both flattening, possibly due to compaction and coalescence by continued growth. Despite their intimate association with the tectonised harzburgite, neither massive nor disseminated chromite has a pervasive deformation fabric.

2.2.6 The Petrological Moho

Only at Vrysin tou Laoudhi [073497] in the south of the WLFC is the transition from the Mantle Sequence to the cumulate sequence preserved. Here, the petrological Moho crops out on the southern flank of a 470m hill. Detailed mapping of the lithological contacts reveals the transition zone that is approximately planar and dips at 28^{o}SE (Figure 2.1).

Figure 2.2 illustrates a detailed stratigraphic column based on a section from the tectonised harzburgite to the layered wehrlite. Harzburgite, with a weak NE-SW vertical foliation, grades into dunite over a 10m transition. This contact is laterally continuous across the entire outcrop. The dunite is massive and forms a laterally variable layer, 20 to 100m thick. Grains of chrome spinel are euhedral, show no sign of deformation and are disseminated throughout a pervasively serpentinised matrix. Alternation between tectonised harzburgite and massive dunite continues over 30m, with dunite layers becoming increasingly persistent and thicker and eventually forming the majority of the outcrop.

Approximately 120m above the first dunite outcrop, diffuse layers of wehrlite occur. Initially the wehrlite appears as bands that vary from 10 to 50m thick. Plate 2.6 illustrates fine scale (3cm) rhythmic layering between wehrlite and dunite. The dunite grades vertically into laminated wehrlite that contains euhedral clinopyroxene and olivine, suggesting cotectic crystallization. Over the final 50m of outcrop, wehrlite increases in pyroxene content, forming thicker and more abundant bands at the expense of dunite. Massive poikilitic wehrlite, forming the final 20m of the section, contains large oikocrysts (10 - 30mm) of clinopyroxene which form a granular texture and surround 0.5 - 1m rounded olivine grains and small (0.02mm) euhedra of chrome spinel. The wehrlite shows no evidence of the plastic deformation that has affected the Mantle Sequence.

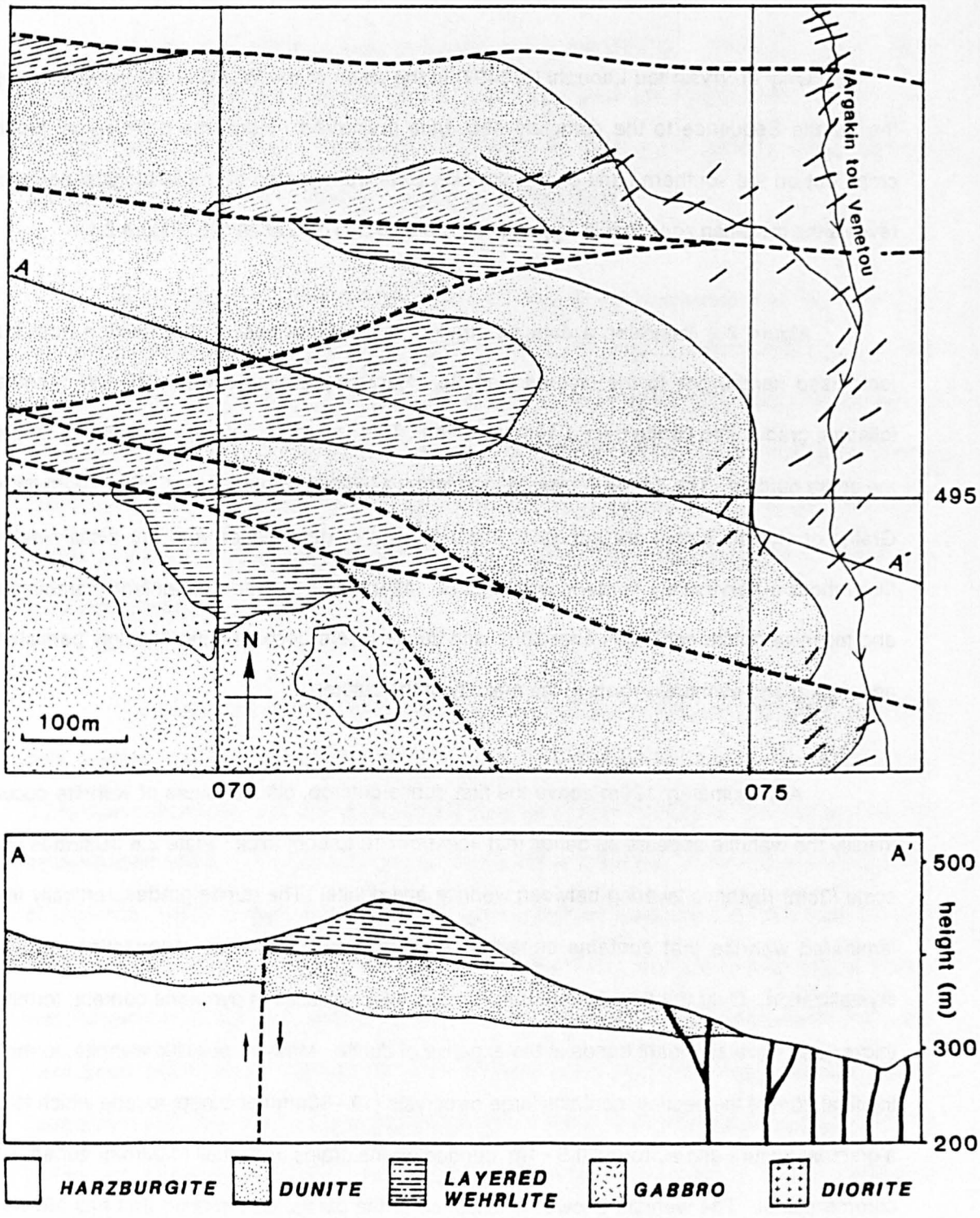

Figure 2.1 Enclosure of an area in the southeast of the WLFC where the petrological-Moho is exposed in the Vrysin tou Laoudhi river section. The petrological-Moho forms a sub-horizontal plane the seperates the Mantle Sequence from the Axis Sequence cumulate ultramafics. The cross-section shows vertical mafic dykes of the Transform Sequence that commonly cross cut the Mantle Sequence.

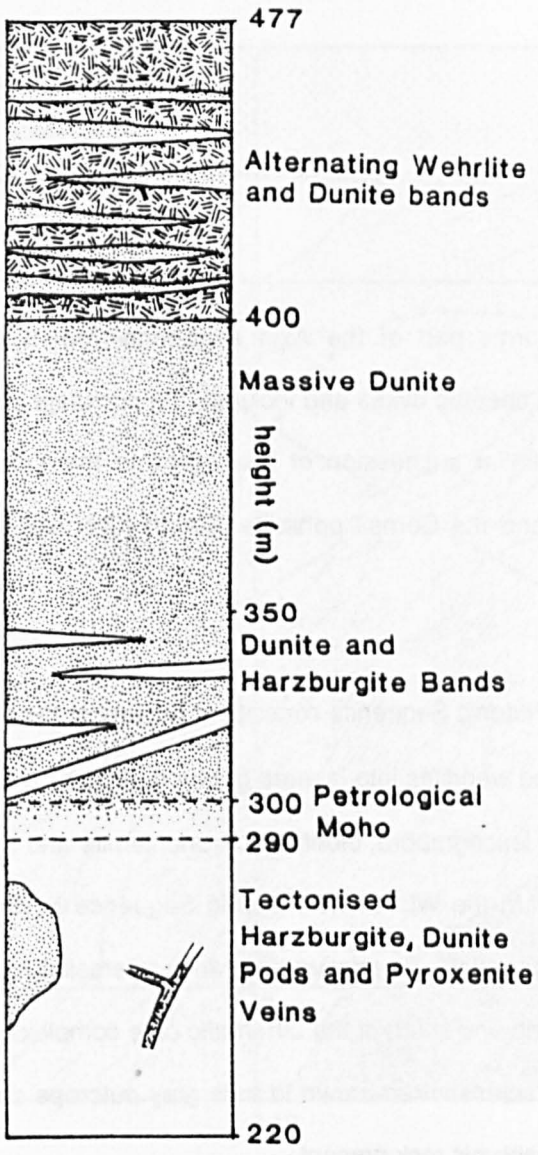

Figure 2.2 Detailed stratigraphic section constructed for the Vrysin tou Laoudhi river section in which the Petrological-Moho is a gradual transition from harzburgite to dunite and layered wehrlite.

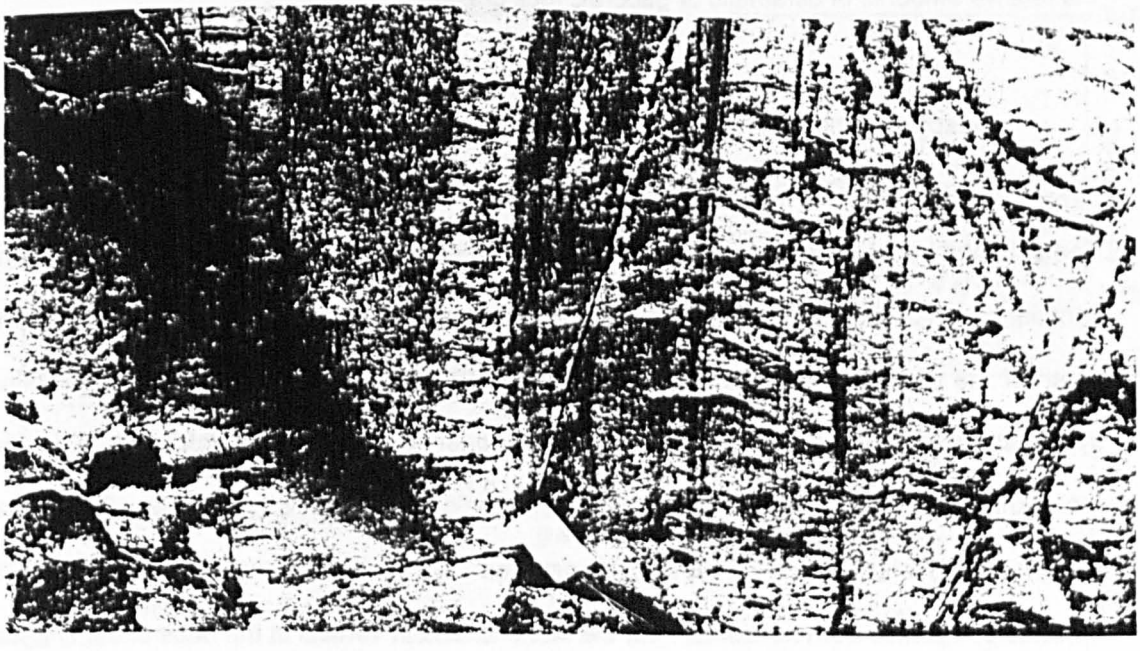

Plate 2.6 Laminated wehrlite from approximately 50m above the petrological-Moho in the Vrysin tou Laoudhi river section.

2.3 The Plutonic Sequence

2.3.1 Introduction

The Plutonic Sequence forms part of the Axis sequence from the top of the petrological Moho to the base of the sheeted dykes and includes the cumulate sequence and the high level plutonic group, a similar succession of lithologies to the Troodos massif (Greenbaum, 1972; Allen, 1975), and the Semail ophiolite, Oman (Glennie *et. al.*, 1974, Browning, 1982).

In stratigraphic order, the Plutonic Sequence consists of dunites at the base passing upwards through massive and layered wehrlites into layered gabbros. The high level Plutonic Sequence contains isotropic gabbro, leucograbbro, diorite and trondhjemite and crops out just below the Sheeted Dyke Complex. In the WLFC the Plutonic Sequence is dismembered, usually forming isolated outcrops (Figure 2.3). Its relative resistance to erosion has resulted in elevated, rugged shoulders to the north and south of the ultramafic core complex. Weathering of the Plutonic Sequence forms characteristic red-brown to pale grey outcrops depending on the relative amounts of ultramafic or gabbroic rock present.

Despite complication by T.S. intrusives, the lithostratigraphy of the Plutonic Sequence has been determined from two nearly continuous sections (Figures 2.4a and 2.4b) Comparisons between these, the Louveras and Argakin tis Kaloshis sections, illustrate lateral variations in thickness, composition and structure of the Plutonic Sequence from the north and south of the complex respectively. Due to restricted exposure and structural complexities, systematic sampling, especially of the cumulate sequence, could not be achieved. Also, like the Mantle Sequence, way up criteria in the Plutonic Sequence is unreliable. Casey and Karson (1981) and Browning (1982) demonstrated the fanning of compositional layering in ophiolite complexes from horizontal near the Moho to almost vertical at the base of the sheeted dykes.

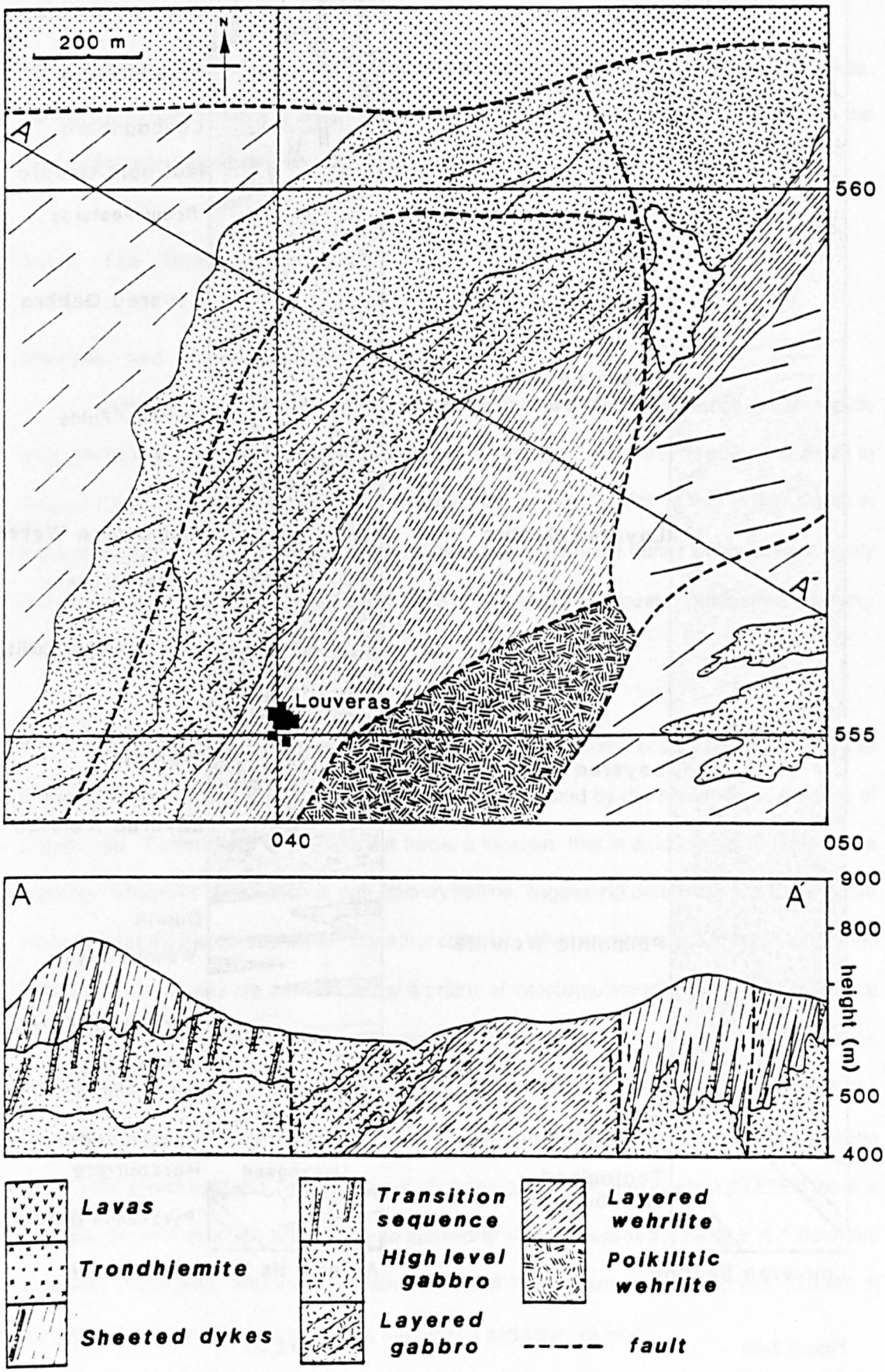

Figure 2.3 Detail of the Louveras area showing the Plutonic Sequence, high level plutonic group and the sheeted dyke complex. Tone shows the strike of the sheeted dykes and the layered rocks.

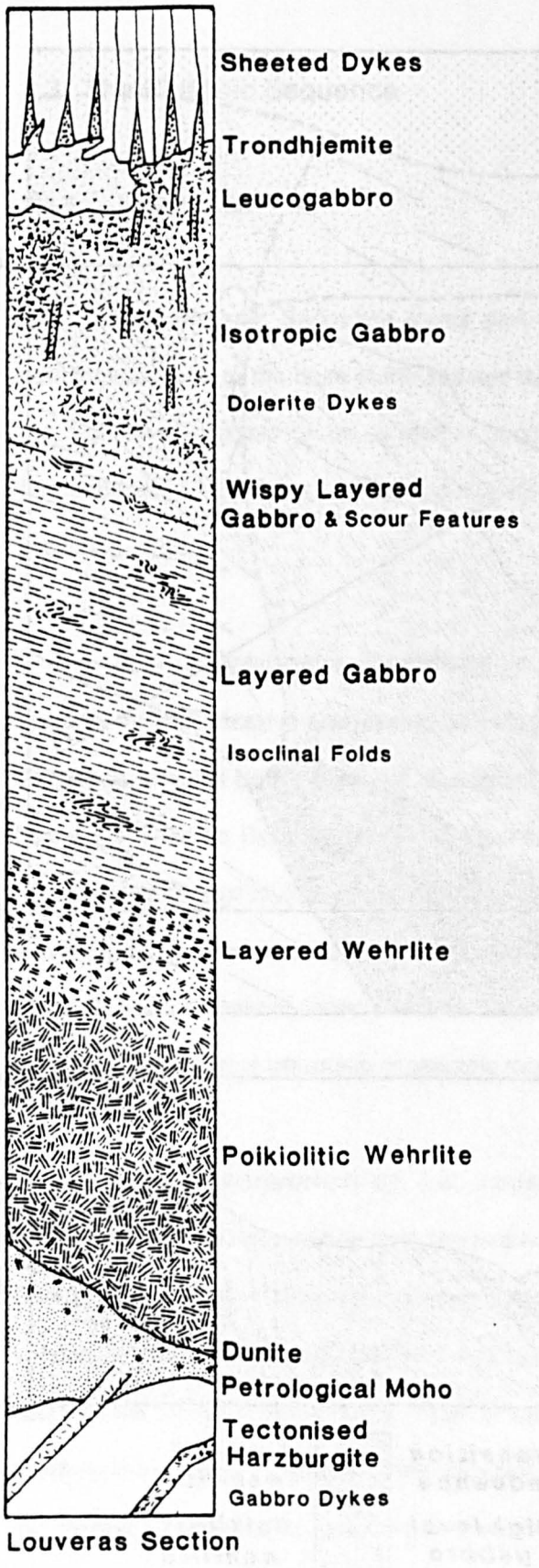

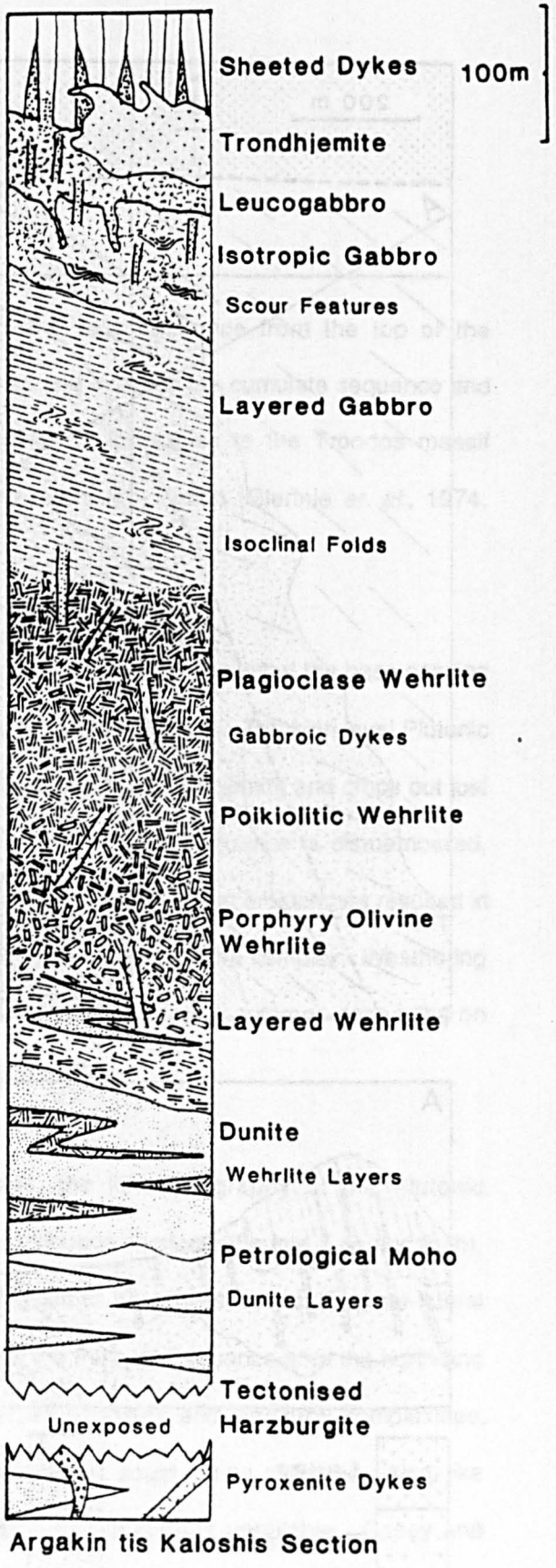

Figure 2.4a

Figure 2.4b

Detailed stratigraphic sections through the Axis Sequence crustal blocks exposed in the Louveras area and the Argakin tis Kaloshis river section respectively. See text for detailed descriptions and explanation.

Rothery (1982) identified compositional layering parallel to the vertical roots of sheeted dykes. As a result perpendicular traverses across the Plutonic Sequence have been located on the basis of the orientation of the sheeted dykes that are assumed to be near vertical.

2.3.2 The Cumulate Sequence

Wehrlite and olivine gabbro

In the Argakin tis Kaloshis section (Figure 2.4b) the cumulate sequence grades rapidly over 2m from tectonised harzburgite into massive dunite. The dunite, described in detail in Section 2.2.3, is laterally discontinuous, wedging out over a distance of 2.7km from 230m in the west to zero in the east. Massive poikilitic wehrlite overlies the dunite with a diffuse, highly irregular contact that strikes 120N, dips 50^{o}SW and is marked by the gradually increasing abundance of clinopyroxene over a 10m zone.

In contrast, in the Louveras section (Figure 2.4a) dunite occurs as layers (0.5m to 2.0m) within wehrlite. Phase layering the wehrlite is defined by the presence or absence of plagioclase. Deformation of the wehrlite forms a foliation that is axial planar to folds in the layering. However the foliation is only intercrystalline, suggesting deformation of the wehrlite while in a semi-consolidated state. Euhedral cumulate olivine grains are 2 to 8mm long, form 70% of the mode, and are surrounded by a matrix of intercumulate clinopyroxene. Individual olivine grains are orientated with their c-axes parallel to one another, giving the rock a laminar, orthocumulate texture. Further up the section, the proportion of olivine decreases with the appearance of plagioclase that occurs as interstitial, idiomorphic grains between clinopyroxene oikiocrysts, and in 0.02 to 1.5m thick layers of olivine gabbro. At one location [056553] there is a porphyritic rock in which idiomorphic to subhedral phenocrysts of olivine (0.5 to 1.5cm) are bimodally distributed, with smaller grains enclosed in allotriomorphic oikocrysts (0.03m) of clinopyroxene, and larger olivine grains are broken and often aligned.

In the Argakin tis Kaloshis river, the poikilitic wehrlite grades up section into layered olivine gabbro. The gabbro is rhythmically layered with Ol & Cpx layers alternating with Cpx & Plag layers on a 3cm and 0.5m scale. The crystallisation sequence of Ol -> Cpx -> Plag is reflected in mineral grading that indicates a southwesterly younging direction. Mesocumulate plagioclase rich layers are often slumped in a style similar to those identified on Troodos (Wilson, 1959; Greenbaum, 1968). Individual layers are locally overturned and thin out laterally over 2 - 4m. This may be the result of synmagmatic tectonism but is more probably due to oversteep layering on the wall of a magma cells becoming gravitationally unstable (Wager & Deer, 1939; McBirney & Noyes, 1979; Casey & Karson, 1981). Layering in the gabbro becomes indistinct upwards over a 50m transition into isotropic gabbro and marks the beginning of the High Level Plutonic Group (HLPG). The isotropic gabbro is idiomorphic-granular has a composition of $Ol_5Cpx_{40}Plag_{55}$ in which the clinopyroxene is partly replaced by actinolite, and the plagioclase is turbid. Wispy phase layering in the gabbros is 2-5cm thick and laterally discontinuous.

In the Louveras section, the gradation from massive poikilitic wehrlite to plagioclase - bearing wehrlite and layered gabbro is more gradual. Interstitial, anhedral plagioclase increases in modal abundance at the expense of olivine, marking the change from plagioclase - bearing wehrlite to olivine gabbro. The olivine grabbro, $Ol_{28}Cpx_{40}Plag_{42}$, is medium grained (2-6mm) granular with subhedral olivine grains partly enclosed by clinopyroxene and plagioclase forming a hypidiomorphic granular intercumulate texture. In contrast to the poikilitic wehrlite, olivine in the olivine gabbro shows a greater degree of equilibrium. Phase layed and mineral graded units, 0.5 to 1m wide, dip steeply towards the west. The crystallisation sequence Ol -> Cpx -> Plag is reflected in the sequence of phase layers that make up rhythmic units and the rapid decrease in abundance of olivine up section. Grain boundary sliding and slumping in the layered gabbro is intense with isoclinal folding of Plag & Cpx and Ol & Cpx bands (Plate 2.7). The intensity of deformation in the Louveras section may be the result of excessive oversteepening of semi-consolidated layers or semi-solid shear, localised in the vicinity of the Arakapas fault belt. Slump and scour features in wispy phase layered gabbro also occur at the

top of the cumulate sequence just below the transition into sheeted dykes. These features including 'channel fill' and cross bedding of mineral layering suggest intense convective circulation encountered during the final stages of crystallisation of the top of a magma cell.

A.S. cumulate blocks

Small isolated blocks of A.S. cumulates, 10m to 100m across, are tectonically entrained throughout the WLFC. They are commonly wehrlite or olivine gabbro that have orthocumulate textures. The occurrence, side by side, of blocks from all levels within the cumulate sequence, indicate extensive vertical displacement. Sample 8-CY2 is a laminated wehrlite that forms part of an elongated block entrained within a serpentinite shear zone [004521]. Although all the olivine is serpentinised, the rock shows an unusual relict orthocumulate texture. Idiomorphic clinopyroxene grains (0.5 to 2mm) are orientated with their c-axes parallel to one another forming an igneous lamination and surrounded by pyroxene forming a relict poikilitik relationship. This unexpected relationship implies a reverse crystallisation sequence of Ol -> Cpx, that is in contrast to that found elsewhere in the A.S. cumulates. Sample 6O-CY82, from another wehrlite block is less serpentinised. Intracrystalline deformation has redistributed olivine by dynamic recrystallisation. Polygonised and neoblastic olivine grains (0.1 to 0.5mm) are sheared around more competent, undeformed clinopyroxene grains producing the anomalous, pseudo-magmatic crystallisation sequence of sample 8-CY82. Since this style of texture is restricted to the isolated cumulate sequence blocks, it is likely that they were pervasively deformed while being tectonically entrained within their host serpentinite shear zones.

2.3.3 High Level Plutonic Group

Between the A.S. cumulates and the Sheeted Dyke Complex are isotropic gabbros, leucogabbros, diorites and trondhjemites that collectively form the High Level Plutonic Group

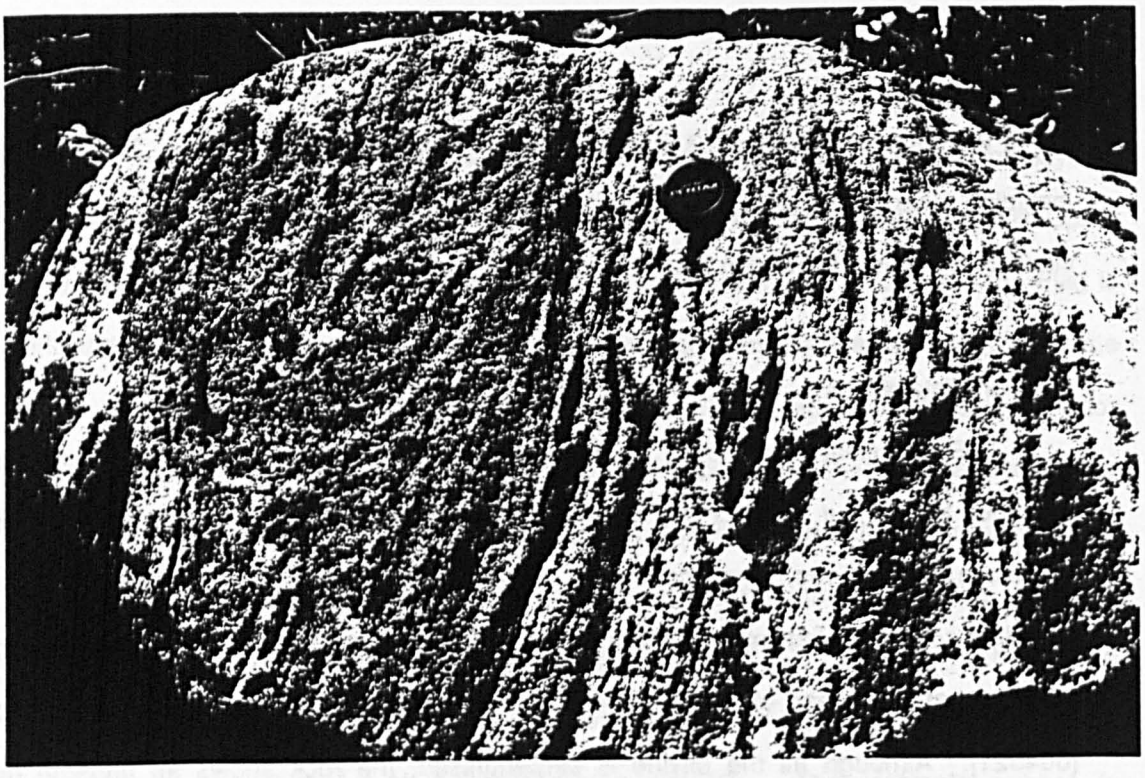

Plate 2.7 A slab showing intensely disturbed layering in layered wehrlite, from the Louveras section. The layering has suffered '*soft state*' deformation as slumping when in a semi-consolidated state.(HLPG). For the Troodos massif, these are interpreted as a combination of roof chill and late-stage fractionates of the cumulate sequence (Allen, 1975; Smewing, 1975). In the WLFC the HLPG grades from and overlies the cumulate sequence, forming only 20-25% of the Plutonic Sequence and thus is similar to other ophiolite complexes.

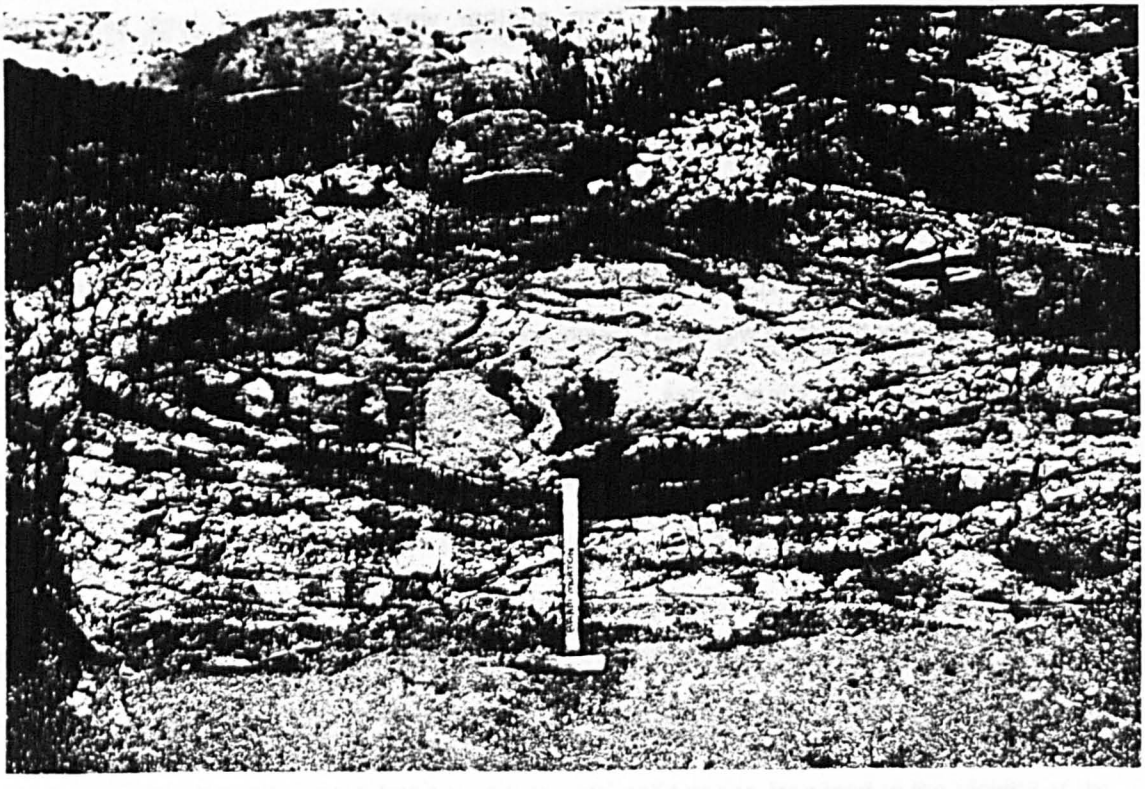

Plate 2.8 A typical '*high level*' gabbro showing an isotropic texture with pegmatitic patches and channelised scour structures: from the gabbro-sheeted dyke transition, Louvaras.

Isotropic gabbro

In the Argakin tis Kaloshis section, isotropic gabbro grades from layered gabbro over a distance of 50m. The isotropic gabbro has a medium grained (0.5 - 3mm) equigranular texture with, $Cpx_{30}Act_5Plag_{60}Qtz_5$ forming interlocking grains that contain (rare) myrmekite patches (Plate 2.8). Alteration of clinopyroxene to chlorite and fibrous actinolite, and plagioclase to epidote, albite and quartz is common and indicates high greenschist facies metamorphism.

In places the high level gabbro has 0.2 to 0.5m diameter pegmatite patches and veins, flasers of finer grained microgabbro and occasionally separates of diorite and quartz gabbro forming a vari- textured rock. In the Argakin tis Kaloshis section the isotropic gabbro varies in thickness from 50m to 260m, and an upward increase in modal plagioclase at the expense of clinopyroxene leads to leucogabbro. This gabbro has an allotriomorphic-granular texture and modal composition of $Plag_{75}(An_{70})Cpx_{20}Act_{20}Qtz_2$ (interstitial myrmekite forms 2% of the mode). In the Louveras section [040555] high level gabbro is intruded by leucogabbro apophyses and dykes that produce multiple and complex cross cutting relationships suggestive of multiple magma cell development. Smewing (1975) and Allen (1975) both report at least three stages of high level gabbro emplacement in the Troodos massif, during which gabbro intruded sheeted dykes, other gabbro and diorite.

Quartz diorite and trondhjemite

In the Argakin tis Kaloshis section, the relationship between the HLPG and the Sheeted Dykes Complex is marked by 1 to 2km long, intrusive pods of quartz diorite and trondhjemite. The majority of diorites and trondhjemites in the WLFC are moderately to strongly altered, weather pale yellow to yellow-brown, and form rugged, elevated terrain. Although Smewing (1975) reports three generations of trondhjemite in the Troodos massif, only two generations have been identified in the WLFC Axis Sequence. Early trondhjemite forms screens, cut by swarms of individual and composite dykes. Late trondhjemite intrudes both high level gabbro and more noticeably the Sheeted Dyke Complex (Plate 2.9). Both generations of trondhjemite occur in the Dhierona area.

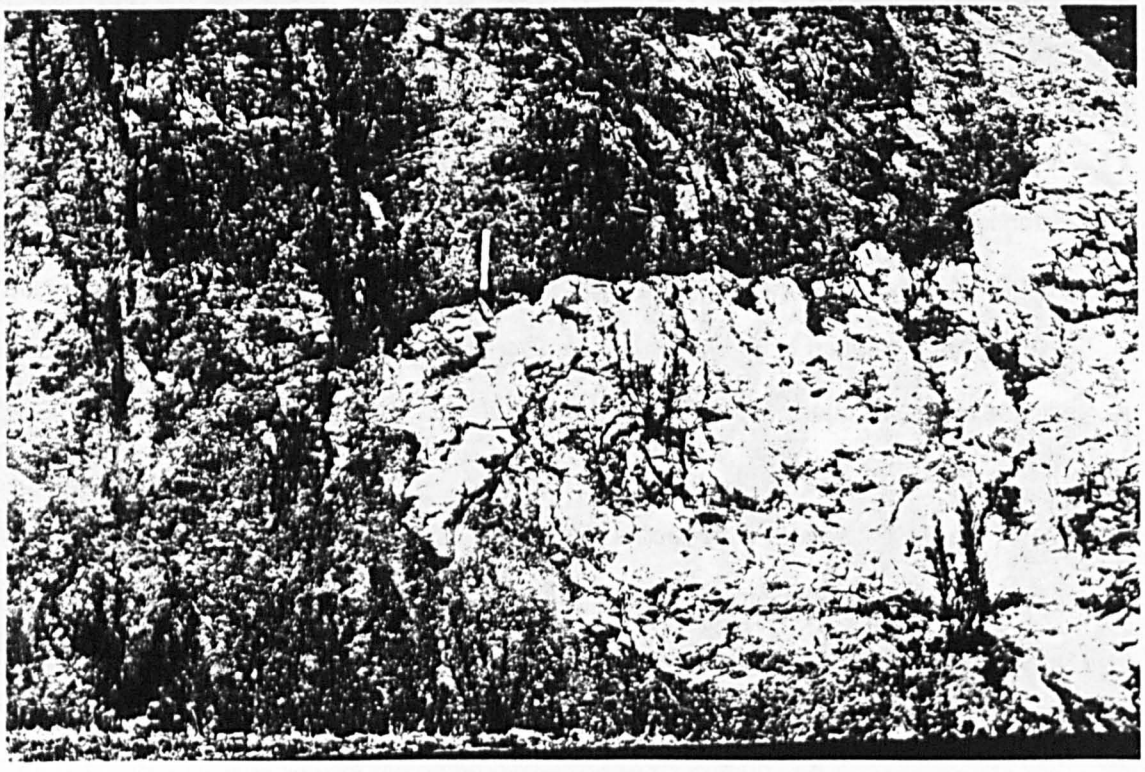

Plate 2.9 Late trondhjemite sheets, apothyses from a larger mass, cut and stop through Axis Sequence sheeted dykes. From an outcrop near Dhierona (see text).

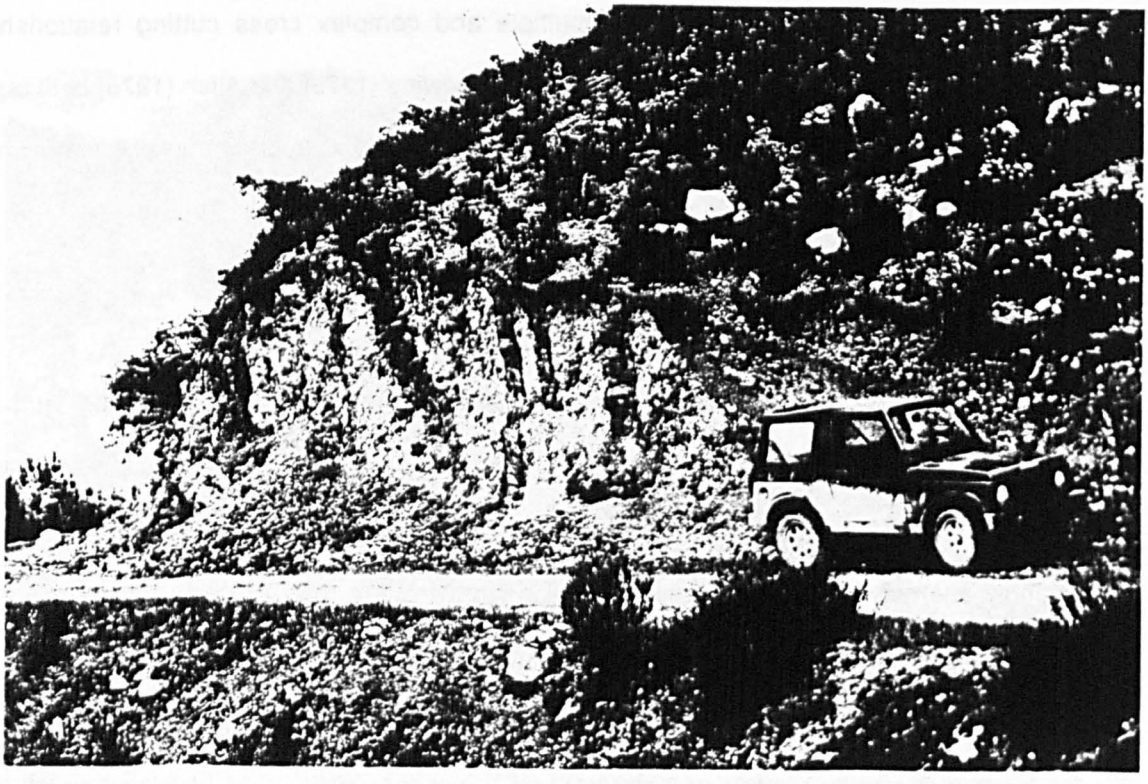

Plate 2.10 A swarm of '*brownstone dykes*', cut disrupted and tilted Axis Sequence sheeted dykes near Louveras. Their colour is characteristic of low grade hydrothermal alteration and sea-floor weathering.

Generations of trondhjemite occur in the Dhierona area. Compared with the early trondhjemite that forms screens 0.02 - 0.5m wide within the Sheeted Dyke Complex, the late trondhjemite contains a higher modal abundance of quartz and forms1 to 2.5km diameter bosses [107552]. A characteristic feature of these later trondhjemites is the presence of abundant xenoliths of dolerite, derived by stoping through the Sheeted Dyke Complex (Plate 2.10). Xenoliths of dolerite are corroded and partially resorbed. Since the solidus temperature of the mafic xenoliths is about 400^{o}C higher than for the trondhjemites, their partial resorption indicates melt - rock reaction rather than thermal assimilation.

In thin section the quartz diorites and trondhjemites are identified by their large modal abundance of quartz. Diorite is medium-coarse grained (0.5 to 3mm) allotriomorphic-granular with plagioclase (An_{35}) as laths forming between 65% and 70% of the mode. Ascicular clinopyroxene grains (up to 40mm long) are ubiquitously replaced by fibrous uralite actinolite. Intergrowth textures between pyroxene and plagioclase suggest cotectic crystallisation although some plagioclase is ophitically enclosed. Magnetite forms 10% of the mode and large 0.8 to 2.2mm euhedral skeletal grains and clusters. The relatively high modal abundance and rapid crystallisation of magnetite indicate a large increase in P_{H_2O} (Osborne, 1958). Alteration of the diorites is ubiquitous with plagioclase partly replaced by zoisite and smectite. Quartz, where present is both an alteration product where it is granular and fine grained, and primary, forming anhedral grains 0.5mm diameter. Abundant prismatic zeolite, possibly laumontite, forms a cryptocrystaline interstitial infill that indicates retrograde metamorphism from greenschist facies to zeolite facies during late stage cooling of the HLPG.

The trondhjemites are petrographically characterised by a coarse grained (4mm to 20mm) massive and granular texture with clinopyroxene (0.5 to 2cm long) that is often overgrown by actinolite and intergrown with granular quartz and laths of plagioclase. Clinopyroxene is also commonly replaced by actinolite that forms fine grained laths in radiating clusters to 2cm in diameter; plagioclase is replaced by smectite, zoisite and epidote, characteristic of hydrothermal metamorphism. Interstitial myrmekite intergrowths form 0.5-2mm

diameter patches. Magnetite is relatively rare and forms disseminated grains that are concentrated especially within actinolite pseudomorphs after clinopyroxene, as an alteration product. In the trondhjemites, saussuritisation and epidote mineralisation is localised along joint and fracture planes. This style of low grade alteration is characteristic of hydrothermal circulation. The presence of rare and unaltered mafic dykes that cross-cut the altered trondhjemites suggests a seafloor setting for the metamorphism.

2.4 Sheeted Dyke Complex

2.4.1 Introduction

The presence of a Sheeted Dyke Complex in an ophiolite complex is the most convincing evidence of its formation at a constructive plate margin (Gass, 1968; Moore & Vine, 1971). Kidd & Cann (1974) developed a model of crustal accretion in which vertical sheeted dykes are emplaced along an oceanic spreading axis, generating 100% extension. Unlike the north-south orientated Troodos Sheeted Dyke Complex (Wilson, 1959), the dominant trend just north of and within the Arakapas fault belt and the WLFC is east-west. The change in strike of the Sheeted Dyke Complex was first identified by Simonian (1975) as a large curvature bend (with a radius of 6km) through 90^{o} anticlockwise into the Arakapas fault belt. Simonian & Gass (1978) interpreted this change in direction as indicative of lateral movement along the east-west trending Arakapas transform fault. By analogy with recent oceanographic studies of fast slipping transform fault zones (Searle, 1983) in which a similar sense of change in orientation of normal faults indicates sinistral shear, the swing in dyke trends into the Arakapas fault belt also suggests left-lateral transform movement.

The A.S. Sheeted Dyke Complex crops out in four main areas in the WLFC, the Louveras area [040552], the Dhierona area [101545], the Akrounda area [060550] and the Venetou area, [055510]. The Sheeted Dyke Complex forms small, 200m high, steep-sided hills that weather pale grey to grey-green in colour, depending on the metamorphic grade.

Within the Sheeted Dyke Complex a range of petrological dyke types ranging from mafic to dioritic in composition cross cut one another. The order in which they cross cut each other varies from one locality to another, suggesting an origin from more than one fractionating magma cell.

2.4.2 Distribution and petrology

Although A.S. dykes occur throughout the Plutonic Sequence and occasionally in the Cumulate Sequence, the transition from high level plutonics into 100% sheeted dykes occurs rapidly over a distance of 20m. In the Louveras section (Figure 2.3), isotropic gabbro is occasionally wispy phase layered, with chaotic and steep mineral banding. Over a distance of 20m up section, cross cutting dykes change from micro-gabbro and coarse-grained dolerite into medium and fine-grained dolerite. Truncated screens of gabbro are common but chilled margins are rare suggesting a high temperature for the host lithologies during dyke emplacement. Although not exposed, it is likely that dyke rooting is similar to that described for the Troodos massif by Allen (1975) and the Semail Nappe, Oman by Rothery (1982).

The most abundant variety of sheeted dykes is a grey, indurate, greenschist facies metadolerite that forms 1.0 to 1.6m wide dykes with parallel sides and strongly chilled margins. One-way chilling of dykes, while individually predominant, is unreliable in trying to identify the location of the palaeo-spreading axis. These metabasite dykes have 0.5 to 1.5mm long laths and elongate grains of plagioclase (An_{28}) forming 65 to 70% of the mode and which are partly saussuritised. Acicular and anhedral grains of clinopyroxene form 25 to 30% of the mode and are commonly altered to uralite actinolite and chlorite. Despite their greenschist facies metamorphism, these metabasites retain a relict igneous hypidiomorphic-granular texture with myrmekitic patches in some of the more evolved samples and disseminated euhedral magnetite forming 5% of the mode.

Brownstone dykes

Cutting the grey greenschist facies sheeted dykes are individual brownstone dykes (Plate 2.11). These dykes have suffered pervasive low-grade hydrothermal alteration with plagioclase and clinopyroxene replaced by smectite, zeolite and zoisite and magnetite oxidised to haematite that weathers to produce the characteristic orange-brown colour of these dykes. This type of alteration has been identified by Cann (1969) for ocean floor basalts that have suffered intense submarine weathering.

In the Louveras area [047553], greenschist facies sheeted dykes have been rotated to sub-horizontal and then been reintruded by near vertical, brownstone facies dykes. Such vertical rotations indicate listric faulting and back tilting of fault blocks, which, cut by later dykes, indicate syn-magmatic sea-floor deformation. Syn-magmatic sea-floor tectonism of the WLFC Axis Sequence is also indicated by the presence of undeformed dykes cutting brecciated and faulted sheeted dykes. It is probable that the listric faulting of the WLFC Sheeted Dyke Complex occurred while it was in close proximity a constructive plate margin, similar to synthetic faults observed in the median valley walls of the FAMOUS and MAR areas (Needham and Francheteau, 1974; Ballard and Van Andel, 1977). The Sheeted Dyke Complex in the immediate vicinity of and within the Arakapas fault belt and WLFC transform fault zone (TFFZ) have a ridge-normal trend. Therefore the listric faulting of the Sheeted Dyke Complex more probably reflects an element of extension across the TFFZ soon after its formation but before A.S. magmatic activity had ceased.

2.5 Discussion and conclusions

2.5.1 Comparison between the WLFC and the Troodos massif

The Mantle Sequence

The Mantle Sequence in the WLFC is more variable than that on the Troodos massif. It has a heterogeneous fabric and lherzolite and plagioclase lherzolite facies are absent. This latter feature suggests a greater degree of mantle depletion following the removal of larger amounts of basaltic melt from the WLFC Mantle Sequence compared with that of Troodos (which Menzies & Allen (1975) concluded was about 12.5%). This interpretation is supported geochemically in Chapter 6 where it is shown that the WLFC Mantle Sequence has undergone a further stage of basaltic melt extraction compared with that in the Troodos massif. In the WLFC, sub-Moho dunite and chromite masses are smaller and more widely scattered than in the Troodos massif, suggesting the magma that formed the WLFC A.S. was supplied from the mantle as smaller batches of melt.

A.S. cumulates

Whereas the Troodos A.S. cumulates are characterised by abundant, repeated ultramafic to mafic cycles that suggest multiple magma influx and replenishment of open system magma chambers (Greenbaum, 1972; Allen, 1975), such rhythmic cyclicity is rare in the WLFC cumulates which appear to change in composition only gradually over their entire cumulate sequence. Slumping of layered gabbros is both abundant and intense in the WLFC whereas on Troodos it is scarce (Simonian, 1975; Allen, 1975). In the WLFC this soft state deformation of the A.S. is most extreme along its northern margin with the Arakapas fault belt. This supports the interpretation of Simonian (1975) that syn-magmatic tectonism was especially localised in the vicinity of the Arakapas fault belt.

In general

The most striking difference in the A.S. between the WLFC and the Troodos massif is the variation in the thickness of the complete crustal sequence and of the individual crustal units. Whereas the A.S. is only about 3.7km thick (see Chapter 5) in the WLFC, on Troodos the succession is 6 to 8km thick (Wilson, 1959; Vine *et al.*, 1973; Allen, 1975; Christiansen, 1977).

This difference in thickness of the A.S. between the two areas is in agreement with the evidence of crustal thinning in the vicinity of oceanic TFFZs, described by Fox *et. al.* (1980). The ratio of the individual crustal units e.g. the Sheeted Dyke Complex, the HLPG and the cumulate sequence, in the WLFC compared with those in the Troodos massif is 30 : 10 : 30 and 30 : 4 : 5 respectively. This may be due to the unusual orientation of the 'spreading ridge' that formed the WLFC A.S. (ie. at a high angle to the Troodos ridge) or due to the different spreading rate between the WLFC and that for Troodos.

It is likely that the WLFC 'spreading ridge' was very intermittent in its production of the WLFC A.S., since the amount of spreading accros the WLFC 'ridge' was small compared with the main Troodos spreading axis. This slow and intermittent spreading requires a smaller input of basaltic melt from the mantle, compared with that of the Troodos massif, and is reflected in the geochemistry of the WLFC A.S. (Chapter 6). Although the WLFC A.S. was formed perpendicular to the main Troodos A.S., it was still generated from part of the same spreading ridge, albeit one that bent in towards the TFFZ. Magmatism within the active transform domain *sensu stricto* did not occure until major extension across the TFFZ produced a transtensional regime in which the T.S. magmas were emplaced, described in Chapters 3 and 4.

2.5.2 Conclusions

(i) The WLFC is host to a Mantle Sequence and A.S. that formed at a constructive ridge axis.

(ii) The Mantle Sequence is more depleated in basaltic components and has a mantle tectonite fabric that is generally perpendicular to that of the Troodos massif.

(iii) In the WLFC the Mantle Sequence is exposed to a maximum depth of 0.8 km below the petrological-Moho.

(iv) The A.S. contains a Cumulate Sequence, a High Level Plutonic Group and a Sheeted Dyke Group that is only 65% as thick as that for the A.S. in the Troodos massif.

(v) The WLFC sheeted dykes have a trend that is perpendicular to those of the Troodos massif.

(vi) The thinning of the A.S. and change in trend of the sheeted dykes towards the Arakapas fault belt and WLFC is in agreement with recent studies of oceanic transform fault zones (TFFZ) in which constructive ridge axes are found to bend in towards the TFFZ close to a ridge - transform - intersection.

(vii) The relatively thin A.S. and the sense in which the sheeted dykes change their direction of strike indicate that the Arakapas fault belt and WLFC are part of a fossil, sinistral TFFZ whose trend is normal to the spreading ridge axis that formed the Troodos massif.

(viii) Following its formation the A.S. was tectonically disrupted and entrained within the fossil TFFZ.

(ix) Syn-magmatic deformation of the A.S. occurred during this tectonism and indicates disruption and magmatic overprinting of the A.S. while in the active domain of a leaky oceanic TFFZ.

CHAPTER 3

The Transform Sequence Intrusive Suite

List of Contents

3.1 Introduction

Within the WLFC, the Axis Sequence (A.S.) has been intruded by wehrlites and gabbros forming small, localised bodies most abundant in the Mantle Sequence. Direct tapping of the magmas that formed these bodies led to the emplacement of multiple mafic dykes and the eruption on the sea-floor of pillow lavas that form the bulk of the volcanic carapace in the WLFC. Since this post Axis Sequence magmatism was emplaced during sinistral transform faulting and is characteristically syntectonic, it has been termed the Transform Sequence (T.S.). On Figure 3.1 the distribution of T.S. intrusives, and the volcano-sedimentary sequence are shown.

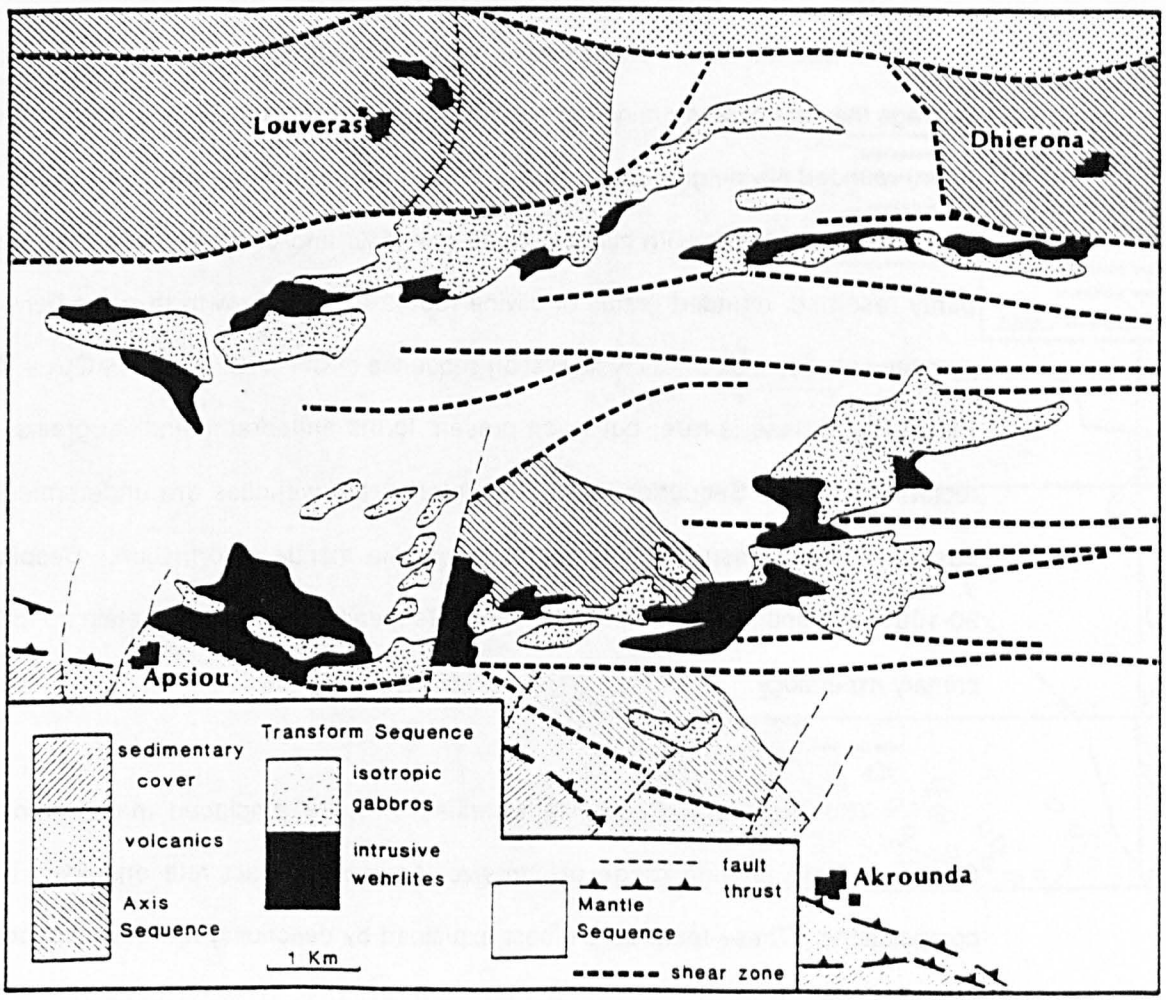

Figure 3.1 Enclosure showing the distribution of major outcrops of Transform Sequence wehrlites, gabbros and lavas and major Axis Sequence blocks.

3.2 Intrusive Peridotites

The oldest members of the T.S. are feldspathic wehrlites, forming small 0.6 to 2.5km long bosses and pods. These intrusive wehrlites cut both the Mantle Sequence and crustal units of the Axis Sequence. They are also cut by later gabbros and dykes of the Transform Sequence, producing an intrusive complex. Where the wehrlites intrude the Mantle Sequence, they typically form small, conical hills with exposure limited to loose blocks at the crest. Weathering of the wehrlites forms characteristic, rust-brown coloured, spongy surfaces with patches of poikilitic pyroxene producing lustrous mottling. Although the wehrlites are intrusive into the Axis Sequence, primary contacts are rarely exposed. Where seen, they are sharp, irregular, truncate earlier structures and fabrics and are devoid of marginal chilling.

These intrusive wehrlites have granular-mosaic textures, with poikilitic interiors. On average they are coarse grained with pyroxene oikocrysts (4 to 28mm) enclosing small (0.2 to 2mm) rounded olivine grains in a ratio of 7:3. In thin section these rocks can be seen to have allotriomorphic texture with clinopyroxene (38-45%) and orthopyroxene (15-20%) enclosing partly resorbed, rounded grains of olivine (30-42%). Intergrowth textures between the two pyroxene phases indicate a crystallisation sequence of Chr -> Ol -> Opx -> Opx + Cpx -> Cpx + Plag. Plagioclase is rare, but when present forms anhedral interstitial grains. Unlike the tectonised Mantle Sequence which they intrude, the wehrlites are undeformed and hence post-date high pressure and temperature, ductile mantle deformation. Despite pervasive 90-100% serpentinisation of the host Mantle Sequence, the wehrlites retain up to 70% of their primary mineralogy.

The Transform Sequence wehrlites that are emplaced mainly into the Mantle Sequence have a wide range of intrusive features, contact relationships, textures and compositions. These features are best explained by describing two selected localities in the following section.

3.2.1 Amirou wehrlite-harzburgite Complex

The largest Transform Sequence intrusive wehrlite is emplaced into the Mantle Sequence at Amirou (Figure 3.2) [040505]. Two facies of wehrlite occur: (i) massive poikilitic wehrlite forming the main body and (ii) a pyroxenitic variety that is especially abundant along the southeastern margin of the intrusion. A lenticular outcrop of dunite occurs along the eastern margin of the wehrlite and is probably part of its cumulate base. The wehrlite has two types of intrusive contact: (i) a sharp, wavy and irregular contact, and (ii) anastomosing veins of wehrlite enclosing xenoliths of harzburgitic country rock. Examples of the sharp, irregular contacts are exposed in the Lakxies area [027530], where they truncate the near vertical mantle foliation (Plate 3.1).

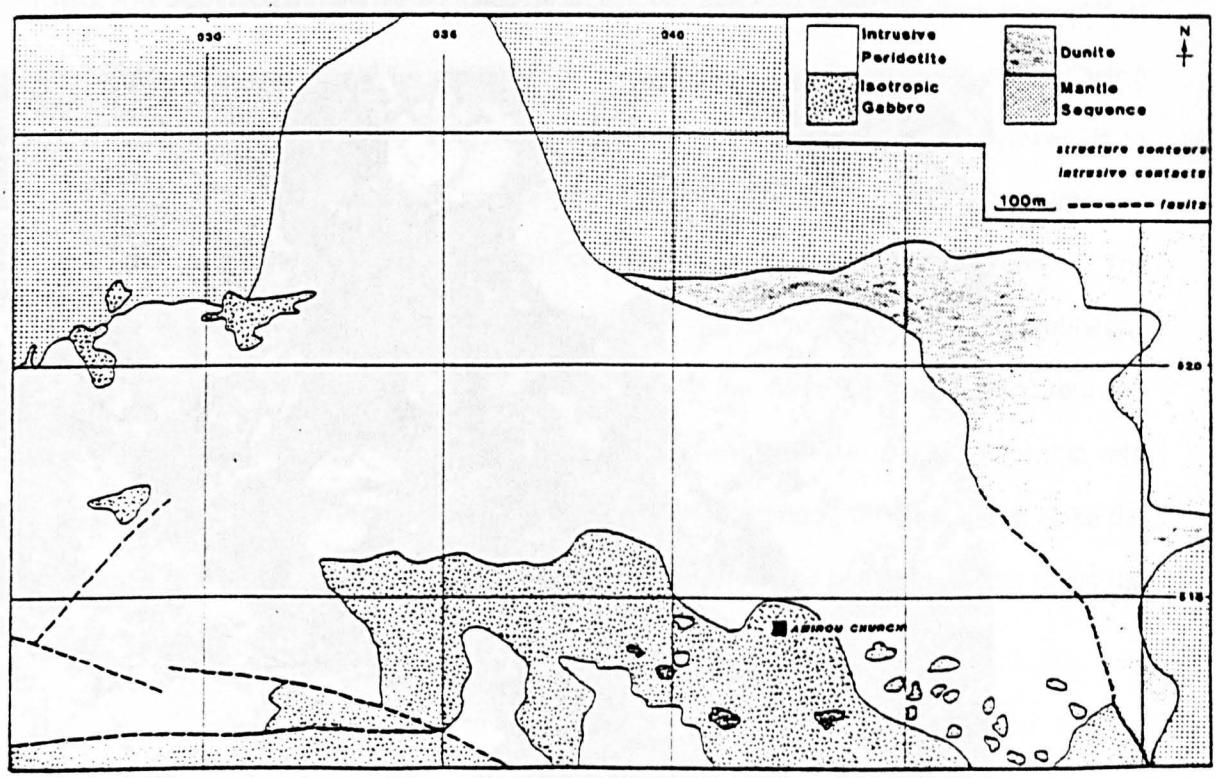

Figure 3.2 Enclosure of the Amirou area showing Transform Sequence wehrlites emplaced into the Mantle Sequence and containing harzburgite xenoliths.

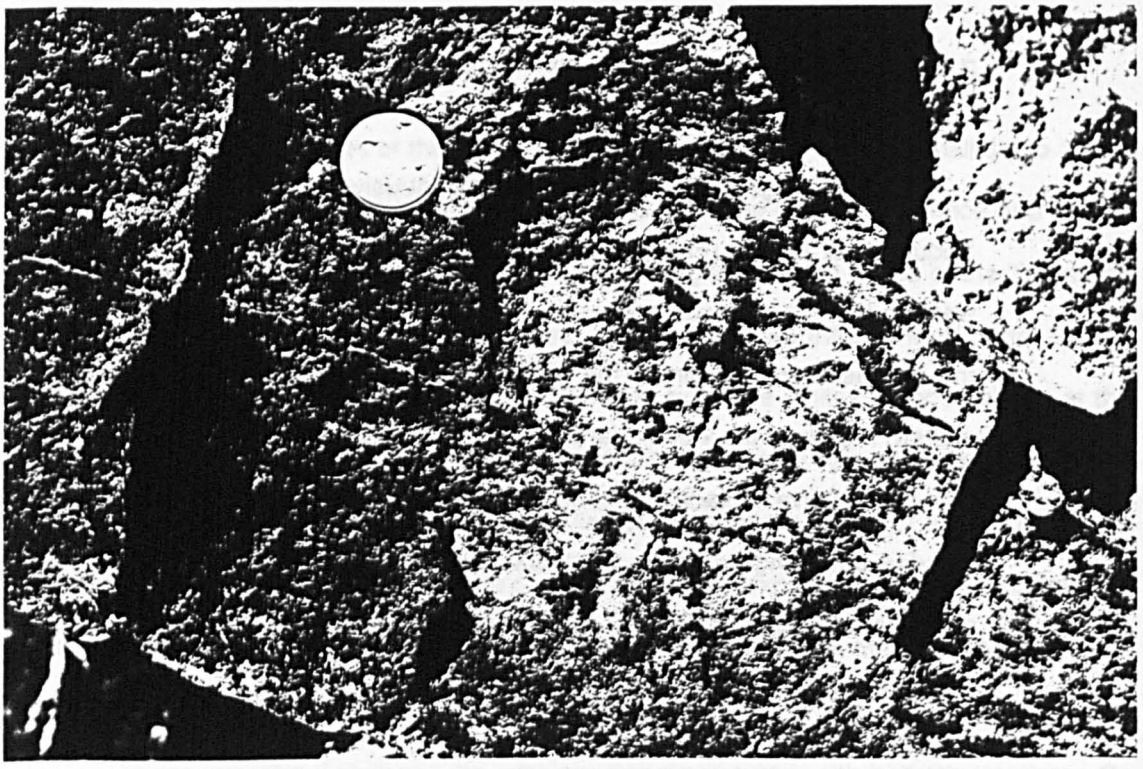

Plate 3.1 Near vertical contact between intrusive wehrlite and tectonised harzburgite. The wehrlite is unchilled and has an irregular margin with its host rock.

Plate 3.2 Photo-micrograph of intrusive wehrlite (field of view, 8mm). Rounded olivine grains and euhedra of chrome spinel are enclosed within clino- and orthopyroxene oikocrysts. Unlike the host harzburgite, the intrusive wehrlite is free of pervasive deformation

The contact is unchilled, indicating that the host Mantle Sequence was at a high temperature when the wehrlite was emplaced.

In thin section (sample 83-CY84) the intrusive wehrlite is a medium-coarse grained (1 - 6mm) rock with an allotriomorphic-granular, orthocumulate texture. Subhedral olivine grains (0.8 - 2.2mm) form 36% of the mode and are enclosed within clinopyroxene (38%) and orthopyroxene (20%) oikocrysts, (Plate 3.2). Intergrowth textures between the pyroxene phases indicate cotectic crystallisation.

At a point 300m due east of Amirou church [043505] the wehrlite contains more modal pyroxene than usual and although the Mantle Sequence crops out about 500m away, the wehrlite contains abundant xenoliths of serpentinised and tectonised harzburgite. The xenoliths are 0.2 to 1m across, angular and cut by anastomosing veins of the invading wehrlite (Plate 3.3). In a stream gully [041504] blue-grey coloured harzburgite xenoliths, form 45% of the outcrop and are enclosed within wehrlite stockworks indicating forcefull intrusion. Over a distance of 200m north of the previous locality, the wehrlite grades from pyroxenitic to subpoikilitic and finally into massive, coarse grained wehrlite characteristic of the main intrusive body. Harzburgite xenoliths (0.5 to 1.2m) continue to crop out over this distance. The pyroxenitic wehrlite is a medium grained (5 to 15mm) hypidiomorphic rock with subhedral orthopyroxene and clinopyroxene grains forming 92% of the mode, partly enclosing rounded serpentinised olivine grains (3 to 5mm). The subpoikilitic wehrlite is allotriomorphic with oikocrysts of ortho- and clinopyroxene enclosing 0.2mm diameter grains of olivine. Like the main body of wehrlite, the pyroxenitic variety is untectonised and hence also post dates the high temperature, ductile mantle deformation.

3.2.2 Intrusive Wehrlite Apophyses

Plate 3.4 illustrates the intrusive relationship between the host Mantle Sequence, wehrlite apophyses and cross-cutting picrite dykes, exposed along the main Yermasoyia to Dhierona road [085517]. Tectonised harzburgite with a subvertical NE-SW trending mantle foliation is cut by 1 to 3m wide dyke-like apophyses of wehrlite. The apophyses taper upward and are offshoots of a subjacent 300m diameter wehrlite boss. Contacts between the wehrlite apophyses and harzburgite are sharp, truncate the mantle fabric and are unchilled.

The wehrlite has an isotropic, hypidiomorphic-granular texture in which olivine (42%) forms subhedral - rounded phenocrysts (5 to 3mm) with marginal embayment produced by partial resorption. Equigranular clinopyroxene (36%), orthopyroxene (18%) and plagioclase (<5%) form a medium grained (3 - 8mm) allotriomorphic groundmass and indicate a crystallisation sequence Chr -> Ol + Opx + Cpx -> Plag. However, the corroded nature of the olivines indicates their earlier formation and re-equilibration with the more evolved melt. The rock is partially altered to serpentinite, epidote and pale green chlorite.

The absence of flow fabrics and a large percentage of matrix suggest emplacement as a liquid-rich magma. The lack of chilled margins is also evidence that the host harzburgite was at a similar temperature to the intrusive wehrlites when first invaded. Later cross cutting, sub-vertical picrite dykes are medium grained, 0.8 to 1.2m wide and have 0.1m wide chilled margins. This, combined with their brittle style of intrusion suggests that both the host harzburgite and intrusive wehrlite was cool and brittle during picrite dyke emplacement.

3.2.3 Chilled Peridotite Margins

In the Dhassina area [07485417] a small 60-80m diameter intrusive boss, emplaced into serpentinised tectonised harzburgite, has a slight reduction in grain size towards its margin. This textural variation is attributed to chilling at the contact with the host harzburgite.

The contact is also sharp and highly irregular with 2 to 4m long apophyses.

At its margin the intrusive wehrlite is medium grained (0.5 to 4 mm) granular with allotriomorphic, poikilitic orthopyroxene (32%) and clinopyroxene (46%) grains enclosing rounded, subhedral olivines (22%) 0.8 to 2.2mm in diameter. In contrast, wehrlite 4m from the contact is more coarsely grained, with oikocrysts (1.6 mm) of orthopyroxene (30%) and clinopyroxene (32%) enclosing rounded olivine grains (38%) between 0.8 and 3mm in diameter. Where partly surrounded by clinopyroxene, some olivine grains have been observed with orthopyroxene reaction rims. Oikocrysts of orthopyroxene exhibit exsolution of clinopyroxene forming blebs parallel to (100). Late alteration of the intrusive wehrlite has formed serpentinite, chlorite and pale green, actinolite, although fresh orthopyroxene remains.

Harzburgite at the contact with the intrusive wehrlite forms very fine grained, granular serpentinite. This suggests that the host was partially serpentinised when, on subsequent intrusion by the wehrlite, dehydration formed recrystallised granular olivine.

3.2.4 Louveras Wehrlite-Gabbro Association

Where the Axis Sequence cumulates are host to later intrusive wehrlites, differentiation between the two is difficult. However, in the Louveras area, high level and layered A.S. gabbros are intruded by small 10 to 30m diameter bosses of poikilitic wehrlite. At [044556] a laminated olivine gabbro has been intruded by an isotropic, equigranular, plagioclase wehrlite. These medium grained wehrlites have up to 15% interstitial plagioclase. Offshoots of feldspathic wehrlite form 3m wide, discontinuous dykes, sills and pods that cut the A.S. gabbros and are medium - fine grained, granular rocks. About 3km southeast of Dhierona, an E-W elongate (5 x 1.5 km) wehrlite is cut by later gabbro and diorite. The intrusive wehrlite does not have a continuous outcrop and the body is parallel to east-west trending serpentinite shear zones.

Plate 3.3 Xenoliths of tectonised harzburgite (with a blue hue) are surrounded and broken up by stockworks of pyroxenitic wehrlite (pale yellow - brown).

Plate 3.4 Intrusive apophyses of T.S. intrusive wehrlite (denoted by *w*) cut by tectonised harzburgite (denoted by *h*) as subvertical sheets, 1.5 to 2m wide. The wehrlite is unchilled, medium grained and has subsequently been cut by chilled picrite dykes (denotet by *p*).

3.2.5 Discussion and Interpretation

Intrusive T.S. wehrlites cut both the Mantle Sequence and crustal units of the A.S. Their intrusive and textural features demonstrate emplacement during cooling, partial serpentinisation and possible uplift of the Mantle Sequence. The formation of apophyses, pods and stockworks suggest the wehrlites were remobilised prior to solidification. Although in the field the T.S. wehrlites resemble the A.S. cumulate ultramafics, they are geochemically distinct (Chapter 6). Despite the geochemical relationship between the T.S. wehrlites and T.S. gabbros (Chapter 6), the intrusive wehrlites do not grade into gabbro in the field. This also suggests that partial remobilisation of the wehrlites prior to solidification filter pressed the remaining liquid which later was intruded as the T.S. gabbros.

Although intrusive wehrlites occur in other ophiolite complexes such as Magame Island (Varne *et. al.*, 1969), the Point Sal Complex (Hopson & Frano, 1977), and the Main Troodos Massif (Wilson, 1959; Dunswater, *pers. comm.*) they only occur at high levels in the ophiolite crustal sequence. These high level peridotites are regarded as intrusive crystal mushes that were emplaced along ridge parallel faults that penetrated deep into partially consolidated, newly formed oceanic crust. A similar interpretation has been made for high level wehrlite dredged from the Mid Atlantic Ridge (Bonatti & Honerez, 1976).

In contrast, their ridge normal elongation, sub-Moho occurrence, semi-consolidated remobilisation and history of syntectonic emplacement suggests that the WLFC, T.S. wehrlites were emplaced within an active transform fault zone. A similar interpretation of a transform fault setting has been made for ridge normal, high level syntectonic intrusive peridotites in the Coastal Complex, Newfoundland (Karson *et. al.*, 1983). Although these latter high level intrusive wehrlites were probably emplaced at a ridge-transform intersection (Karson *et al., op cit*), the WLFC, T.S. wehrlites intrude the Mantle Sequence and are the product of leaky transform fault magmatism.

3.3 Intrusive Gabbro-Diorite Complexes

Following the emplacement of the majority of intrusive wehrlites (see Chapter 3.2), gabbronorites, diorites and trondhjemites were emplaced at all structural levels within the WLFC Axis sequence. These plutons form elongated, isolated bosses, 1 to 5km long, that are generally orientated NE-SW. Like the intrusive wehrlites that preceded them, these later mafic plutons most commonly cut the Mantle Sequence and are readily identifiable by their characteristic buff coloured weathering. Intrusive roof relationships between the gabbro-diorite complexes are usually exposed in deeply incised gullies while the host Mantle Sequence and T.S. wehrlite crop out along the ridges. Textural similarities between these intrusive mafic complexes and the high level A.S. plutonic group make distinction between the two difficult. In all, six structural and textural facies have been identified in the gabbro-diorite complexes:

i) anastomosing veins and stockworks of pegmatite

ii) apophyses of microgabbro

iii) main body, isotropic gabbro

iv) microgabbro autoliths

v) aplite apophyses,

vi) diorite-trondhjemite bodies.

With the exception of (vi) all these features are clearly exposed in a river section, south of Dhierona, that has been chosen as a type locality, described below. The significance of the gabbro-diorite complexes is discussed in terms of syntectonic magmatism and closed system fractionation in Section 3.3.8.

3.3.1 Pegmatite Veins and Stockworks

The appearance of pegmatite veins is a characteristic, distal manifestation of the intrusive gabbro-diorite complexes. Commonly observed cutting an ultramafic host, these pegmatites are often accompanied by localised serpentinisation and epidote veining, indicating fluid mobilisation. They are most abundant directly above, and persist for up to 350m

from, major mafic intrusions. Closer to the main gabbro-diorite plutons, anastomosing pegmatite stockworks up to 3m in diameter cut the host rocks, (Plate 3.5). Pegmatitic veins over 0.05m wide are commonly composite with microgabbroic centres. Pegmatites invading brecciated and sheared country rock are evidence of brittle faulting prior to intrusion (Plate 3.6). Although pegmatite veins and stockworks that truncate mantle tectonite fabrics are not macroscopically deformed, microscopic investigation reveals protocataclastic textures (Plate 3.7).

Sample 4-CY84 is typical, exhibiting a medium - coarse grained (2-6mm) allotriomorphic - granular, protocataclastic texture. Plagioclase (petrographically identified as An_{58}) forms 65% of the mode and is present as both subhedral phenocrysts (3-6mm) and as part of an equigranular groundmass. Polygonisation, undulose extinction and tapering of periclase twins indicate intracrystalline strain. Orthopyroxene forms 20% of the mode and is present in the groundmass and as occasional large phenocrysts (4-6mm). The orthopyroxene grains are commonly hypidiomorphic, kinked and have ragged, mosaic textured cataclastic areas.

Plate 3.8 reveals reaction rims of clinopyroxene around and between disrupted fragments of cataclastic orthopyroxene grains that suggest deformation preceded final crystallisation of the pegmatite vein. In the allotriomorphic groundmass, ragged and stained grains of clinopyroxene (0.3-0.8 mm) are partially replaced by uralite, actinolite and epidote. Magnetite forms 2% of the mode, is deformed with cuspate margins and occurs as anhedral, interstitial grains (0.3-0.6 mm).

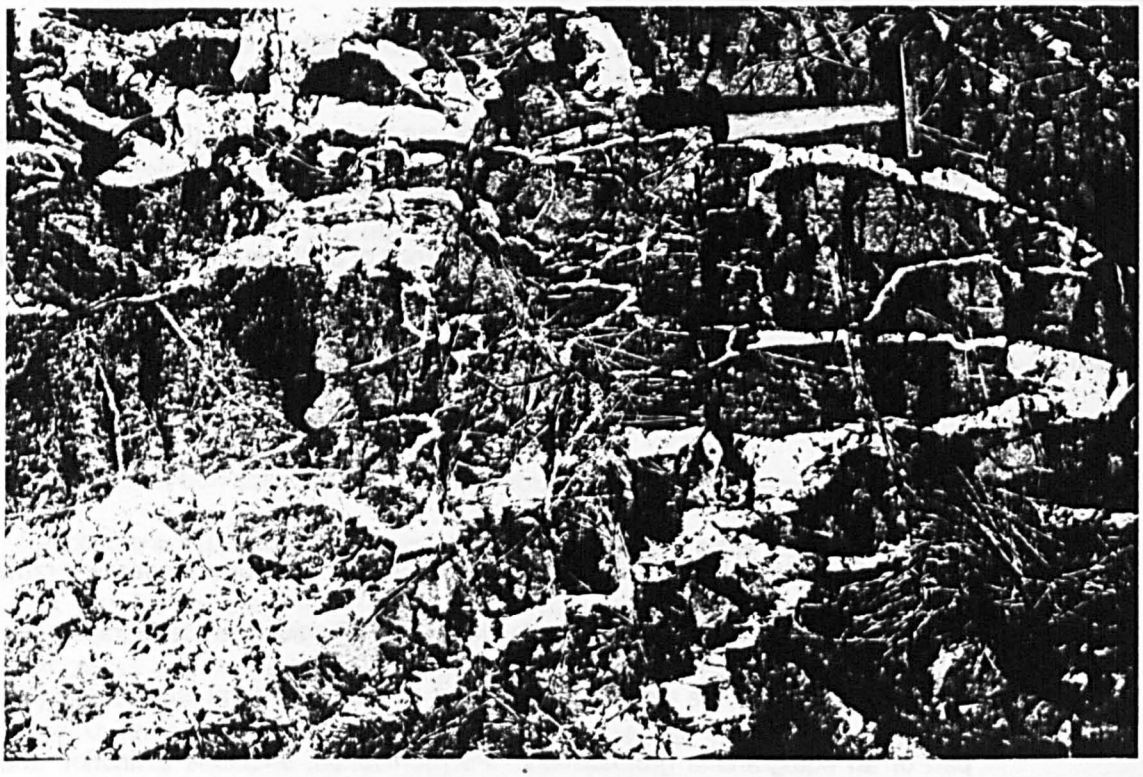

Plate 3.5 Anastomosing stockwork of pegmatite gabbro invades tectonised harzburgite, 250m from the main gabbro outcrop.

Plate 3.6 Pegmatite gabbro partially fills brecciated, tectonised harzburgite, resulting in a net veining effect suggesting the harzburgite had been brecciated prior to subsequent invasion by the T.S. gabbro.

Plate 3.7 Photo-micrograph of pegmatite gabbro from a stockwork invading harzburgite. Unlike its tectonised harzburgite host, the gabbro has not suffered high P and T deformation. However, it does have a protocataclastic texture indicating brittle shear, Field of view, 8mm.

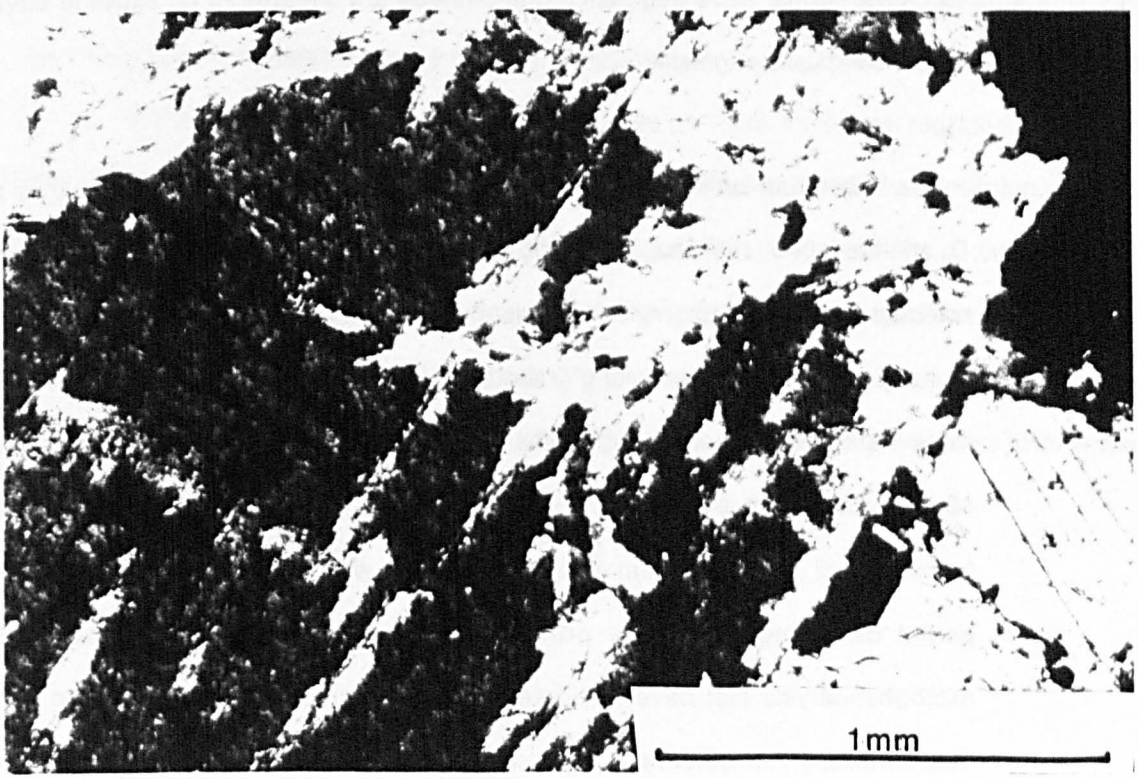

Plate 3.8 Photo-micrograph showing a cataclastic orthopyroxene grain from a gabbro stockwork invading harzburgite. The grain has been fractured prior to subsequent overgrowth by clinopyroxene, indicating synmagmatic deformation.

3.3.2 Microgabbroic Apophyses

With increasing proximity to the main gabbro-diorite complexes, microgabbroic veins and dyke-like apophyses become progressively more abundant at the expense of pegmatites. These intrusives vary between 0.2m and 0.7m wide, the largest cropping out near the contacts with the main plutons [0605430] (Plate 3.9). Where they exceed 0.3m in width the apophyses are medium-fine grained but with 5 to 10mm wide, chilled margins, indicating intrusion into a cool host. Close examination of harzburgite where it is in contact with the larger microgabbroic apophyses reveal 50mm rims of fine grained, granular serpentinite that is texturally unlike the rest of the ultramafic host (Plate 3.10). These rims are interpreted as thermal dehydration reaction products of serpentinite that formed granular, recrystallised olivine during emplacement of the microgabbro and prior to subsequent re-serpentinisation. This suggests that partial serpentinisation and cooling of the Mantle Sequence took place prior to gabbro emplacement. In places apophyses in excess of 0.5m wide taper away from the main gabbroic outcrops. Some have pegmatitic margins and are interpreted as extreme developments of earlier composite pegmatite veins.

Deformation of the microgabbroic intrusions is variable. Although they post date the D_1 mantle fabric (see Chapter 5) and are macroscopically undeformed, they commonly have protocataclastic to protomylonitic, microscopic textures. Sample 7-CY83 is typical of the majority of apophyses, exhibiting granulation and partial recrystallisation. The microgabbro is more mafic than the earlier pegmatites, consisting of 48% clinopyroxene, 5-8% orthopyroxene, 40-47% plagioclase and about 2% magnetite. Plate 3.11 illustrates equigranular clinopyroxene forming small (0.05 to 0.1mm) grains occasionally with ragged edges, undulose extinction and partial disaggregation. The orthopyroxene is present as subhedral, 0.05 to 0.2mm microphenocrysts that have also been partially fragmented by deformation. Petrographic determinations of undeformed plagioclase compositions vary from An_{35} to An_{60} with a mean of An_{55} being most common in the groundmass. The grain size of the plagioclase is bimodal with 90^{o} of the plagioclase forming mosaic textured, polygonised grains. Porphyroclastic

phenocrysts (0.6 to 2mm) are subhedral with undulose extinction and tapered periclase twins. Mosaic textures and partial disaggregation illustrate cataclastic matrix development. Olivine is very rare with only one rounded grain enclosed within a orthopyroxene grain having been observed. Magnetite, where present, forms less than 1% of the mode as small (0.01mm) euhedra. The crystallisation sequence, Ol -> Opx + Opx + Cpx -> Cpx + Plag ± Mgn is characteristic of the gabbro-diorite complexes.

3.3.3 Major Gabbroic Plutons

The outcrops of the major gabbroic plutons are elongated NE-SW, vary between 1 and 5km long by 0.3 to 1.2km wide and constitute 15% of the occupied by the Mantle Sequence. The majority of these T.S. gabbros form steep-sided bosses.

Serpentinised harzburgite in contact with, and incorporated as, roof pendants and xenoliths in the gabbroic plutons [053543] have a fine grained, granular appearance similar to the recrystallised serpentinite at the margins of the intrusive microgabbroic apophyses (Section 3.3.2). Although these xenoliths range from 0.2m to 0.5m long, are rounded and most abundant near the roofs of the plutons, they do not show any evidence of assimilation. Apart from xenoliths of country rock, the main T.S. gabbros often have autoliths of finer grained, more mafic gabbro, described in Section 3.3.4. Texturally, the main gabbros are variable, medium to coarse grained equigranular and isotropic with pegmatite patches 0.2m to 0.6m in diameter, some of which are pyroxenitic. In places, finer grained gabbroic facies form wispy flaser textures, similar to the High Level Plutonic Group (Plate 3.12).

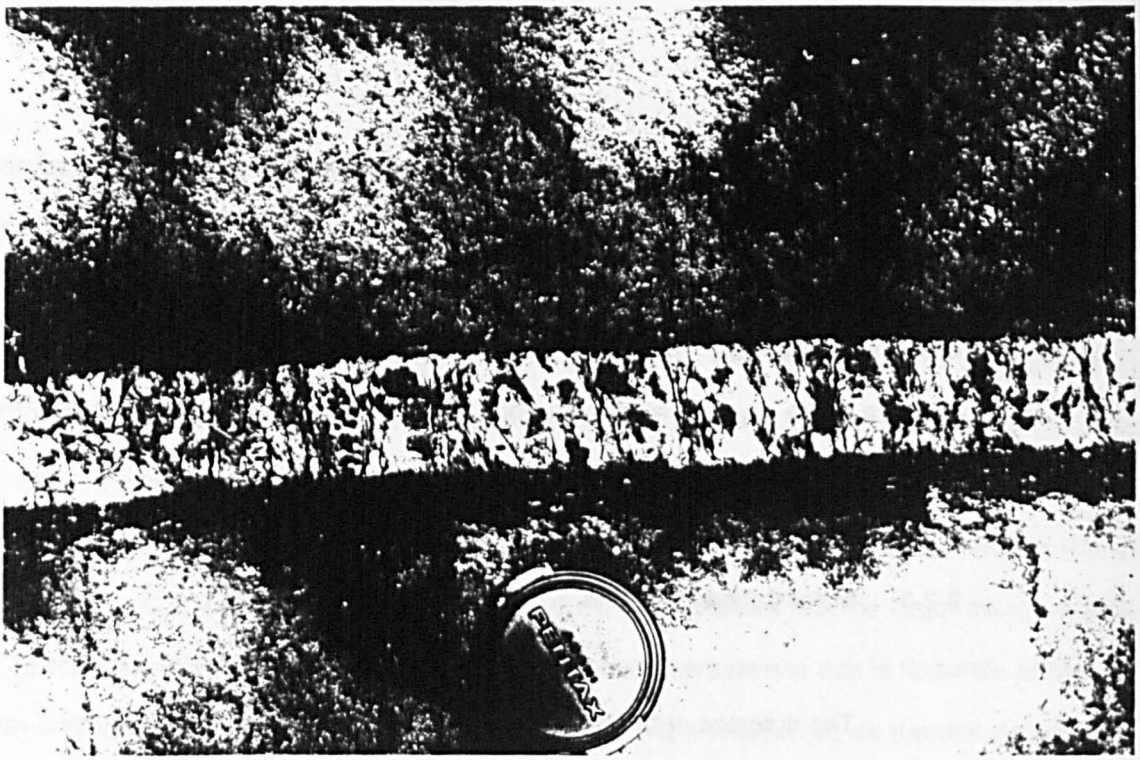

Plate 3.9 Microgabbroic apothysis cuts tectonised harzburgite and truncates the high P and T mantle deformation fabric.

Plate 3.10 Detail of contact between a T.S. gabbroic apothysis and its tectonised harzburgite host. The harzburgite has a very fine grained texture at the contact, suggesting thermal dehydration reaction during gabbro emplacement and hence its prior partial serpentinisation.

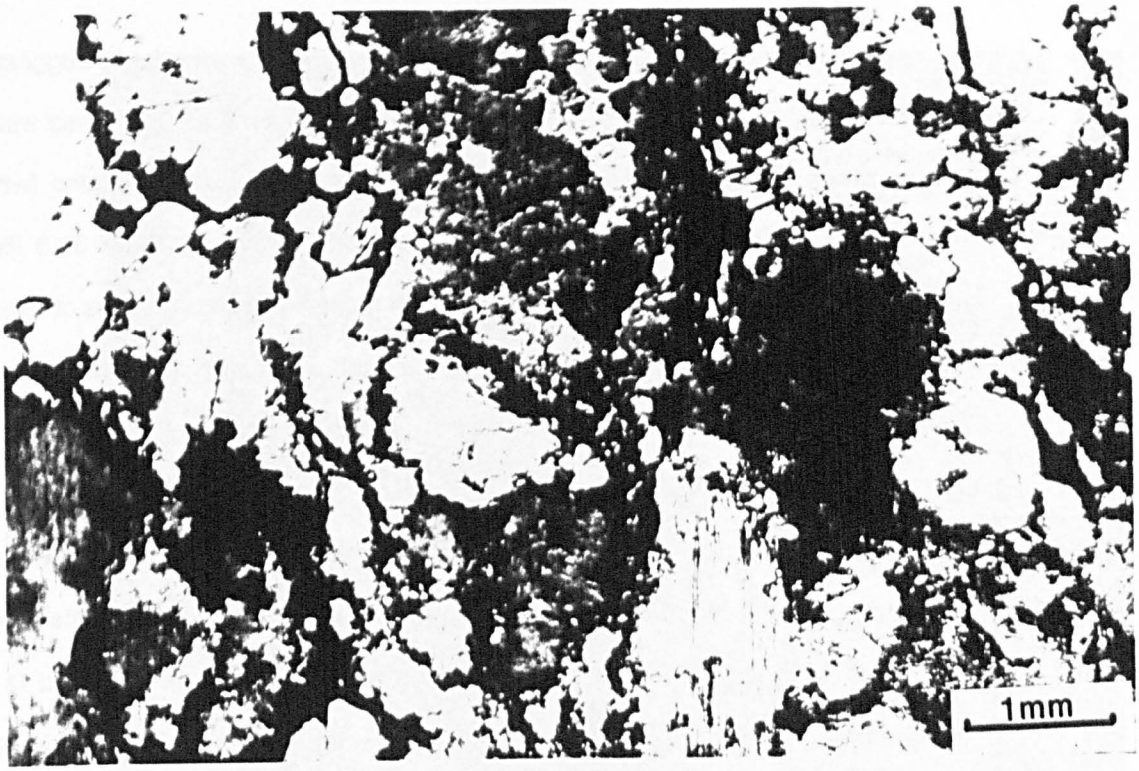

Plate 3.11 Photo-micrograph of moderatly deformed, protocataclastic and strained gabbro from a gabbroic apothyses that cuts harzburgite of the Mantle Sequence.

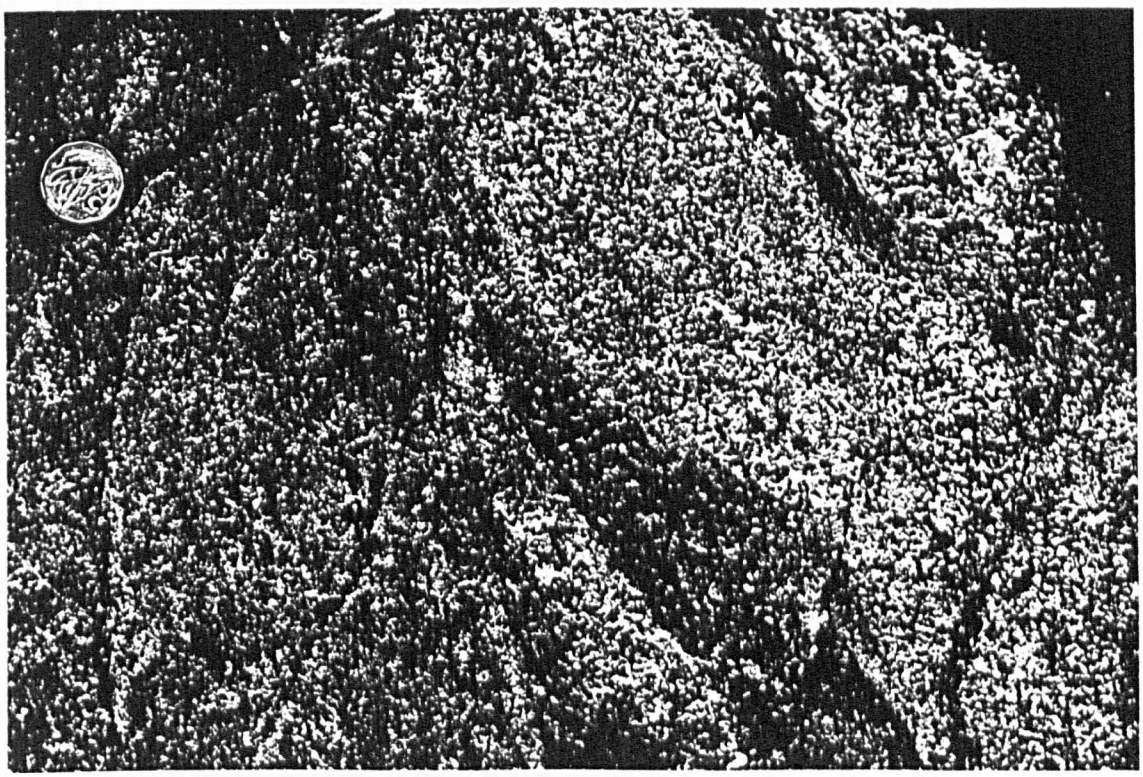

Plate 3.12 Typical , isotropic T.S. gabbro with a varitextured appearance and flazers of finer grained microgabbro.

The association of some plutons with major E-W trending faults suggests a structural control of magma emplacement. Where the gabbroic plutons are in contact with serpentinite shear zones they are often ultramylonitic. Elsewhere, gabbroic margins (which are only moderately chilled) commonly have protocataclastic textures. Plate 3.13 illustrates late autoveining of a gabbro by irregular 0.1 to 0.3m wide, N-S trending dykes of microgabbro that suggest extension parallel to the length of the gabbro main pluton during its final stages of crystallisation.

In thin section, the gabbro from the interior of the plutons is medium-coarse grained, equigranular, hypidiomorphic and which is strained but *not* cataclastic (Plate 3.14). Although described as gabbroic, the rock contains up to 24% orthopyroxene and is therefore a gabbronorite. The orthopyroxene occurs as strained and cracked grains (0.2 to 0.6mm), occasionally with clinopyroxene reaction rims. Equigranular clinopyroxene forms 18% of the mode, anhedral, strained grains, partly enclosed by subhedral plagioclase (An_{55}) which forms 58% of the mode. The majority of strain has been accommodated by slight mosaic recrystallisation and deformation of plagioclase. Relict plagioclase phenocrysts have tapered periclase twins and undulose extinction. Like the microgabbro apophyses, the main gabbros contain less than 1% magnetite, forming 0.2mm euhedra, and a similar crystallisation sequence of Opx + Cpx -> Cp + Plag ± Mgn.

In contrast, gabbro at the contact with tectonised harzburgite is generally protocataclastic (Plate 3.15), with an allotriomorphic - granular texture. Clinopyroxene is especially granulated and brecciated. These grains occur as both ragged 0.8 to 2mm porphyroclasts and strained 0.1 to 0.4mm groundmass grains that form 48% of the mode. Orthopyroxene forms 5% of the mode, is less deformed and occurs as 2mm porphyroclasts. Plagioclase, petrographically determined as An_{55}, is extensively sheared with mosaic polygonisation of 0.8 to 3mm porphyroclasts that partly enclose both clinopyroxene and orthopyroxene. In extreme cases, some gabbro margins are ultramylonitic.

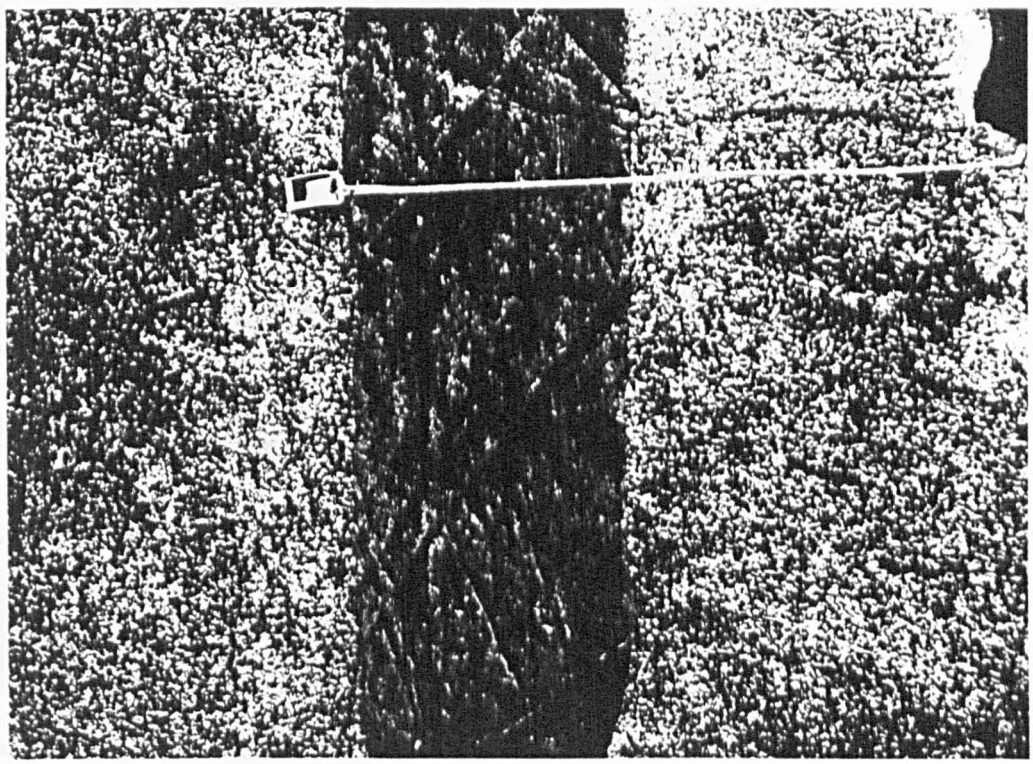

Plate 3.13 Late, fractionated dykes of microgabbro autovein their parental host. These dykes typically trend perpendicular to the length of the gabro plutons that they cut.

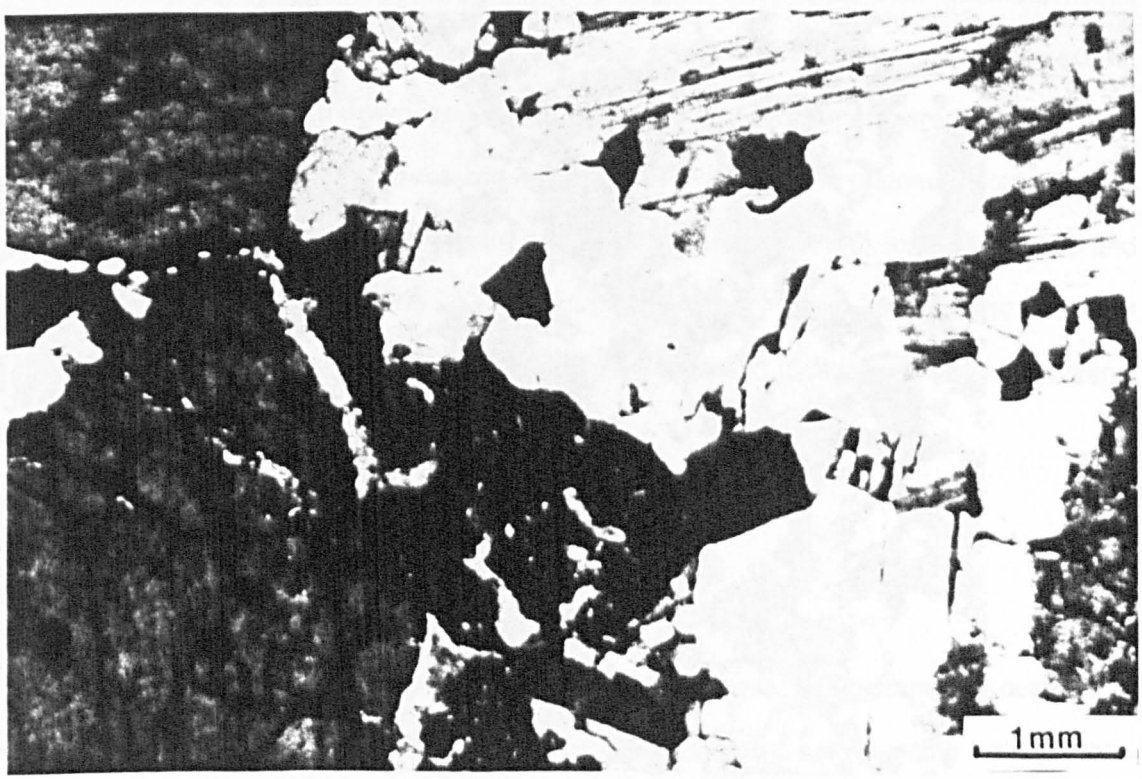

Plate 3.14 Photo-micrograph of T.S. gabbro from the interior of a major outcrop, showing a hypidiomorphic - granular texture. Deformation of the gabbro has been relatively weak and has only strained the rock fabric.

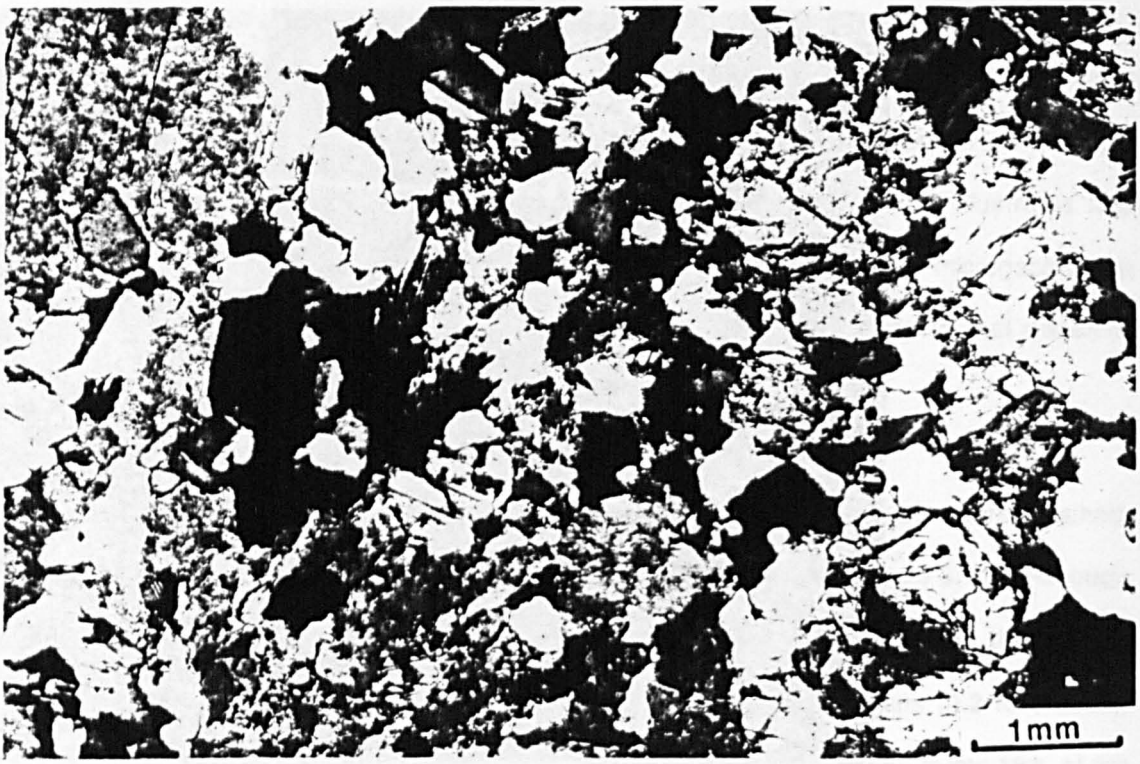

Plate 3.15 Protocataclastic gabbro from the margins of a major outcrop. Disaggregation and strain of the grains reflects a moderate amount of brittle deformation.

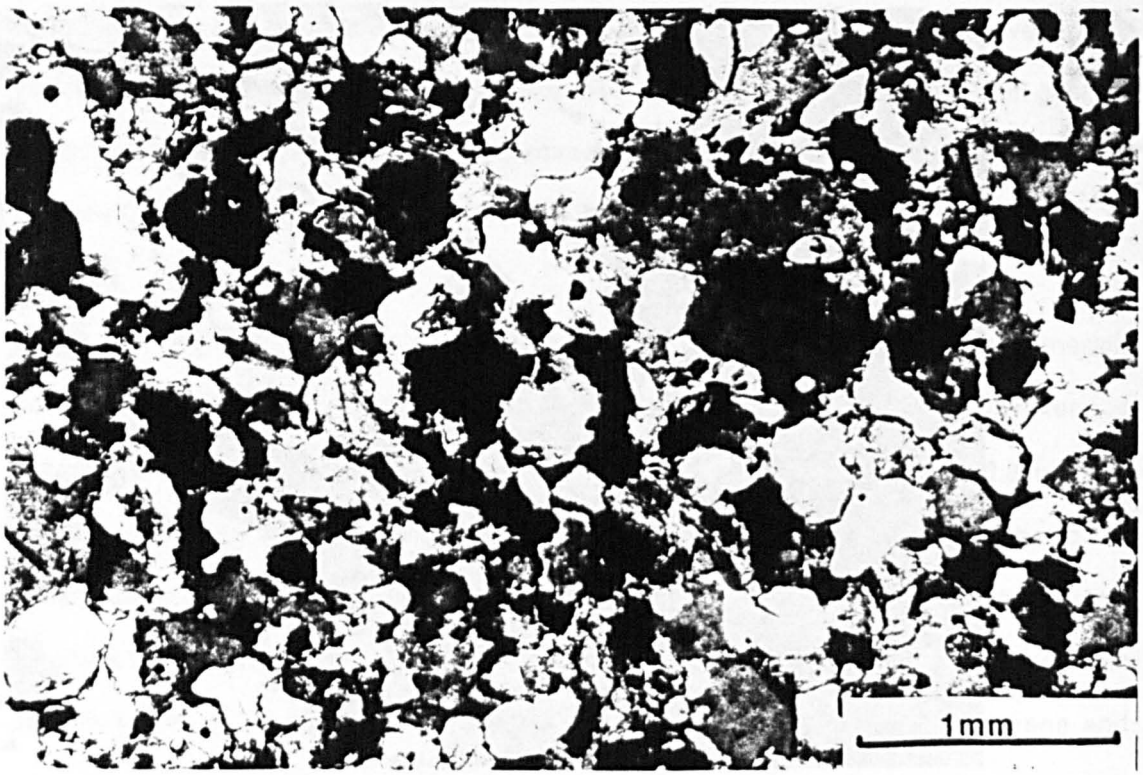

Plate 3.16 Photo-micrograph of an ultramylonitic margin to a T.S. gabbro pluton in the vicinity of a major east - west shear zone. The rock is completely recrystallised reflecting extreme, ductile deformation.

Sample 13-CY83 is from a contact with tectonised harzburgite, 230m south of an E-W trending serpentinite shear zone [091524]. Plate 3.16 illustrates a very fine grained, equigranular, recrystallised texture in which clinopyroxene (36%), orthopyroxene (26%) and plagioclase (38%), petrographically determined as An_{56}, form hypidiomorphic-rounded grains with characteristic 120° triple junctions, indicating textural equilibrium.

3.3.4 Gabbroic Autoliths

Near the roofs of some gabbronorite bodies, abundant, fine grained gabbroic xenoliths occur, interpreted as chilled margins later incorporated within their parent intrusions as autoliths. These inclusions are generally angular, 0.2 to 0.5m across, have distinct margins and do not show any evidence of assimilation. In contrast to their only moderately strained hosts, they are commonly strongly deformed, exhibit protocataclastic textures and hence are evidence of syntectonic magmatism. Although the autoliths appear more mafic, their modal composition of $Opx_{28}Cpx_{22}Plag_{50}$ is only slightly more than their gabbroic hosts. Microscopic examination of the autoliths reveals a fine grained protocataclastic texture. Clinopyroxene and orthopyroxene porphyroclasts (0.5 to 3mm) are ragged, have orthocumulate overgrowth textures and are supported within a fine grained protocataclastic groundmass. Orthopyroxene grains are occasionally seen with (100) exsolution blebs and reaction rims of clinopyroxene. The groundmass that forms 20% of the mode is hypidiomorphic, equigranular and consists of granulated and disaggregated clinopyroxene, orthopyroxene and plagioclase.

3.3.5 Aplite Apophyses

Associated with the roof apophyses of the main gabbroic plutons are outcrops of leucogabbroic aplite or beerbachite. These leucocratic intrusions back-vein the main gabbroic bodies and have irregular contacts with the overlying and surrounding country rock. They are medium grained, have a sugary texture and are devoid of marginal chilling. On weathering,

they form prominent cream coloured outcrops that are readily identifiable when in contrast with the ultramafic host. Occasionally aplite dykes are observed forming sheets penetrating over 100m above the main aplite outcrops. It is evident from their intrusive relationships that the aplites are a late stage in the intrusion of gabbro-diorite complexes. As such they also post-date much of the tectonism accompanying pluton emplacement. In thin section the aplite is medium - fine grained (0.5 to 1mm) with equigranular plagioclase An_{45} (72%), clinopyroxene (20%) and interstitial, allotriomorphic quartz (5%). Alteration is pervasive with about 60% of the clinopyroxene having been altered to epidote and actinolite, and 80% of the plagioclase saussuritised. The extent of the alteration, compared with the only moderate uralatisation of the main gabbroic outcrop, suggests that extensive, late hydrothermal fluids were channelled along the aplite margins resulting in autometasomatism.

3.3.6 Diorite-Trondhjemite Bodies

Commonly located in the roofs, and above the main outcrops of the gabbroic plutons, diorite and trondhjemite occur as isolated bodies up to 200m across. On weathering, the diorites form pale grey exposures whereas the trondhjemites are characteristically cream coloured. Due to their susceptibility to low grade alteration, these feldspathic intrusions are rarely fresh and form rounded exposures with friable surfaces that make sampling difficult. These leucocratic intrusions are medium to coarse grained and invade the country rock as veins, dykes and bosses that are occasionally observed intruding the main gabbroic plutons. Their spatial and temporal relationship to the main gabbroic complexes suggest the diorite-trondhjemite bodies are late stage fractionates formed by extreme magmatic differentiation of the earlier T.S. gabbroic intrusions. As such, they are similar in origin to the trondhjemites of the Troodos Massif, interpreted by Wilson (1959), Greenbaum (1972) and Allen (1975) as late fractionates of high level magma cells. In the WLFC the diorite-trondhjemites form an evolutionary suite characterised by an increasing modal abundance of quartz and feldspar and decreasing amounts of ferromagnesian phases.

Sample 49A-CY84 [54650595] is typical of the majority of this group, being a medium to coarse grained hypidiomorphic quartz diorite with a modal composition of $Plag_{60}$ Qtz_{20-25} Cpx_{12-20} Act_{5-10} Mgn_{0-3}, in which equigranular (3-10 mm) plagioclase grains (An_{38-50}) are often strained, fractured and saussuritised. Quartz is present as anhedral and subhedral grains (0.2 to 0.8 mm) and forms radial myrmekite aggregates with sodic-plagioclase (Plate 3.17). Ascicular clinopyroxene grains, altered to and overgrown by tremolite and pale green actinolite, are characteristic, and are up to 15mm long with length to breadth ratios around 15:1. In the more mafic diorites, magnetite forms skeletal, cruciform grains up to 2mm across, indicating rapid crystallization. The texture of both the ascicular clinopyroxene and skeletal magnetite, together with primary amphibole, suggests crystallization from a hydrous-melt. A high fluid content would enhance rapid ion diffusion and hence pyroxene and amphibole c-axis growth (Putnis and McConnell, 1980). An increase in PH_20 and fO_2, would also enhance rapid magnetite crystallization.

The most evolved, silicic variety, sample 304-CY83 [06425503], is a trondjhemite that intrudes harzburgite of the Mantle Sequence and has 62% modal quartz. The rock is medium grained, with an allotriomorphic-granular texture (Plate 3.18). Quartz forms (0.8 to 1.6mm) equidimensional grains and 8mm diameter radiating, myrmekitic patches. Sodic plagioclase constitutes 36% of the rock the majority forming subhedral, equidimensional grains. The trondjhemite are almost devoid of ferromagnesian phases with only actinolite (less than 1% of the mode) forming pale green, ascicular and anhedral grains; magnetite is absent.

Plate 3.17 Photo-micrograph of diorite occuring near the roof of a T.S. gabbro pluton. The rock is characterised by the presence of myrmekite patches and acicular clinopyroxene grains that are overgrown by actinolite.

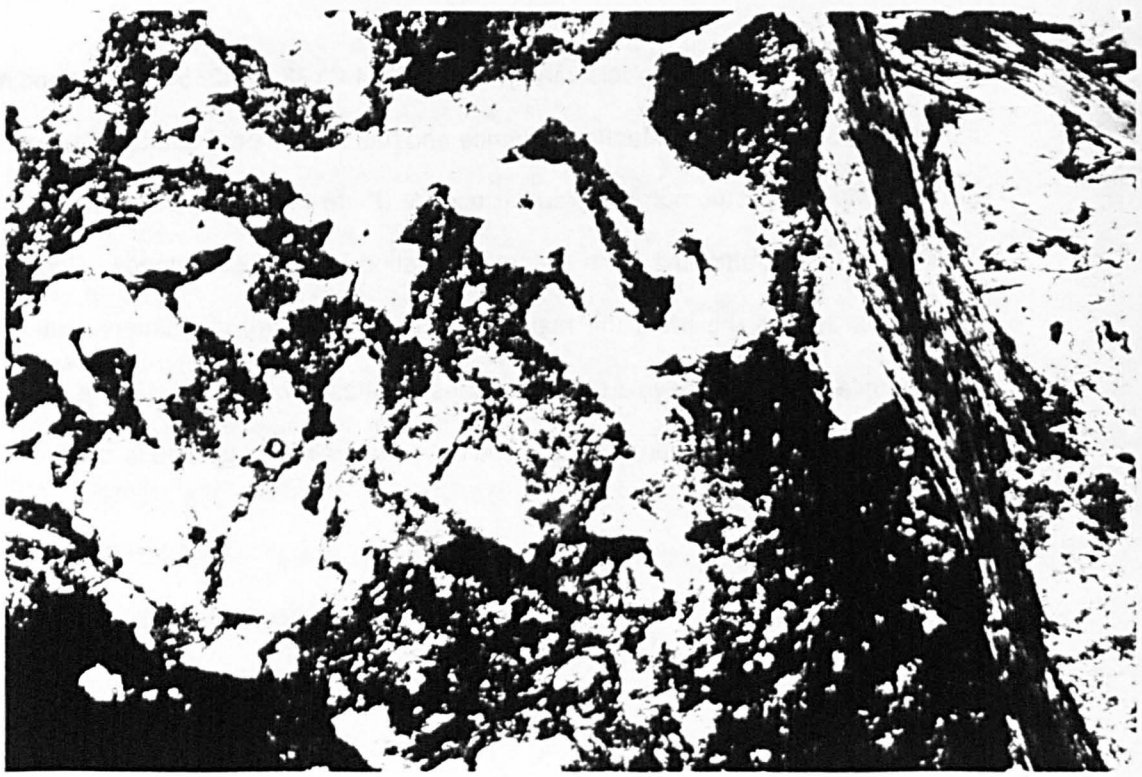

Plate 3.18 Photo-micrograph of trondhjemite. The rock is coarse grained and consists mainly of equigranular quartz and plagioclase. Both this and Plate 3.17 have an 8mm field of view.

3.3.7 Type Section

All the features described above, with the exception of the diorite - trondhjemite bodies are exposed in a stream section that flows eastwards into the Kyprissa gorge from above the Dhierona to Yermasoyia road (Figure 3.3). In this section, a 2km long NE-SW elongate gabbroic intrusion, emplaced into the Mantle Sequence, has chilled, cataclastic margins, dykes and aplite apophyses.

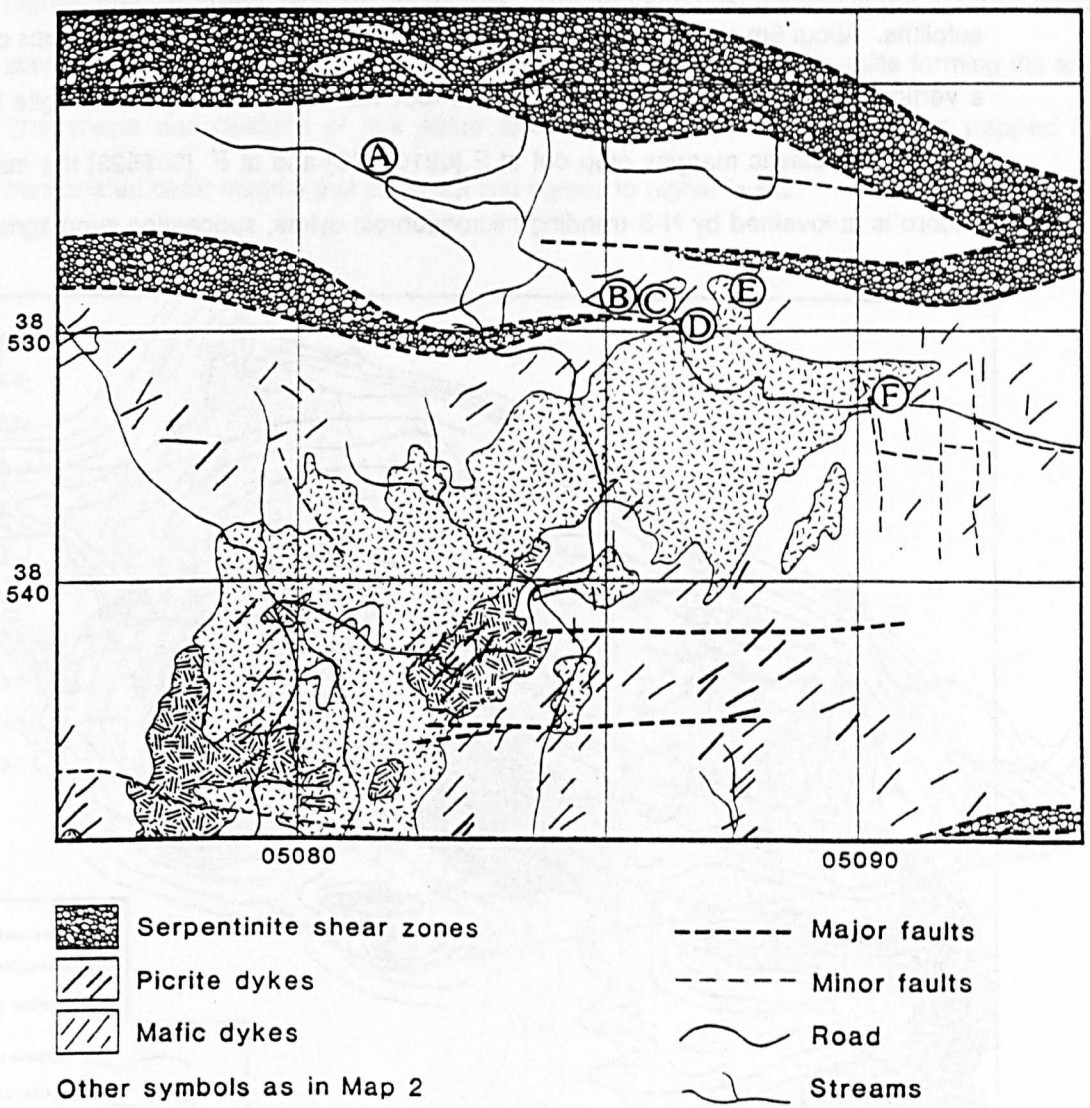

Figure 3.3 Enclosure of type locality for T.S. plutonic rocks, showing the position of detailed localities A to F that are discussed in the text.

Starting at A, Figure 3.3 [081528] ; the host harzburgite becomes increasingly cut by 5 to 50mm wide veins of serpentinite and epidosite. At a point 300m west of the main gabbro outcrop, the veins become anastomosing and composite with pegmatite gabbro cores. Occasionally dense stockworks of pegmatite anastomose and brecciate harzburgite. At B (Figure 3.3) [085526] the host ultramafic is brecciated and sheared by a major vertical E-W trending fault that has subsequently been invaded by a network of pegmatite veins. Microgabbroic apophyses first appear at C [08505255] and rapidly increase in abundance over 100m until at D [086525], the main body of gabbro crops out. The main gabbro is medium grained, isotropic and varitextured, containing pegmatite patches, fine grained flasers and autoliths. About 5m above locality D [08655265], an 80m long pod of aplite crops out, forming a vertical apophysis that forms part of the roof with the enclosing harzburgite host. Fine grained, cataclastic margins crop out at E [09105235] and at F [085523] the main body of gabbro is autoveined by N-S trending microgabbroic dykes, suggesting synmagmatic, E - W tension.

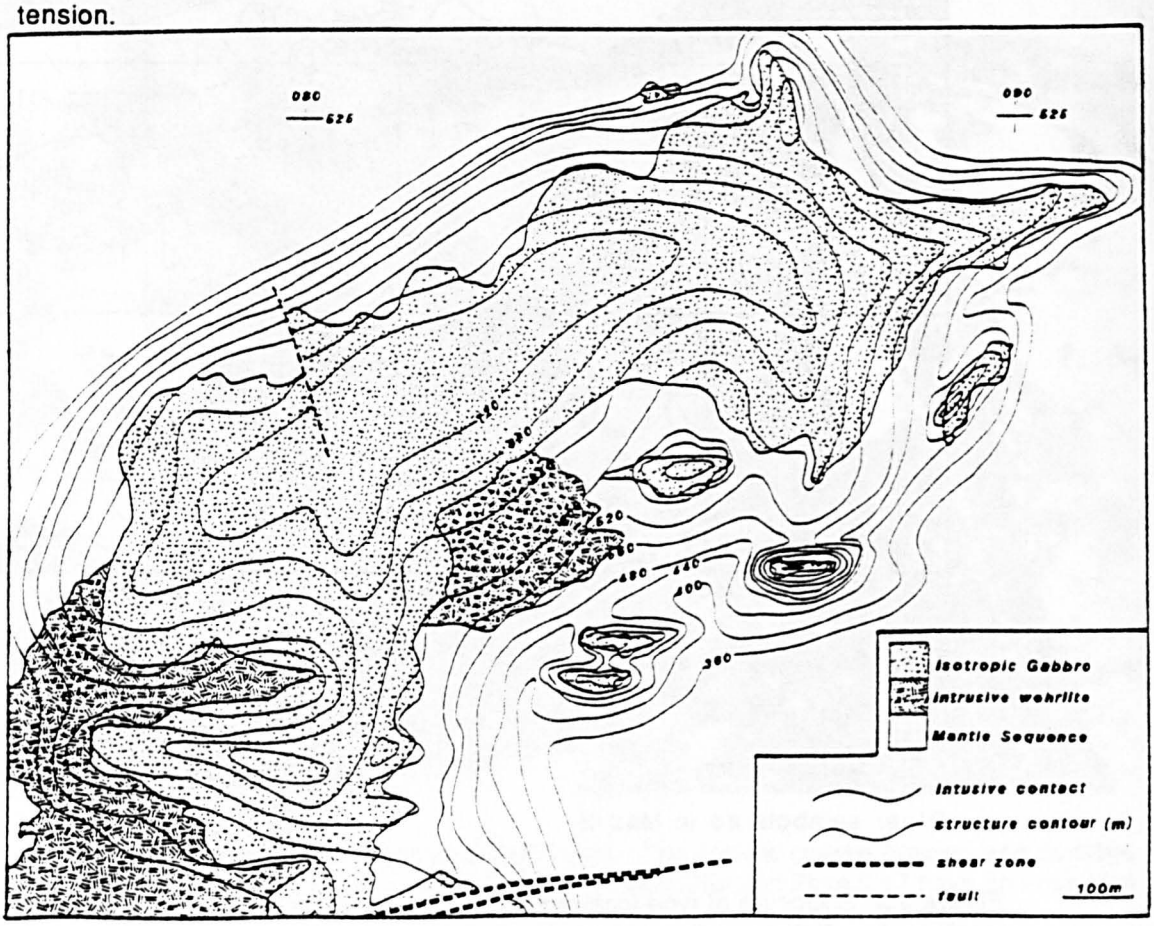

Figure 3.4 Structure contouring of T.S. gabbro pluton is constructed from the intersection of its margin with the steep topography of the area.

Structure contouring of the margin of the pluton, based on its outcrop and topography, (Figure 3.4) reveals the high level, roof relationship between it and the surrounding Mantle Sequence. The shape of the intrusion is irregular with a small lobe forming where the gabbro invades an E-W trending serpentinite shear zone. Trend surface analysis based on an isometric section projected obliquely from the southeastern corner of the pluton (Figure 3.4) illustrates a highly irregular surface topology to a boss which has prominent vertical apophyses and steep margins. Comparison between the structure contours and outcrop of the intrusion shows that country rock xenoliths and roof pendants are most abundant in the highest outcrop levels, near the pluton roof. The northernmost outcrop of the intrusive gabbro complex [086526] contains a 100m diameter, conical apophysis, with aplite forming the apex. The shape and position of this aplite apophysis suggests formation from trapped and fractionated basic magma that could not find egress to higher levels.

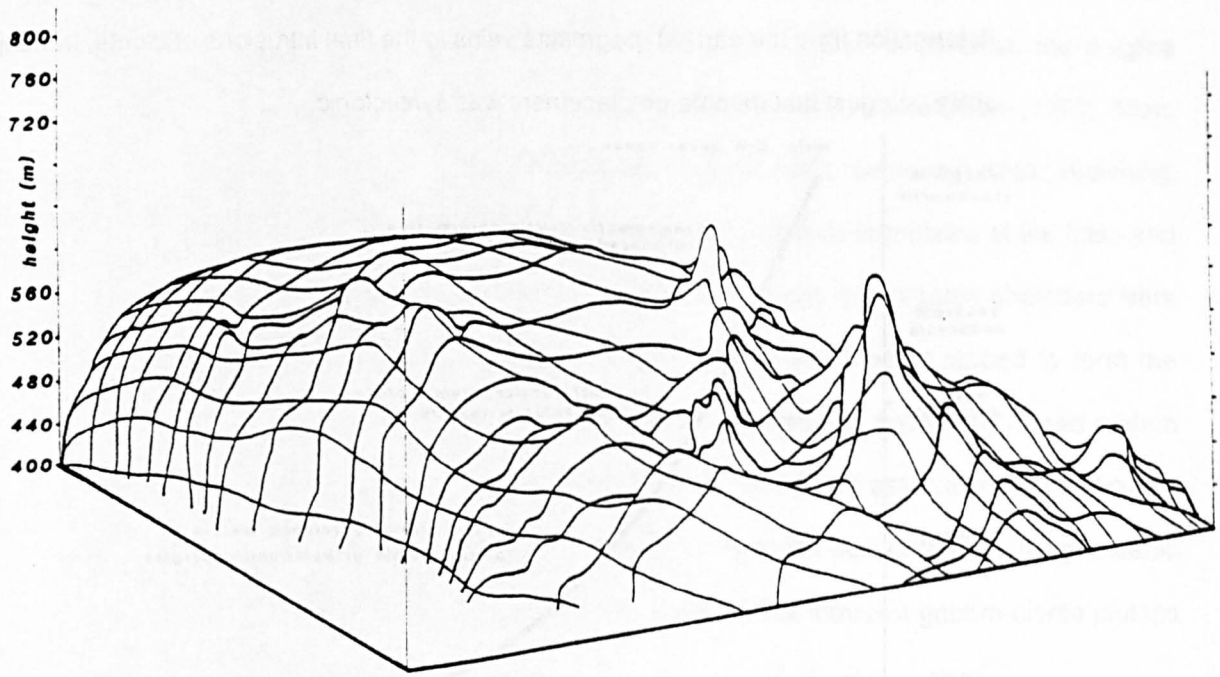

Figure 3.5 Trend surface analysis of the surface of the major T.S. gabbro (detailed in Figure 3.4), projected from its southsouthern corner and generated from NE - SW and NW - SE composite sections, clearly illustrates the pinicular shape of the gabbro apothyses and the steep sides of the main boss.

Harzburgite, exposed in the road section above the main gabbroic outcrop [082526], is extremely serpentinised and veined by fibrous white asbestos, probably chrysotile. Similar alteration of the harzburgite above other large intrusive gabbro-diorite complexes, suggests extensive hydrothermal circulation during magma emplacement and cooling. Identification of areas of altered harzburgite, veined by epidote, pegmatite, gabbro and chrysotile may indicate the position and the approximate size of major gabbroic intrusions up to 160m below the surface. On this circumstantial evidence, it is possible that there are many more gabbroic intrusions, as yet unexposed, emplaced into the Mantle Sequence beneath the floor of the WLFC.

3.3.8 Discussion and Interpretation

Figure 3.6 summarises the relationship between the intrusive history of the gabbro-diorite complexes and their tectonic evolution. The decreasing degree of penetrative deformation from the earliest pegmatite veins to the final intrusions of diorite, trondhjemite and aplite, suggest that magma emplacement was syntectonic.

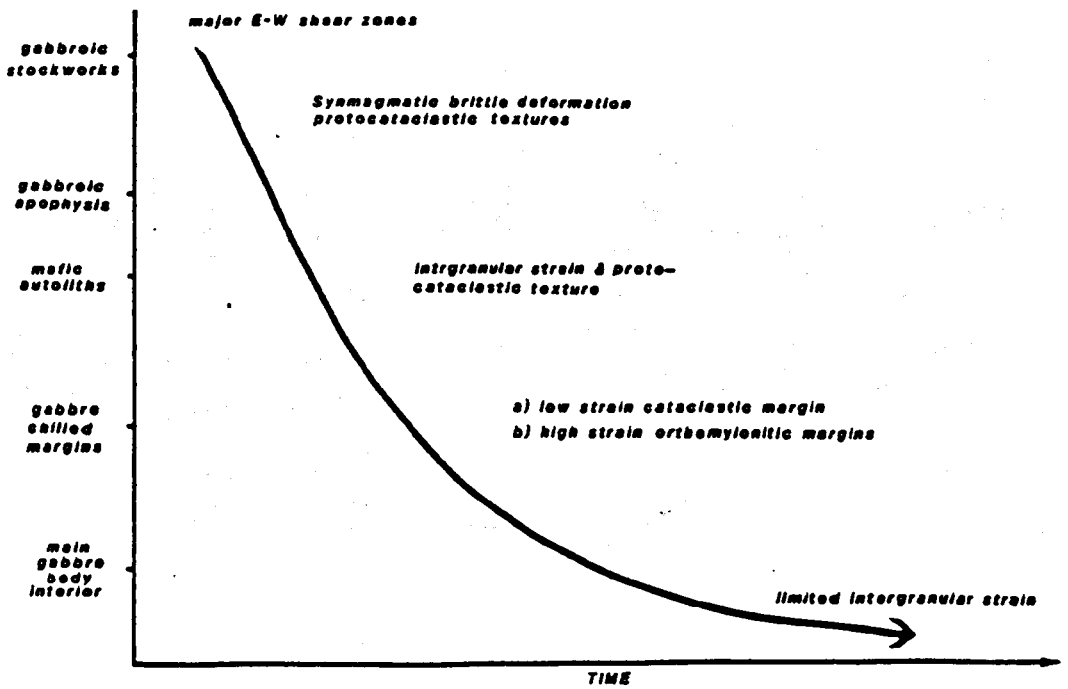

Figure 3.6 Schematic event diagram showing the various degrees of deformation suffered by the major T.S. gabbro (Figure 3.4) during its emplacement; eg. E - W shear zones localised early gabbro stockworks.

Protocataclastic pegmatites with clinopyroxene overgrowths of granulated orthopyroxene grains, and the inclusion of cataclastic autoliths in a relatively undeformed gabbroic host, are both conclusive evidence that magmatism was syntectonic. Post-consolidation deformation formed protocataclastic and ultramylonitic margins. This later deformation was probably the result of the continuation of faulting and shearing in the host country rock that may have localised the major gabbro intrusions. This is supported in Chapter 5 where the preferential NE-SW trend of elongated gabbro-diorite complexes is compared with prismatic tension gashes and interpreted as magma emplacement into major lithospheric fractures during active sinistral, transtensional transform deformation.

The steep topography of the WLFC has allowed structure contouring of pluton margins. Trend surface analysis reveals most of these intrusions to be steep-sided bosses. Although not cumulate, the gabbroic intrusions include a range of compositions from orthopyroxene-rich, mafic gabbronorite to trondhjemite that occur at all levels within each plutonic body and suggest closed system magma fractionation. In contrast, the magma systems that formed the Axis Sequence on Troodos (Wilson, 1959; Greenbaum ,1972; Allen, 1975) and the Semail Nappe, Oman (Pallister & Hopson, 1981; Smewing, 1981; Browning, 1984) have an ordered magmatic stratigraphy with cyclic, layered cumulates at the base and evolved, silicic lithologies at the top. These constructive ridge axis magma chambers were periodically replenished with batches of primitive magma while being tapped to form the sheeted dyke complex and volcanic carapace. However, although apparently closed system fractionates, the intrusive gabbro-diorite complexes in the WLFC are associated with and cut by multiple mafic dykes. These dykes and the basalts forming the bulk of the overlying volcanic suite are both petrologically and geochemically related to the intrusive gabbro-diorite plutons (see Section 6).

3.4 Post Gabbro-diorite Dyke Systems

Abundant mafic and picrite dykes cut the Mantle Sequence and are associated with and intrude some of the gabbro-diorite complexes. Three dyke sets have been identified and are described below:

i) an early E-W trending set of greenschist facies metabasites

ii) a later NE-SW trending set that includes picrites and plagioclase phyric varieties, and

iii) a final set of N-S trending, brownstone facies metabasites.

Increasing retrograde metamorphism from lower amphibolite facies to subzeolite facies affects the dyke sets from (i) to (iii) respectively. The structural significance of the dyke trends is discussed in Chapter 5. Finally, variations in composition and metamorphic grade with time are discussed in terms of derivation from small, localised magma chambers and emplacement during cooling and uplift of the WLFC.

3.4.1 Early E-W Trending Dykes

The earliest set of mafic dykes in the WLFC are 1 to 1.5m wide, near-vertical metabasites. Figure 3.7, a rose diagram in which the direction and frequency of dykes cutting the Mantle Sequence are plotted, illustrates two sets; (i) a conjugate dyke suite trending 080N and 110N and (ii) the main set trending 040N.

Although these dykes are especially abundant near the margins of the WLFC, where they cut Axis Sequence crustal units, and constitute only 18% of all theTransform Sequence mafic dykes. The 080 - 110N trending dykes often form localised swarms that are occasionally cut by later gabbros, dykes, faults and serpentinite shear zones. The dykes have 0.01 to 0.02m chilled margins and are generally aphyric, medium grained metadolerites with clinopyroxene (48%) and plagioclase (52%) An_{53} laths forming a hypidiomorphic - granular texture. Orthopyroxene, where present, forms 0.2 to 0.5mm grains, partially altered to chlorite. Metamorphism occurred under variable conditions between greenschist and lower amphibolite

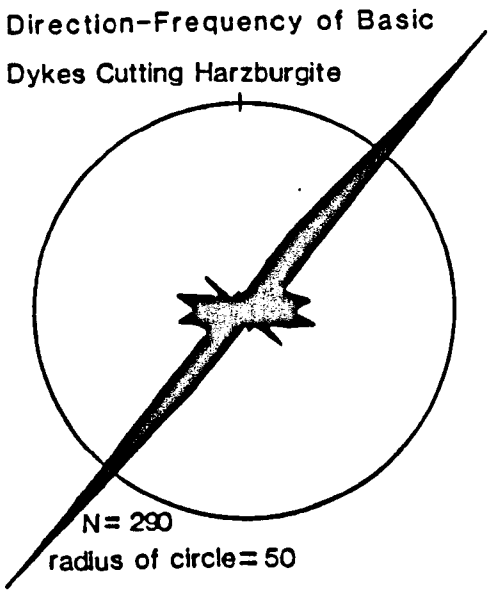

Figure 3.7 Rose diagram of direction of T.S. dykes that cut the Mantle Sequence. The major set trends 040 with a smaller conjugate set trending 080 and 110N.

facies (i.e. epidote-quartz assemblages). In the greenschist facies dolerites, clinopyroxene is occasionally pseudomorphed by green uralite, actinolite and epidote whereas plagioclase, although sometimes fresh, is often replaced by granular epidote. Dykes of this suite that cut the lowest structural levels (e.g. the Mantle Suite) have been metamorphosed to low amphibolite facies in which clinopyroxene is completely pseudomorphed by uralite actinolite, and plagioclase is altered to albite and, more rarely, epidote and quartz.

3.4.2 NE-SW Trending Dykes

The most abundant set of dykes are generally metabasites that trend NE-SW and include mafic and picrite varieties. They are most abundant near the centre of the WLFC where they cut the Mantle Sequence and T.S. intrusive peridotites and gabbros. In places [084512], especially in the vicinity of some major gabbroic intrusions, these dykes occur as dense swarms that form locally 'sheeted' or multiple composite units. These dykes trend between 030N and 046N, are subvertical and have chilled intrusive contacts. On the Dhierona- Yermasoyia road

[077499] fine grained, mafic dykes cutting serpentinised harzburgite bifurcate upwards (Plate 3.19), suggesting both magma emplacement from below and that $P_f = P_l$, ie. approximate parity between the intrusive pressure of the basaltic magma and the lithostatic overburden pressure respectively. Serpentinised harzburgite in contact with the dykes is fine grained and granular, suggesting dehydration to olivine from serpentinite and subsequent re-serpentinisation (Plate 3.20). Polygonisation of some dyke margins is evidence of large temperature gradients between the basalt and the host Mantle Sequence during dyke emplacement.

Plate 3.21 illustrates a slightly deformed, mafic dyke cutting the foliated matrix of an E-W trending serpentinite shear zone [085524]. Characteristically, these cross-cutting dykes are the lowest metamorphic grades of the NE-SW trending suite and are commonly vesicular. This NE-SW trending dyke set contains multiple picrite dykes that are largely synchronous with the mafic varieties, although a late set in the Venetou area [064506] post-dates major block faulting and the onset of uplift of the Mantle Sequence. The picrite dykes uniformly trend 040N, form dense swarms and are occasionally sheeted with strong marginal chilling (Plate 3.22). Flow alignment of olivine grains parallel to dyke margins is evidence of emplacement as phenocryst-rich melts. An outcrop of chilled picrite dykes [08255175] cutting intrusive wehrlite that was emplaced into tectonised harzburgite, identifies both the intrusive sequence and cooling history of the Mantle Sequence during Transform Sequence magmatism. Like the mafic dyke varieties, the picrites range in metamorphic grade from lower amphibolite facies (early ones) to lower greenschist facies (eg. the late, Venetou suite).

There are three distinct petrographic types of dyke in the NE-SW trending set; (i) olivine rich picrites, (ii) pyroxene phyric mafic dykes with Ol -> Ol + Cpx crystalline sequences, and (iii) plagioclase phyric varieties with Opx + Cpx + Plag but no olivine. The petrographic composition of the dykes is such that they could represent a single fractionation suite.

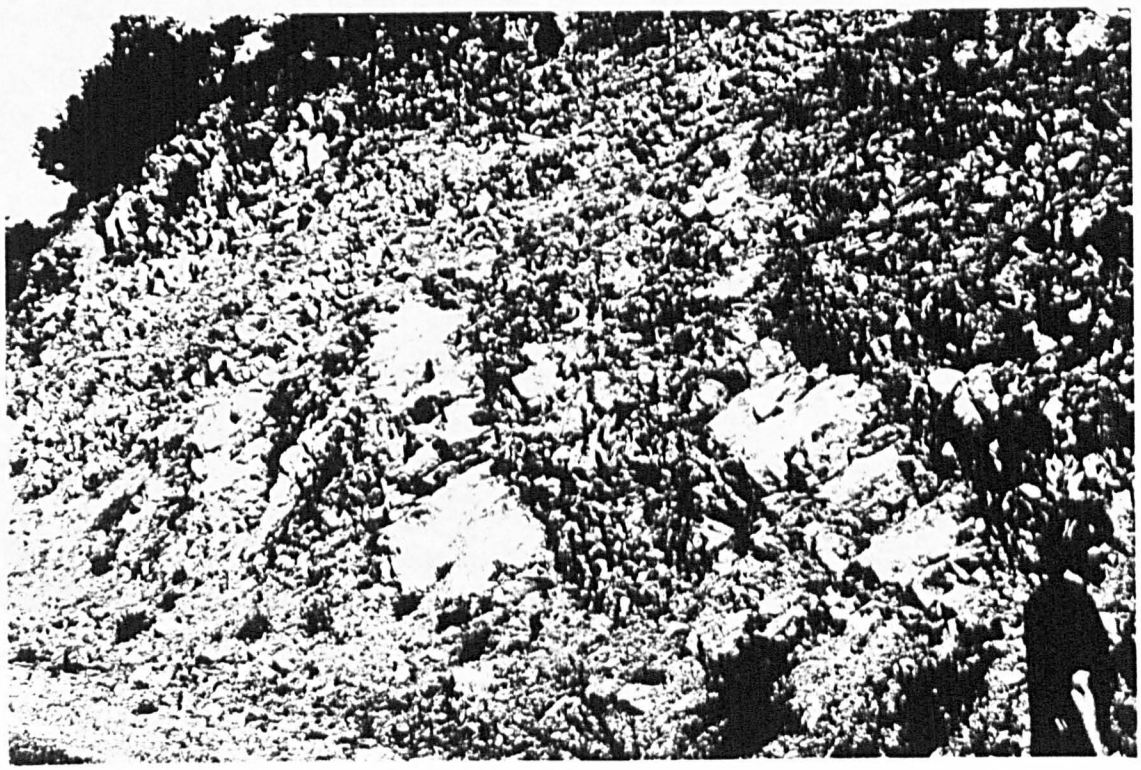

Plate 3.19 A swarm of mafic dykes cut the Mantle Sequence and bifurcate upwards. In places these dykes are seen as 'locally' sheeted' swarms.

Plate 3.20 Detail of margin of a mafic dyke in contact with serpentinised harzburgite. At the contact the serpentinite is fine grained and granular.

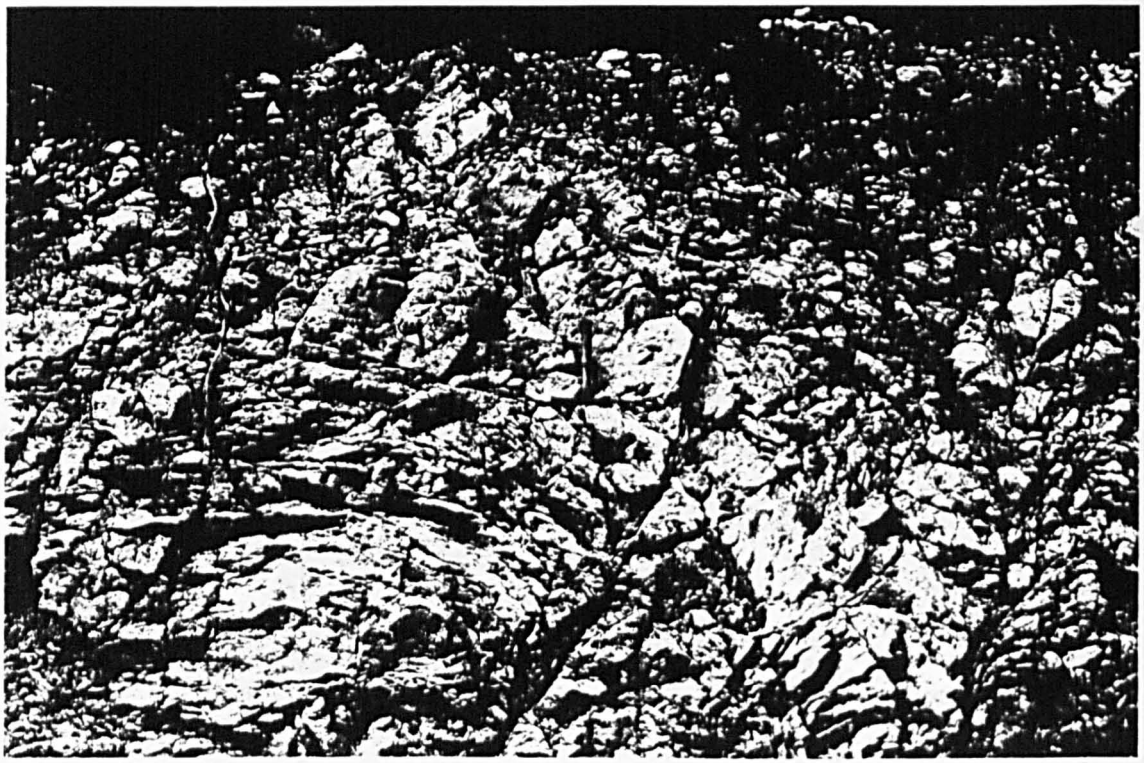

Plate 3.21 A slightly deformed mafic dyke cuts a serpentinite shear zone illustrating the close relationship between tectonism and T.S. magmatism.

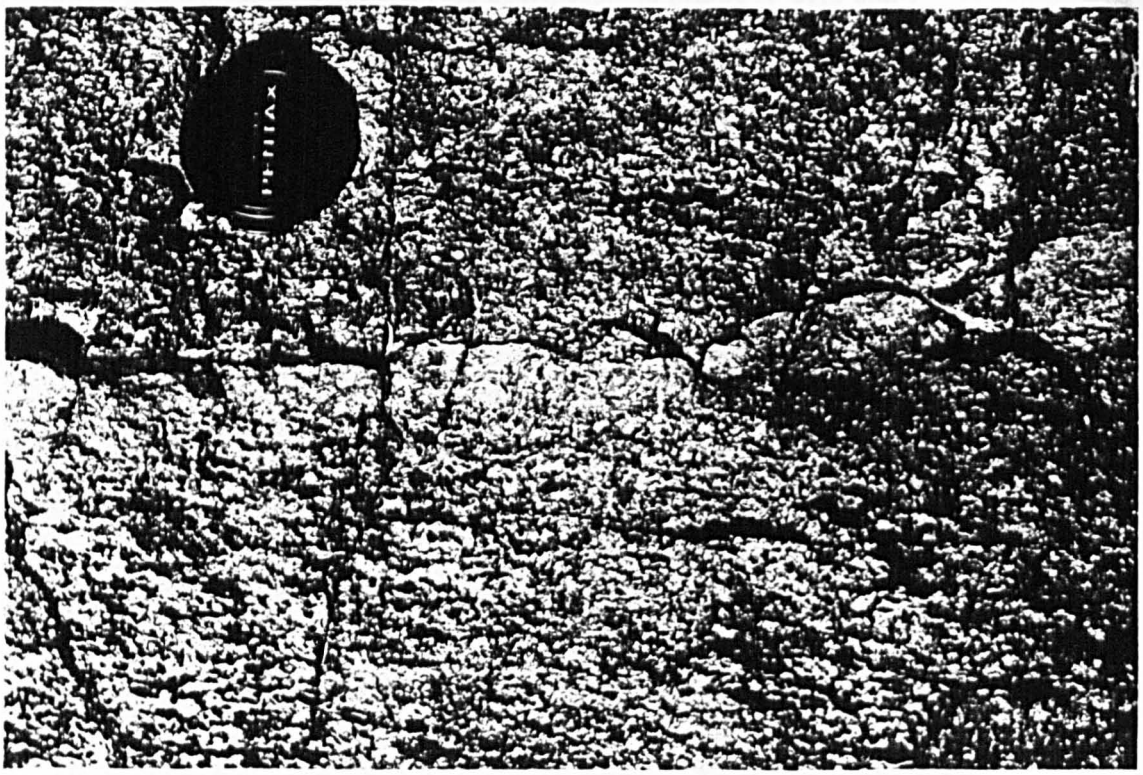

Plate 3.22 Detail of chill contacts between units of a composite picrite dyke that cuts the Mantle Sequence.

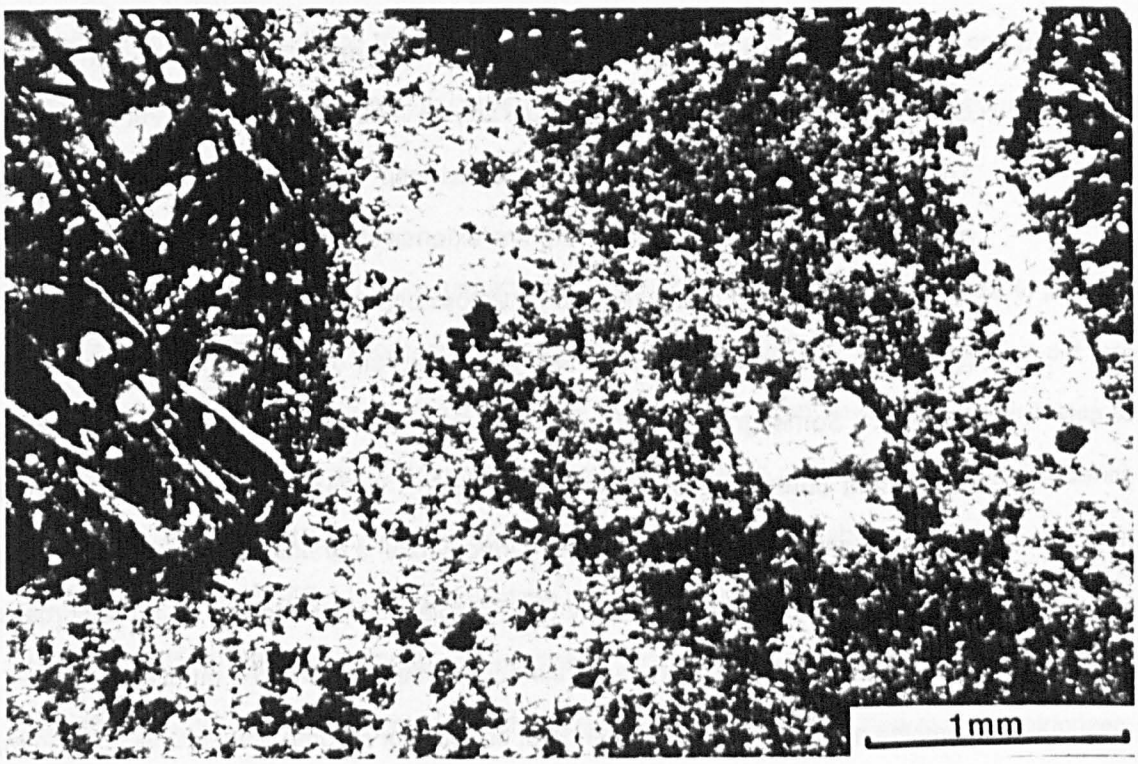

Plate 3.23 Photo-micrograph of a picrite dyke. Olivine phenocrysts are corroded, partially serpentinised and surrounded by a matrix of granular olivine, clinopyroxene and (rare) plagioclase.

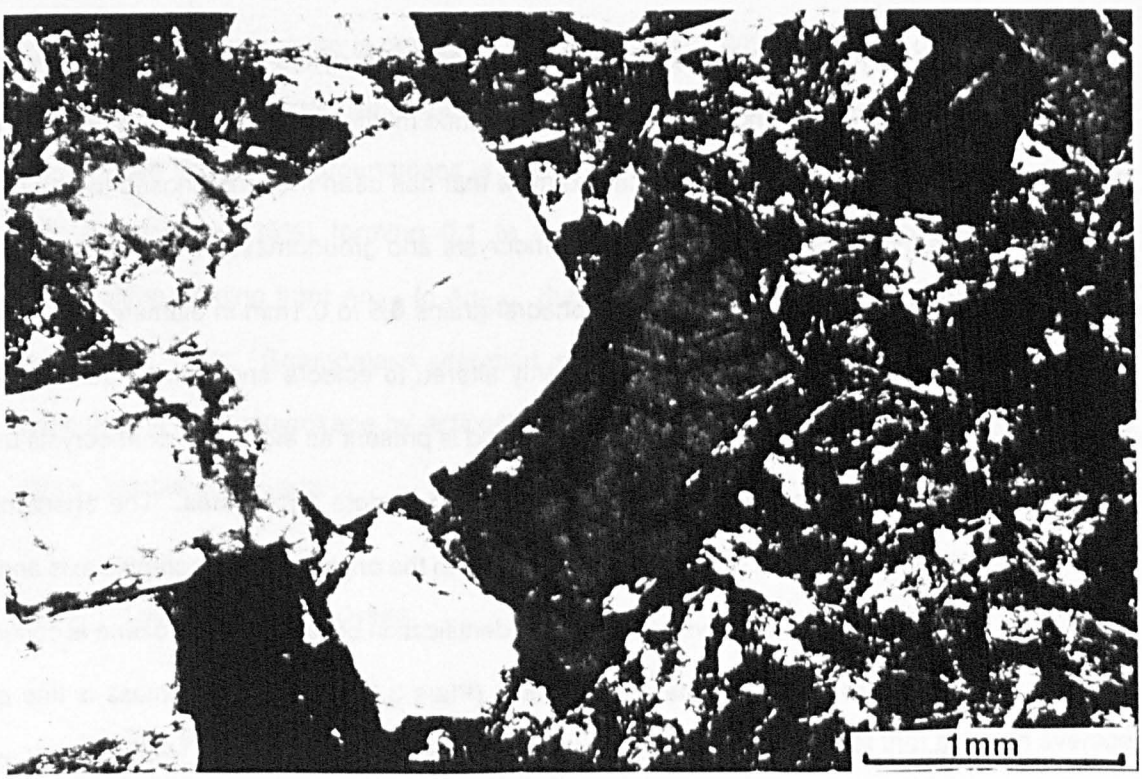

Plate 3.24 Photo-micrograph of metabasite dyke that cuts the Mantle Sequence and trends 040N. Clinopyroxene phenocrysts are fresh, but the groundmass is partially saussuritised.

(i) Plate 3.23 shows a typical picrite dyke metamorphosed to high greenschist facies. Olivine phenocrysts ($Fo_{89.1}$ - $Fo_{89.3}$), ranging in size from 0.3 to 2mm, form 46% of the mode. They are subhedral and slightly embayed with ghost crystal outlines formed by dusty magnetite. The olivine phenocrysts are extensively altered with serpentine filled cracks and blades of pale green actinolite growing across crystal boundaries. Clinopyroxene phenocrysts (En_{90} Di_{46}) form 5% of the mode, are euhedral, 0.2 to 2.8mm in diameter and are often twinned. Some grains form small clusters whereas others are intergrown with olivine suggesting cotectic crystallisation. Alteration is variable, with fibrous tremolite growing perpendicular to the (110) cleavage. Orthopyroxene grains are small (0.08 to 0.1 mm), form 1 to 2% of the mode and are largely (70%) replaced by tremolite. The groundmass is very fine grained and granular with relict clinopyroxene and olivine, otherwise altered to epidote, tremolite and quartz. The presence of euhedra of chrome spinel (0.08 to 0.4 mm) both within relict olivine grains and in the groundmass emphasises the primitive composition of the picrite melt.

(ii) The majority of NE-SW trending, mafic dykes contain olivine, orthopyroxene and clinopyroxene phenocrysts set in a fine grained matrix that is devoid of plagioclase (Plate 3.24). Sample 186D-C783 is a typical example that has been metamorphosed to greenschist facies. Clinopyroxene, present as both phenocrysts and groundmass, is the most abundant phase, and forms 45% of the rock as subhedral grains 0.5 to 0.1mm in diameter. Saussuritisation is common with many phenocrysts partly altered to epidote and fibrous, pale green actinolite. Orthopyroxene forms 12% of the mode and is present as elongated phenocrysts 0.8 to 1.8mm long that are pseudomorphed by chlorite and epidote aggregates. The orientation of these secondary minerals is approximately parallel to the original crystallographic axis and mimics the original orthorhombic crystal structure. Identification of relict orthopyroxene is confirmed by the presence of clinopyroxene reaction rims (Plate 3.25). The groundmass is fine grained and granular with serpentinite pseudomorphs, probably after olivine, forming 43% of the rock. Clinopyroxene is also present as granular grains, partly altered to epidote. Although

186D-C783 is a dyke cutting the mantle sequence, its low metamorphic grade combined with zeolite filled vesicles, 1 to 1.5mm in diameter, suggest emplacement into a cool country rock at shallow structural levels.

(iii) Apart from the diorite and aplite dykes that can be traced directly back to parental gabbroic apophyses, the most evolved members of the NE-SW trending dyke set are clinopyroxene and plagioclase phyric varieties. They range from lower amphibole facies to lower greenschist facies, are medium grained, strongly chilled and cut the Mantle Sequence and lower members of the Axis Sequence. They are especially abundant in the southern central part of the WLFC. Fresh plagioclase phenocrysts range in composition from An_{40} to An_{52}, are 0.8 to 11mm in diameter, euhedral and form 5 to 11% of the mode. With increasing metamorphic grade, the plagioclase phenocrysts range from fresh to pervasively epidotised. Clinopyroxene (augite) phenocrysts form 15 to 20% of the mode, are commonly euhedral and range in size from 2 to 8 mm. Orthopyroxene phenocrysts are characteristically elongate, subhedral and up to 1mm long. Some grains are skeletal, indicating rapid crystallisation. Alteration of orthopyroxene is pervasive and approaches 100%, with laths of epidote, chlorite and actinolite growing parallel to the host c-axes. Where clinopyroxene reaction rims occur, they remain fresh. The groundmass is commonly medium grained, hypidiomorphic-granular with plagioclase (35%) forming 0.1 to 0.5mm laths, and petrographically determined composition ranging from An_{42} to An_{53}. Subhedral to anhedral clinopyroxene forms up to 34% of the mode. Groundmass alteration is pervasive at higher metamorphic grades with replacement of clinopyroxene by actinolite and epidote, and plagioclase by albite, and more rarely, epidote and quartz.

3.4.3 Late Brownstone Dykes

The youngest dykes in the WLFC are a sinuous, bifurcating set that have an average N-S trend and cut all levels of the Axes and Transform Sequences, including high level gabbros, trondhjemites, sheeted dykes and the lowest levels of the volcanic sequence.

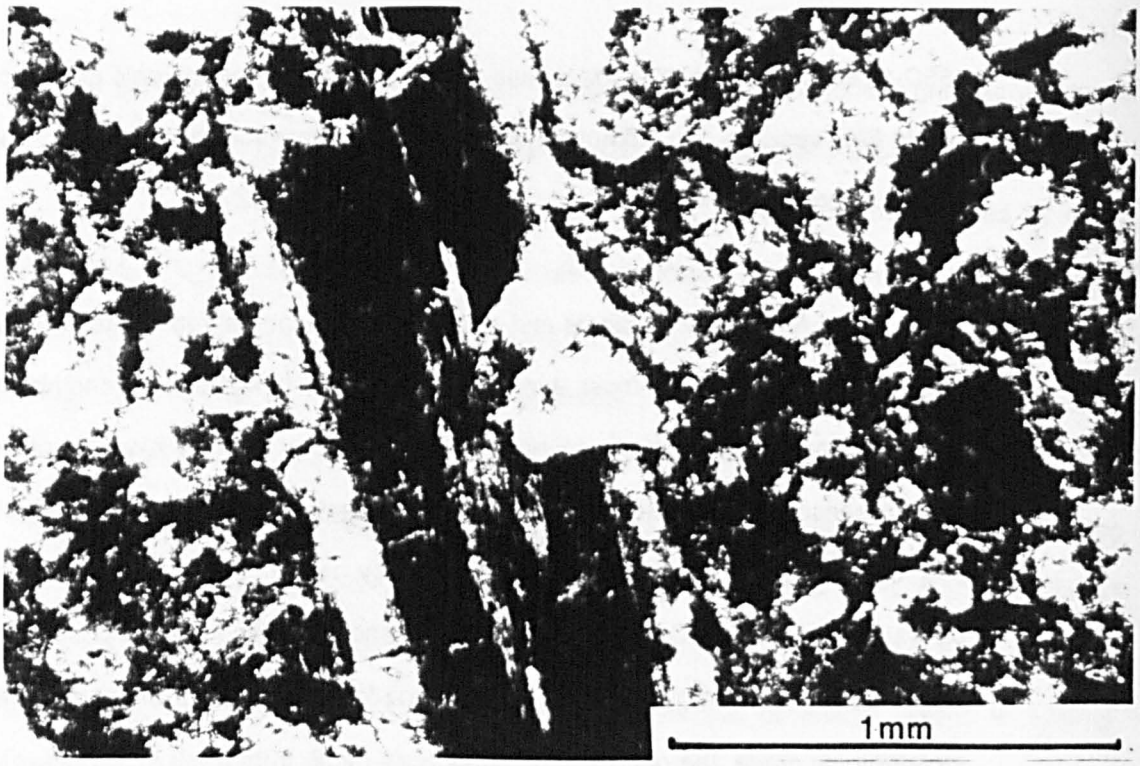

Plate 3.25 Orthopyroxene phenocryst in a meta-basite dyke that cuts the Mantle Sequence. Although the orthopyroxene grain is pseudomorphed by aggregates of chlorite and epidote, it is identified by the presence of clinopyroxene rims.

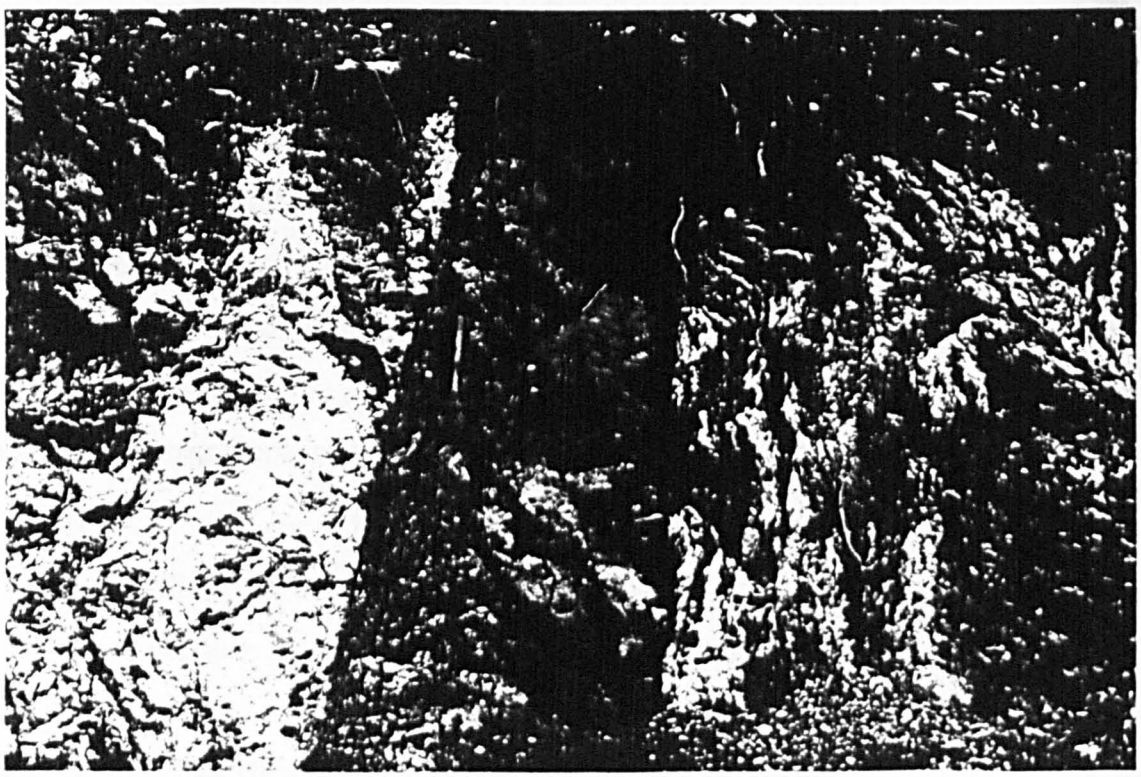

Plate 3.26 Brownstone dyke cuts serpentinite shear zone, suggesting the country rock was at a low temperature when intruded by the dyke.

Pervasive propylitisation indicative of low grade, brownstone hydrothermal alteration is characteristic of the suite which, on weathering, are friable and brown in colour. Brownstone facies metamorphism (Cann, 1969) affects present day oceanic basalts of seismic layer 2A and has been found to within a depth of 1km below the seafloor (Cann, 1979; DeWitt and Stern, 1976; Haynes, 1974). In the WLFC, 'brownstone' sheets are sinuous and form irregular, branching dykes and sills and occasionly cut serpentinite shear zones (Plate 3.26).

The dykes are generally medium grained, doleritic, with both euhedral plagioclase and clinopyroxene phenocrysts 0.5 to 3mm in diameter, forming 15% and 8% of the mode respectively. The groundmass is medium grained, except where marginally chilled and contains granular clinopyroxene and laths of plagioclase forming a trachytic texture. Although pervasively altered to zeolite and clay minerals, some original igneous textures remain.

3.4.4 Interpretation

Early E-W trending T.S. dykes are aphyric, cut the Mantle Sequence and A.S. crustal units and are at high greenschist metamorphic facies. They are cut by a later dyke set that trend NE-SW and range in metamorphic grade from greenschist to high zeolite facies. This later dyke set contains a range in composition, from picrite, Ol + Opx + Cpx phyric to Cpx + Plag phyric varieties. Although from both their mineralogy and geochemistry (see Chapter 6) these dykes have a common fractionation trend, the various petrological groups mutually cross-cut one another. These cross-cutting relationships suggest the dykes were derived from several independantly evolving magma chambers. Such an interpretation agrees with the field evidence for several, isolated parental gabbro plutons, mostly emplaced in the Mantle Sequence. The last set of dykes to be emplaced in the WLFC are sinuous, brownstone sheets that cross-cut all previous intrusions. Although the three dyke sets were emplaced at a similar structural level, they show a progressive decrease in metamorphic grade with time. This retrograde history reflects cooling and possible uplift of the WLFC during magmatic activity in an oceanic setting.

3.5 Conclusions

The WLFC is dominated by ultramafic and mafic plutons and hypabyssal dykes that were emplaced into the tectonically disrupted Axis Sequence crustal units and uplifted Mantle Sequence, illustrated in Figure 3.8. As a result the lithospheric structure and magmatic complexity of the WLFC is in marked contrast to the comparatively ordered, layered structure of most coherent ophiolite complexes (eg. The Main Troodos Massif; Wilson, 1959; Greenbaum, 1972; Allen, 1975: The Semail Nappe, Oman; Pallister *et al.*, 1983; Browning, 1982; Lippard *et al.*, 1986: The Bay of Islands Complex; Malpas, 1978). The anomalous lithospheric structure of the WLFC is not compatable with its formation at a conventional constructive plate margin.

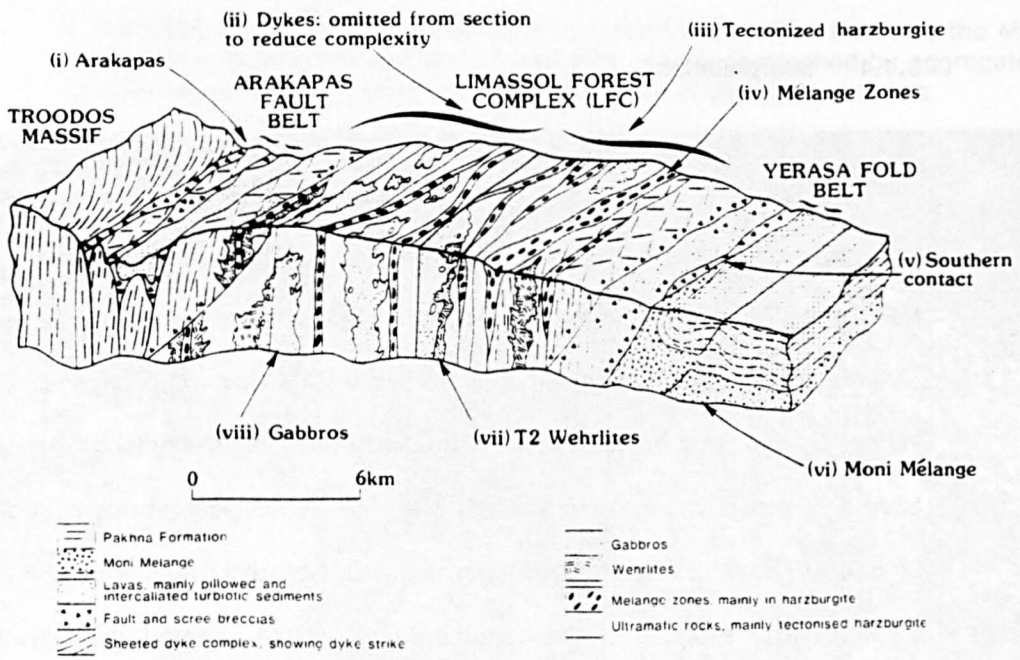

Figure 3.8 North - south block diagram showing the main petrographic and structural features of the WLFC. (i) Arakapas fault belt; an east - west trending zone of sheared sheeted dykes and lavas. (ii) T.S. mafic dykes cut all levels including the Mantle Sequence; main trend 040N. (iii) Tectonised harzburgite forms the main lithology of the Mantle Sequence and is host to most of the T.S. plutonic rocks. (iv) Serpentinite shear zones generally trend east - west. (v) Inverted unconformable contact with umbers and/or moni melange resting on basaltic pillow lavas. (vi) A sedimentary olistostrome of possible trench origin. (vii) Early phase of T.S. magmatism. (viii) T.S. gabbros emplaced after wehrlites but generally prior to mafic dyke intrusion.

The change from plutonic to hypabyssal intrusion, the increase in degree of marginal chilling and the retrograde metamorphic history of the T.S. magmas is evidence that the WLFC was cooling and being uplifted while in an oceanic setting. The synmagmatic disruption and uplift of the Axis and Mantle Sequences are the result of deformation and magmatic activity in the active domain of a leaky oceanic transform fault zone (Figure 3.9). The presence of both ultramafic and mafic plutons, emplaced at high structural levels, may explain the occurrence of similar lithologies within present day oceanic transform fault zones (Miyashiro *et al.*, 1970; Bonatti *et al.*, 1977; Fox *et al.*, 1980).

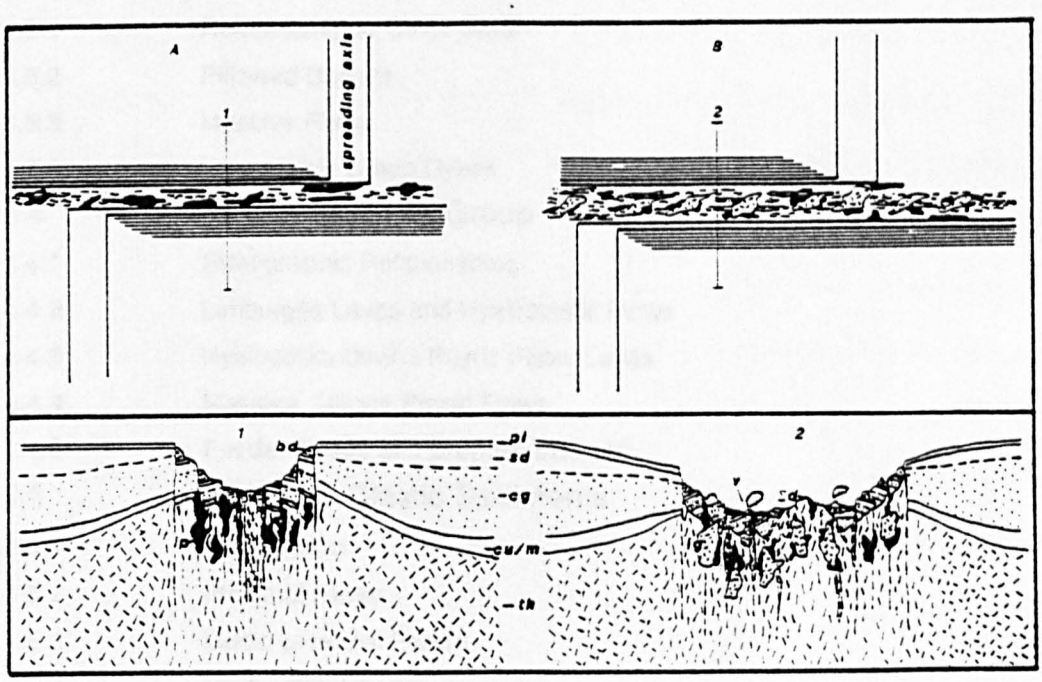

Figure 3.9 Schematic diagram showing a possible, leaky transform environment within which the WLFC T.S. plutons and dykes were emplaced. A. Early transform movement during which wehrlites were intruded at depth into the Mantle Sequence beneath an active transform segment. B. Later transform movement involving extension across the complex, causing tectonic thinning of the Axis Sequence crust and emplacement of gabros and dykes into the active transform domain. *bd = breccia deposits, pl = pillow lavas, sd = sheeted dykes, cg = cumulate gabbro, cu/m = cumulate ultramafics, th = tectonised harzburgite: ig = isotropic gabbro, ip = intrusive wehrlite, Σd = serpentinite diapir, v = volcano.*

CHAPTER 4

VOLCANOSEDIMENTARY SEQUENCE

List of Contents

4.1 Introduction

A sequence of lavas and intercalated sediments form an almost continuous outcrop along the southern and southwestern boundary of the WLFC with the overlying Cretaceous and Tertiary sediments. The lavas are predominantly pillow basalts, although massive flows also occur, intercalated with both coarse clastic and argillaceous sediments. This volcanosedimentary sequence forms a carapace, up to 1.5km thick to the WLFC The lavas are morphologically, petrographically and geochemically (see Section 6) most similar to the Upper Pillow Lavas of the Troodos massif (Smewing, 1975) and the boninitic basalts described by Simonian (1975), Simonian & Gass (1978) and Bechon (1982) from the Arakapas fault belt. Based on their metamorphic facies, abundance of intrusive dykes and the presence of vitreous flows the lavas have been divided into three suites, (i) the Basal Group, (ii) the Lower Lava Group and (iii) the Upper Lava Group. The clastic and argillaceous sediments found interbedded with the volcanics are similar to deposits identified by Simonian (1975) from the Arakapas fault belt, but which are generally absent from the rest of the Troodos massif.

Although the volcanosedimentary sequence crops out in the south of the WLFC, near Mathikaloni, it is both folded and faulted (Figure 4.1). The most complete development is found near and to the south of Kapillio (Figure 4.2) where the sequence has been stratigraphically logged, sampled and described in detail. Finally, in discussion, the volcanosedimentary sequence is compared to the Troodos Upper Pillow Lavas including the Arakapas fault belt lavas, and is described in terms of syntectonic eruption and micro-basin development .

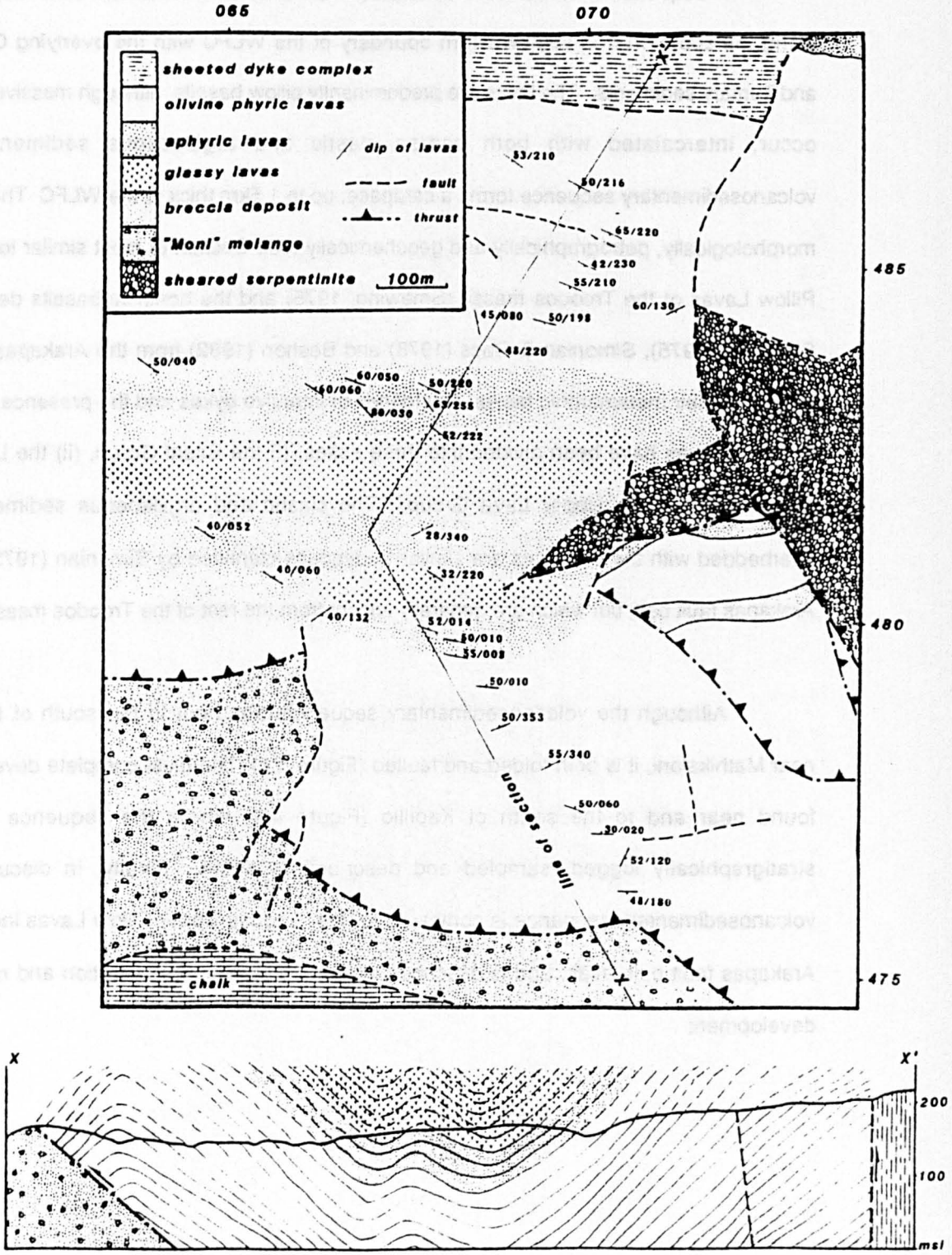

Figure 4.1 Map and cross section of the volcanosedimentary sequence in the Mathikaloni area showing the generally synclinal structure.

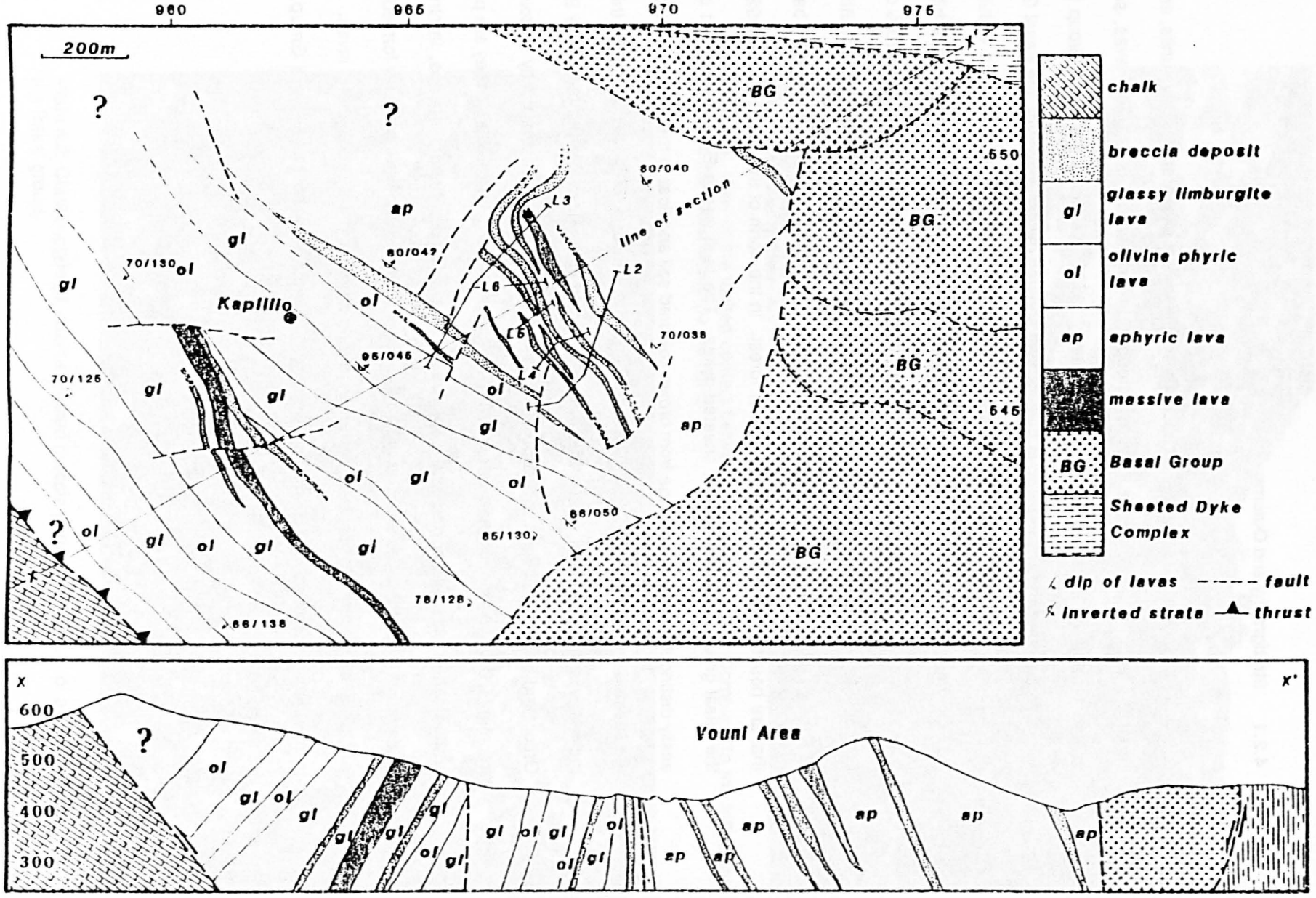

Figure 4.2 Map and cross section of the volcanosedimentary sequence in the Kapillio area showing the progressive unconformity between the Lower and Upper lava groups.

4.2 The Basal Group

4.2.1 Stratigraphy and Outcrop

Although termed the Basal Group, these, the lowest stratigraphical lava units, are not regarded as comparable to the transition group from sheeted dykes to pillow lavas, *sensu stricto*, termed the Basal Group on Troodos (Bear, 1958). Neither is the Basal Group in the WLFC found overlying any immediate basement of sheeted dykes. However, the Basal Group is the lowest structural unit of the volcanosedimentary sequence cropping out within the WLFC. It grades upwards into the overlying Lower Lava Group, the boundary being arbitrarily chosen as the limit above which anastomosing, cross cutting dykes form less than 20% of the outcrop. As such, the main area of the Basal Group crops out between 2 and 3.5km southwest of Kapillio, forming a relatively subdued topography of haematised, brown weathering basalts that are host to a moderately dense conifer forest. In the north of the outcrop area [992548] the basal group is faulted against sheeted dykes. The fault trends E-W, the contact being easily distinguished by the change from brown coloured soil and float to the pale grey colour of the sheeted dyke complex (Plate 4.1). Breccia deposits, although rare, are up to 100m thick in the Karavlis area [997550], where they are intercalated with units from the top of the Basal Group and overlying Lower Lava Group (Figure 4.3). These breccias are mostly of doleritic fragments, 0.5m to 1mm in diameter, derived from the sheeted dyke complex. They are poorly graded, often clast supported and occasionally intercalated with argillaceous, laminated mudstones (Plate 4.2). The breccias form a fan shaped outcrop and were probably formed as a fault talus, suggesting vertical fault movement during eruption of the Basal Group lavas. Both to the west and south, the Basal Group grades upwards into the Lower Lava Group, the transition being gradational.

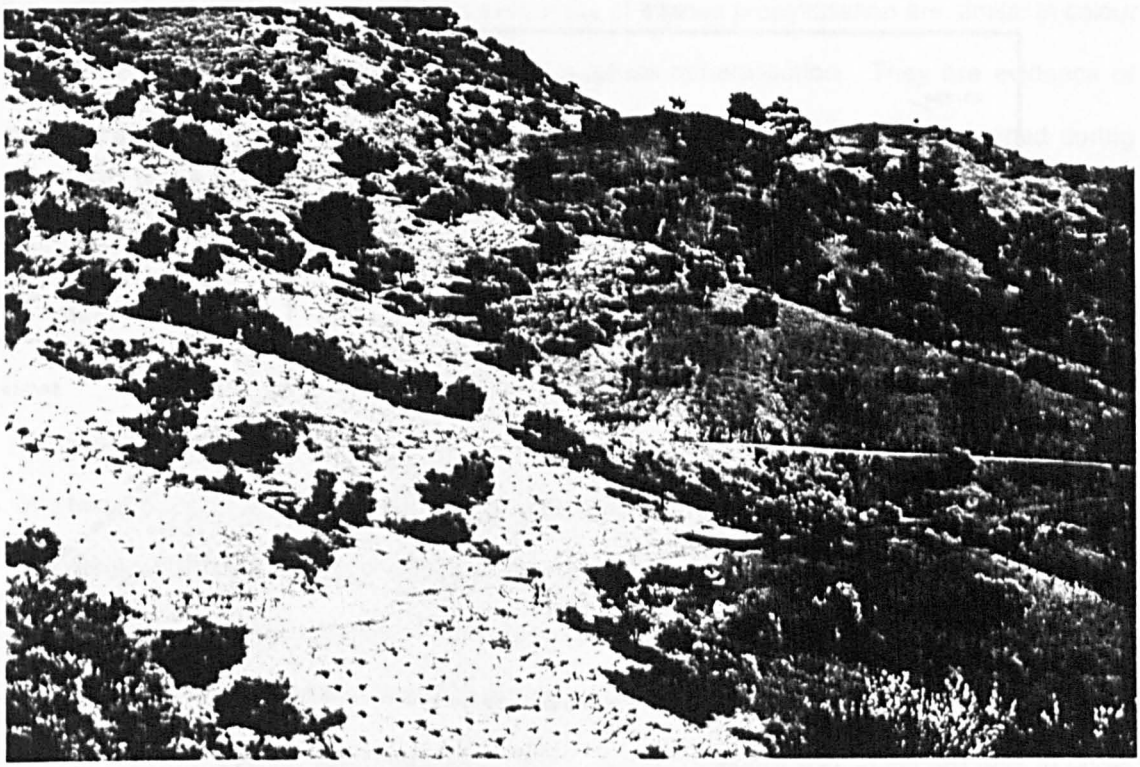

Plate 4.1 View of the faulted contact between the Sheeted Dyke Complex (to the left of the field) and the Basal Group (to the right).

Plate 4.2 Clast supported, coarse grained breccia deposit that is part of a fault talus deposit in the Basal group.

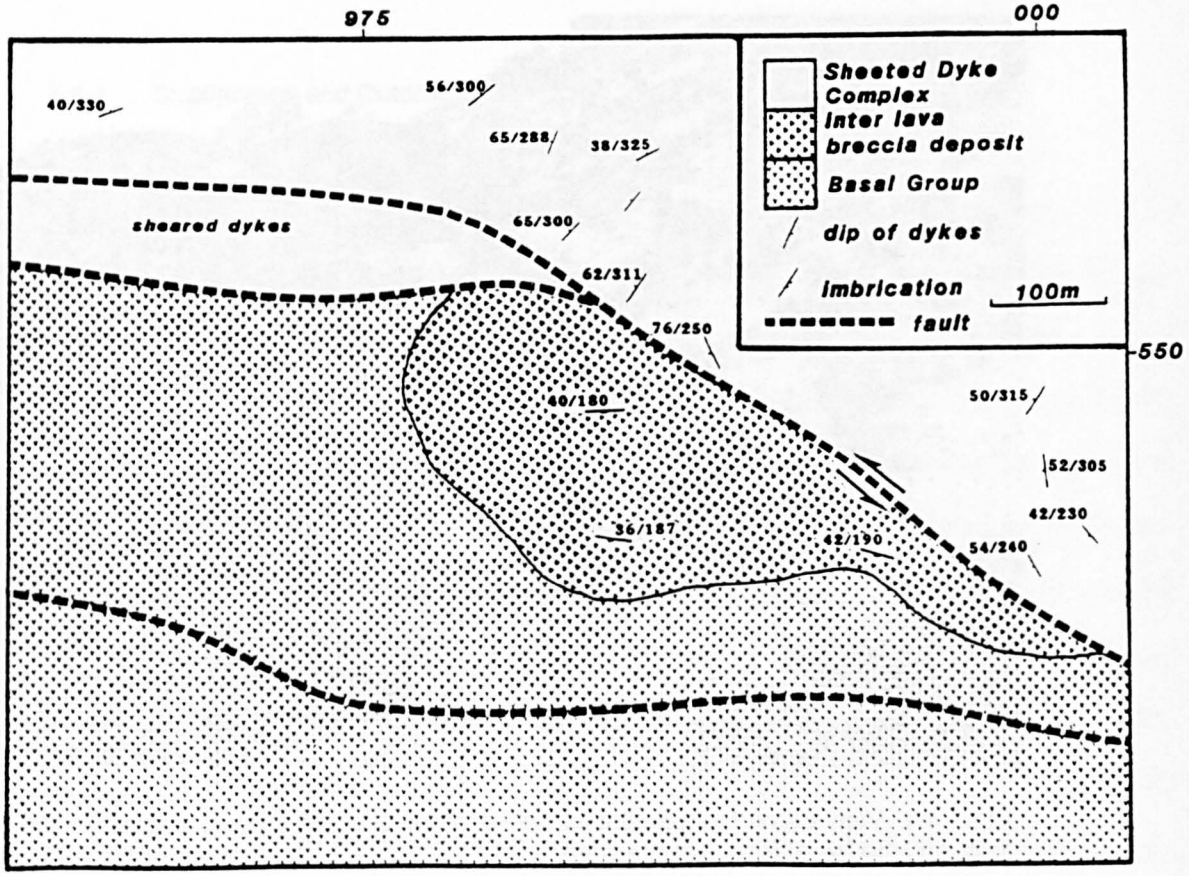

Figure 4.3 Outcrop map showing the position of a breccia deposit that forms a talus fan, intercalated within the Basal Group, with material derived from the Sheeted Dyke Complex to the north.

4.2.2 Basal Group Lavas

The general morphology of the Basal Group is one of disrupted, rounded pillow lavas, between 0.2 and 3m in diameter, cut by abundant aphyric and plagioclase micro-phyric dolerite dykes. The pillow lavas are medium grained, have fine grained, 10 to 20mm wide chilled margins, but no glassy selvedges. However, some margins are variolitic with 3 to 6mm diameter spherulites. The lavas are sparsely vesicular, with carbonate and zeolite amygdales, 1 to 5mm in diameter. Haematisation is characteristic with abundant veins of zeolite, calcite and occasionally, quartz cutting the lavas, especially where disrupted. Northwest of the Yerasa-Louveras road [00375352], brecciated basaltic fragments have rinds of hematite and limonite. Such alteration is especially abundant where faulting has tectonically brecciated the

Basal Group Lavas, or in the vicinity of small intrusive bosses, usually of gabbro [977551] or wehrlite [00255320]. These orange-brown areas of intense propylitisation are similar in colour to gossens, but are rarely associated with sulphide mineralisation. They are evidence of intense hydrothermal circulation (Cann, 1979) however, and were probably formed during sea-floor fracturing and magmatism, similar to fault zone hydro-thermal systems found on present day oceanic ridges (Williams *et al.*, 1979; CYMEX, 1979; Rona *et al.*, 1984).

The highly altered state of the Basal Group precluded any detailed petrology and prohibited primary geochemical analysis (see Section 5). The Basal Group Lavas are divided into two groups, (i) aphyric, and (ii) olivine micro-phyric. The former are the more abundant and are medium grained, granular and have an intersertal texture. Clinopyroxene is ubiquitously replaced by uralite and chlorite. Plagioclase, although turbid, has been both albitised and in places propylitized. Vesicles form 5% of the mode, are small (0.5 to 1mm) and are filled with fibrous zeolites, zoisite, carbonate and, rarely, quartz. Epidote was observed only in cross cutting veins from lavas cut by late intrusive bodies (see Section 4.2.4). The olivine micro-phyric lavas have similar compositions and textures, but contain microphenocrysts of olivine, now replaced throughout the rock by orange iddingsite. The olivine grains are up to 1mm in diameter, anhedral and occasionally skeletal. They are set in an altered ground mass of granular clinopyroxene and interstitial plagioclase, although the latter is less abundant than in the aphyric varieties. Apart from the presence of iddingsite, alteration is identical to the former aphyric lavas and is characteristic of zeolite facies or low greenschist facies metamorphism.

4.2.3 Basal Group Dykes

Intrusives into the Basal Group Lavas are abundant with swarms of doleritic dykes being by far the most plentiful. These brown weathering dykes vary between 0.5 to 1.5m wide, are sinuous and discontinuous. The most common trend is E-W, but 40N and 120N directions are also present. The density of dykes increases from abundant individuals occupying 20% of the outcrop to swarms and localised sheeted swarms forming up to 45% of the Basal Group.

Pillow lavas in the high density dyke swarm areas occur as disrupted and broken screen often with zeolite, carbonate and, more rarely, epidote veining. The disruption affecting the pillow lavas also affects the dykes, making both distinction between extrusive and intrusive members difficult as well as obscuring dyke trends and pillow lava orientations. By analogy with the Troodos Basal Group (Bear, 1959; Wilson, 1959) the proportion of dykes varies directly with the depth of exposure within the Group. However, nowhere in the WLFC do dykes exceed 50% of the outcrop. The nearest exposure of the Troodos Basal Group crops out just south of Kalakhorio on the Agros-Yerasa road, where they are associated with the Arakapas fault belt basement (Bear, 1960; Simonian, 1975).

Although altered and propylitised, the doleritic dykes preserve a felted, holocrystalline igneous texture. The dykes are generally aphyric, although a number of olivine and plagioclase subphyric varieties were observed. The olivine micro-phyric dykes contain 0.5 to 1mm, euhedral microphenocrysts of olivine in a granular olivine and clinopyroxene bearing, medium grained groundmass. Occasionally, plagioclase occurs as 0.5 to 1.5mm microphenocrysts in an intersertal and pilotaxitic groundmass of plagioclase and clinopyroxene blades. Alteration of the dykes is pervasive with uralitisation of most clinopyroxene grains, albitisation of plagioclase, that has later been altered to clays, and replacement of olivine by iddingsite. Vesicles, although rare and less than 1mm in diameter are ubiquitously filled with zeolite, zoisite and occasionally carbonate. All the dykes are at moderate to high zeolite metamorphic grades.

4.2.4 Late, High Level Plutons

Small intrusive bosses of microgabbro, although rare, are also observed cutting and locally altering the Basal Group. Figure 4.4 illustrates an isolated gabbroic boss [99995351], elongated E-W, 100m long by 60m wide, that intrudes disrupted Basal Group lavas and dykes causing quartz epidosite and carbonate veining in the immediate vicinity. The microgabbroic outcrop is in the centre of a 300m wide, 2.5km long, E-W striking zone of brecciation and intense propylisation and haematisation. The alteration zone is extensive compared to the

relatively trivial size of the gabbro outcrop, and is probably of tectonic origin. Both propylisation and gabbro emplacement were most likely localised along a broad E-W fault zone, although no major offset has been found. About 1km due east of the gabbro boss, an intrusive plug of poikilitic wehrlite forms a 50m diameter outcrop [998537]. The wehrlite is easily distinguished by its dark brown weathering compared to the pale brown of the surrounding basalts. The wehrlite is micropoikilitic with oikocrysts (0.3 to 1 cm) enclosing 0.08 to 0.2mm diameter grains of olivine, now pervasively serpentinised. Like the intrusive microgabbro boss to the west, the intrusive wehrlite lies within the E-W trending brecciation and alteration zone. Both of these gabbroic and wehrlitic intrusions are petrographically identical to the plutonic members at the Transform Sequence and probably relate to it.

4.2.5 The Yerasa Inlier

An approximately 1 km^2 outcrop of mafic to ultramafic lithologies forms an inlier that occupies a slight topographic depression within the lowest units of the WLFC Basal Group, (Figure 4.4). This outcrop, termed the Yerasa Inlier, is bounded on all sides by shears, the northern and southern of which are north dipping, high angle thrust faults, and the north-south trending ones being vertical, strike-slip faults. Despite the Inlier having been tectonically elevated, the bounding thrust faults do not extend for more than 150m into the surrounding Basal Group and therefore represent only small vertical throws, up to 300m, illustrated in Figure 4.4b. As such the Yerasa Inlier is a tectonic window, exposing the non-volcanic basement immediately below the Basal Group, a structural level that is generally unexposed in the WLFC. Although the lavas of the Basal Group do not lie directly on the mafic-ultramafic lithologies, such a relationship may be expected. Indeed, in the Vavla area, Simonian (1975) reported pillow lavas lying directly on serpentinised ultramafics, confirming the possibility of such a relationship.

The geology of the Yerasa Inlier is illustrated in Figure 4.4a. The inlier is divided in two by a N-S trending, vertical strike slip fault filled with sheared serpentinite. Sigmoidal drag of vertical sheared serpentinite foliation across the fault axes indicates a dextral sense of

movement, (Figure 4.5). The inlier consists of three distinct lithological associations:

(i) a serpentinised, tectonised harzburgite of mantle origin

(ii) layered and laminated wehrlites and gabbros

(iii) cross cutting peridotite and gabbroic bosses and later mafic dykes.

The tectonised harzburgite is pervasively serpentinised and grades into sheared serpentinite melange zones towards its contacts with the surrounding Basal Group. Its enstatite foliation, although strong is orientationally inconsistent. Otherwise, the harzburgite is identical to that from the WLFC mantle sequence, described in Chapter 2.2. Layered and laminated wehrlites and gabbros in tectonic contact with the serpentinized harzburgite, are identical to the cumulate members of the Axis Sequence, described in Section 2.4. The wehrlites are medium and coarse grained. Phase layering on both a centimetre and metre scale is formed by variations in the abundance of olivine and clinopyroxene. In places, cumulate medium grained layered gabbros grade from the wehrlites.

The harzburgite and cumulates have been observed cut by coarse pyroxenite, pyroxenitic wehrlite, isotropic gabbro bodies and a number of doleritic dykes. The pyroxenite and pyroxenitic wehrlite form irregular 50m diameter outcrops with steep intrusive contacts that cut the harzburgite foliation, [992538]. These intrusive ultramafic pods are in turn cut by a medium grained, isotropic gabbro that also cuts the harzburgite host, at [99155368] and [99205340] respectively. The gabbro is massive, varitextured and has pegmatitic patches and large dyke like apophyses. It also contains 1 to 10m xenoliths of harzburgite and layered wehrlite cropping out up to 50m from the main contact with the harzburgite host, [991537]. The isotropic gabbro also cuts the overlying Basal Group where it forms an irregular contact, between [990538] and [987536].

Cutting the harzburgite, layered wehrlite-gabbro complexes and intrusive peridotites and gabbros are multiple, dolerite dykes. These dykes are vertical, 1 to 1.5m wide, medium grained aphyric and plagioclase subphyric and have 10 to 20mm wide, chilled margins. Their E-W to NE-SW trends are similar to dykes in the near Basal Group.

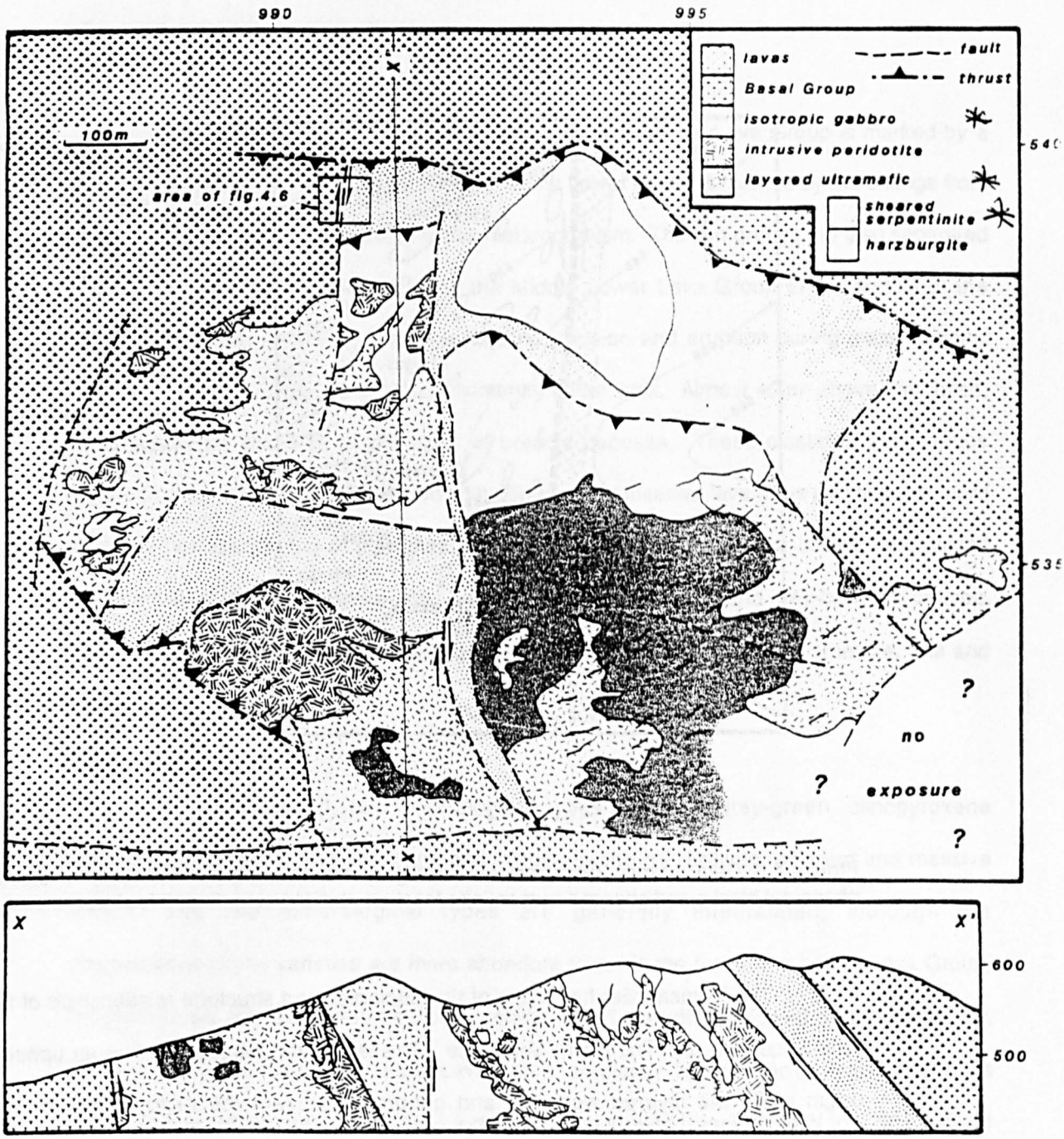

Figure 4.4 Detailed map and cross-section of the Yerasa inlier showing its relationship with the surrounding volcanosedimentary sequence. The Yerasa inlier is essentially an imbricate of inclined sheets, thrust into the Basal Group, forming a tectonic window into the plutonic basement. The eastern and western margins of the inlier are, however, primary igneous contacts, suggesting that the basement rocks forming the inlier have not been transported over a very great distance.

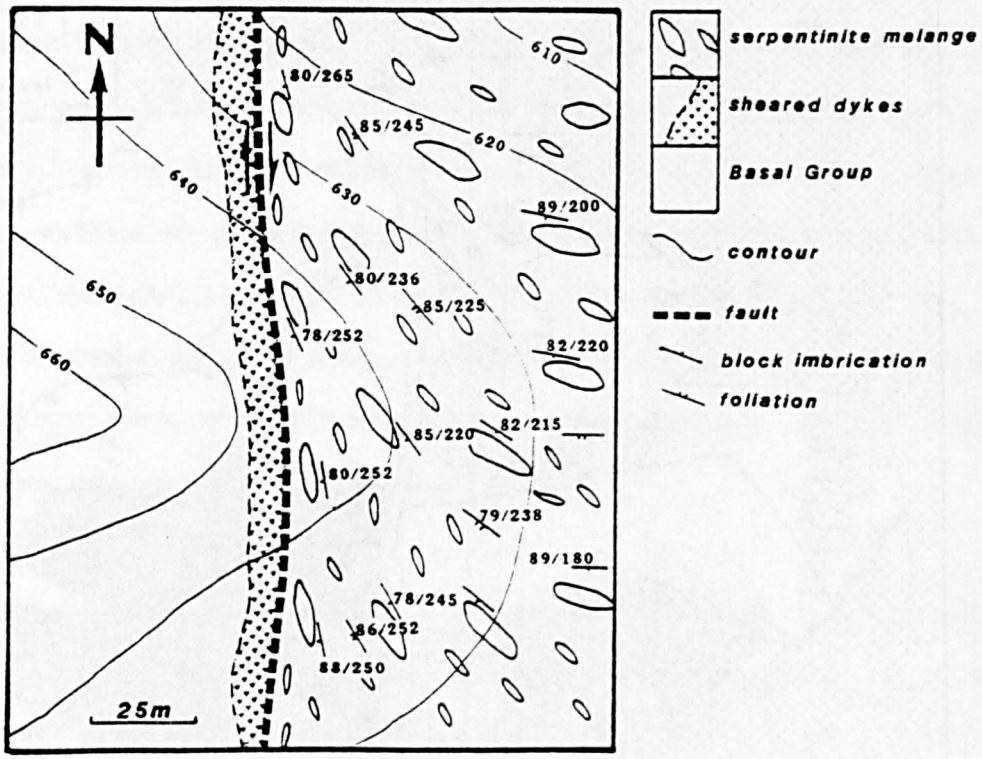

Figure 4.5 Detailed map, from enclosure in Figure 4.4, showing the orientation and position of phacoidal blocks and sheared serpentinite foliation, that indicate dextral fault movement.

The Yerasa Inlier has many of the lithologies and structural relationships of both the Axis Sequence and Transform Sequence. The tectonised harzburgite has an upper mantle origin while the layered wehrlites and gabbros represent the plutonic part of the Axis Sequence. The intrusive peridotites, gabbros, and cross cutting dolerite dykes are identical to the Transform Sequence described in Section 3. As such, the Yerasa Inlier represents the disrupted basement up to 300m below the Basal Group in the WLFC. This is in direct contrast to the basement of sheeted dykes on Troodos.

4.3 The Lower Lava Group

4.3.1 Relationship to other Units

The boundary between the Basal Group and the Lower Lava Group is marked by a maximum abundance of 20% dykes. The top of the Lower Lavas is marked by the change from pervasive zeolite facies to subzeolite facies metamorphism. The two groups are also separated by a progressive unconformity affecting the Middle Lower Lava Group to the Middle of the Upper Lava Group, providing evidence of tilting, erosion and eruption during major tectonic activity. The Lower Lava Group is approximately 800m thick. Almost 400m above their base, the Lower Lavas are host to a number of breccia deposits. These clastic to argillaceous sediments occur as sheets, intercalated with pillowed and massive lava flows that become more abundant towards the top of the Lower Lava Group. Unlike the orange-brown, haematised colour of the altered Basal Group, the Lower Lavas are pale-brown and grey-brown at outcrop. Fresh surfaces are grey-green, reflecting pervasive, low grade alteration to smectite, illite and zoisite.

Within the group, two mineralogical types occur (i) grey-green, clinopyroxene subphyric pillow lavas, and (ii) olivine and clinopyroxene microphyric, pillowed and massive flows. The two mineralogical types are generally intercalated, although the clinopyroxene-phyric varieties are more abundant towards the top of the Lower Lava Group. Morphologically the lavas vary between coherent and disrupted pillowed basalts to planar, massive lava flows. Unlike the Upper Lava Group, no glassy, hyalophyric or hyaloclastic flows occur. Dykes cutting the Lower Lavas form individual sheets trending 040N to 120N and are mineralogically similar to the Upper Lava Group.

4.3.2 Pillowed Basalts

Grey-green, clinopyroxene subphyric lavas form 0.8 to 1.3m diameter, rounded pillows with 10 to 15mm wide chilled selvedges and abundant zeolite and carbonate filled vesicles. The vesicles range from 0.8 to 1.5mm diameter, are most abundant towards the top of the pillows and can be used as a way-up criteria. Chilled margins are often spherulitic with 2 to 5mm diameter variolites, probably formed as a result of devitrification, Plate 4.3. Occasionally individual pillow tops were observed with paheohoe surface textures indicating steep southerly downslope flow directions, Plate 4.4. In the Muttin tis Pernias area, 1.5km NW of Yerasa Inlier, clinopyroxene-phyric pillow lavas are elongated, 3m long by 0.5m in diameter. The elongation trends westwards and coincides with a dip of 25^{o} to 30^{o} (Plate 4.5). Although not common, elongated pillow tubes also occur to the southeast of the Yerasa Inlier [99495199] where they also dip west at 30^{o}. In the Kapillio area, individual pillowed flows are often discontinuous, decreasing in thickness from 5m to 2m over 20m along strike. Often pillows are flattened at the base of a flow compared to the overlying ones, suggesting rapid extrusion and burial before complete solidification.

In contrast to the grey-green, clinopyroxene-phyric and aphyric basalts just described, the other pale brown weathering lavas of the Lower Lava Group are small, olivine micro-phyric pillows. Individual pillows range from 0.4 to 0.8m diameter, have 20 to 30mm thick, vesicular devitrified and hyalopilitic rims. Vesicles (0.5 to 3mm) are abundant toward, the tops of the pillows where they are ubiquitously filled with white zeolites and carbonate. Like the grey-green lavas, individual flows range from 2 to 5m thick and are discontinuous along strike. Olivine microphenocrysts are characteristically replaced by orange iddingsite. Pink, anastomosing zeolite veins cutting the pillows are common. The smaller size and semi-vitreous chilled selvedges suggests a higher temperature and lower viscosity of these basalts, compatible with their more mafic mineralogical composition. Semi-brecciated and fragmented pillow lavas are most common near the top of individual flows.

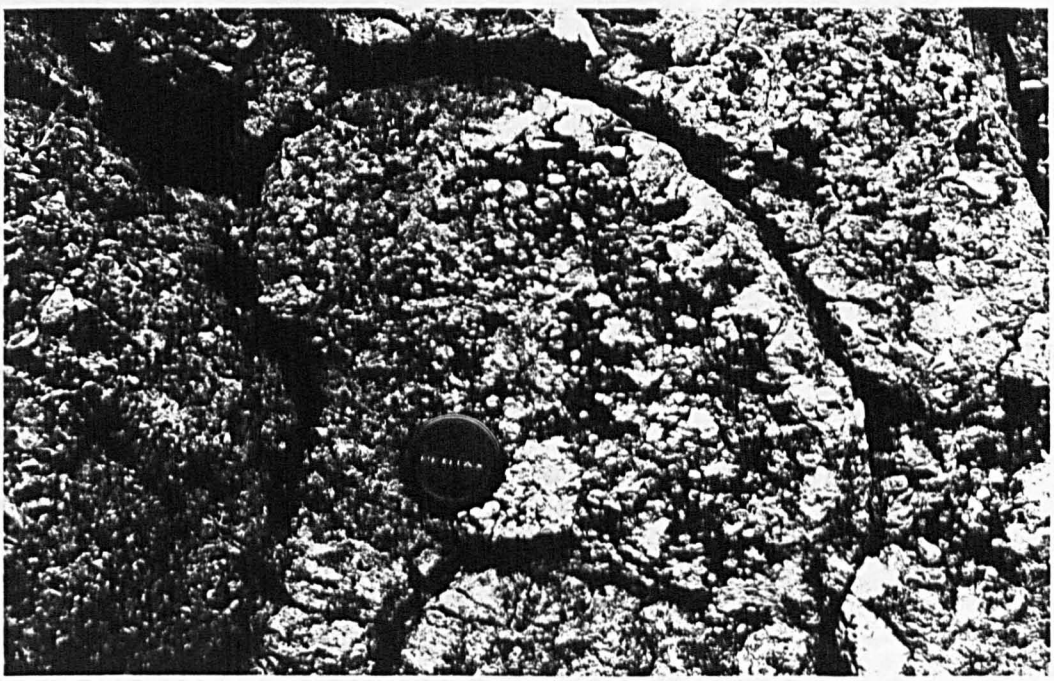

Plate 4.3 Devitrified Lower Group Lavas with characteristic weathering surface in which variolites form a nodular texture.

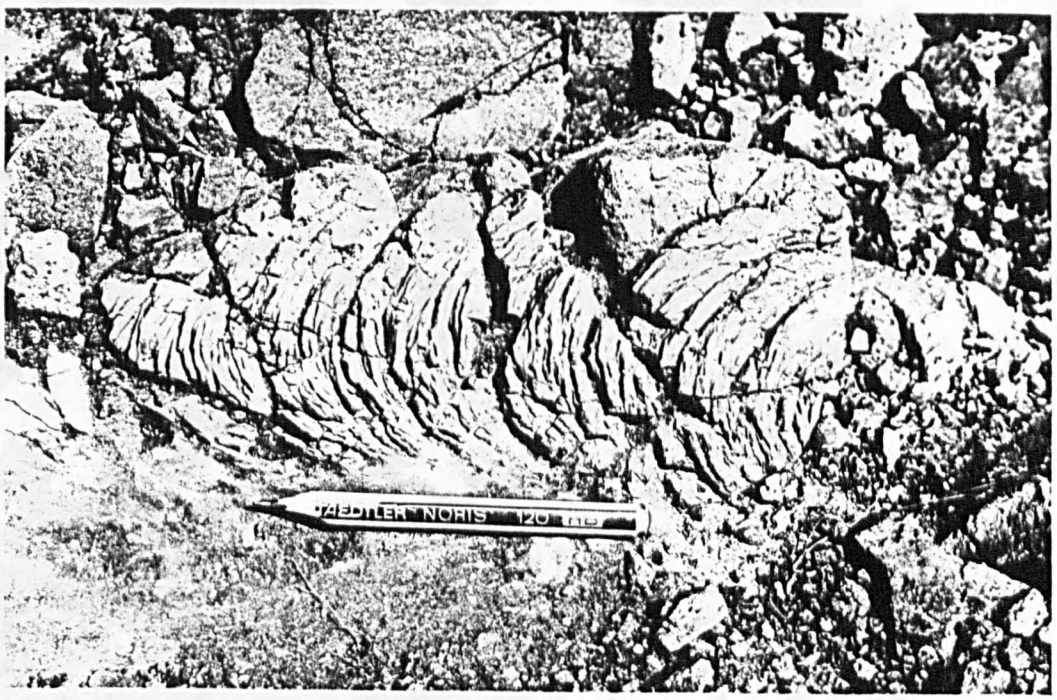

Plate 4.4 Pahoe - hoe surface texture to a basalt flow in the Akrounda area. The surface coils indicate a southerly flow direction for the basalt.

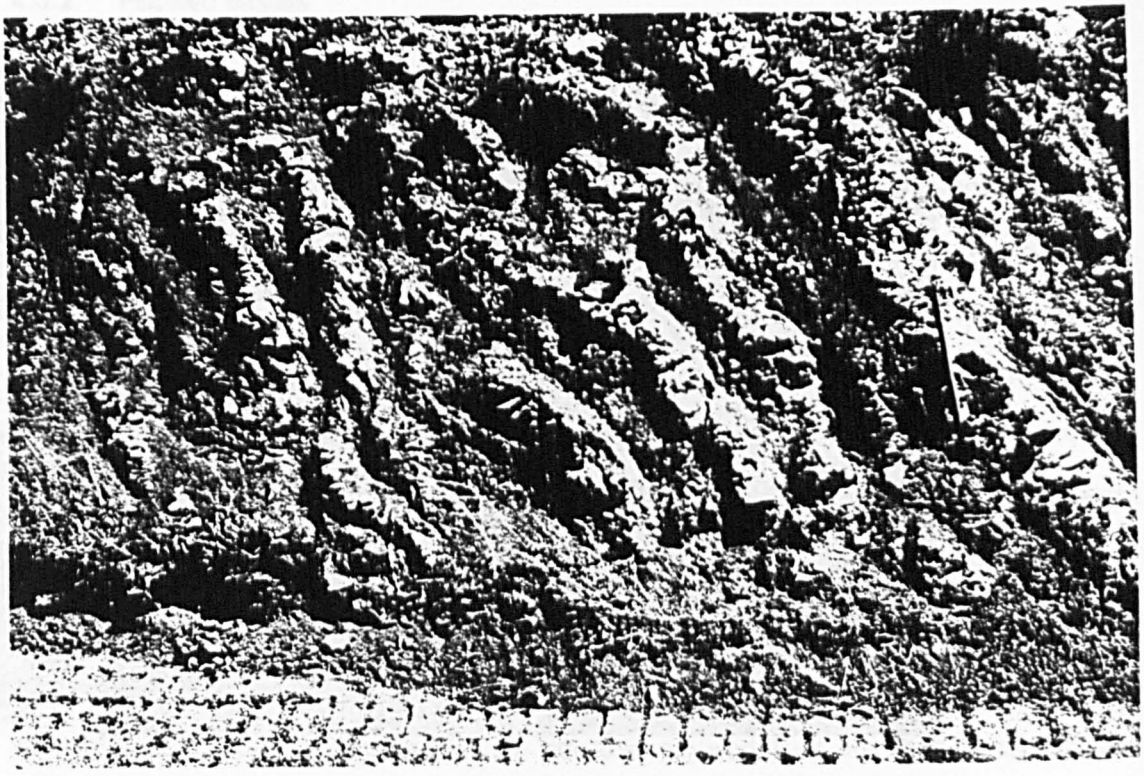

Plate 4.5 Elongated pillow tubes indicating eruption down a steep palaeo-slope.

Plate 4.6 Photo-micrograph of intersertal clinopyroxene phyric, basaltic pillow lava. Clinopyroxene grains (augite) are commonly twinned. Field of view is 8mm.

There is a complete range in brecciation from fractured, coherent pillows and pillows with fragmented selvedges to chaotically brecciated basalts. Despite being disrupted, their recognisable pillow form suggest the fragmented lavas have not been significantly transported. A possible mechanism for their formation may have been eruption onto and subsequent slumping down steep palaeoslopes. The term "collapse breccia" has been applied to by Xenophontas & Gass (*pers. comm.*) to describe this phenomenon.The two varieties of pillow lavas are petrographically similar, except for the presence or absence of olivine microphenocrysts.

Plate 4.6 illustrates an intersertal, clinopyroxene-phyric basalt, typical of the Lower Lava Group. Hypidiomorphic-granular clinopyroxene constitutes 38% of the mode and ranges from 1.2mm phenocrysts to 0.05mm grains in the groundmass. Phenocrysts of clinopyroxene occur as glomeroclusters of up to ten grains, have slightly embayed margins and are occasionally twinned. They are generally fresh except where replaced by zoisite and minor chlorite. The groundmass is intersertal, holocrystalline and fine grained with granular clinopyroxene and acicular plagioclase laths forming semi-variolitic sprays. Commonly albitised plagioclase, An_{28-34}, forms 52% of the mode and crystallised later than clinopyroxene. Where the lavas are olivine-phyric, olivine grains are euhedral, often skeletal, form less than 5% of the mode and range from 0.3 to 0.7mm in diameter. Vesicles are abundant (2 to 5% of the mode), spherical, range from 0.2mm to 1mm in diameter and are filled with granular zoisite, radiating zeolite and occasionally carbonate. Alteration of the basalts includes iddingsite after olivine, turbid plagioclase and occasional replacement of clinopyroxene by granular zoisite, indicative of zeolite facies metamorphism.

4.3.3 Massive Flows

Detailed stratigraphic logging in the Kapillio area reveals massive clinopyroxene-phyric and aphyric lava flows between 20m and 1.5m thick. The massive flows are discontinuous along strike, forming flattened lens shaped bodies. Figure 4.6 illustrates a cross section across

the largest massive lava flow that crops out between forest boundary posts FC 195 and FC 194 [76755475], and which is 21m thick by 182m in length. At its thickest point the top of the flow is doleritic, medium-grained, massive and aphyric. The grain size increases downwards over 12m where it grades into coarse dolerite. A further 8m thickness occurs over which the grain size steadily decreases until at the base the flow becomes basaltic. The massive flow overlies a 1.5m thick breccia deposit that is baked and cut by downward penetrating, 10 to 50mm wide chilled basaltic wedges. In turn, the flow is also overlain by 10m of coherent aphyric pillow lavas. Because the outcrop dips at a high angle, vertical sections through the margins of the massive flow are well exposed. The northwestern margin is complex, being interdigitated with multiple breccia units and overlain by pillow lavas. Interfingering of the massive flow and the breccia units is evidence of lateral penetration into the breccia deposits. In contrast, the southwestern contact progressively onlaps the underlying pillow lavas and breccias. The overall asymmetry of the massive flow indicates fault dominated control of the northwestern margin. Elsewhere in the Lower Lava Group, massive aphyric and clinopyroxene-phyric flows, between 0.5m and 1m thick are betwen 50 and 100m wide. These flows are fine-grained, have planar lower and upper surfaces, and often overlie laminated, argillaceous silts and mudstones. Their laterally consistent thickness and sheet morphology are evidence of rapid magma eruption on to a relatively even and horizontal seafloor.

Petrologically the dolerite lava flows are medium grained, holocrystalline with a hypidiomorphic-granular texture. Plate 4.7 is a photomicrograph showing clinopyroxene and olivine micro-phyric basalt with an intersertal groundmass of plagioclase and clinopyroxene. Augite grains 0.2 to 1mm in diameter are euhedral, and form 2% of the mode. Alignment along (100) axes of augite grain is probably due to flow within the massive lava. Olivine microphenocrysts are relatively rare, form less than 1% of the mode, range from 0.3 to 0.7mm in length and are skeletal and barrel shaped, indicating rapid crystallisation. The groundmass contains clinopyroxene (60%) and intersertal, acicular plagioclase (38%). Weak flow alignment of plagioclase laths has produced a patchy trachytic texture.

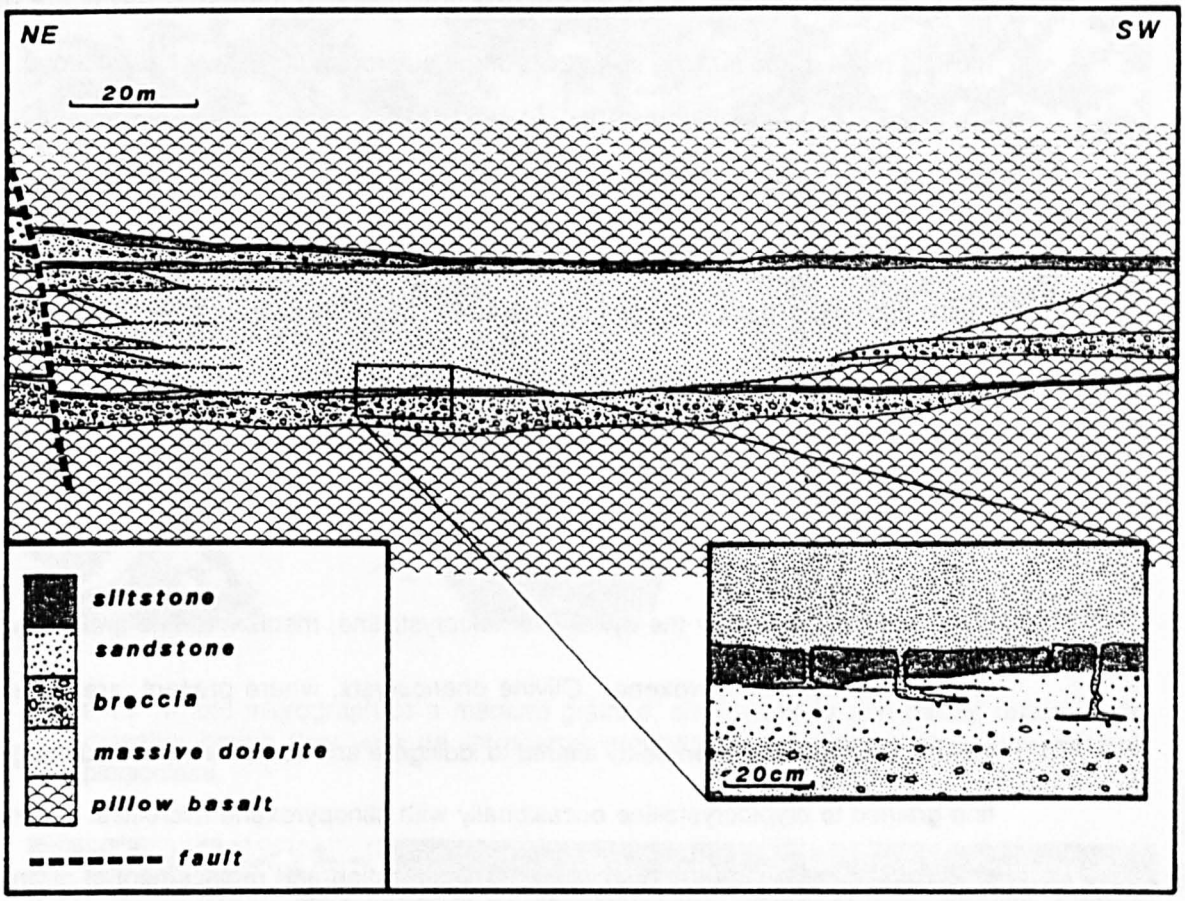

Figure 4.6 Section through a Massive lava flow in the Lower Lava Group that crops out in the Kapilio area. Inset detail shows a graded deposit overlain by chilled basalt forming the base of the massive flow. Veins of the overlying basalt have been injected into the sediment.

Vesicles, although most abundant towards the top of the flow, range from spherical to elliptical, 0.3 to 0.7m in diameter and are filled with fibrous zeolite, zoisite and occasionally by carbonate. Alteration of the dolerite flows is to low greenschist facies, high zeolite facies with clinopyroxene (augite) partly replaced by granular epidote, zoisite and quartz. Olivine is replaced by iddingsite and groundmass plagioclase has been albitised. This relatively high grade of alteration compared to the low zeolite facies of the surrounding pillow lavas may be a result of autometasomatism due to the large thickness of the massive flows (ie. greater that 20m) .

4.3.4 Lower Lava Group Dykes

Unlike those in the Basal Group, intrusives into the Lower Lavas are restricted to multiple mafic dykes forming up to 20% of the outcrop of the Lower Lavas Group. The dykes are subvertical and have a bimodal trend of 040N and 120N (Plate 4.8). They are 1 to 1.6m wide, fine-grained with 30 to 50mm thick chilled margins, and cross cut one another, the 120N set being the youngest in the Kapillio area. They are also observed intruding and locally baking clastic and argillaceous sediments (Plate 4.9). Unlike the pale weathering lavas that they cut, the dykes weather dark brown, fresh surfaces being almost black. Mineralogically, the dykes are most similar to the lavas of the overlying Upper Lava Group and are probably feeders to them.

Petrographically the dykes are holocrystalline, medium to fine grained with granular olivine and pilotaxitic pyroxene. Olivine phenocrysts, where present, are euhedral, 0.5 to 1.5mm diameter and often partly altered to iddingsite and serpentine. Chilled margins are very fine grained to cryptocrystalline occasionally with clinopyroxene microlites. Alteration of the mafic dykes is moderate and includes serpentinisation and replacement of olivine grains by iddingsite, replacement of the groundmass by smectite, illite and zeolite, and carbonate filling of vesicles. As such, their zeolite metamorphic facies is the same as that of their Lower Lava Group host.

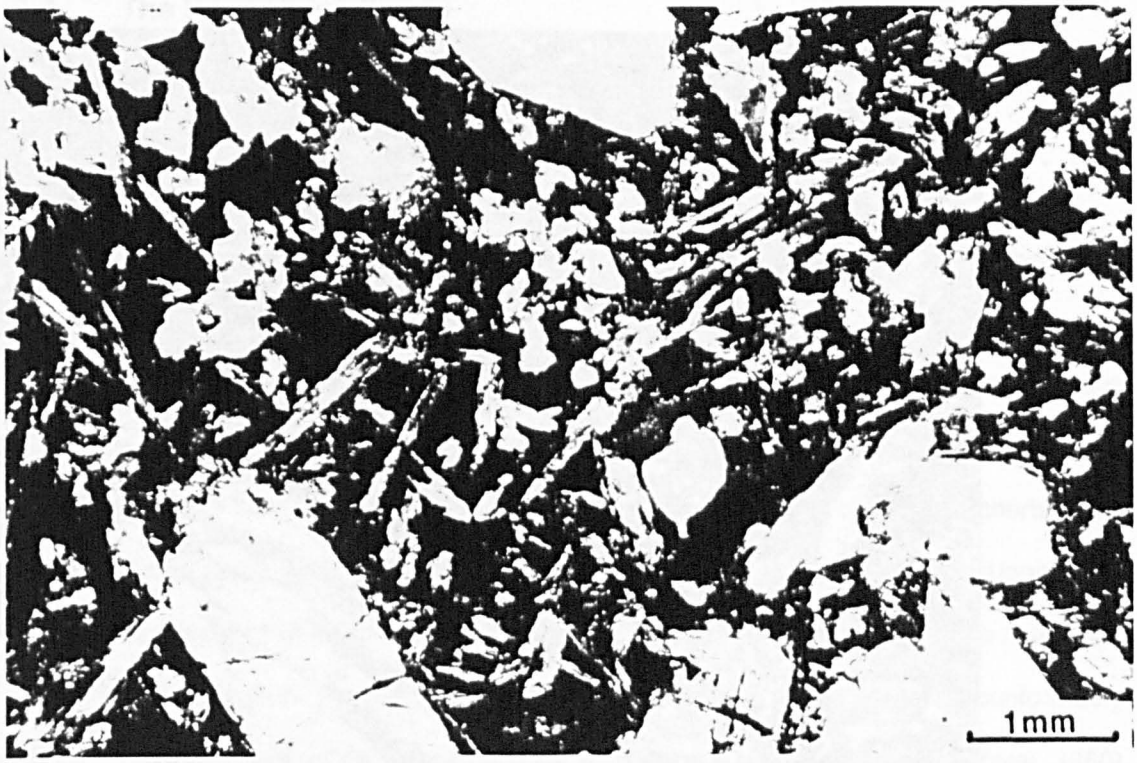

Plate 4.7 Photo-micrograph of a medium grained, clinopyroxene and olivine micro-phyric massive basalt flow with an intersertal groundmass of olivine, clinopyroxene and plagioclase.

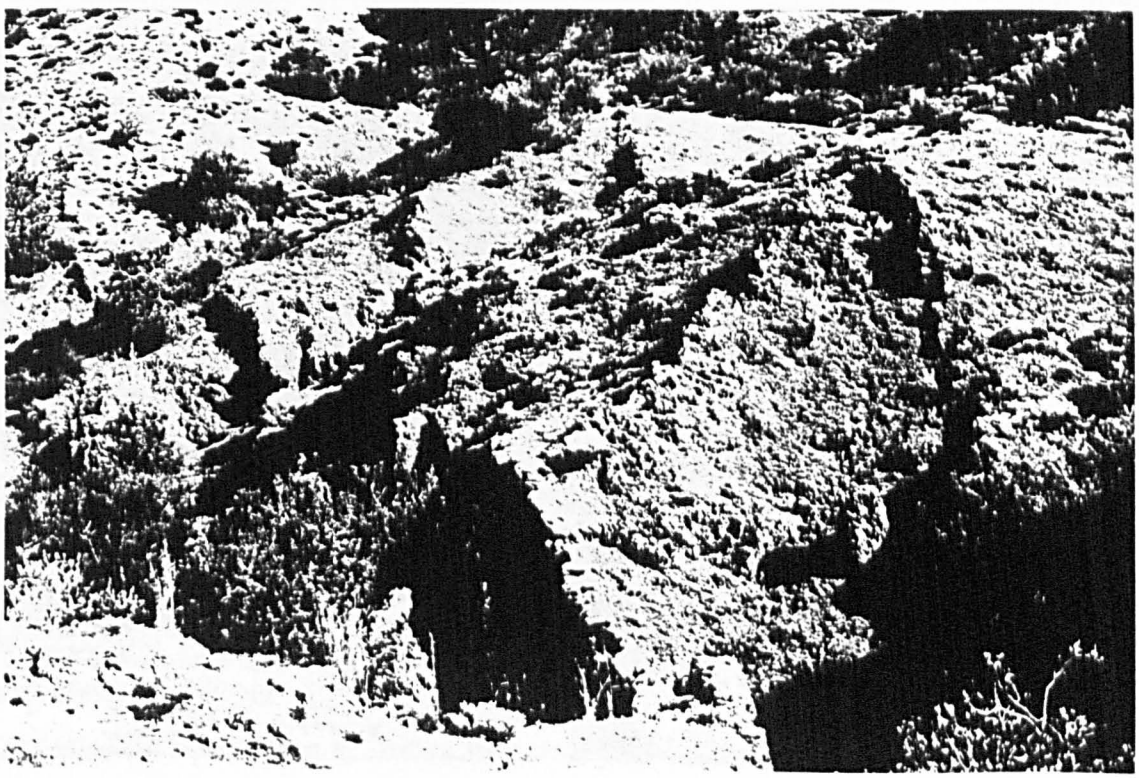

Plate 4.8 Conjugate dyke set cuts the Lower Lava Group at Kapillio, the dykes trend 040 and 120N.

Plate 4.9 Mafic dykes cut coarse grained deposit in the Kapillio area.

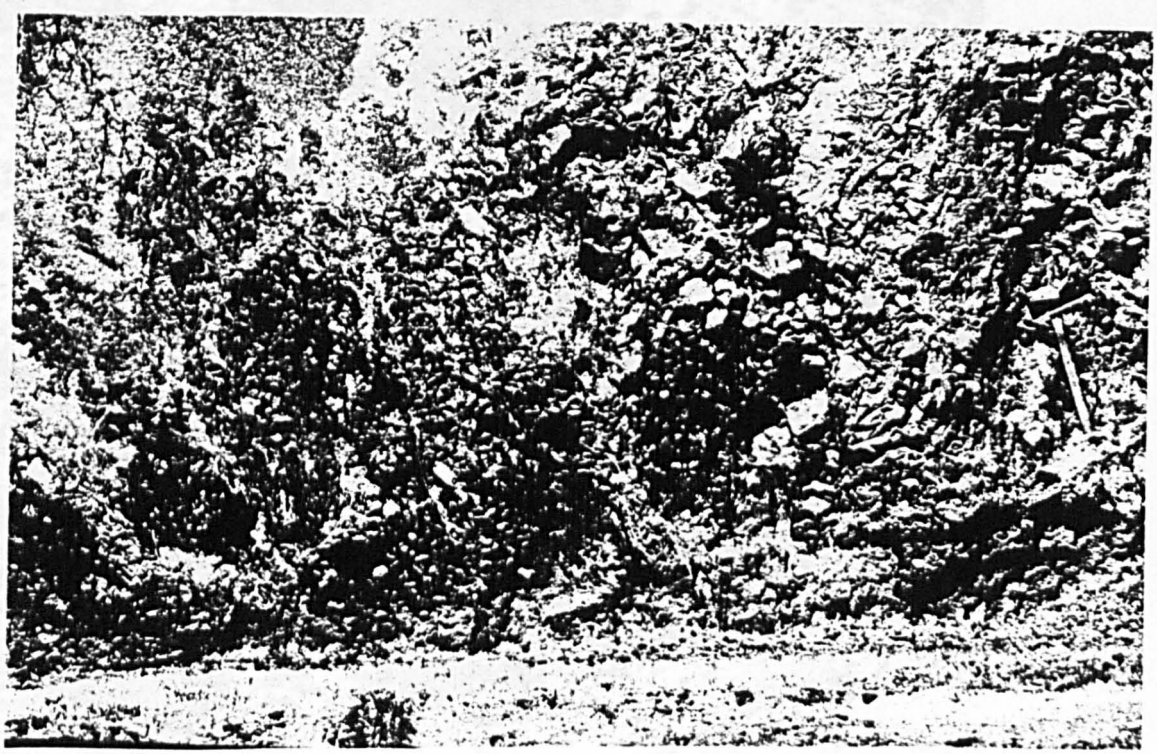

Plate 4.10 Limburgite lavas, in the Kapillio area, form a characteristic outcrop of small, dark coloured and vitrious pillows.

4.4 The Upper Lava Group

4.4.1 Stratigraphic Relationships

The Upper Lava Group is distinguished from the Lower Lava Group by the absence of zeolite facies metamorphism, and the incoming of glassy, olivine-phyric pillow lavas and hyaloclastic flows. As a result, the Upper Lavas weather dark brown and form coherent, tough exposures. The upper limit to the Upper Lava Group is faulted out and hence not observed in the Kapillio area. Instead the lavas are thrown against near vertical chalks and cherts of the Lapithos Group (Bear, 1960). However, between Mathikaloni and Akrounda, the Upper Lava Group is interdigitated with and overlain by manganiferous sediments (Umbers) and radiolarian cherts of the Perapedhi Formation. These deposits, up to 10m thick, are unconformably overlain by a sedimentary melange, the Moni Formation (Late Maestrichtian; Morel, 1960) consisting of a bentonitic clay matrix in which olistoliths of quartzose sandstone, recrystallised limestone, ribbon cherts and lavas are entrained.

The Upper Lavas can be divided into three main mineralogical and textural groups: (i) olivine (and rarely orthopyroxene) microphyric, glassy pillow lavas, (ii) hyalopilitic, olivine microphyric pillow lavas, and (iii) halocrystalline, olivine-phyric massive flow. The pillow lavas also have three morphological types: (i) pillowed basalts, (ii) fragmented pillows (iii) hyaloclastite flows. Although mafic dykes cut the upper lavas, they rapidly decrease in abundance up through the sequence, where they are occasionally observed terminating in extrusive edifices.

4.4.2 Limburgite Lavas and Hyaloclastic Flows

Characteristic of the Upper Lava Group are dark brown to black, glassy pillow lavas (Plate 4.10). Although initially described as *'limburgites'* (Bear,1960; Smewing, 1975), Simonian (1975) preferred to classify them only as *'glassy lavas'* on the basis that they are oversaturated with respect to SiO_2. However since they contain olivine and clinopyroxene

phenocrysts in a hyalopilitic matrix that exceeds 20% vol. of glass, the term limburgite has been retained as a textural term that is devoid of any compositional implication. Limburgite lavas are especially prominant in the vicinity of Kapillio village where they form the Lower Units of the Upper Lava Group, (see Figure 4.2). These vitriophyric basalts are variably brecciated and grade from pillowed lavas into hyaloclastic flows, the transition usually occurring up through the sequence.

Morphologically, the pillow lavas are small, 0.3 to 0.8m in diameter, often elongated, up to 3m long, and have holovitreous margins forming 20% to 30% of the mode of each individual pillow. Individual limburgite flows range from 2 to 10m thick and are laterally impersistent over 150 to 200m along strike. Glassy margins are more resistant to weathering and occasionally form shells to hollow lava tubes. The relative abundance of southwest dipping, elongated pillows compared to massive sheet flows suggests eruption predominantly on moderate or steep palaeoslopes. In places [96653], baked, red, fine grained material forms interstitially between limburgite pillows. Although not fossiliferous, this cryptocrystalline material may be baked pelagic mudstone, indicating slow, sporadic pillow eruptions or high sedimentation rates.

There is a range of hylaclastic textures from rounded cobbles of glassy basalt surrounded by a matrix of shattered, highly friable black glass fragments (Plate 4.11), to flows consisting of only shattered black glassy fragments. Partial alteration of the hyaloclastites to palagonite and veining by carbonate is common. Fresh surfaces have a blue hue and indicate alteration of glass to chlorophaeite. Compared to the more coherent, limburgite pillowed flows, the hyaloclastite flows are impersistent along strike and wedge out from 4.8m to zero thickness over 50m laterally, eg. [96755425].

Figure 4.7 illustrates a vertical section through a limburgite pillow lava that grades vertically upward into an overlying hyaloclastite [96255425]. The coherent limburgite pillows (0.3 to 0.5m diameter) become increasingly enclosed within shattered glass shards, probably

derived from spauled glassy pillow selvedges. The proportion of shattered glassy matrix increases from 10% to 60% over 1.5 m, where it supports isolated, rounded and exfoliated basaltic clasts ranging from 10mm to 80mm in diameter. These rounded, aphanitic and glassy clasts are friable and readily disintegrate into matrix sized fragments. The top 1 to 0.3m of the flow consists entirely of shattered basaltic glass. The hyaloclastite is massive and coarse grained with particle sizes ranging from 0.2 to 6mm. At a locality 300m south of Kapillo church, a 1.8m thick hyaloclastite crops out with no underlying coherent or brecciated base suggesting either *in situ* disintegration of an entire limburgite flow, or transport from a more coherent flow. If the latter were the case, then the massive nature of the deposit indicates downslope mass transport such as slumping or debris flow (Figure 4.8).

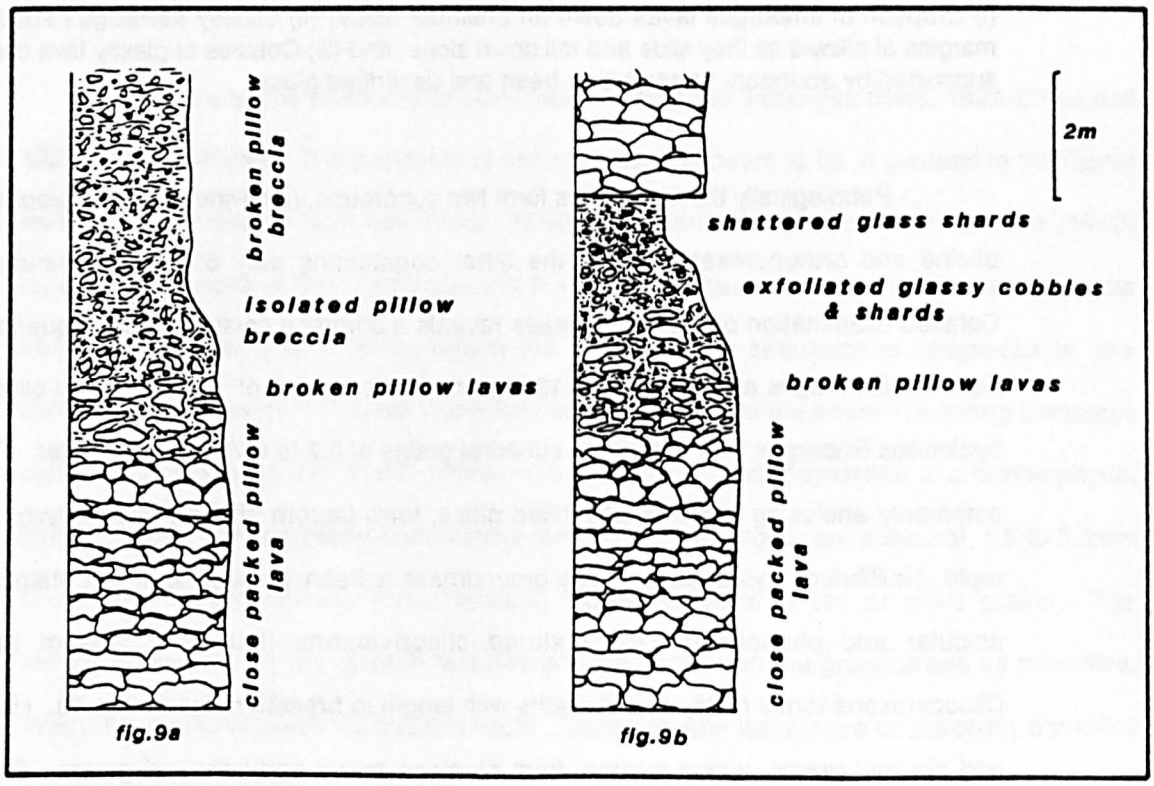

Figure 4.7 (a) Graphic log of '*in situ*' hyaloclastite flow that grades upwards from close packed and coherent limburgite pillow lavas, through increasingly broken limburgite lavas. (b) Graphic log of '*transported*' hyaloclastite flow that fines upwards from a base that rests directly on coherent and close packed pillow lavas.

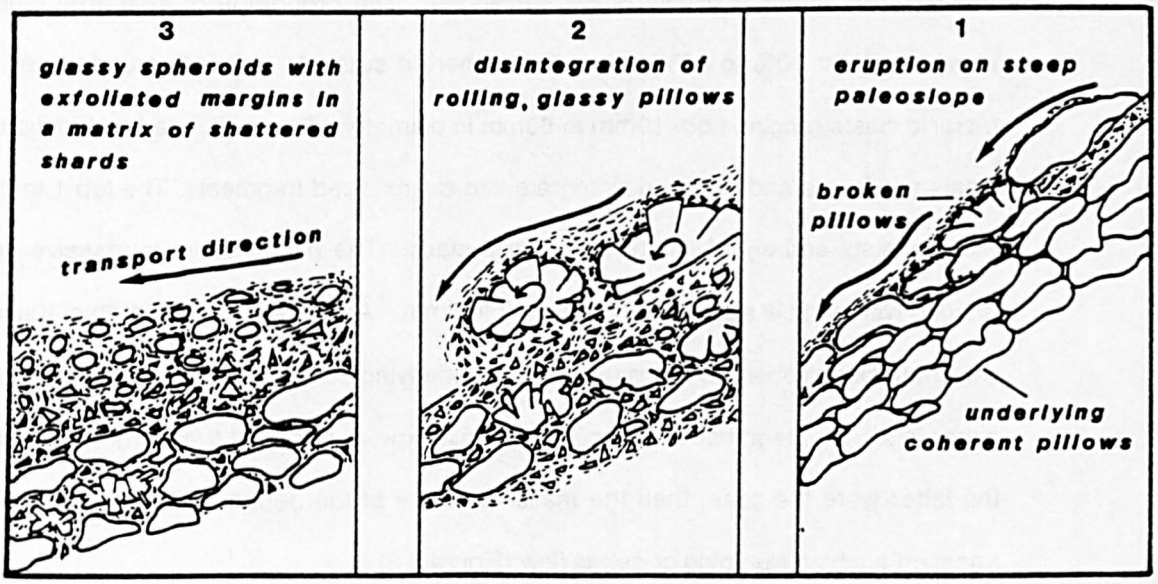

Figure 4.8 Postulated three stages in the formation and deposition of hyalocastiic flows: (i) Eruption of limburgite lavas down an unstable slope, (ii) Glassy selvedges spaul from the margins of pillows as they slide and roll down slope, and (iii) Cobbles of glassy lava come to rest, supported by abundant fragments of fresh and devitrified glass.

Petrologically the limburgites form two subgroups, (i) olivine-phyric, hyalopilitic, and (ii) olivine and orthopyroxene-phyric, the latter constituting only 8% of all limburgite flows. Detailed examination of the two varieties reveals a common crystallisation sequence of Ol -> Opx -> Cpx; Plag is absent. Plate 4.12 is a photo-micrograph of the core of an olivine-phyric, hyalopilitic limburgite with skeletal to euhedral grains of 0.2 to 0.7mm in diameter. The grains, commonly enclosing cores of devitrified glass, form lantern shaped phenocrysts indicating rapid, equilibrium crystallisation. The groundmass is fresh, hyalopilitic and contains dendritic, acicular and plumose quench textured clinopyroxene that form 75% of the mode. Clinopyroxene forms highly acicular laths with length to breadth ratios of 8 to 10. Herringbone and skeletal grains, where curved, form plumose swirls and helictical grains, (Plate 4.13). Minute spherulitic clusters 0.01 to 0.05mm in diameter indicate insipient nucleation points, (Plate 4.14). Although these clusters appear to be of clinopyroxene, Cameron *et. al.*, (1980) identify identical occurrences as primary amphiboles and refer to them as 'indicative of significant amounts of primary H_2O'. Attempts to analyse the clusters by microprobe proved

unsuccessful due to their minute size and skeletal habit. Interstitial glass is clear, fresh and forms 13% of the mode. Where it is altered, the glass has been hydrated to palagonite and clay minerals (probably smectite). The limburgites contain sphericle vesicles 0.9 to 0.3mm in diameter, forming 3% of the mode. The vesicles are mostly empty, although some have been filled with fibrous zeolites.

Plate 4.15 illustrates a vitriophyric, limburgite selvedge in which 0.4 to 0.8mm, subhedral olivine grains are set in a hyalopilitic groundmass of highly acicular clinopyroxene (28% of the mode) and clear glass forming 62% of the mode. The pillow margins contain 1% vol. of vesicles that range from 0.3 to 0.02mm in diameter, are irregular, elongate and occasionally filled with carbonate. The irregularity of the vesicles compared to those towards the centre of pillows may be due to rapid plastic deformation of the molten lava envelope during eruption and solidification.

Orthopyroxene phenocrysts were found in only two limburgite flows, 192A-CY84 and 192B-CY84, [965549]. The presence of orthopyroxene appears to be in contrast to the Upper lavas of the Arakapas fault belt (Bear, 1960; Simonian, 1975). However, Bechon (1982) reports orthopyroxene from some parts of the Arakapas fault belt, especially as phenocrysts from units termed type C lavas, where the crystallisation sequence of ol-opx-cpx is rare compared to the majority of lavas in the fault belt, but similar to the entire Transform Sequence plutonics and lavas in the WLFC. Plate 4.16 illustrates an orthopyroxene and olivine-phyric, glassy basalt. Orthopyroxene phenocrysts form 61% of the mode, are euhedral, 1.5 to 0.2mm in diameter and commonly form radiating glomeroclusters of ten or more grains. The orthopyroxene has *in situ* growth textures and also occurs in the groundmass as microlites, indicating equilibrium with the basaltic liquid. Clinopyroxene jackets are occasionally observed growing parallel to (100).

Simonian (1975) reports similar occurrences, that he interpreted as a result of local depletion of Mg ions with respect to Ca and Al around growing orthopyroxene grains, thereby

pushing the crystal into the clinopyroxene stability field and allowing clinopyroxene jackets to form simultaneously with orthopyroxene elsewhere. Such a heterogeneous textural assemblage is metastable and is characteristic of rapid crystallisation and undercooling during quenching. Similar heterogeneous crystallisation textures from quench basalts and limburgites has been described from the Argilla formation in Orthris ophiolite complex (Hynes, 1974; Menzies, 1976).

Unlike the straight extinction of many low Ca orthopyroxenes the phenocrysts in samples 192A-CY84 and 192B-CY84 have 0 to $6^{o}\ \gamma \wedge$ (100) oblique extinction, suggesting a distorted orthorhombic crystal lattice. The distortion may be a function of rapid cooling, but is more probably due to a higher proportion of Ca ions, allowing the lattice to partially invert to a monoclinic state. The latter is supported by the relatively high CaO composition of the orthopyroxene phenocrysts, determined by microprobe analysis (see Apendix 6). As such, the orthopyroxene phenocrysts are more correctly clinoenstatite and probably inverted from protoenstatite during cooling below $985^{o}C$ (Boyd and Schairer, 1964). Although clinoenstatite is exceptionally rare in naturally occurring rocks, it has been identified in the groundmass of boninite lavas from Cape Vogel, Papua New Guinea (Dallwitz, 1968; Walker & Cameron, 1983).

4.4.3 Hyalopilitic, Olivine-Phyric Pillow Lavas

Olivine-phyric pillow lavas with glassy margins with hyalopilitic interiors are most abundant towards the top of the Upper Lava Group where they form the majority of flows. These mafic lavas form dark brown weathering pillowed flows that are laterally persistent, typically cropping out as 3.5m thick units over 100 to 160m along strike. Individual pillows are round, range from 0.5 to 0.8m diameter and have 15 to 30mm thick glassy selvedges. Vesicles, concentrated towards the tops of the pillows are generally empty, although some are observed filled by a white zeolite. Compared to the limburgite, these flows are more pervasively altered with olivines ubquitously altered to orange iddingsite.

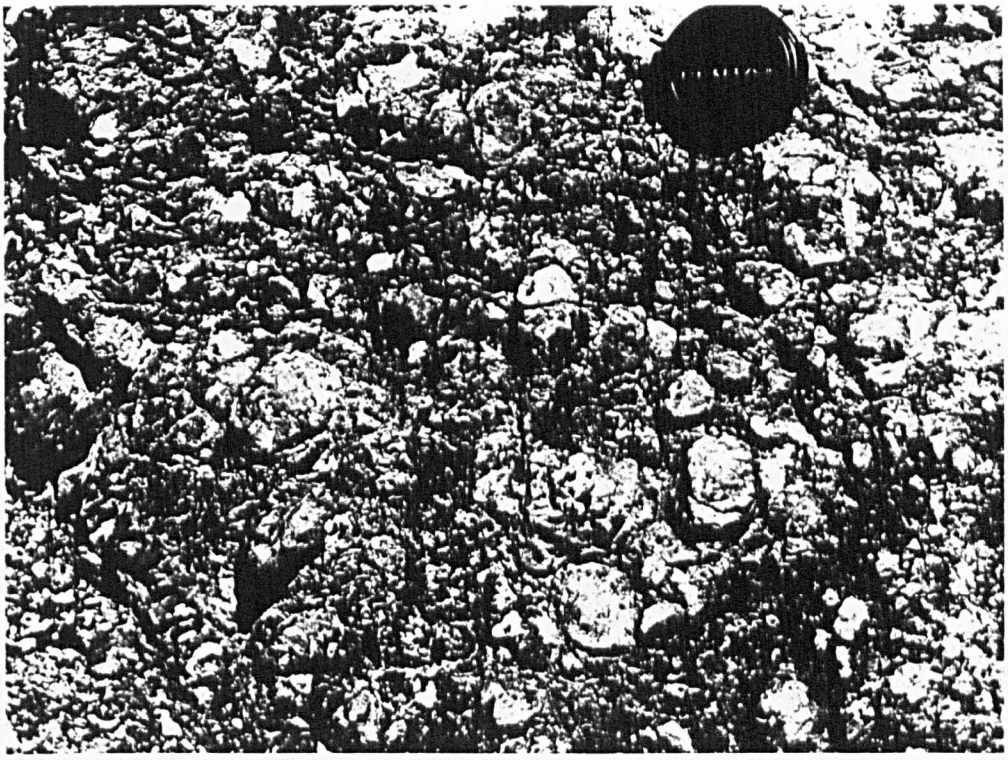

Plate 4.11 Black glassy fragments and cobbles of glassy basalt form an hyaloclastic flow interbedded with pillow lavas and sediments.

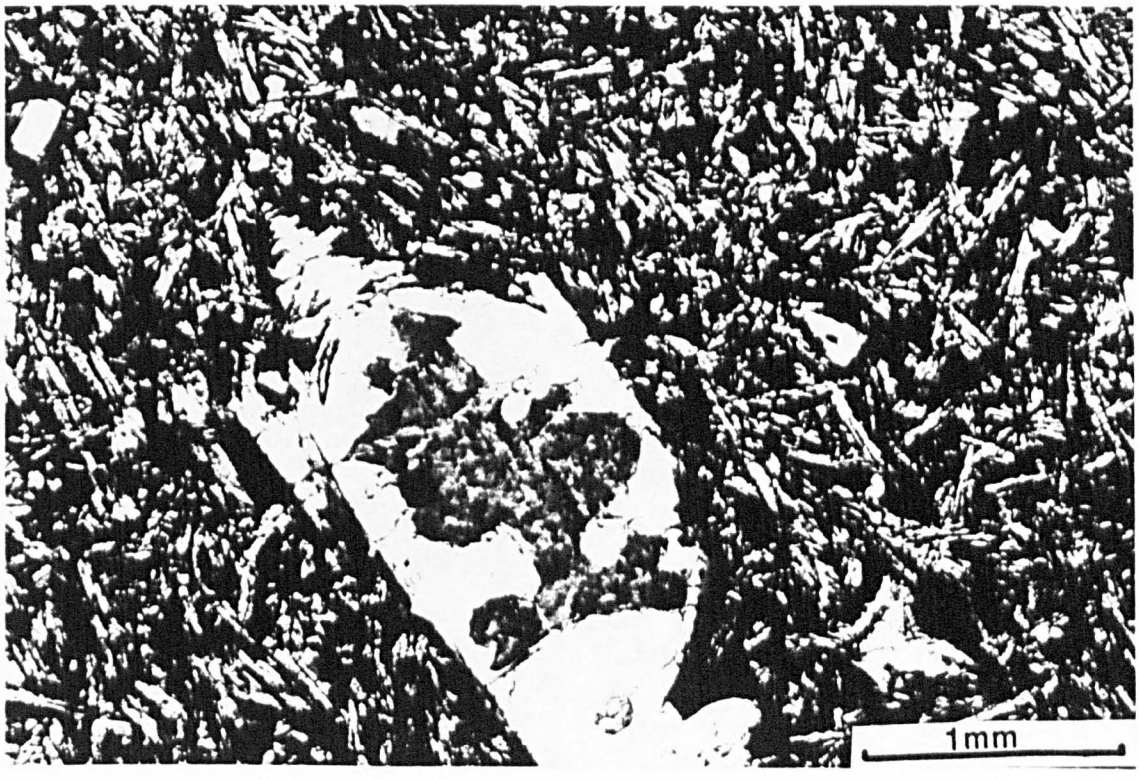

Plate 4.12 Photo-micrograph of the glassy core of a limburgite flow containing skeletal olivines and laths of clinopyroxene, set in a groundmass of plumose clinopyroxene and glass.

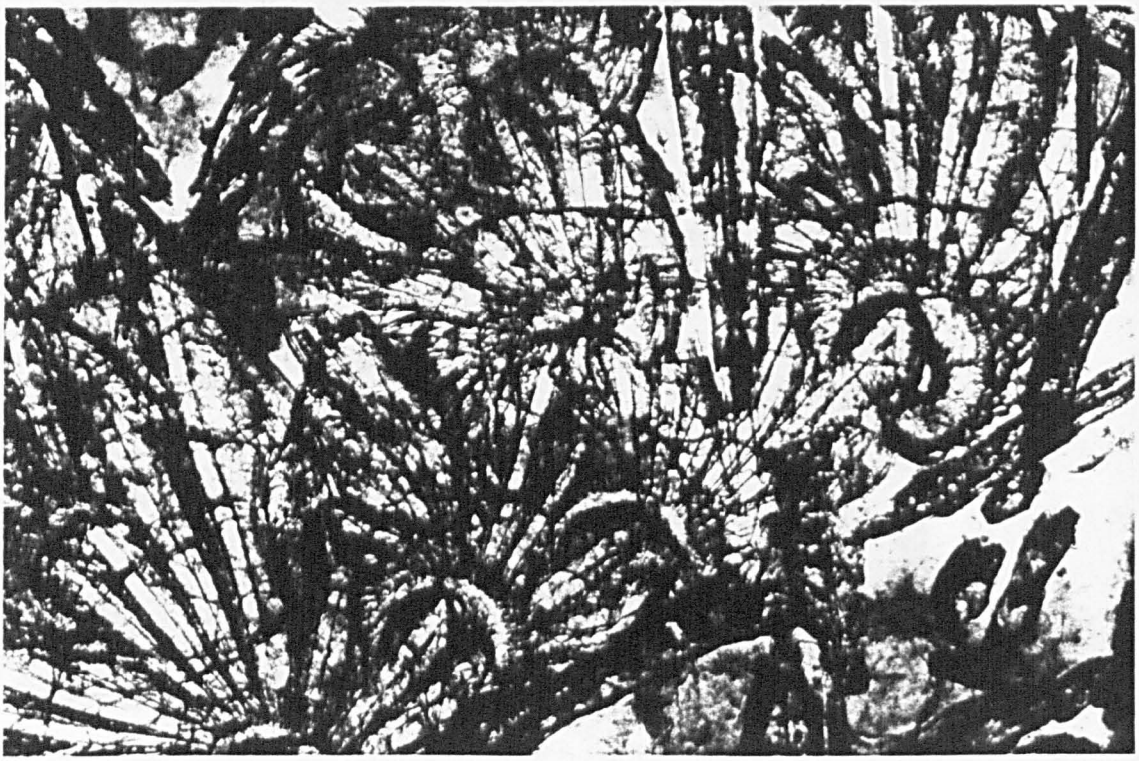

Plate 4.13 Quench textured, plumose and herring bone clinopyroxene set in glass, form the groundmass to many limburgite flows. × 300

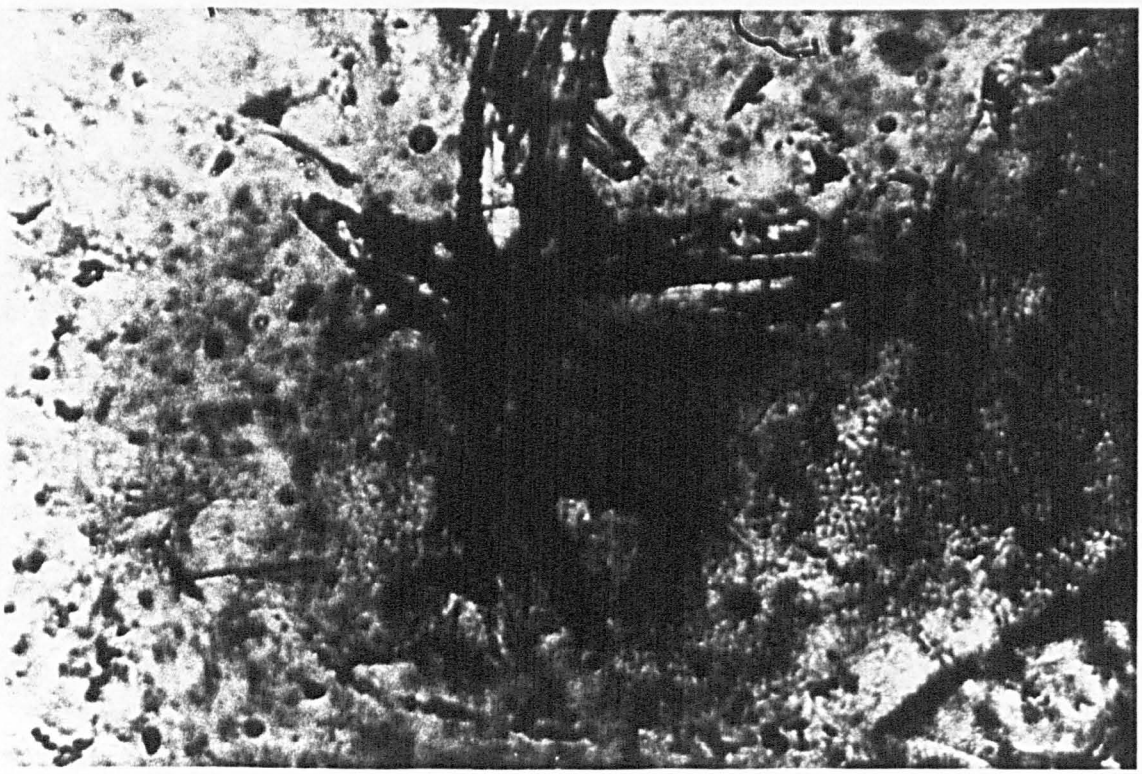

Plate 4.14 Spherulite clusters (reportedly of amphibole) suggesting a high content of magmatic volatiles, born out by whole rock analysis of fresh glass that shows a mean volatile content of about 3%. × 600

Plate 4.15 Photo-micrograph of fresh glass, with micro-phenocrysts of olivine and clinopyroxene; photographed in polarised light with sensitive tint plate. × 150

Plate 4.16 Photo-micrograph of limburgite flow rich in low Ca, clinopyroxene (1st order grey). The low Ca pyroxene has sub-parallel extinction, low birefringence and is identified as clinoenstatite. ×150

Like the Lower Lavas, the hyalopilitic olivine-phyric lavas are intercalated with breccia deposits, sandstones and laminated siltstones. They are also interbedded with manganoan, argillaceous sediments (umbers) that increase in thickness up to 1.5m upward through the section, (Plate 4.17). The abundance of manganoan sediments may suggest rapid sedimentation rates, but more probably indicate increasingly longer breaks in lava eruption. Unlike the limburgites, the olivine-phyric lavas rarely form elongate pillow tubes, nor do they commonly grade into fragmented, disrupted flows. This, combined with their lateral persistence suggests seafloor eruption on moderately shallow palaeoslopes, possibly between periods of major fault activity.

Petrographically, the olivine-phyric, hyalopilitic lavas are similar both in their mineralogical composition and quenched textures to the limburgite lavas. Olivine forms 11.5% of the mode and ranges from 1mm to 0.07mm phenocrysts and groundmass grains respectively. Olivine phenocrysts are euhedral and sometimes skeletal indicating rapid equilibrium crystallisation. Globuloclusters of up to six phenocrysts occur, suggesting partial olivine accumulation. The groundmass is fine-grained with acicular augite, up to 52% of the mode, entrained within brown interstitial glass, forming an hyalopilitic to felted texture. Clinopyroxene blades range from 0.1 to 0.3mm long, are highly acicular with length to breadth ratios up to 12. Flow banding forms a pseudotrachytic texture. Interstitial glass is often partially devitrified and replaced by palagonite or clay minerals. Vesicles are common, especially near the top of the pillows, and on average, form 4.5 to 8% of the mode. They range from 0.2 to 0.4mm in diameter, are sphericle and empty.

4.4.4 Massive, Olivine-Phyric Flows

Although not as common as in the Lower Lava Group, massive flows also occur in the Upper Lavas. Figure 4.9 illustrates a section through a 62m thick unit that dips at 60^{o} toward 215N, that crops out in the Kouspari area 0.64km west of Kapillio. Exposure of the flow is obscured towards the north, but can be traced almost continuously south where it is faulted up to a high angle and wedges out between an underlying breccia deposit and overlying

manganoan shales and lavas (Plate 4.18). In the Kouspari area where the massive flow is at its thickest, it is mineralogically bimodal with an olivine-phyric base and aphyric top.

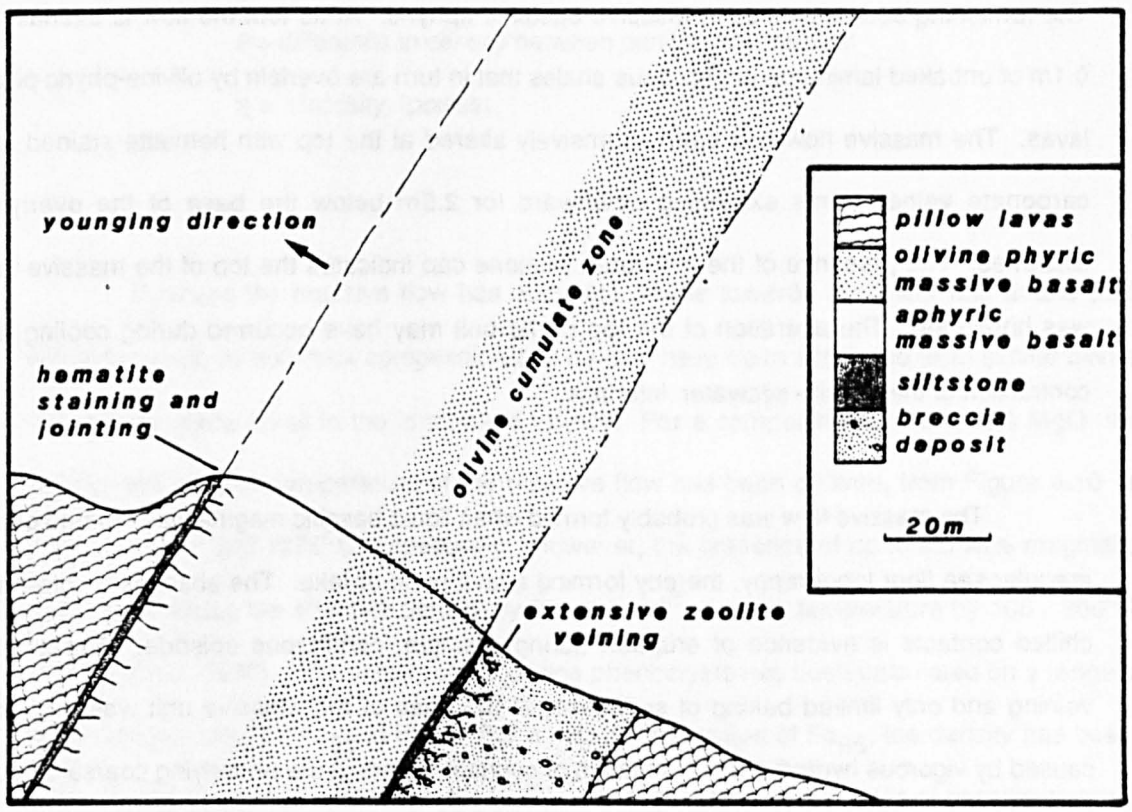

Figure 4.9 Section of cumulate olivine, massive lava flow, dipping at 60^{0} toward 215N. The base chills against baked clastic sediments, the top of the flow is altered and has hematite staining and jointing, and is overlain by a laminated shale unit.

The massive basalt flow is fine grained at its base and grades upwards into massive dolerite towards the centre of the unit. At its base, the massive lava overlies 0.2 to 0.3m of baked, zeolite veined, laminated argillaceous mudstones and hyaloclastic laminated sandstones that grade upwards from an 8m thick pink weathering breccia. These sediments are also incorporated in the base of the massive flow as 0.3m long rafts. The rock is altered, weathers pink-brown and has a friable surface. Euhedral olivine grains, 0.5 to 2.0mm in diameter (mean of 1.5mm) have an almost constant abundance of 15% of the mode until, at 30m above the base of the flow, it rapidly decreases from 12% of the mode to zero over 0.75m. The remaining 30m thickness of massive basalt is aphyric. At its top, the flow is overlain by 0.1m of unbaked laminated argillaceous shales that in turn are overlain by olivine-phyric pillow lavas. The massive flow has been extensively altered at the top with hematite stained and carbonate veined joints extending downward for 2.5m below the base of the overlying siltstones. The presence of the laminated siltstone cap indicates the top of the massive lava was horizontal. The alteration of the top of the unit may have occurred during cooling and contraction of the basalt - seawater interface.

The massive flow was probably formed when liquid basaltic magma was erupted on an irregular sea floor topography, thereby forming a lava pond or lake. The absence of internally chilled contacts is evidence of eruption during a single, continuous episode. The zeolite veining and only limited baking of sediments at the base of the massive unit was probably caused by vigorous hydrothermal circulation of connate waters in the underlying coarse breccia deposit, rapidly dissipating the temperature gradient at the contact. The time taken for the massive flow to effectively solidify has been estimated from the settling rate and distance travelled by olivine phenocrysts. From Figure 4.9 the aphyric portion of the unit is 32.3m compared with 29.7m for the olivine-phyric, lower half. The laterally continuous horizon above which olivines are absent is evidence of stagnant magma conditions during cooling. By using Stokes Law, which describes the settling velocities of approximately spherical particles in viscous fluid mediums, it is possible to estimate the terminal velocity of euhedral olivine pheocrysts in a basaltic magma (Shaw, 1969).

Stokes Law states that:

$$V = \frac{2\,gr2\ (\Delta P)}{9\eta}$$

where V = terminal settling velocity (cm sec^{-1})

r = partical radius (cm)

g = graviation acceleration (cm sec^{-1})

P = difference in density between partical and medium

η = viscosity (poises)

Because the massive flow has cumulate olivine towards the lower half and is thus heterogeneous, its bulk rock composition and density have been estimated from similar olivine microphyric pillow lavas in the immediate vicinity. For a composition of 12.1 wt% MgO the density and eruptive temperature of the massive flow has been derived, from Figure 4.10 at 2.705 gm cm^{-3} and 1275^{o}C respectively. However, the presence of up to 2.5 wt% magmatic water may reduce the effective density by 0.1 gm cm^{-3}, and the temperature by 100 - 200^{o}C (Sparks *et. al.*, 1980). The density of the olivine phenocrysts has been calculated on a range of compositions between Fo_{80} to Fo_{90}. For a mean composition of Fo_{85}, the density has been taken as 3.3955 gm cm^{-3} (Deer *et. al.*, 1966). Although viscosity estimates of basaltic magmas are highly contentious and range between 3000 poises for the parental, primitive basalt (Hess, 1960; Wager and Brown, 1968) to 100 and 1000 poises (Goode, 1976), experimental data on mid-ocean ridge basalts indicate a range from 50 to 500 poises (Shaw, 1972; Murase and McBirney, 1973; Fuji and Kushiro, 1977; Sparks & Pinkerton, 1978). Taking Sparks *et. al.* (1980) and Huppert & Sparks (1980) viscosity of 300 poises for primitive MgO rich basaltic magmas and by calculating the settling velocity, the time taken to drop through d, the thickness of the aphyric layer is assumed to approximate the crystallisation period of the magma, E.

Based on a viscosity of 300 poises, taken as most representative of primitive MORB, the crystallisation period for the massive flow is approximately eleven days.

4.4.5 Feeder Dykes and Eruptive Edifices

Cross cutting dykes with 040N and 120N trends, similar to ones in the Lower Lava Group, crop out in the Upper Lavas in the vicinity of Kapillio. These late dykes have 0.1m glassy margins, are 1 to 1.5m wide, bifurcate along strike and are often observed cutting breccia deposits.

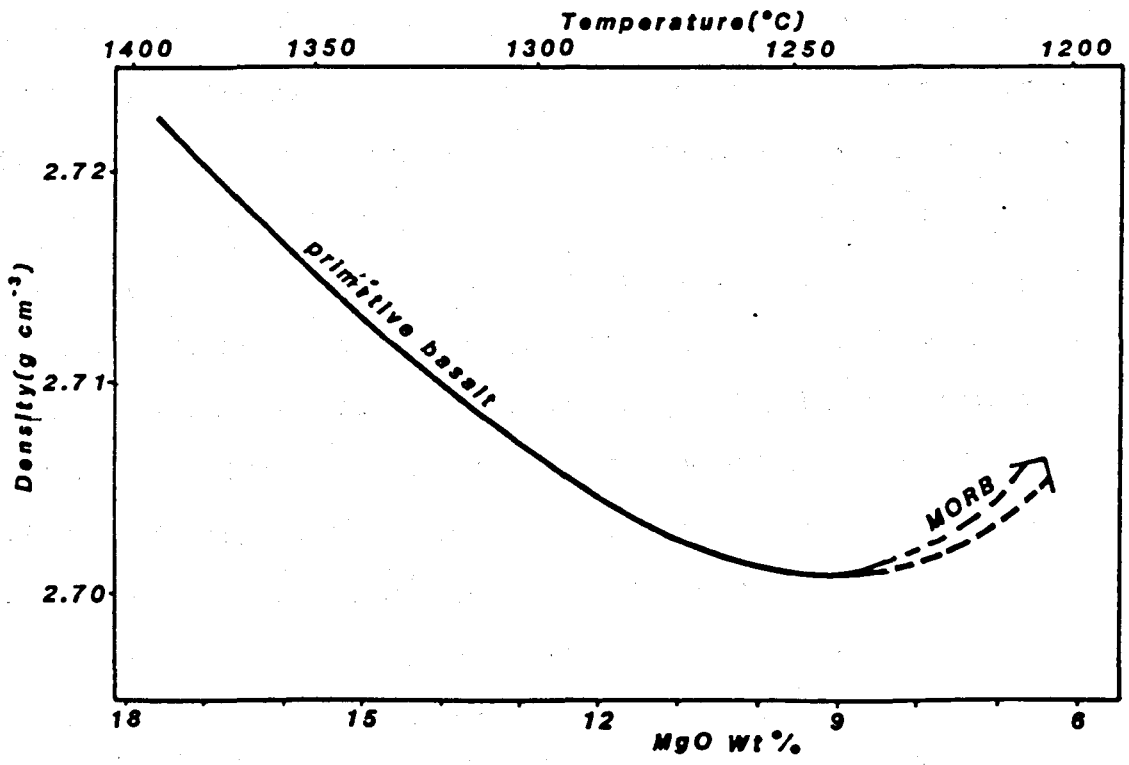

Figure 4.10 Correlation between density, temperature and Wt % MgO, taken from Sparks & Huppert (1983).

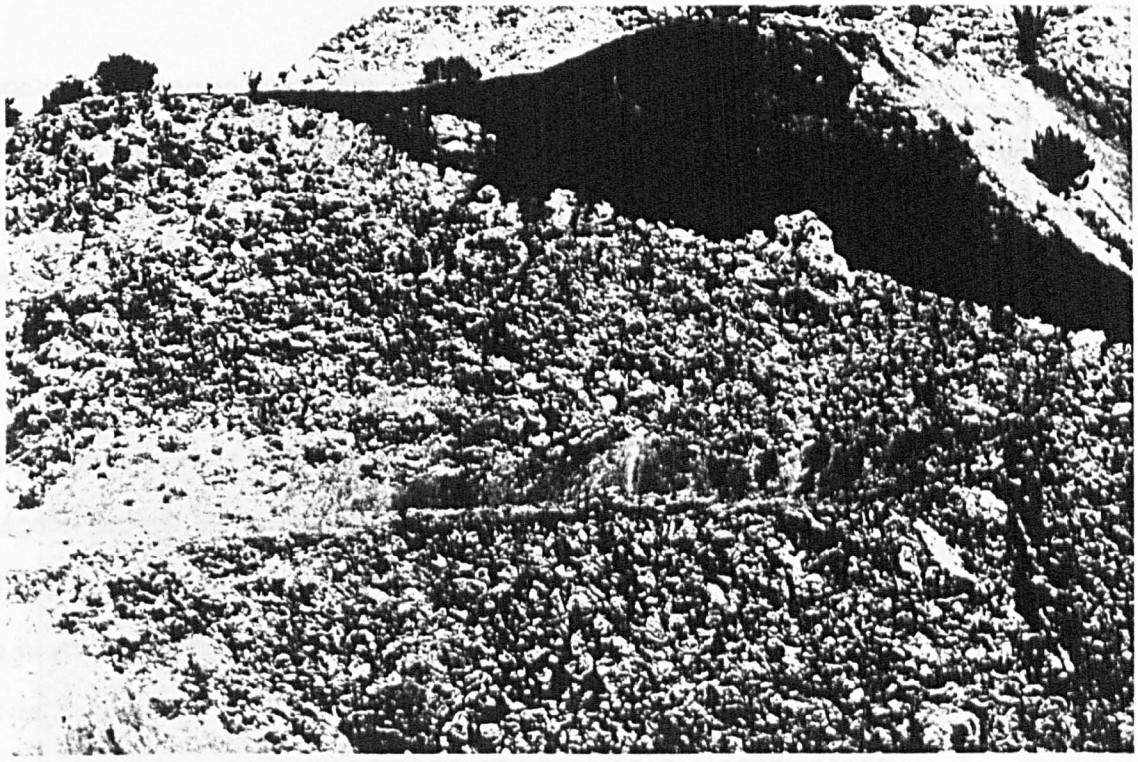

Plate 4.17 Manganoan sediments (umbers) interbedded with olivine phyric, hyalopilitic lavas in the Mathikaloni area.

Plate 4.18 Olivine phyric, massive lava flow wedges out between an underlying coarse grained, clastic breccia deposit and an overlying laminated silt stone unit and pillow lavas.

Figure 4.11 is a sketch of a volcanic feeder and edifice that crops out near Kapillio [970597] in which dykes intrude faults and indicate a close relationship between magmatism and tectonism. The feeder dyke thins upwards from 2.2m to 1.2m over 75m and terminates as a splay of micro-dykes, veins and associated pillow lavas. The top of the feeder dyke also coincides with a 0.5m thick unit of breccia, coarse sandstone and laminated siltstone that indicates both a horizontal palaeo-seafloor as well as an hiatus in lava eruption. The edifice is formed from small 0.3 to 0.8m diameter glassy pillow lavas, many of which are elongated and brecciated indicating eruption down a palaeoslope. At the base of the edifice, elongated pillows dip at 5^{o} away from the core of the feeder, with respect to the palaeohorizontal. The pillow lavas grade upward into increasingly brecciated, clast supported units, possibly *in situ* collapse breccias that have a weak imbrication dipping at 31^{o} with respect to the palaeohorizontal.

Figure 4.12 illustrates three stages in the evolution of the volcanic edifice; (i) following an indeterminate period of volcanic quiescence, basaltic magma is emplaced along a fault plane forming a fissure eruption, (ii) initial eruption on the seafloor forms small glassy pillow lavas that dip at 5^{o} away from the fissure, (iii) continuous eruption forms a conical edifice 25m high and approximately 43m in radius, with elongated and brecciated lavas forming a slope of 31^{o}.

Petrographically, the feeder dykes are identical to the glassy pillow lavas. They are generally olivine microphyric with euhedral phenocrysts 0.2 to 0.8mm in diameter and set in an hyalopilitic to felted groundmass of pyroxene (augite) and interstitial glass. The proportion of glass varies from 30% at the margins to less than 1% in the centre of the thickest dykes. Alteration of the dykes varies inversely with the proportion of glass. Vitreous margins are generally intact with only moderate devitrification, however dyke centres are commonly pervasively altered with glass replaced by illite and smectite and olivine by iddingsite. Augite remains intact and small 0.08 to 0.2mm vesicles are filled with zeolites.

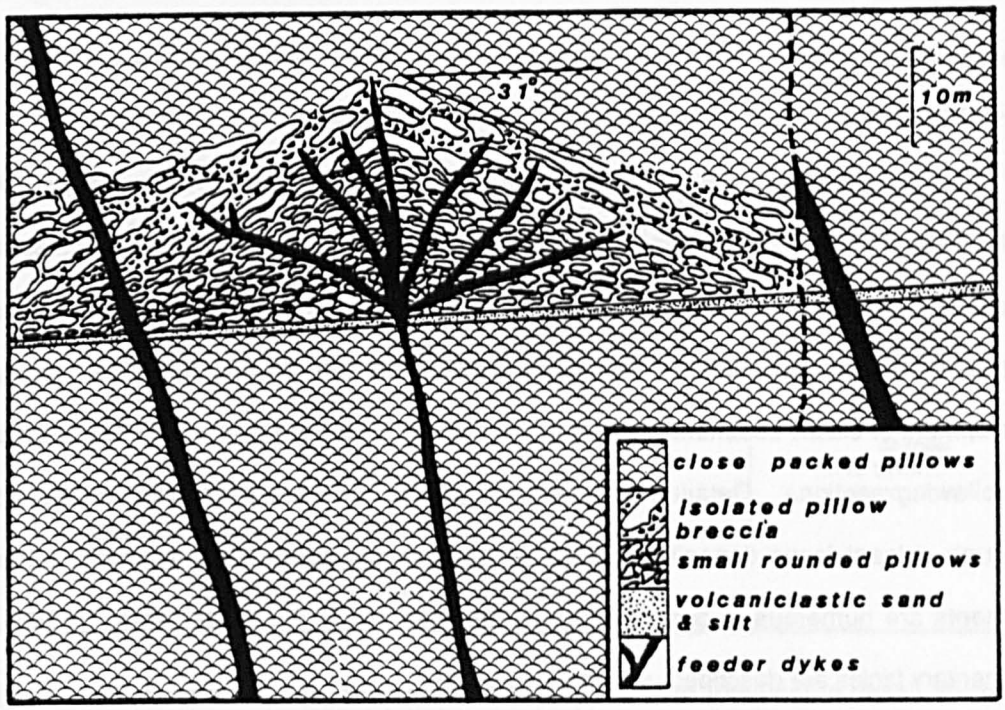

Figure 4.11 Sketch section of a volcanic edifice and feeder dykes that crop out in the Kapillio area. The edifice forms a pile of pillow lavas that become increasingly elongated and brecciated up section, and that have a palaeo-angle of repose of 31°.

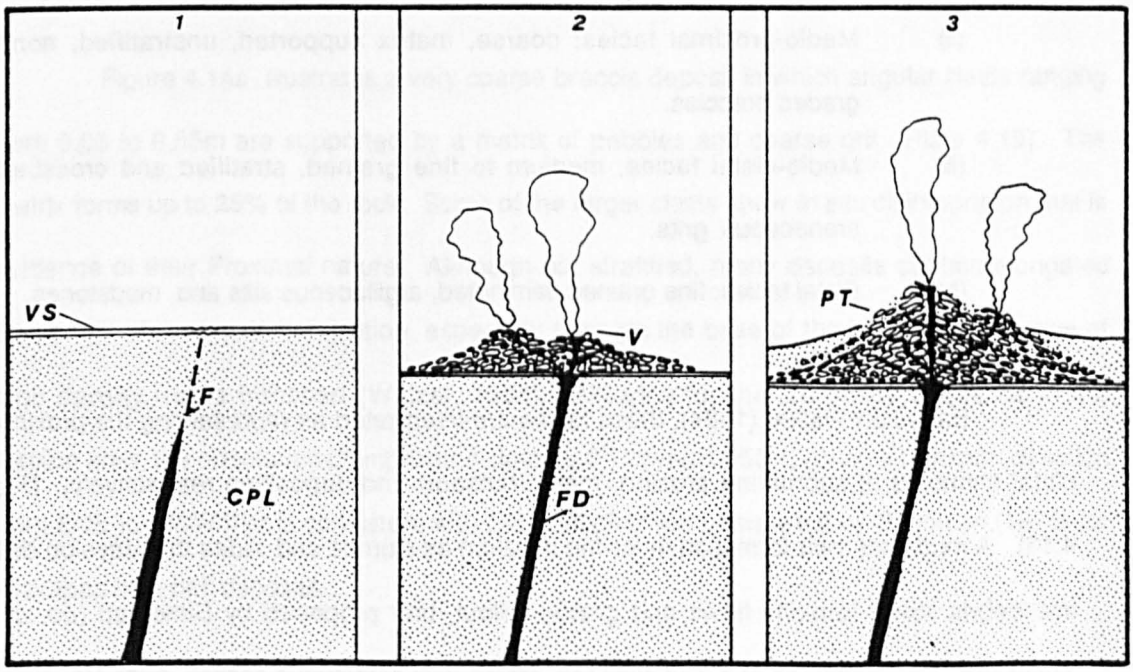

Figure 4.12 Postulated three stages in the development of a volcanic edifice. (1) Fault localises intrusion of a feeder dyke that egresses to the surface, (2) Eruption of small rounded pillow lavas from a number of minor vents and feeders, (3) Eruption of elongated pillow tubes, some of which disintegrate down unstable slopes, and partial burial of the volcanic edifice by lavas from neighbouring vents.

4.5 Interlava, Clastic Sediments

4.5.1 Introduction

Interbedded with the Lower and more especially, the Upper Lava Groups are a variety of clastic sediments, predominantly volcaniclastic in origin. The provenance, transport and deposition of similar deposits occurring throughout the Arakapas fault belt has been described as transform fault deposits by Simonian (1975). In the WLFC, the most substantial development of clastic sediments occurs in the Kapillio area from where they are described in the following sections. Detailed sedimentary graphic logs are presented in Appendix 3. Although volcaniclastic deposits in the Kapillio area are predominantly mafic, ultramafic fragments are numerous in coarse interlava breccias in the Akrounda area. In total, four sedimentary facies are described, summarised below.

(i) Proximal facies; coarse, matrix supported, unstratified, reverse graded breccias.

(ii) Medio-proximal facies; coarse, matrix supported, unstratified, normally graded breccias.

(iii) Medio-distal facies; medium to fine grained, stratified and crossbedded arenaceous grits.

(iv) Distal facies; fine grained, laminated, argillaceous silts and mudstones.

Based on Walker (1984), these facies are interpreted as representing the proximal to distal members of submarine erosion, mass transport and deposition respectively, (Figure 4.13). A model for their formation involving initiation as slumps and slides that develop distally into debris flows, turbidity flows and gravity fallout, first proposed by Simonian (*op. cit.*) is discussed. Basin analysis of a well exposed, structurally continuous section in the Vouni area, 0.5km east of Kapillio, illustrates a history of both fault controlled basin development and localised volcanic eruption.

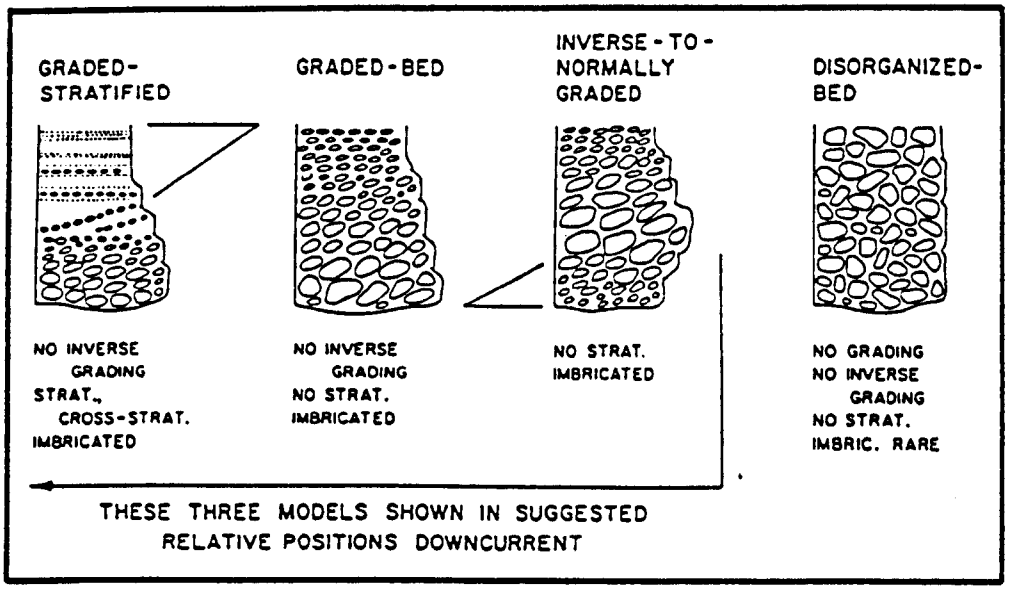

Figure 4.13 Four models for the various facies types from Proximal to distal, showing their relative, down current positions, see text for details (after Walker, 1984).

4.5.2 Proximal Facies

Figure 4.14a illustrates a very coarse breccia deposit in which angular clasts ranging from 0.05 to 0.55m are supported by a matrix of pebbles and coarse grit, (Plate 4.19). The matrix forms up to 25% of the rock. Some of the larger clasts show *in situ* disintegration that is evidence of their Proximal nature. Although not stratified, many deposits contain elongated clasts that show a-axis imbrication, especially towards the base of the breccias, indicative of high density, mass transport (Walker, 1984). Allowing for the dip of the sequence in the Kapillio area, the orientation of imbricated clasts is 5^{o} towards 050N, giving a transport direction from ENE to WSW that is consistent with the E-W direction interpreted by Simonian (1975) for Arakapas fault belt deposits.

Although it is often normally graded, the Proximal facies commonly exhibits reverse grading near the base. Large boulders up to 0.55m in diameter occur up to 1.5m above the base where they are supported by a mixture of matrix and smaller clasts that increase in size

downwards. Occasionally large boulders are found at the top of Proximal facies units where they protrude, forming an irregular surface to deposits. Such reverse grading, described in detail by Fisher (1971) is due to shear in a high viscosity matrix at the base of a debris flow; the height above the base of the flow of the largest diameter clasts depending on the speed, viscosity and matrix content during transport (Dott, 1963; Middleton and Southard, 1984). The reverse or ungraded portion of the Proximal facies can exceed 50%, the remaining upper portions usually being normally graded, with clasts decreasing in size to 5 cm, supported by a matrix of medium to fine-grained grit. Although only a small number of channelised scours were observed, their ENE-WSW trends are similar to the imbrication directions described above. Where the Proximal facies overlies fine-grained, laminated siltstones, rip-up clasts, flame structures and drop stone features are often observed.

In one Proximal facies unit (log 5), partially disrupted dykes are preserved, moderately intact, indicating only moderate internal deformation of the unit during transport and deposition, characteristic of slump or slide deposit (Walker, 1980; Helwig, 1970). The distribution of the Proximal facies is highly variable with units wedging out laterally from 3m to zero thickness over 50 m. More commonly, the Proximal facies is observed grading into finer grained breccias of the Medio-proximal facies, described below in Section 4.5.3. Coarse Proximal facies units are also observed interbedded with the other three facies types (Figure 4.14a), suggesting more than one apex of sediment influx.

Morphologically the Proximal facies is sheet-like, indicating unconfined, non-channelised deposition. The composition variation of the Proximal facies is summarised in table 4.1. Although everywhere polymict, in the Kapillio area it is comprised of 46 to 68% of pillow lava basalt, 46 to 28% greenschist dolerite of sheeted dyke origin and 0 to 4% isotropic gabbro. Deposits that are rich in dolerite clasts are also rich in gabbro (Plate 4.20). Simonian (1975) describes similar deposits derived from an uplifted block of sheeted dykes forming Mt. Muttitou Dhios, 3km southwest of Kalokhorio. In the Akrounda area, Proximal facies breccias contain ultramafic clasts, including mantle derived harzburgites.

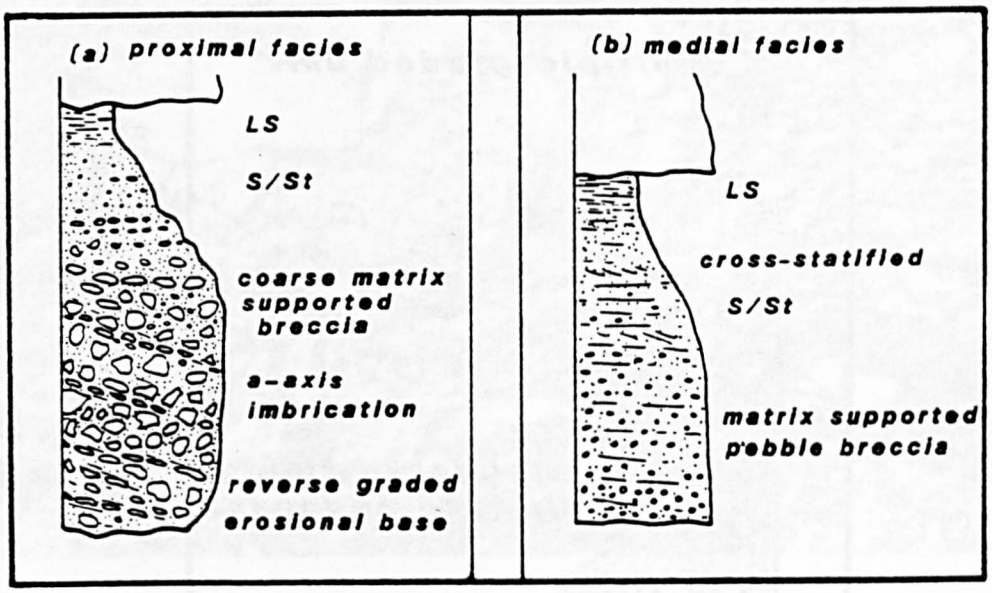

Figure 4.14 Graphic logs showing the differences between the proximal and medial facies. Note the reverse grading of the proximal facies indicating debris flow transport

4.5.3 Medio-proximal Facies

Figure 4.14b illustrates a generalised profile of a matrix supported breccia deposit. This, the Medio-proximal facies, has a matrix of very fine sand and silt that forms between 15 and 22% of the mode Clasts are very angular, unsorted and range from 0.15 to 0.02m in diameter. Unlike the Proximal facies, the Medio-proximal facies is normally graded throughout, but is most prominant in the upper 33% of individual units, Plate 4.21. a-axis imbrication forming a pseudo-stratification is common and gives a consistent direction of transport from east to west. Figure 4.15 illustrates a profile of a multiple breccia unit in which a number of coarse bands stagger the overall fining upwards sequence, indicating repeated input surges of coarse material. This suggests a low frequency mechanism, possibly earthquake vibration and acoustic fluidisation (Melosh, 1983), that triggered and supported multiple sediment surges. Unlike the Proximal facies, coarse, Medio-proximal facies units have erosional bases, indicating turbulent, high energy deposition.

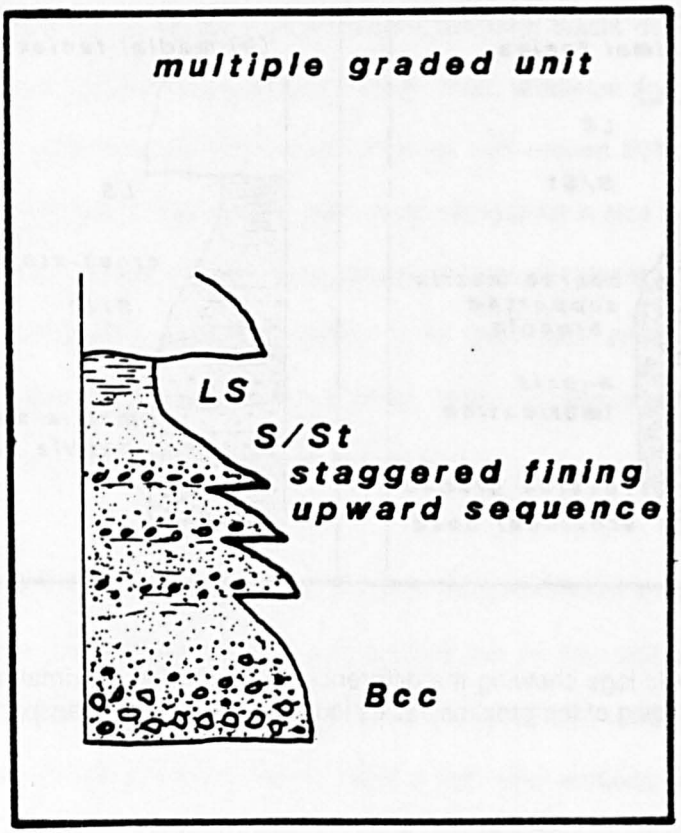

Figure 4.15 Detail of graphic log showing a multiple graded unit of repeated coarse to fine units, capped by a laminated silt stone unit. *LS* = laminated silt stone: *S/St* = sand stone: *Bcc* = breccia .

The distribution of the Medio-proximal facies is laterally variable. Although individual beds could not be traced extensively along strike, it is evident from detailed logging that 1.5m thick units wedge out over 50 to 60 m. However, since sediment transport directions are generally east to west and the Medio-proximal facies units are only observed pinching out laterally from north to south, their full axial extent is unknown. Morphologically, the Medio-proximal facies is sheet like, with a larger width to thickness ratio than the Proximal facies.

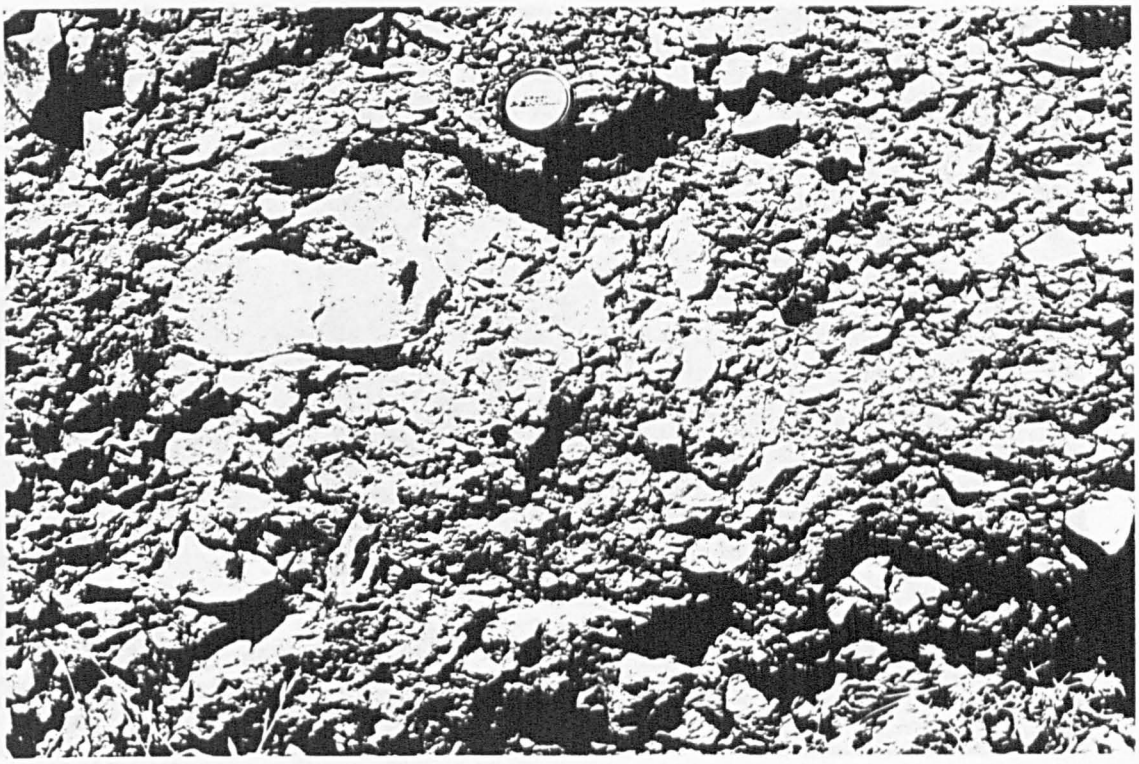

Plate 4.19 Proximal facies, very coarse, clast supported massive breccia deposit.

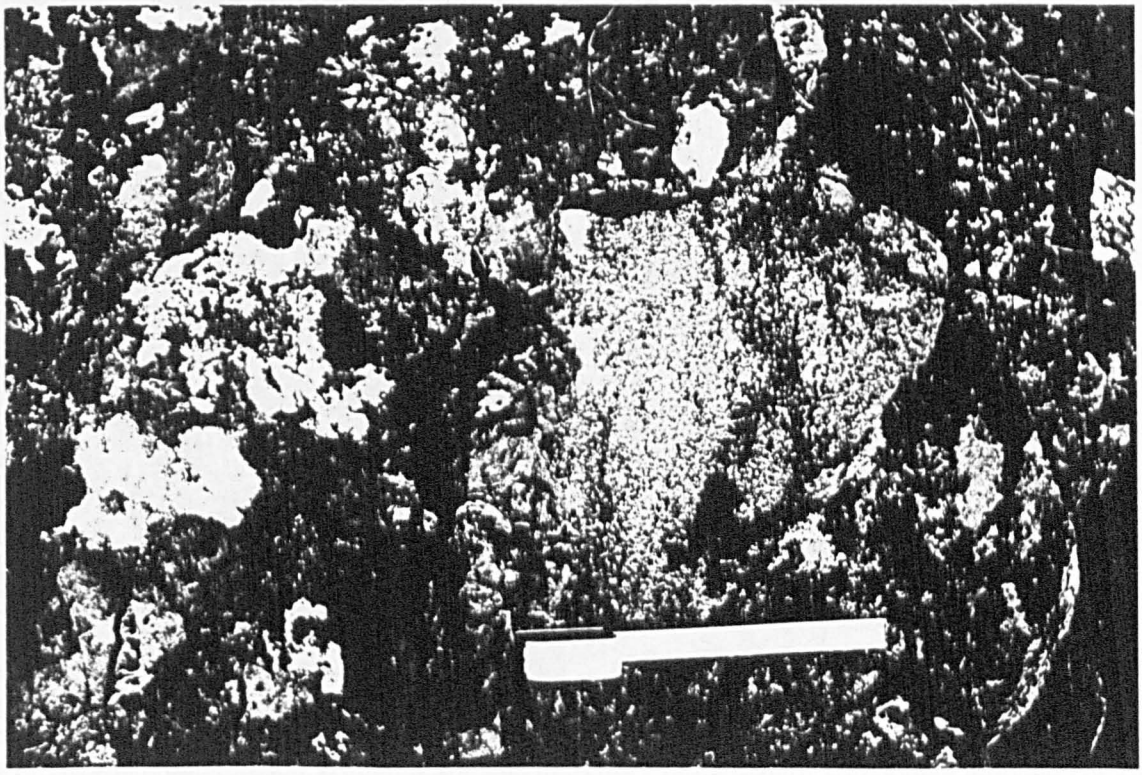

Plate 4.20 Large (0.5 to 1.5m) boulders of isotropic gabbro within very coarse, Proximal breccia deposit, Kapillio.

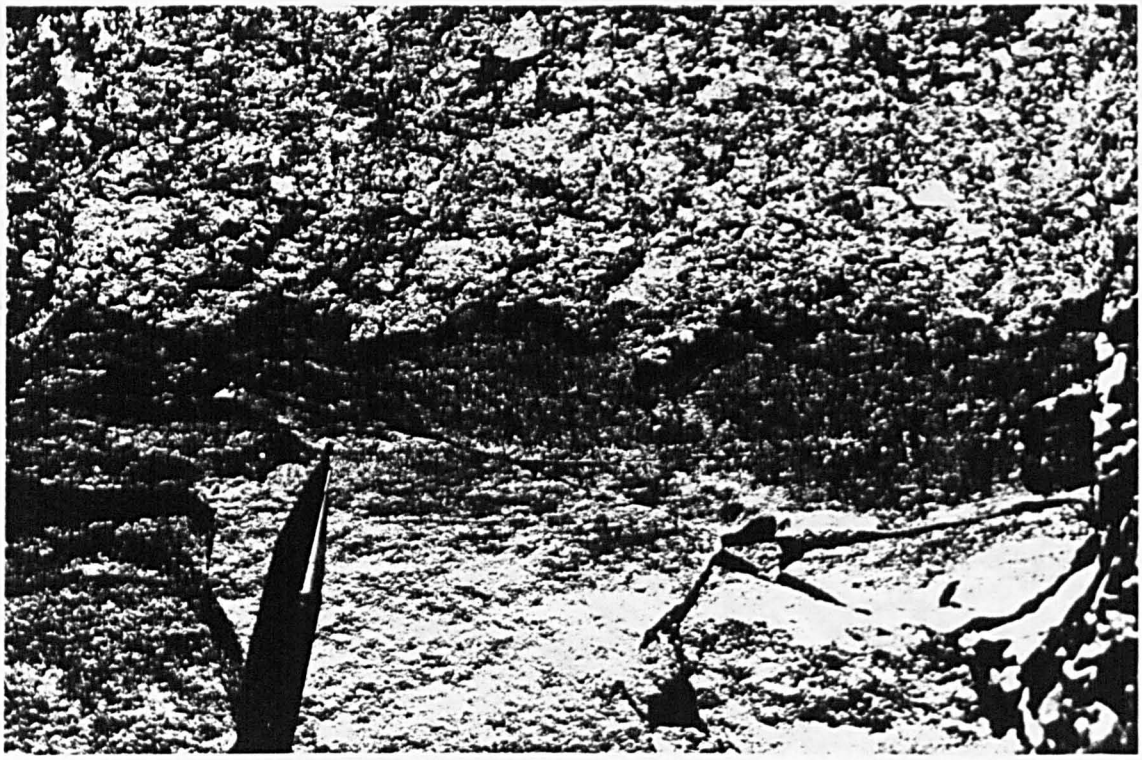

Plate 4.21 Normally graded, fining upward unit of the medium grained, Medio-proximal facies, showing basal scour and fill features.

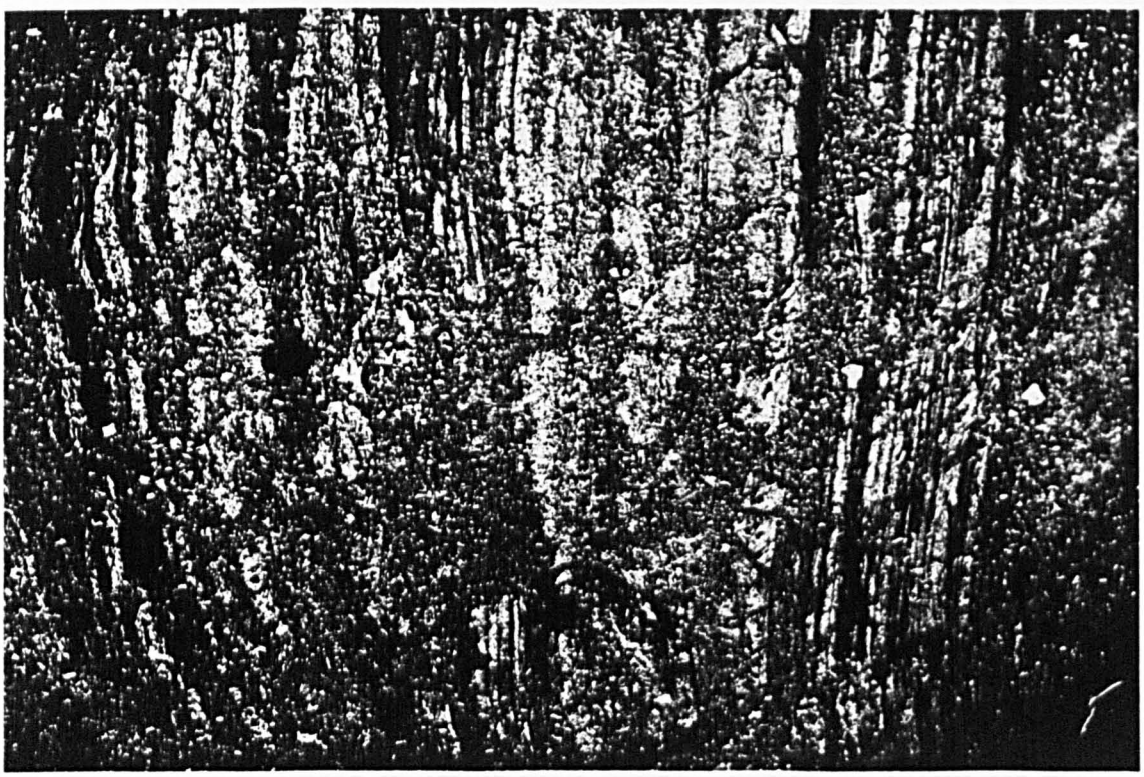

Plate 4.22 Well stratified, laterally continuous, medium grained arenaceous and volcaniclastic grits of the Medio-proximal facies that have been tilted to near vertical at a point 2km south of Kapillio, along the southern margin of the WLFC.

Where complete, the Medio-proximal facies vertically into pebbles and grits, often capped by laminated silts of the distal facies. The latter are often eroded by coarse, overlying deposits. Compositionally, the Medio-proximal facies is identical to the Proximal facies, either consisting predominantly of pillow lava fragments or greenschist dolerite and isotrophic gabbro clasts. However, the matrix in the former facies is both finer-grained and contains a higher fraction of argillaceous material.

4.5.4 Medio-distal Facies

In the Hussein Bey area [970531], 1.5km south of Kapillio, 0.1 to 0.6m thick graded units, of medium to fine grained arenaceous grits and laminated silts are interbedded with pillow lavas of the Upper Lava Group. Plate 4.22 illustrates a thick unit and well bedded, stratified and graded arenaceous grits, dipping steeply towards the south west. Grain sizes range from very coarse grit (2 to 1mm) to fine silt (less than 0.1mm). Although not matrix supported a 15% of silt and hematised mud surrounds angular and poorly sorted clasts, indicating deposition by turbidity flow (Middleton and Hampton, 1976; Hampton, 1972). Although coarser grit units have some clast imbrication, the most characteristic feature of the Medio-distal facies is its stratification. Although laminar at their base, beds tend to have fine cross stratification of the finer portion, (Figure 4.16) indicating a transition to turbulent flow conditions, (Hampton, 1972). Assuming a sub-aqueous flow density of 103 poises, turbulent conditions would be expected in velocities in excess of 3m sec^{-1} (Middleton and Southard, 1984). Like the coarser facies described above, the Medio-distal facies grits have erosional bases, occasionally observed with siltstone rip-up-clasts. Plate 4.23 illustrates penecontemporaneous deformation of a 1.5m thick sequence of multiple graded, medium to fine grained grits, overlain by 0.5m of laminated argillaceous siltstones. Laminated silts within the sequence have been plastically domed upwards, forming an envelope to coarser grits that have been chaotically disrupted. A possible mechanism involving rapid dewatering and subsequent slumping was first attributed to similar soft sediment deformation in coarse arenites from the Pre-cambrian, Torridonian formation of N.W. Scotland (Shelly *et.al.*, 1963); such structures are also indicative of fast sedimentation

rates. Interbedded within the Medio-distal facies grits are ferro-manganoan argillaceous sediments (umbers). These dark brown, massive and laminated deposits are found close to and lying directly upon uneven pillow lava surfaces. Interbedded grits occur towards the top of umbiferous units, suggesting a depositional history involving pillow lava eruption, hydrothermal exhalation and deposition of umbers followed by arenaceous turbidity deposits.

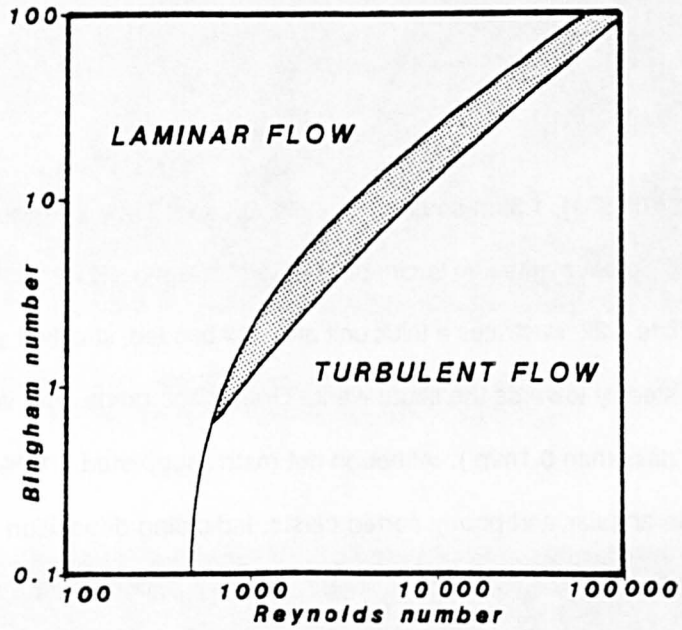

Figure 4.16 Relationship between the Bingham number (ie.plasticity) and Reynolds number, showing fields for laminar and turbulent flow.

Unlike the coarser Medio-proximal and Proximal facies described above, the Medio-distal facies forms laterally continuous sheets. Individual beds up to 0.2m thick, can be traced over several hundred meters along strike. Such lateral continuity suggests shallow palaeoslopes (as little as 0.05^{o}, Middleton and Hampton, 1984) consistent with the grits being moderately distal members of the coarser debris flows and slides of the Medio-proximal and Proximal facies respectively. In the Hussien Bey area, the grits were found to be predominantly volcanoclastic. Petrographically the grits are medium to fine grained, poorly-sorted and moderately well stratified. Clasts are extremely angular, generally range from 0.03 to 2mm in diameter and are set in a matrix of very fine grained, haematised silt and clay. Although the matrix forms between 16% and 25% of the mode, the sediments are typically clast supported. Rip-up clasts of dark brown, manganoan mudstone form flakes distributed throughout the

coarser grits. Lithofragments of volcanic glass, often altered to clay and palagonite, as well as hyalopilitic basalt, consititute the bulk of the clasts. Highly angular shards and acicular splinters, 0.2mm wide by 1.5mm long suggest grain transport was both cushioned and relatively short. These hyalopilitic lithofragments are identical to the limburgite lavas of the Upper Lava Group, described in Section (4.4.2).

The predominantly Upper Lava provenance of the Medio-distal facies is supported by the presence of crystal fragments that include augite, olivine, plagioclase and orthpyroxene, in decreasing order of abundance (Plate 4.24). Olivine grains are subhedral to anhedral and generally serpentinised. Augite and orthopyroxene grains are fresh, but plagioclase is often turbid. The rare presence of rutile chlorite, zoisite and zeolite grains indicates erosion of zeolite and greenschist facies sources. hematite is abundant, especially in the matrix where it forms from the breakdown of granular magnetite. Calcite is present both as a replacement of serpentinised olivine and as an authigenic mineral filling grain boundary cavities. No detrital carbonate occurs, consistent with formation of the Troodos massive beneath the carbonate compensation depth (C.C.D) (Robertson & Hudson, 1974).

Unexpectedly, quartz grains were found in the volcaniclastic grits in the Hussein Bey area, where they constitute 1.6% of the mode The quartz grains are clear, rounded with serrated margins and internal cracking, and are well sorted ranging from 0.1 to 0.2mm in diameter. The shape and sorting of quartz grains indicates a greater degree of transport than the basaltic grains, and are hence more distal. However, free quartz is rare in both the WLFC and the Troodos massif, occuring only in evolved trondhjemites and occasionally as a metamorphic phase. Terrigenous sediments are reportedly absent from the Troodos massif (Wilson, 1959; Bear, 1960; Gass, 1960 ; Mores & Vine, 1971), but do occur in the Moni and Mamonia formations that overlie the ophiolitic basement, (Henson *et. al.* ,1949; Lapierre, 1968; Robertson, 1977). If the quartz grains are terrigenous in origin, then they may have a similar origin to the quartzitic lithologies in the formations mentioned above. The presence of such terrigenous quartz in the volcaniclastics of the WLFC is problematic since it may involve

transport across a destructive margin trench (Robertson *op. cit.*).

Fossiliferous material, although not observed by Simonian from sediments in the Arakapas fault belt, is present in the Hussein Bey area of the WLFC. Sample 181-CY84 contains two fragments of radiolarian tests, a 0.15mm diameter central capsule with radiating spicules, and a 0.2mm fragmented central capsule, (Plates 4.25a and 4.25b), respectively. Although incomplete, the chemical preservation of these silicous, opaline tests is remarkable since they are readily dissolved under alkaline conditions or during even low grade metamorphism. Although the radiolarions could not be identified sufficiently to give any reliable stratigraphic age to the sediments, they do demonstrate deposition under deep marine, pelagic conditions.

In summary, the texture, composition and morphology of the Medio-distal facies indicates deposition under pelagic conditions from locally derived, unchannelised turbidity flows.

4.5.5 Distal Facies

Very fine grained, laminated muds and silts form the distal facies. These orange brown to dark brown sediments were often observed both grading upward from fine grits and as overlying beds to coarse breccia deposits. In contrast to Simonian (*op. cit.*) who describes abundant scour and flute casts, characteristic of high velocity density flows, the distal facies in the WLFC is laminated and stratified (Plate 4.26), indicative of quiet conditions of deposition. Although individual distal facies units rarely exceed 0.15m in thickness, they can be traced over 50 to 60m laterally, where they directly drape over underlying pillow lavas.

Plate 4.23 Medio-distal facies, arenaceous grits with disturbence of bedding, probably slumping, with undisturbed beds both above and below indicating penecontemporaneous deformation.

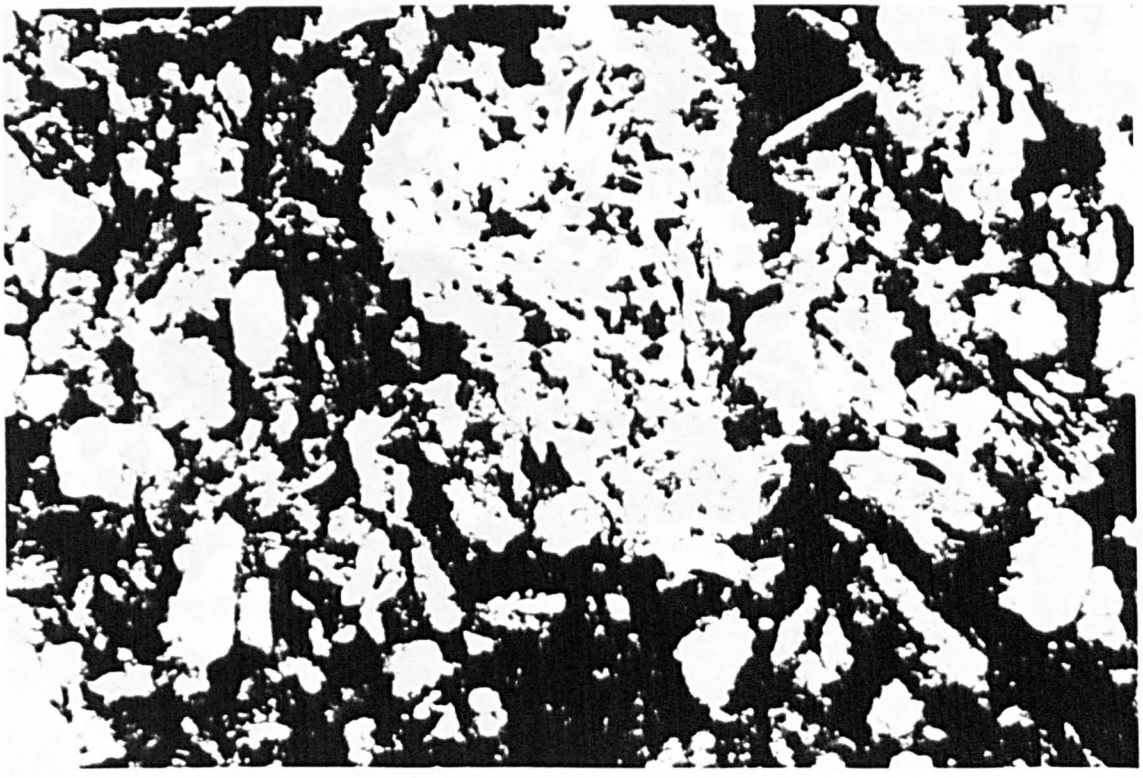

Plate 4.24 Photo-micrograph of arenaceous grit showing fragments of basaltic glass, basalt, dolerite and mafic crystals (olivine and clinopyroxene). × 100

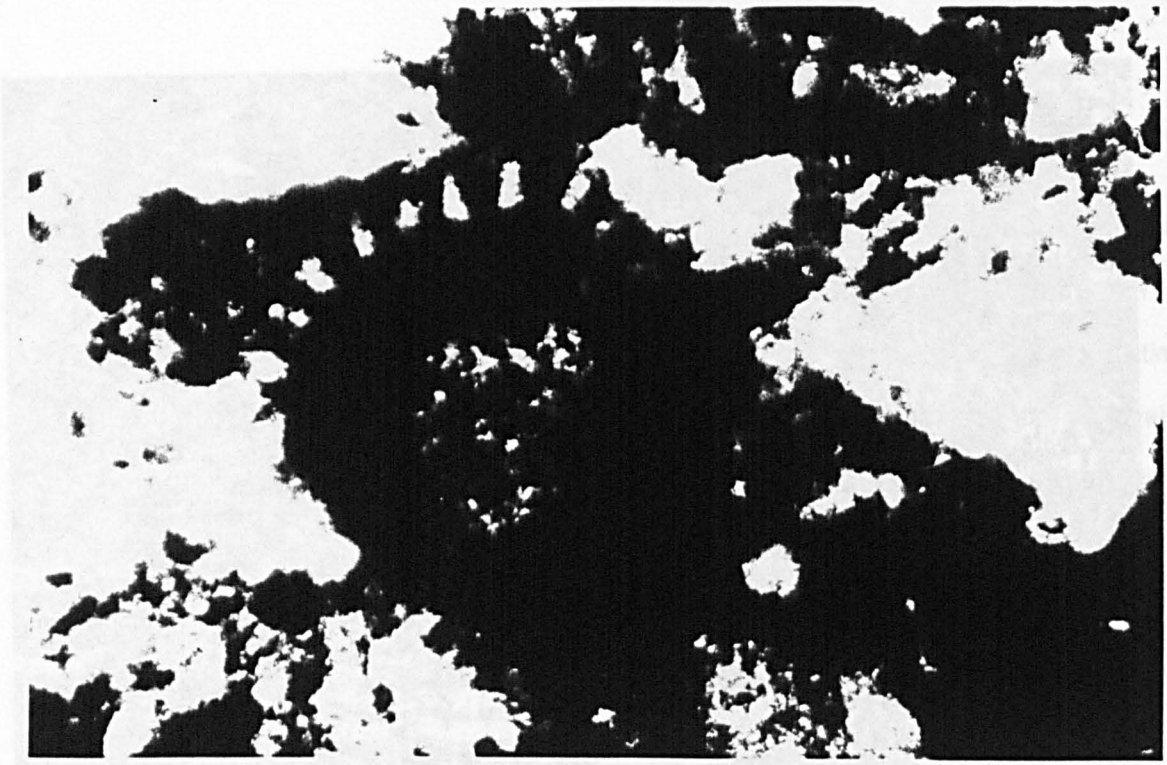

Plate 4.25a Photo-micrograph of a 1.5mm diameter perforated organic test, possibly of radiolarian origen.

Plate 4.25b A 0.2mm fragmented central capsule showing perforated carapace segment, possibly of similar origen to Plate 4.5a.

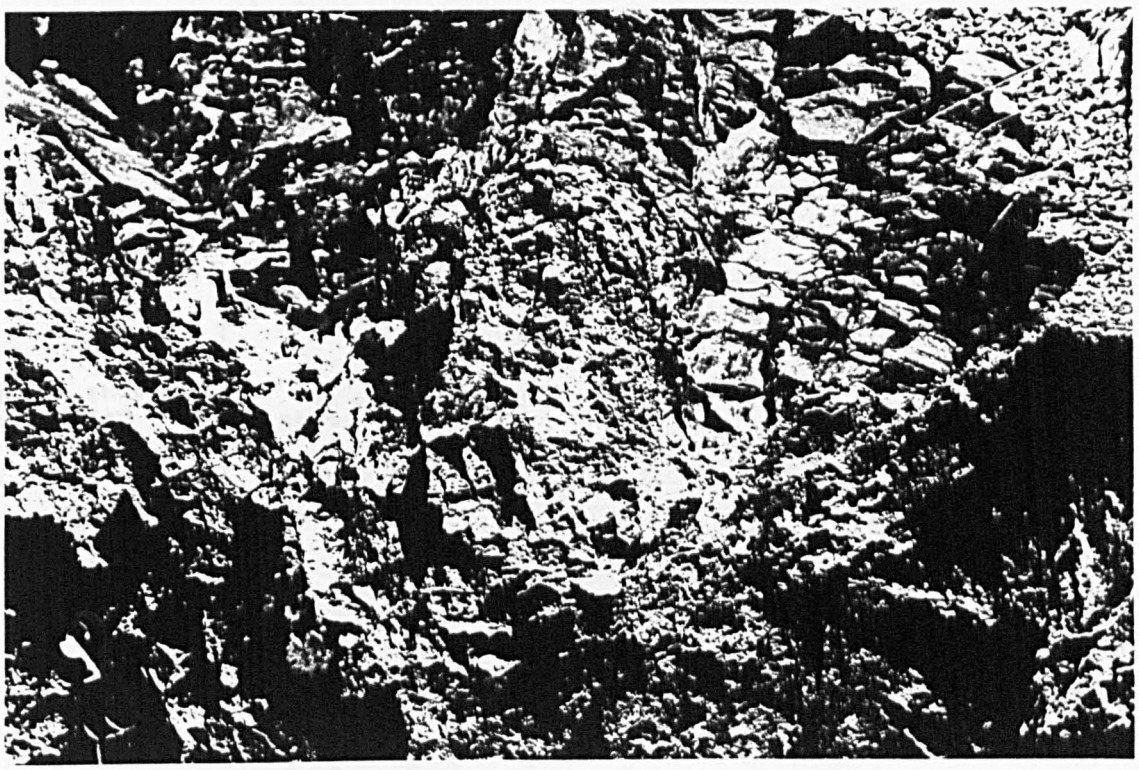

Plate 4.26 Laminated silt stone of the Distal facies drapes directly over pillow lavas indicating low energy deposition.

Due to the very fine grain size and authigenic alteration of clasts, the mineralogy of the Distal facies silts has been difficult to determine. However, the majority of identifiable clasts are of similar volcaniclastic composition to the coarser Medio-distal facies. The characteristic brown colour of the silts is due to authigenic haematisation of disseminated magnetite. The very fine grain size, normal and grading, lateral persistence of individual beds and the phenomenan of sediment draping all suggest fractional deposition by gravity fallout. As distal members of the coarser facies described above, the laminated silts and muds probably settled out of the water column following mass slumping or sliding that threw the finer fraction up as an aqueous suspension.

The relationship between the four facies types is summarised in Figure4.17 (after Hampton,1972; and Simonian 1975).

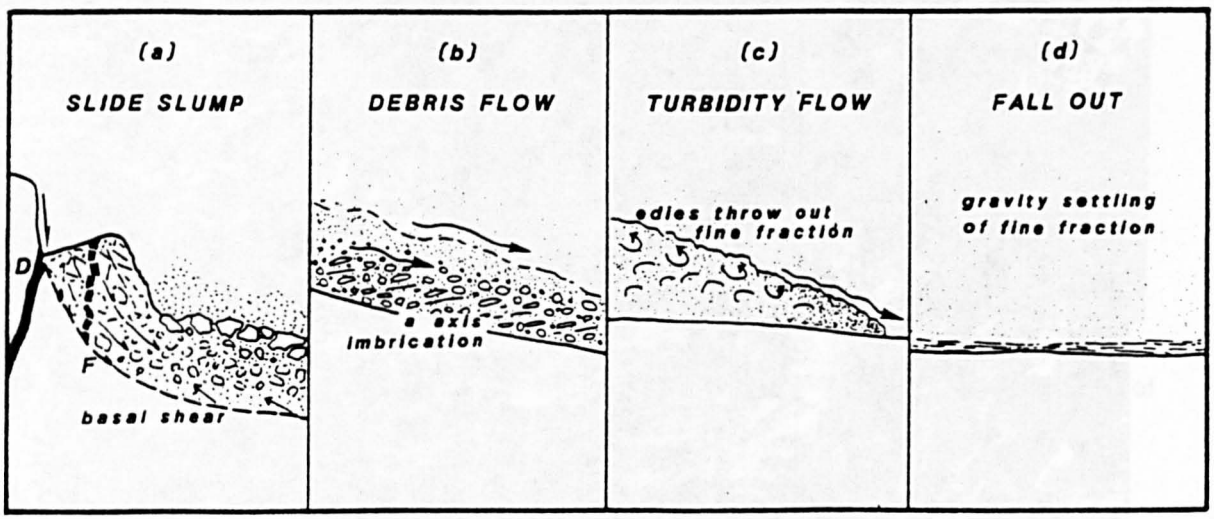

Figure 4.17 Schematic diagram showing the different styles of transport and deposition for the four facies types (a) Proximal, (b) Medio-proximal, (c) Medio-distal, and (d) Distal.

4.5.6 Basin Analysis

Figure 4.18 (the pullout enclosure) illustrates seven cross correlated, logged sections from the Vouni area [967567], summarising detailed logged sections presented in appendix 3. Major unit correlation was verified in the field, although individual beds could not be reliably traced due to their limited exposure and lateral facies variation. Although the Vouni section is not representative of the entire volcanosedimentary sequence, it is approximately coincident with the boundary between the Lower Lava and the Upper Lava groups. From bottom to top, the section has been divided into six lava units and five clastic units, described below. The section was constructed using the top of clastic unit 1, that was found to be almost planar, as a datum .

NW

Figure 4.18 Basin analysis: no vertical exaggeration

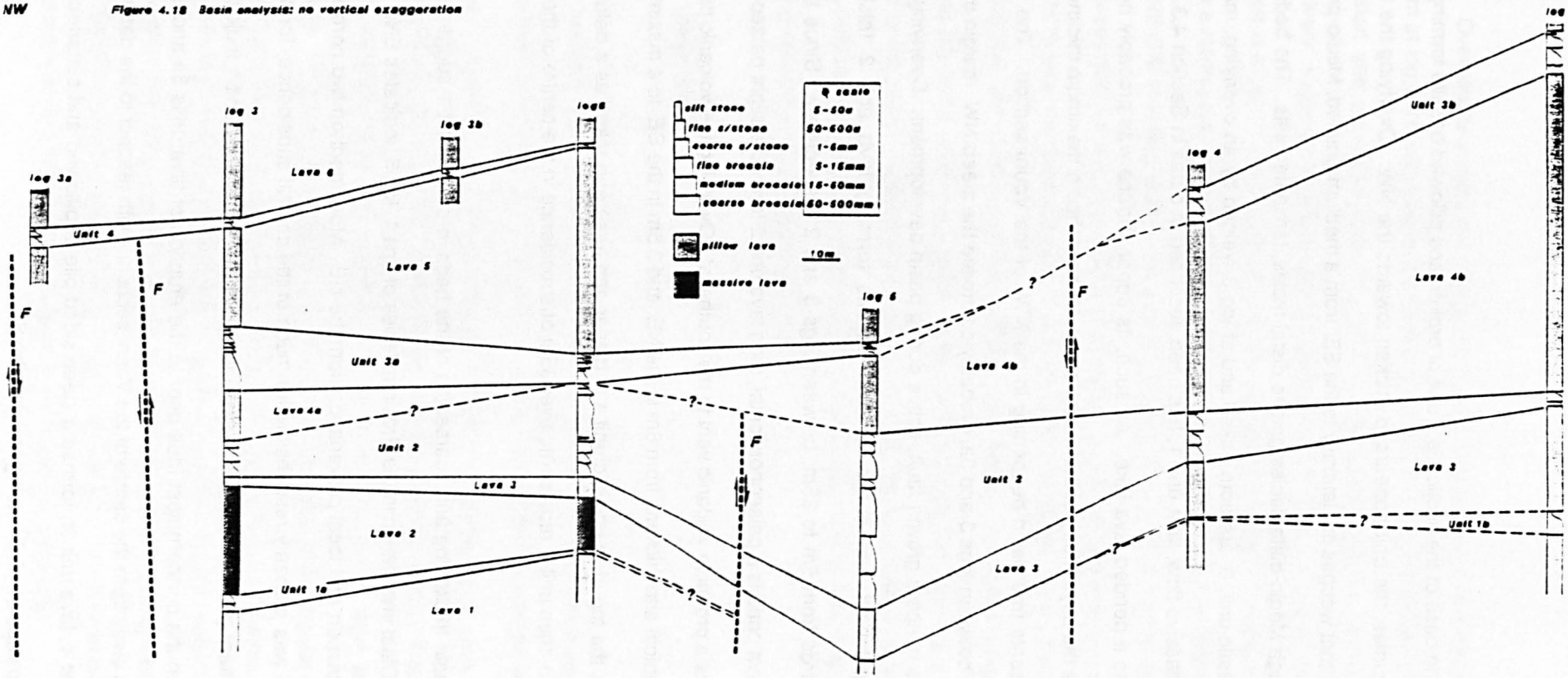

At the base of the section is a unit of broken and pillowed basalts forming lava unit O. From field studies, the unit appears to thicken towards the NW. Overlying the lava unit is a clastic unit, 0 that wedges out laterally to the SE from a medium grained, Medio-proximal facies breccia through Medio-distal facies grits to distal facies, laminated silts. The beds forming the top of the clastic unit, 0, are both baked and at log 3, veined by an overlying, massive basalt flow. The massive flow, lava unit 1, has been described in detail in Section 4.3.3, where it is interpreted as a ponded lava lake. As such, its upper surface was probably horizontal and planar. Thus the asymmetry of the massive unit, that reached a maximum thickness of 20m at log 3, represents true basin deepening in the NW of the Vouni section. The vertical fault, cropping out between logs 3 and 3a, probably controlled the steep NW margin of the massive flow and was hence a growth fault, active during basin development. Overlying the massive lava flow, pillowed and autobrecciated basalts forming lava unit 2 thicken steadily southeastwards from 5m to 25m, between logs 3 and 2 respectively. Since the top of the underlying lava pond is a palaeohorizontal, then lava unit 2 formed a slight palaeoslope of 3.3^{o}, rising towards a probable volcanic vent to the southeast. Overlying the volcanic pile, clastic unit 1 is asymmetrical and thickens from 8m in the NE and 3.5m in the SE to a maximum of 40m at log 5. Since the top of the clastic unit 1 is planar and has been taken as a datum line for the entire section, then unit 1 represents over 35m of subsidence in the centre of the Vouni area.

Rapid thickening and coarsening of the beds in clastic unit 1 suggests fast rates of deposition. Clast imbrication in the Proximal facies of unit 1, log 5, indicates ENE to WSW axial sediment transport and local provenance from the NE. Movement on two normal faults either side of log 5 was probably responsible for much of the central subsidence, forming a NE-SW syn-sedimentary graben. A slight basement high at the top of clast unit 1 indicates continued movement on the northernmost fault prior to the eruption of lava units 3a and 3b. Both lava units thicken away from the centre of the Vouni section. With respect to the datum line defined by clastic unit 1, lava unit 3b formed a steep sided pile of pillowed and autobrecciated basalts with a palaeoslope of 18.5^{o}, rising towards the SE.

Overlying lava unit 3a to the NW, is a clastic wedge, unit 2, that thickens from 3m at log 5 to 14m at log 3 indicating slight subsidence in the NW of the Vouni section. However, both imbrication and gradation from Proximal to Medio-distal facies, between logs 3 and 5 respectively, suggests sediment transport from NE to SW. Overlying lava unit 3b to the southwest is a clastic unit 3. This unit has an unusual distribution, pinching out just north of log 4, down a steep palaeoslope. The unit may, however, be faulted out between logs 4 and 5 by a late NE-SW trending fault, indicated on Figure 4.18. Lava unit 4 both progressively transgresses clastic unit 2, lava unit 3b and clastic unit 3 from north to south, as well as thinning from 52m to less than 24m between logs 6 and 3a respectively. Since the beds immediately underlying lava unit 4 are mostly thin bedded, laminated and laterally persistent silts, then it is likely that the lavas were erupted on a horizontal seafloor and formed a sloping lava pile elevated to the south. The formation of such a palaeoslope is supported by the presence of Medio-proximal and Medio-distal facies beds, forming clastic unit 4, that progressively onlap the underlying volcanic pile towards the southwest.

4.5.7 Interpretation

Interlava clastic sediments, mainly volcaniclastic in composition are stratigraphically most abundant in the vicinity of the Lower to Upper Lava Group transition where they form a progressive unconformity. Facies analysis reveals four facies types from coarse Proximal breccias to distal, laminated silts. Sedimentary analysis of the three most Proximal facies types indicates mass transport and by slide or slump, viscous debris flow and turbidity flow respectively. The most distal facies has sedimentary characteristics of quiet condition, gravity fallout, although some current reworking also occured. In three most Proximal facies, sediment was predominately transported from the ENE to the WSW. Basin analysis of a NW to SE section in the Vouni area reveals a tectonically active NE to SW graben system in which the centre of deposition fluctuated between the NW and centre of the Vouni section, controlled by differential subsidence rates across a number of major axial growth faults.

Sediment provenance was local and from the ENE, coincident with a major WNW-ESE trending fault system that upthrows to the north.

Figure 4.19 illustrates a model of basin development in which listric faulting along WNW-ESE faults caused back rotation of the Kapillo block. Simultaneously, NE-SW trending, normal faults formed a graben system along which fault scarp deposits were transported. Faults forming the southeastern margin of the basin system also localised volcanic vents, probably fissures, from which elevated piles of pillow lava and autobreccia formed. Further listric faulting on the WNW-ESE fault system continued to rotate the Kapillo block forming a progressive unconformity by subsequent erosion and deposition. The structural control of the basin fits a regional structural framework, described in Section 6, in which the major WNW-ESE listric fault system represents tensional activation of the principal shear direction and the NE-SW trend of the Vouni graben is parallel to the synthetic shear direction indicating sinistral, tear-apart basin development.

4.6 Discussion and Conclusions

The volcanic sequence in the WLFC, consisting of pillowed and massive lavas, autobreccias and dykes, can be divided into three groups; (i) the Basal Group, (ii) the Lower Lava Group and (iii) the Upper Lava Group. The WLFC lavas are mineralogically similar to the most primitive end-members of the Troodos Upper pillow lavas (Smewing *et. al., op. cit.*; Pearce, 1975; McCulloch, 1983). In particular, limburgite lavas in the WLFC Upper Lava Group petrographically resemble boninite type lavas from the Troodos Massif (Cameron *et. al.*, 1979; Cameron *et. al.*, 1980; Schminke, 1983; Cameron, 1985) and basaltic komatiites or high magnesium andesites in the Arakapas fault belt (Simonian, 1975; Simonian & Gass, 1975; Bechon, 1982).

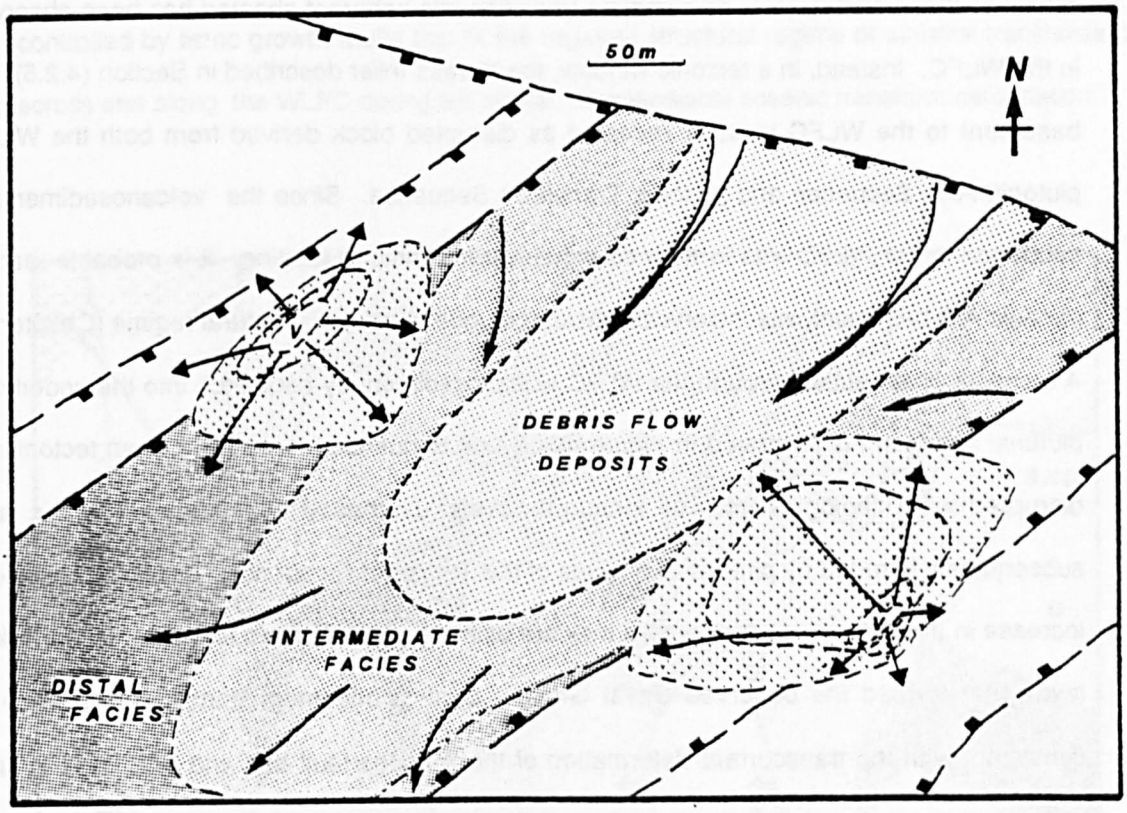

Figure 4.19 Interpretation of the environment of formation of the Kapillio volcanosedimentary sequence in which a small graben developed with the main clastic supply from a fault scarp in the NE of the area. Material was reworked both axially and along the edges of the small graben, marginal faults of which localised volcanic eruptions (v).

Although orthopyroxene is included in the WLFC paragenetic sequence, it is rarely developed as a phenocryst phase. Likewise, plagioclase phenocrysts are rare and never observed co-existing with olivine. Aphyric basalts consisting of olivine, clinopyroxene and plagioclase represent cotectic crystallisation. Although both Simonian and Bechon (*op. cit.*) interpret the variation in the crystallisation sequences of AFB basalts as a function of differing primitive lava compositions, the WLFC basalts are related by simple crystal fractionation to a single primitive magma composition. Hence the WLFC forms a volcanic regime distinct from either the Arakapas fault belt or Troodos massif. A thorough examination of the paragenesis of the WLFC lavas is appraised geochemically in Chapter 6.

Although the base of the lavas consists of a basal group of brecciated lavas and dykes similar to those on Troodos, no complete transition into coherent sheeted has been observed in the WLFC. Instead, in a tectonic window, the Yerasa Inlier described in Section (4.2.5), the basement to the WLFC lavas is revealed as disrupted block derived from both the WLFC plutonic Axis Sequence and plutonic Transform Sequence. Since the volcanosedimentary sequence in the WLFC was formed during sinistral transform faulting, it is probable that its plutonic A/S basement was tectonically disrupted under a similar structural regime (Chapter 5). A reconstructed section through the WLFC volcanosedimentary sequence into the underlying plutonic basement is illustrated in Figure 4.20 Axis Sequence blocks have been tectonically disrupted with lithologies from all structural levels juxtaposed against one another, and subsequently intruded by plutons and dykes of the Transform Sequence. Cross cutting dykes increase in abundance upwards where they are ultimately intruded into and extruded as pillow lavas that formed the observed Basal Group. Such a basement transition sequence is consistent with the transcurrent deformation of the Arkapas fault belt and WLFC. It is also supported by the occurrence of upper pillow lavas that lie directly over serpentinised ultramafics in the Vavla area of the Arakapas fault belt (Simonian, 1975).

The debris flow and turbidity flow deposits of both the Arakapas fault belt and WLFC are laterally extensive and form sequences up to 200m thick in the Layia area (ie. the eastern Arakapas fault belt; Simonian, 1975). In contrast, volcaniclastic interlava sediments in the northern Troodos massif are very coarse grained, unstratified, clast supported, lava breccias set in a matrix of orange brown, fine grained mud, and interpreted as Proximal fault scarp, talus deposits, (Gass, 1960; Gass & Smewing, 1973; Smewing, 1975; Schmincke *et. al.*, 1983). Such coarse, proximal deposits do not form laterally extensive units and never exceed a few metres in thickness. The more substantial development of interlava sediments in the Arakapas fault belt and WLFC areas is evidence of a more active tectonic regime (ie. a transform fault zone) than that during formation of the Troodos massif at a constructive margin. This is born out by the presence of large throw vertical faults in the WLFC and Arakapas fault belt from which sheeted dyke and isotropic gabbro fragments, and, in the Akrounda area, ultramafic lithologies

were derived and deposited. Basin analysis in the Kapillio area indicates graben formation, controlled by listric growth faults that fit the regional structural regime of sinistral transtension across and along the WLFC during left lateral, transtensional oceanic transform deformation.

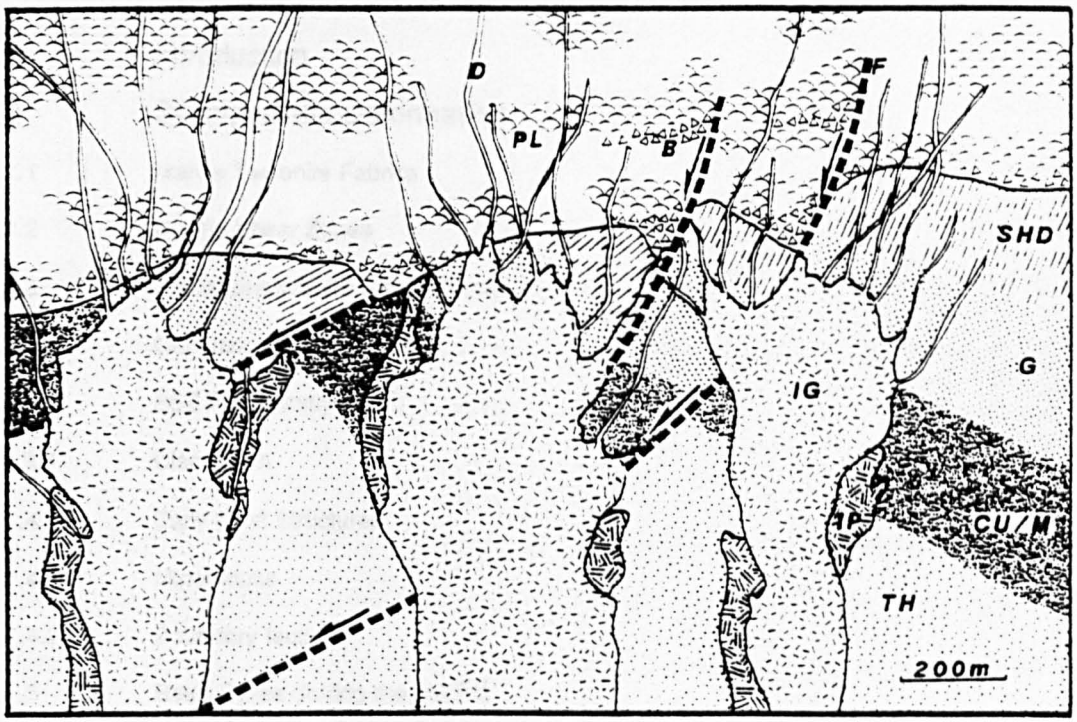

Figure 4.20 Schematic section for the transition from the basement to the volcanosedimentary sequence in the WLFC. The basement consists of faulted and tilted blocks in which: *SHD = Sheeted Dyke Complex, CU//M = cumulate ultramafics, TH = tectonised harzburgite, (and correspond to the Axis Sequence); IG = isotropic gabbro , IG = intrusive wehrlite, D= maficdykes, PL = pilow lavas (and correspond to the Transform Sequence): F = fault.*

CHAPTER 5

STRUCTURAL AND TECTONIC EVOLUTION

List of Contents

5.1 Introduction

This Chapter deals with the structural and tectonic evolution of the Western Limassol Forest Complex (WLFC), firstly during its formation as oceanic lithosphere in the Late Cretaceous (97-65 Ma) and secondly during its subsequent history as an elevated and eroded ophiolite complex in the middle Miocene (11.6-6.0 Ma). The various syn- and post- magmatic events are dealt with in order of decreasing age. Since all WLFC magmatism is interpreted as oceanic in origin (see Chapter 5), syn-magmatic tectonism is considered coincident with the formation of the WLFC and includes mantle tectonite fabrics, ductile shear zones, brittle serpentinite shear zones, early fault structures, large scale folding and uplift and the tectonic implications of gabbro and dyke emplacement. These features are then discussed in terms of tectonic activity within an oceanic transform regime.

All post-magmatic deformation that affects both the WLFC and the Upper Cretaceous and Miocene sedimentary cover is coincident with the emergence of the area as an ophiolite complex. Although neither an underlying basement nor a metamorphic aureole has been found for the Troodos and WLFC ophiolite complex, it is therefore on this basis, considered autochthonous. All post-magmatic structures are here termed emplacement features. These emplacement features include the Yerassa fold belt, high angle reverse faults and Recent north-south faults, and are discussed in terms of north-south regional compression; no major thrust zones indicating obduction processes have been identified, although these may occur at depth. Finally, the structural and tectonic evolution of the WLFC is summarised in a list of conclusions based on the data presented in this Chapter. However, first a brief explanation of the method of data presentation and analysis is given.

In the following sections, the majority of the structural data are presented on Lambert equal area, lower hemisphere projections. To aid comparison between data sets of varying size (Starkey, 1977) the projections have been contoured using the STATIS programme

developed by N.G. Woodcock on the Cambridge University Main Frame IBM-370 computer. The programme also analyses the distribution and fabric shape of the data using the eigenvector method of Watson (1965 and 1966). Normalised eigenvalues S_1, S_2 and S_3 define three eigenvectors, V_1, V_2 and V_3 which approximate the Fisher Mean (Fisher,1953), an intermediate value and the pole to the best fit great circle respectively. Woodcock (1977) developed K and C parameters to quantify the shape and strength of fabric distributions by making two axis, logarithmic comparisons of normalised eigenvalues (Figure 5.1).

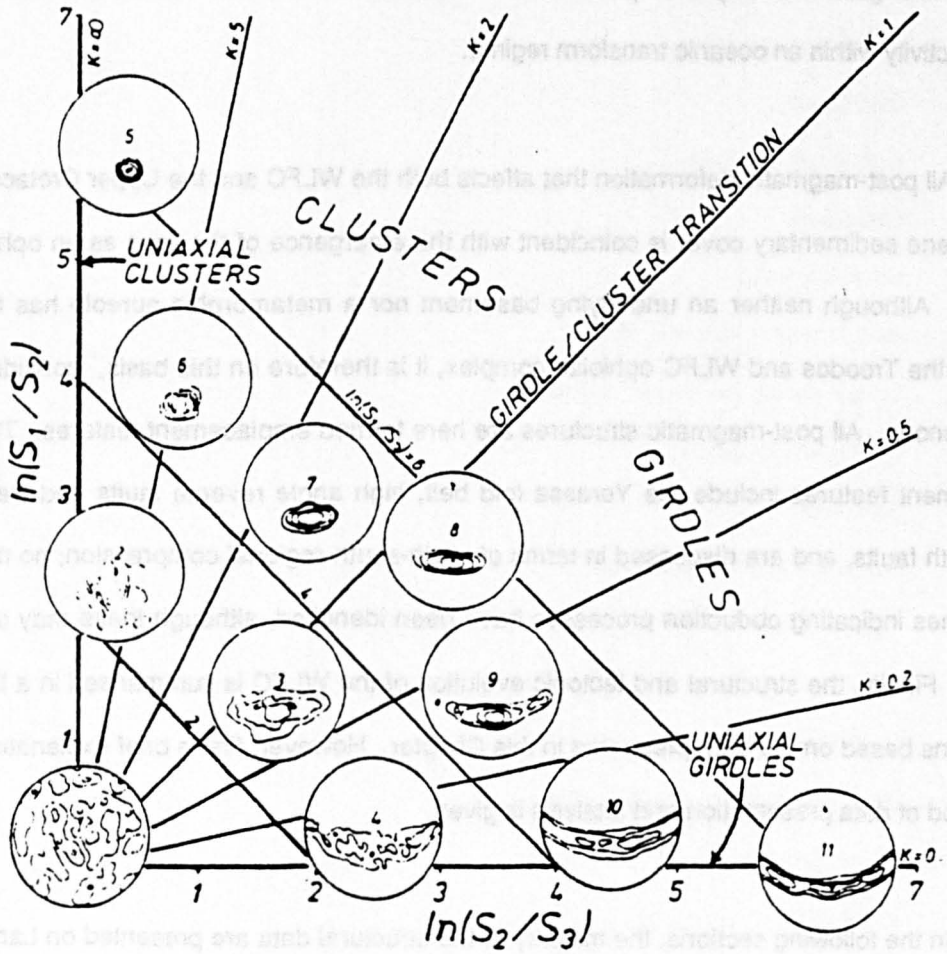

Figure 5.1 Fabric shape and strength plotted using eigen vectors S1, S2 and S3, where K = ln (S1/S2) / ln(S2/S3) varies with the strength of distribution cluster and the value C = ln(S1/S3) varies proportionally with the strength of any prefered fabric orientation.

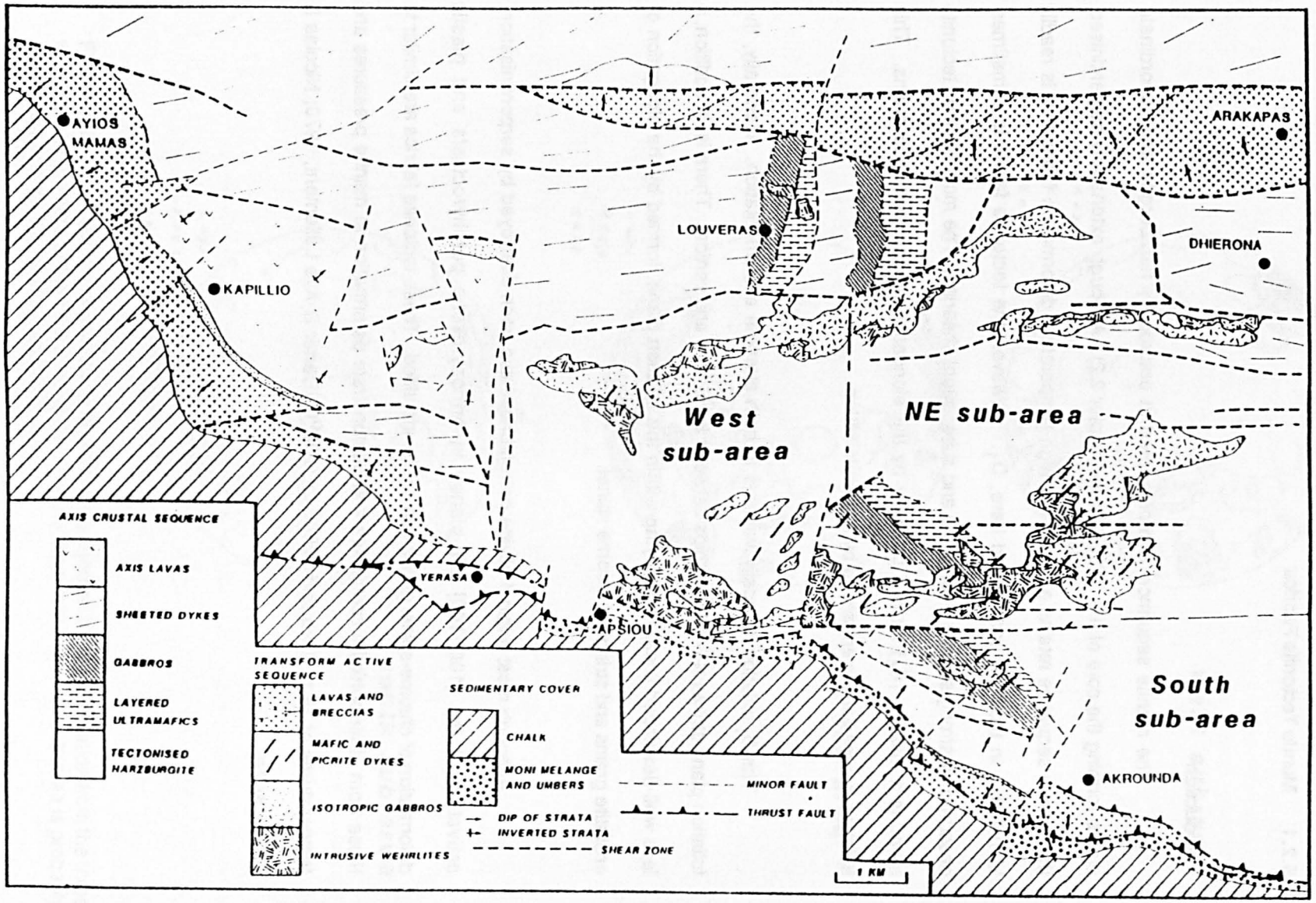

Figure 5.2 Map of the WLFC showing the three structural sub-areas from which the mantle fabric data has been taken.

5.2 Syn-magmatic Deformation

5.2.1 Mantle Tectonite Fabrics

Introduction

The mantle sequence is represented at outcrop by harzburgite and subordinate dunite forming the core of the WLFC (see Chapter 2.2). Although extensively serpentinised, the mantle sequence retains a pervasive, high temperature deformation fabric that is readily identifiable in the field and termed here, D_1. However, the tectonite fabric is sometimes obscured by strong surface weathering and subsequent shearing. The most obvious tectonite fabric is a foliation (S_1) formed primarily by the elongation of orthopyroxene grains. This foliation is occasionally enhanced by serpentinisation.

The S_1 foliation is locally variable in both strength and orientation. Generally, the foliation plane strikes NE-SW and dips between 80°S NW, and vertical. There is, in addition, a less well-developed linear fabric, lying within the foliation plane, formed by the elongation of enstatite grains and strings of chrome spinel.

Although most original olivine petrofabrics have been destroyed by serpentinisation, activation of the (100)[100] slip-planes in orthopyroxene porphyroclasts and plastic deformation of chrome-spinel grains can still be identified. These tectonite fabrics are similar to those from other ophiolite complexes and demonstrate deformation at mantle pressures and temperatures of 15 to 20kb and 1000° to 1200°C (Carter & Ave Lallement, 1970; Nicolas & Poirer, 1976).

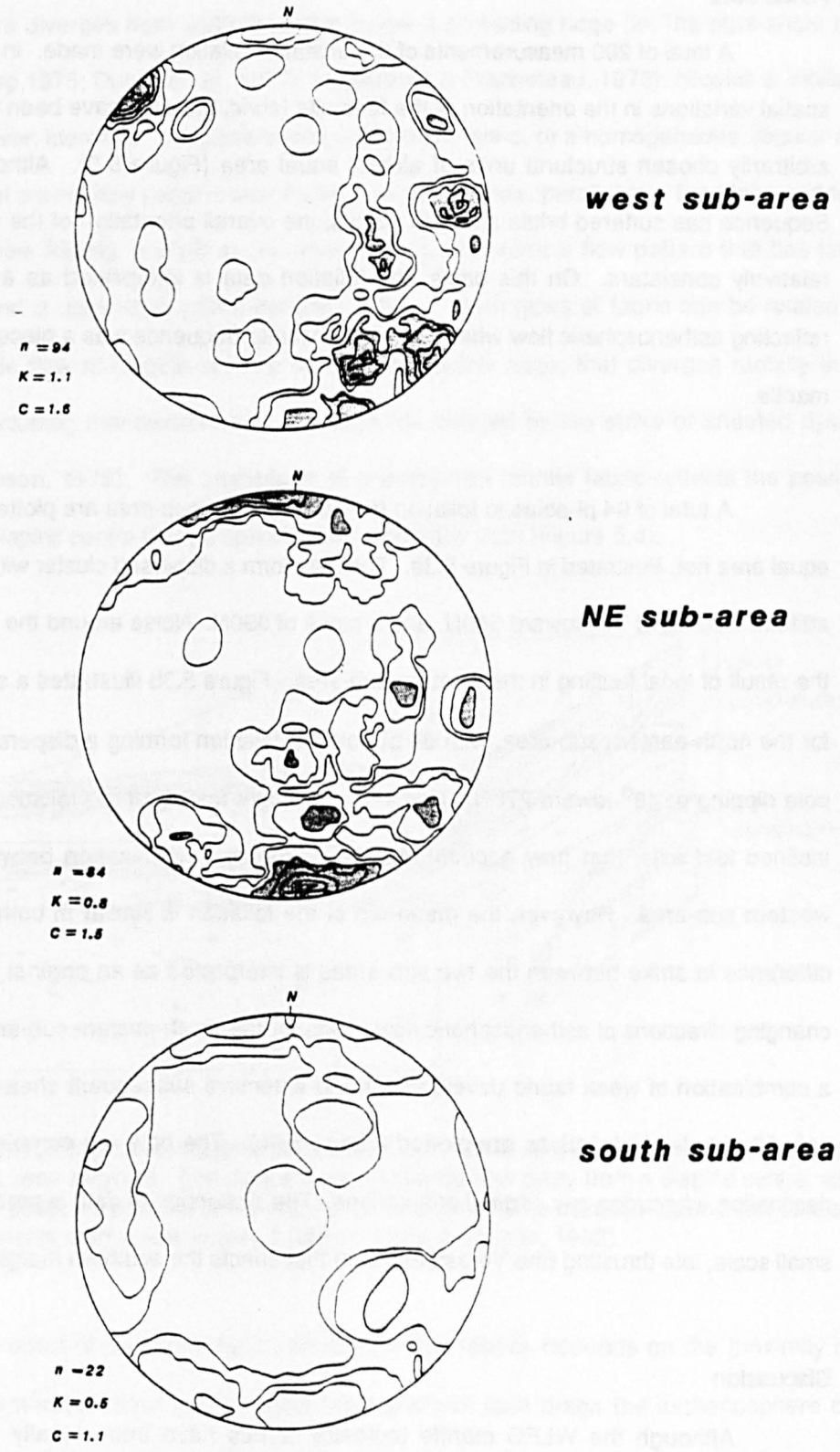

Figure 5.3 Lambart equal area lower hemisphere projection of mantle foliation from the three sub-areas of the core of the WLFC. Dispersion of the data from the south sub-area is probably due to disturbance by local Miocene thrusting.

Fabric Data

A total of 200 measurements of the enstatite foliation were made. In order to examine spatial variations in the orientation of the tectonite fabric, the data have been divided into three arbitrarily chosen structural units of almost equal area (Figure 5.2). Although the Mantle Sequence has suffered brittle shear in places, the overall orientation of the tectonite fabric is relatively consistant. On this basis, the foliation data is interpreted as a primary feature, reflecting asthenospheric flow when the WLFC Mantle Sequence was a piece of oceanic upper mantle.

A total of 94 pi-poles to foliation from the western sub-area are plotted on a contoured equal area net, illustrated in Figure 5.3a. The data form a dispersed cluster with a mean foliation attitude dipping at 71^{o} toward 360N, and a strike of 090N. Noise around the mean is probably the result of local faulting in the western sub-area. Figure 5.3b illustrates a similar distribution for the north-eastern sub-area, with 84 pi-poles to foliation forming a dispersed girdle about a pole dipping at 48^{o} toward 275N. This indicates slight folding of the foliation about a steeply inclined fold axis, that may account for the difference in declination between this and the western sub-area. However, the mean dip of the foliation is similar in both sub-areas. The difference in strike between the two sub-areas is interpreted as an original feature reflecting changing directions of asthenospheric flow. Data for the south-eastern sub-area are few due to a combination of weak fabric development and extensive subsequent shearing. As a result, only 22 pi-poles to foliations are plotted (Figure 5.3c). The data are completely dispersed in declination, obscuring any original orientations. The dispersion of data is probably the result of small scale, late thrusting (the Yerasa fold belt) that effects the southern margin of the WLFC.

Discussion

Although the WLFC mantle tectonite fabrics have been locally faulted, they still preserve asthenospheric flow fabrics produced during the formation of the WLFC as oceanic lithosphere. Many authors consider such mantle flow fabrics to form where rising

asthenosphere diverges from vertical ascent below a spreading ridge (ie. the right-angle turn model of Sleep,1975; Dutea *et. al.*, 1977; Tapponnier & Fracheteau, 1978). Nicolas & Viollette (1982), however, identified two generations of tectonite fabric, (i) a homogeneous, regular and sub-horizontal plastic flow pattern, consistent over large areas, parallel to a flat Moho and free from large scale folding, and (ii) an inhomogeneous, sub-vertical flow pattern that has large scale folds and is discordant with a deformed Moho. Both types of fabric can be related by vertical mantle flow at diapiric centres along a spreading ridge, that diverges radially in all directions, including that parallel with the ridge (as defined by the strike of sheeted dykes) (Vogt & Johnson, 1975). The orientation of a preserved mantle fabric reflects the position relative to a diapiric centre that an ophiolite was obducted from (Figure 5.4).

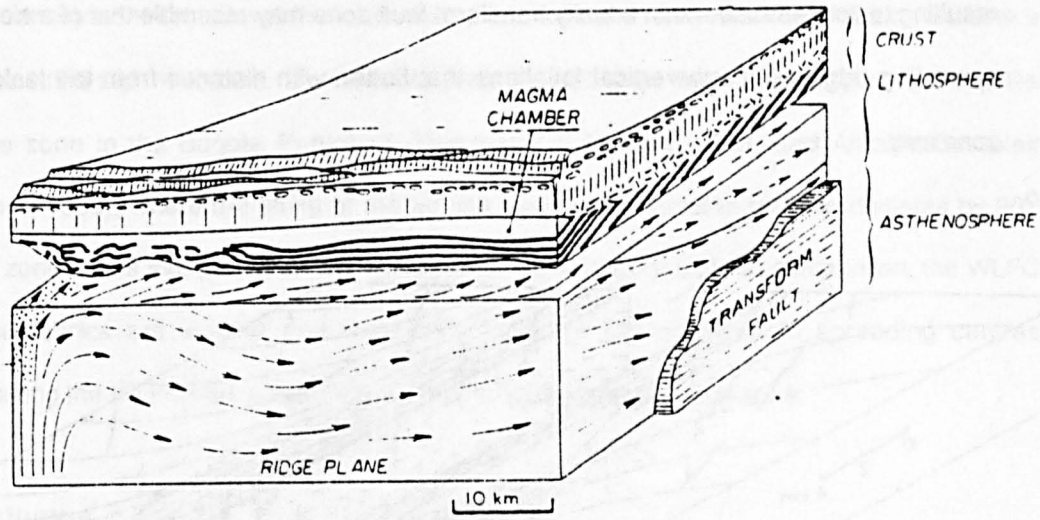

Figure 5.4 Block diagram of oceanic lithosphere, cut parallel to a spreading axis and an active transformfault zone segment. The diagram shows mantle flow away from a diapiric centre, along the ridge and deflected paralllel to the transform fault zone. The transform fault zone acts as a 'dam' that prevents mantle flow across it (after Nicolas & Violette, 1982).

The effect of transform faults on mantle flow fabrics depends on the proximity of a ridge-transform intersection and whether the transform fault drags the asthenosphere or is driven by it. Vogt & Johnson (1975) predicted that along-ridge asthenospheric flow would be obstructed by, and eventually be deflected parallel to, transform faults. Nicolas & Viollette (1982) consider such transform controlled mantle fabrics to form sub-vertical foliations and

transform parallel lineations (Figure 5.4). Mantle fabrics within transform faults are likely to depend on whether the structure is 'tight' (ie. transcurrent or transpressional) or 'leaky' (ie transtensional). If the former, then deformation will probably be governed by asthenospheric drag with the transform zone effectively decoupling the opposing motion of the adjacent lithospheric plates. The resulting mantle fabrics will be sheared across and along the transform zone, producing a wide shear zone with an oblique mylonite fabric, similar to that of the Bagota Peninsula, Papua New Guinea (Figure 5.5). In contrast, if a transform fault is sufficiently 'leaky', then it may effectively be considered as an oblique, slow spreading ridge (Vogt & Johnson, 1975). If lithospheric plate motion is driven by asthenospheric flow rather than by tensional forces (Boudier & Coleman, 1981), then differential plate motion across a 'leaky' transform zone may be accommodated by divergent mantle flow, rather than by mantle-shear decoupling. The resulting tectonite fabric within a leaky transform fault zone may resemble that of a slow, oblique spreading ridge, with sub-vertical foliations that flatten with distance from the leaky fracture zone axis.

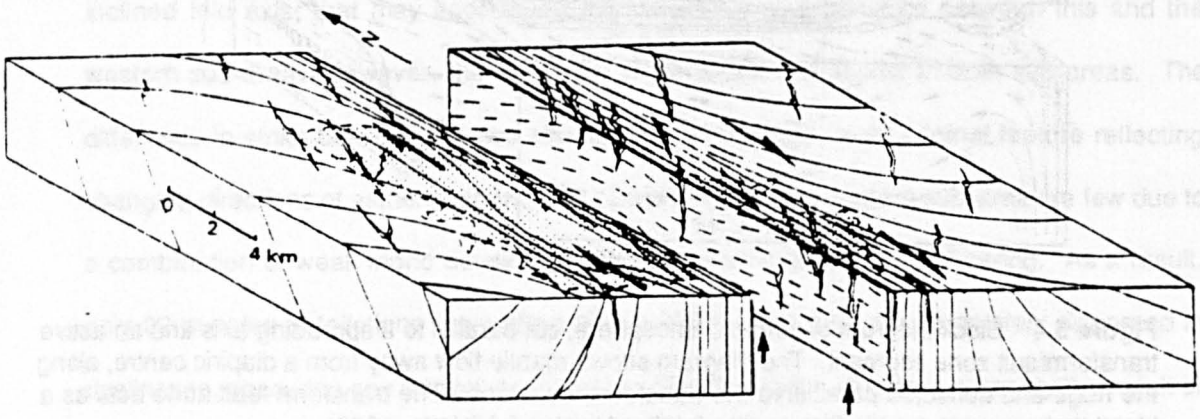

Figure 5.5 Block diagram showing the change of orientation for the mantle tectonite fabric across a postulated palaeo-transform fault zone in the Bagota Peninsula, Papua New Guinea. The mantle tectonite fabric has been dragged and sheared across the transform fault zone, effectively decoupling the opposing plate motions (after Prinzhofer & Nicolas, 1980)

vertical with respect to the Moho plane. Later, in a more detailed study, Bartholomew (1982) recorded two foliations, an early, deformed foliation and a later, stronger, vertical, NW-SE fabric. Bartholomew also identified a mantle lineation that dips steeply SE. Although both Nicolas & Viollette (*op. cit.*) and Bartholomew (*op. cit.*) attributed the tectonite fabrics to vertical diapiric flow of mantle material beneath the Troodos spreading ridge, neither authors were able to say in which direction the palaeo-spreading axis lies with respect to the Troodos ophiolite. In comparison, the NE-SW to E-W striking, near vertical mantle foliation found in the WLFC is compatible with asthenospheric flow being deflected by transform structures (Vogt & Johnson (1975).

If the tectonite fabric in the WLFC is,however, dominated by mantle shearing (ie. the 'tight' transform model, above) then the vertical fold axis and NE-SW striking foliation indicate a dextral strike-slip movement. Such an interpretation has been made for the 3km wide mylonite mantle zone in the Bogota Peninsula (Prinzhafer & Nicolas, 1980) and Antalya Complex (Reuber, 1985), where the strike of the Mantle Sequence, enstatite foliation deviates by 90^{o} into a zone that is interpreted as a fossil transform fault (Figure 5.5). In comparison, the WLFC mantle fabrics are weaker and more akin to those formed beneath spreading centres suggesting the WLFC was a 'leaky' rather than a 'tight' transform fault zone.

Conclusion

The mantle tectonite fabric in the WLFC is similar to mantle spreading fabrics from other ophiolite complexes. Although variable in strength and orientation, the enstatite foliation dips steeply NW and strikes NE-SW in the west and ENE-WSW in the north-east, where it has been deformed around a sub-vertical fold axis. Unlike the mylonitic mantle fabrics of the Bogota Peninsula and Antalya complex, the WLFC has a spreading fabric that suggests 'leaky' transform activity. As such, the WLFC mantle fabrics suggest an asthenospheric plume coincided with a 'leaky', sinistral, transtensional transform fault zone (Figure 5.6).

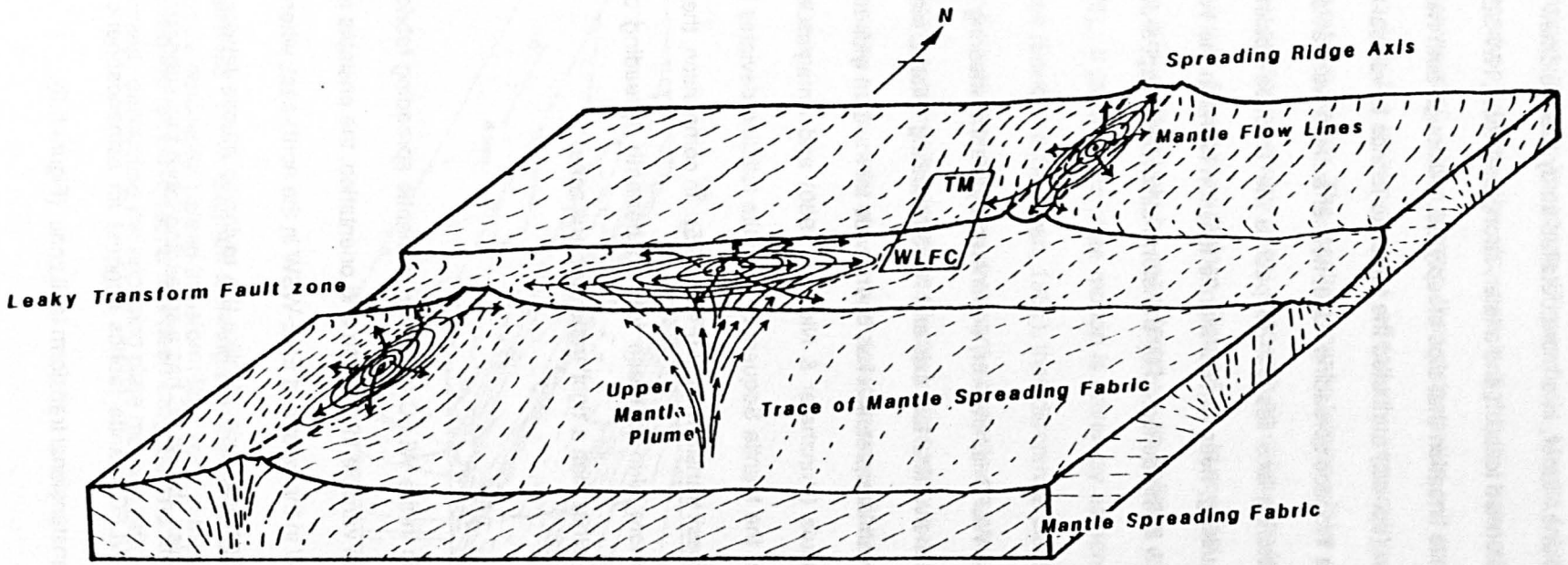

Figure 5.6 Block diagram showing the reconstructed plate configuration and mantle flow beneath the WLFC. The mantle flow fabric suggests that there was a mantle diapir to the west, within the transform domain. This configuration is in contrast to 'tight' transform fault zones, in which the mantle appears to be sheared between the opposing plates. The WLFC appears to have been 'leaky' with the opposing plate motions decoupled by the generation of oceanic lithosphere within the transform domain.

B J Murton 1986 148 Chapter 5

5.2.2 Ductile Shear Zones

Introduction

Ductile shear zones although relatively rare are up to three metres wide, and cut T.S. gabbros and occasionally the mantle sequence. In the latter, the mantle tectonite fabric (S_1) is deformed by the ductile shear zones which are also cut by later brittle serpentinite shear zones (see Section 5.2.3), thus identifing the mylonites as S_2 structures formed during D_2 deformation. The presence of cross-cutting and subsequently deformed basic dykes identifies the D_2 as syn-magmatic and hence, oceanic deformation. Although only 23 serpentinite and 32 basic ductile shear zones have been measured, they are all east-west trending, sub-vertical structures with sub-parallel sides. Granulation and dynamic recrystallisation forms a foliated, fine-grained fabric that is evidence of ductile mylonite deformation (Sibson, 1977; Penrose, 1982).

Macroscopic fabrics in gabbroic, ductile shear zones form the most common type of mylonite in the WLFC. Sharp boundaries between mylonite zones and their undeformed protolith walls indicating strain softening and locallised deformation along discrete (0.1 - 0.2m wide) shear zones (Ramsay & Graham, 1970; White *et. al.*, 1980). Although shear zone walls are commonly parallel, occasional necking and brittle extensional fracturing (illustrated in plate 5.1), indicates a brittle-ductile transition, possibly in response to a decrease in temperature, or an increase in shear strain rate, or both. Macroscopic mylonitic banding is formed by mafic and leucocratic compositional segregation and grain size variation. Such banded shear zones are most common in the stream section, [05079-38135] (Plate 5.2).

Orientation data

Figure 5.7a illustrates 37 sub-vertical, basic shear zones with an average strike of 085N, that is close to the mean 091N trend of the 23 sub-vertical, ultramafic mylonite zones (Figure 5.7b). Where present, elongated and flattened amphibole, pyroxene and feldspar

grains form a macroscopic vertical foliation and horizontal lineation, both sub-parallel with the shear zone walls and indicating strain by strike-slip displacement. Since the angle (θ) between the principal finite elongation (the foliation) and the shear zone walls decreases with increasing shear strain (γ) both the sense and amount of offset can be determined (Ramsay & Graham, 1970; Ramsay, 1985). The total shear strain (S) is related to the angle θ by;

$$S = {}^{x}\int_{0} \gamma \, dx \qquad \text{where } x \text{ is the width of the shear zone.}$$

Plate 5.3 shows an oblique and slightly sigmoidal fabric developed across a gabbroic mylonite. The angle and resultant shear strain vary between 5^{o} and 7.6^{o} and 11.5γ to 7.5γ respectively. Since, in this example x = 12cm, the total shear displacement (S) is only 125cm. This calculated total shear strain is similar to an adjacent mylonite where θ varies between 8^{o} and 26.75^{o}, with the resultant shear strain between 7γ and 1.5γ respectively. Since the width of this mylonite is 22 cm, S = 115 cm. Since the mylonite foliations form 'Z' shaped, sigmoidal patterns across the shear zones, both mylonite fabrics indicate sinistral shear movement (Ramsay, 1980).

Asymmetric Microfabrics

In the absence of displaced markers, shear zone walls or olivine or quartz petrofabrics, Simpson & Schmid (1983) recommend analysis of microfabrics (Figure 5.8). Such features as asymmetric augen structures (A) (Eisbacher, 1970; Lister & Price, 1978; Berthe *et al.*, 1979), asymmetric pressure shadows (B & C) (Ghosh & Ramberg, 1976), composite planar fabrics, disrupted, broken grains (D) and oblique elongated and polygonised grains (F) to determine shear sense or vorticity along a mylonite zone. The following sections describe orientated samples, each cut in two mutually perpendicular directions, (ie. normal to the foliation and perpendicular to the lineation).

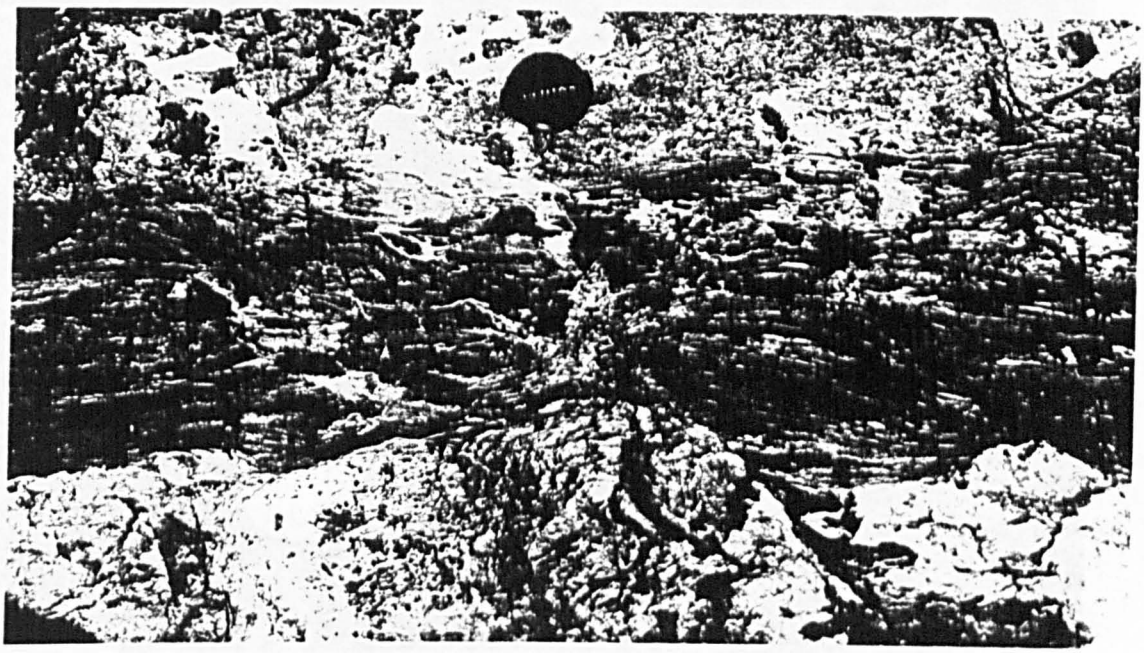

Plate 5.1 Banded mylonite zone in Transform Sequence gabbro showing pinching, necking and pull-apart indicating a brittle - ductile transition.

Plate 5.2 Strongly foliated mylonite zone in a transform sequence gabbro. The banding trends E - W and indicates high strain.

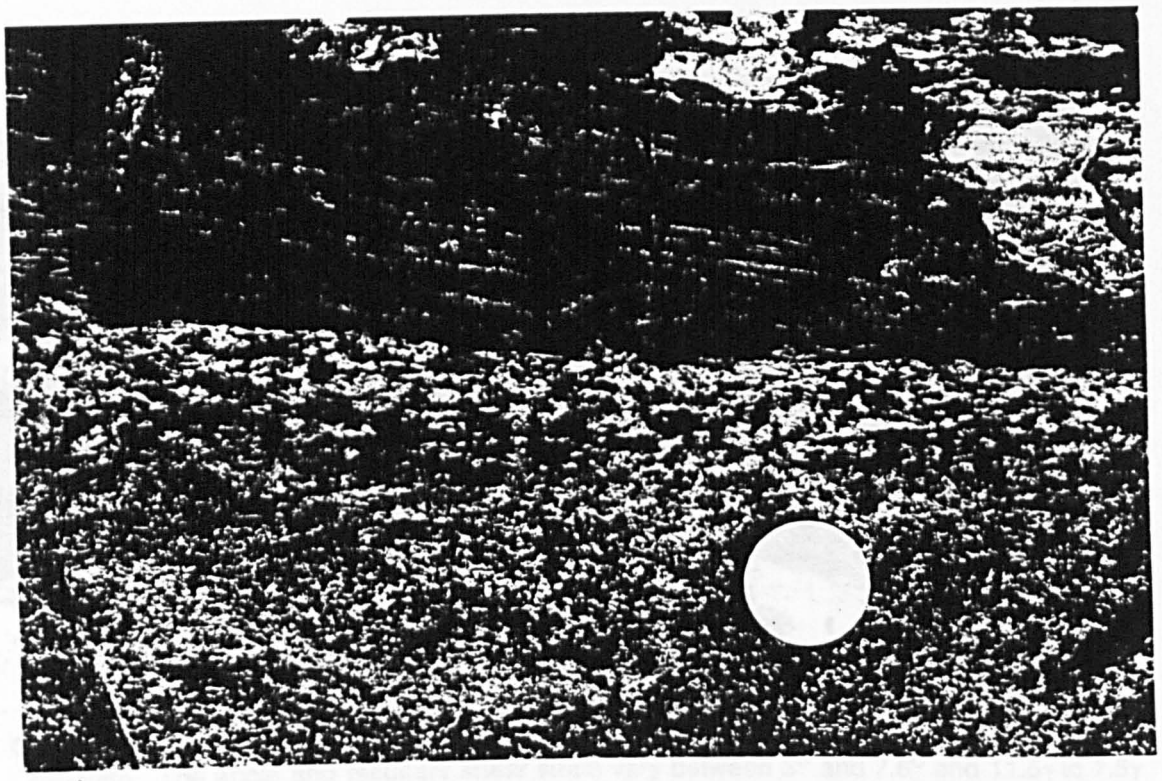

Plate 5.3 Mylonite zone developed in a Transform Sequence gabbro showing a sharp contact with the undeformed wall of the protolith indicating strain weakening. The mylonite foliation is oblique to the walls of the shear zone and is evidence of sinistral shear. Total strain >20γ.

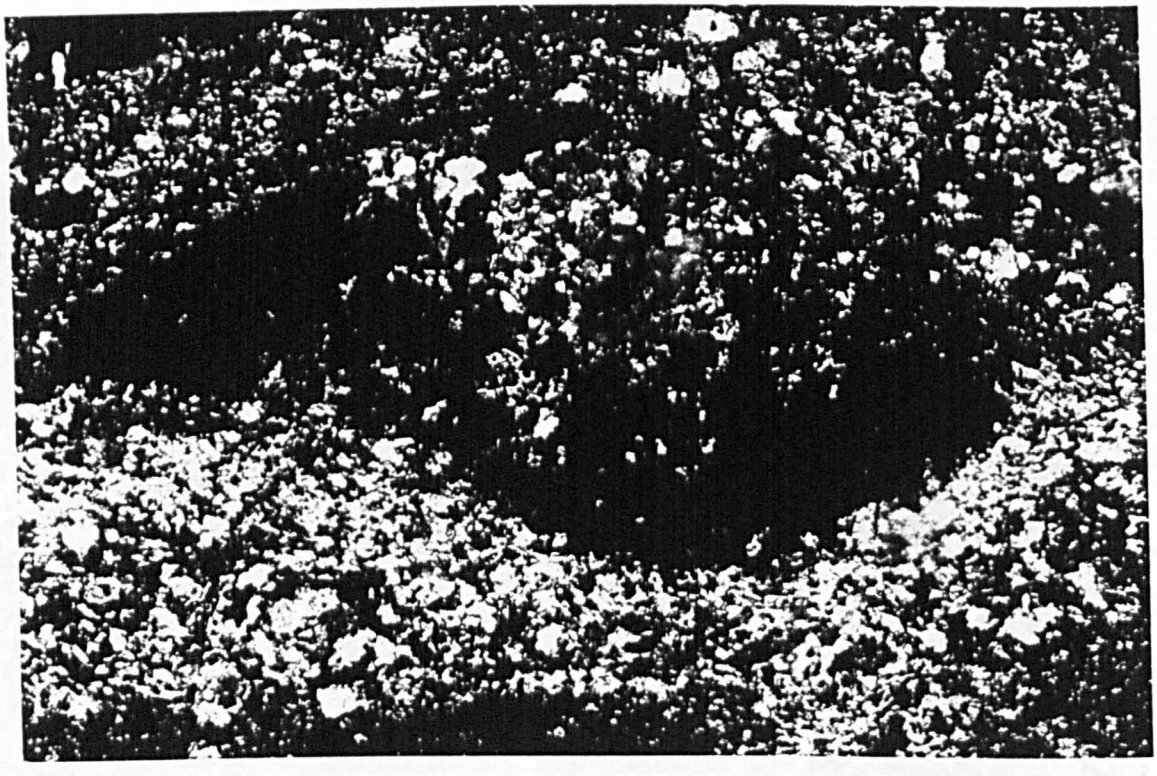

Plate 5.4 Photo-micrograph of an asymmetric retort-shaped orthopyroxene grain (in extinction) with aggregated recrystallised top margin. The shape of the grain indicates sinistral shear (X 40)

Sample 230-C783 is a laminated, mylonite shear zone in harzburgite. The fine grained groundmass of 100 to 200 μm neoblastic olivine is evidence of high deviatoric stresses greater than 2 kbars and rapid strain rates at temperatures of about 800°C (Nicolas & Le Pichon, 1980; Nicolas & Poirer, 1976). Strong microfabric symmetry indicates high shear strain, probably in excess of 20γ. A section cut normal to the foliation illustrates rotation of porphyroclasts and their strain shadows by ductility contrasts between relict grains and their recrystallised matrix, (Ramsay *op. cit*). Also shown is a retort shaped orthopyroxene porphyroclast with a granulated edge, that has been rotated anticlockwise into the foliation (Plate 5.4). This, combined with 'S' shaped asymmetric strain shadows, suggests sinistral shear.

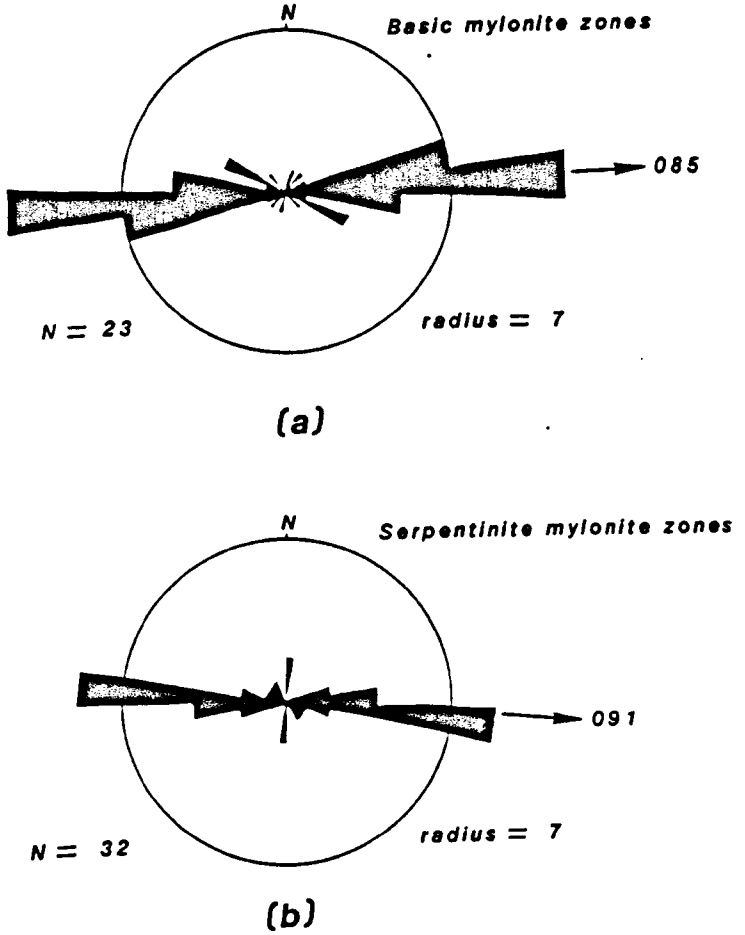

Figure 5.7 Cumulative direction v frequency diagrams for (a) mafic and (b) serpentinite, ductile shear zones (mylonites). The shear zones are vertical, their average trends are indicated.

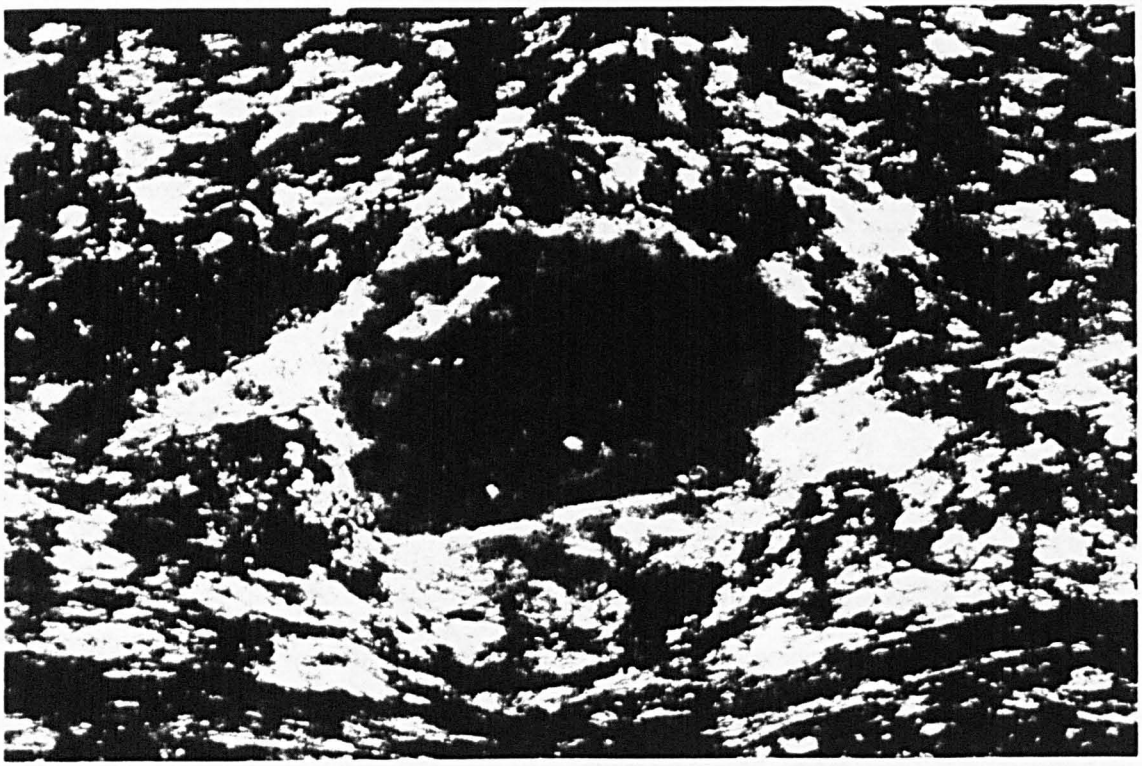

Plate 5.5 Photo-micrograph of an asymmetric augen structure formed from a deformed clinopyroxene porphyroclast. The grain has polycrystalline 'tails', showing anticlockwise rotation and micro-folded foliation indicating sinistral vorticity (X 100).

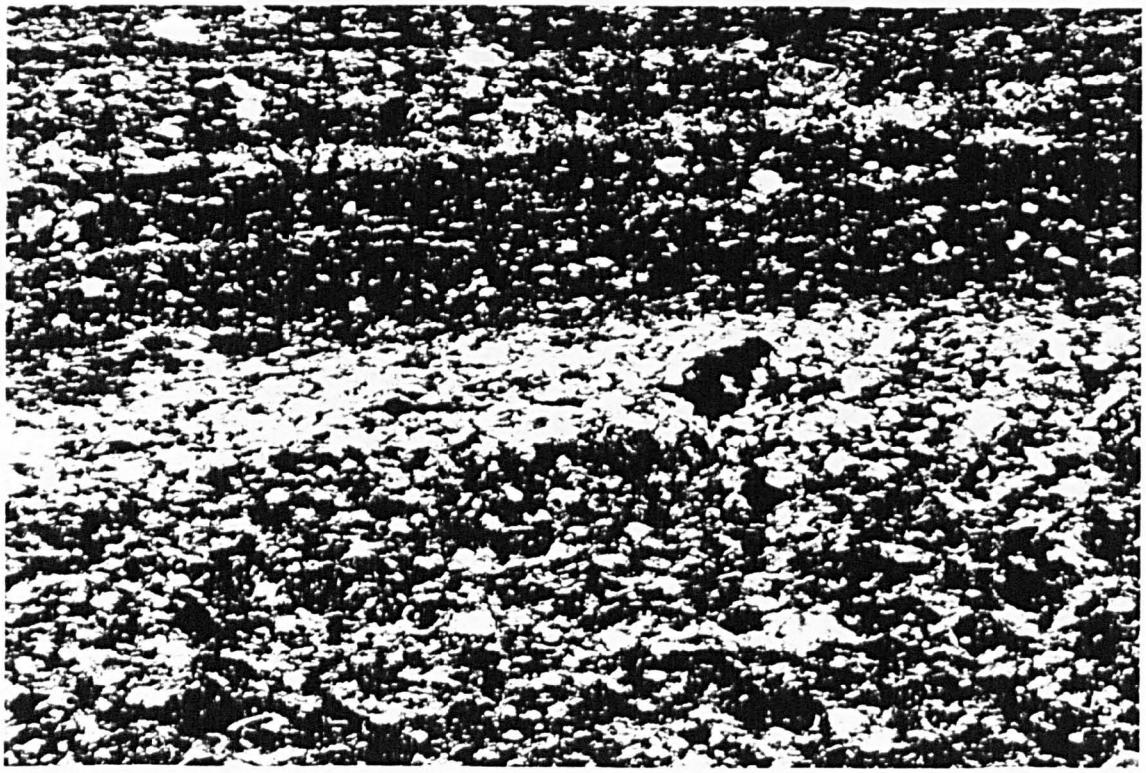

Plate 5.6 Photo-micrograph of a fine grained banded mylonite (from a T.S. gabbro) in which the grains are rounded and the laminations are laterally continious indicating very high shear strain (X100)

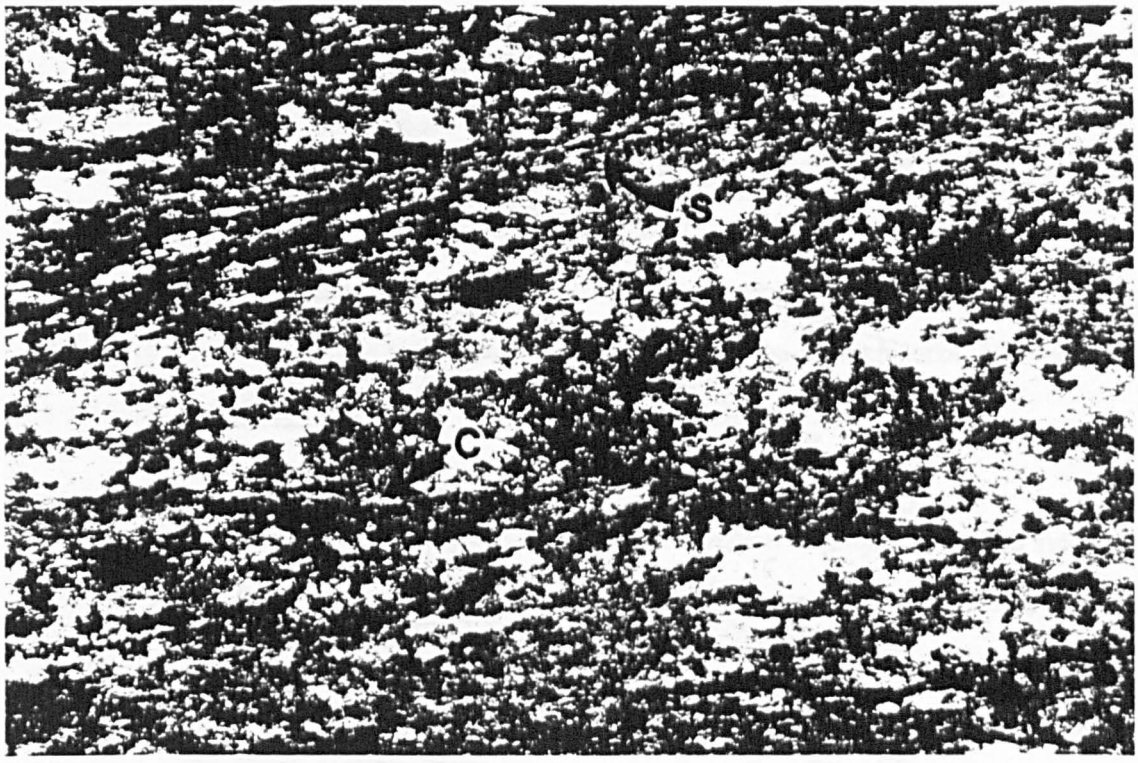

Plate 5.7 Photo-micrograph of a very fine grained mylonite in gabbro (x 40) showing the development of 'S and C-Structures (arowed). The foliation parallel to the frame is an S-Structure and forms part of the principal foliation. The plane that is oblique to the frame, and to the main foliation fabric, is secondary and approximates to a reidal shear indicating a sinistral shear sense.

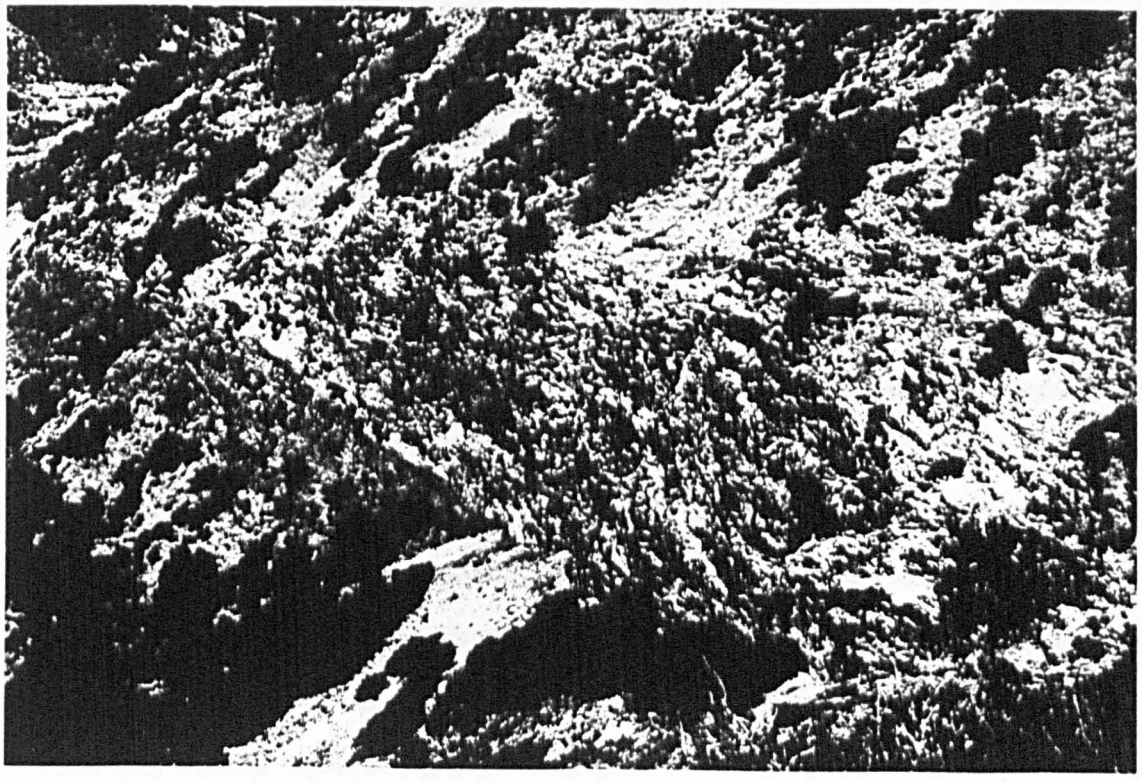

Plate 5.8 Outcrop of a serpentinite shear zone in the field. The foliated serpentinite fabric is oblique to the shear zone wall and suggests sinistral strike-slip movement.

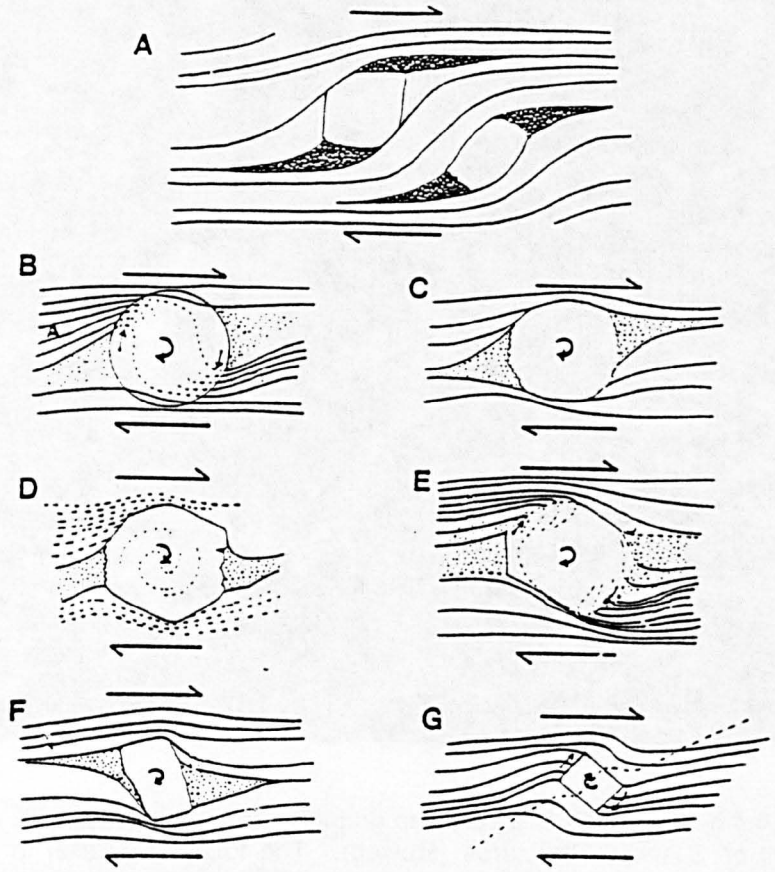

Figure 5.8 Schematic diagram of asymmetric augen structures formed within foliation planes (taken from Simpson & Schmid, 1983). The direction of vorticity or shear is indicated (and is opposite from those in the text). **A** The tails of rotort-shaped grains are composed of fine grained material of the same composition as the host porphyroclast. **B** Rotated porphyroblastic grain, the foliation outside of which forms small micro-folds at the point of entry into the grain, that is also bounded by rotated pressure shadows. **C** and **E** Rotated porphyroblasts with pressure shadows and foliation. **F** Rotated feldspar with associated pressure shadows. **G** Rotated rigid inclusion in sheared silicon putty (after Gosh & Ramberg, 1976).

Plate 5.5 illustrates the development of asymmetric augen structures and polycrystalline tails of the host grain and strain shadows. The retort-shaped porphyroclast has been rotated into parallelism with the foliation and now shows elongation and rounding with increased shear strain. Both the oblique orientation of the grain relative to the foliation and micro-folding of the foliation into the strain shadows is further evidence of sinistral shear displacement. The presence of a subhorizontal linear fabric in this rock suggests that strike-slip displacement was accompanied by vertical dip-slip movement.

In specimen 129-C783, a fine grained laminated mylonitic gabbro with a well formed vertical foliation, relict grains of plagioclase are cracked, strained, partially rotated and have deformed asymmetric pressure shadows (Plate 5.6) also indicating anticlockwise porphyroclast rotation and hence sinistral shear movement (Ghosh & Ramberg, 1976; Simpson & Schmid, 1983). A horizontal, fine grained, linear fabric lying in the plane of the foliation also indicates formation by strike-slip deformation.

The microscopic foliation formed by grain size variation in sample 135-C783 indicates both high total shear strain and high strain rates. The orientation of the shear and foliation fabrics (the S- and C- surfaces of Berthe *et al.*,1979) is evidence of a sinistral sense of movement (Plate 5.7). Where present, acicular amphiboles growing parallel to the S-surface fabric and into undeformed clinopyroxene grains indicate syntectonic growth at temperatures less than 1000^{o}C. In this sample, a strong, horizontal linear fabric, parallel to the foliation, is produced by the elongated amphibole c-axis.

Conclusions

Angular relationships between mylonite foliation planes and shear zone walls indicate high total strain (greater than 15γ) and a sinistral sense of shear. Most mylonites are formed from gabbroic protoliths and are strongly foliated. Where shear zone walls and offset markers are absent, asymmetric microfabric analysis commonly indicates sinistral shear movement. Some mylonite shear zones have suffered both horizontal and vertical displacement. Some undeformed dykes cut, and have been subsequently deformed by, mylonitic shear zones. These date the formation of the D_2 mylonites as coincident with T.S. magmatism. Syntectonic growth of amphiboles and fine grained recrystallisation of groundmass olivine indicate temperatures of formation of betwen 400 and 800^{o}C for the basic mylonites. In contrast, the serpentinite mylonites can only form below 450^{o}C (Rayleigh & Paterson, 1985) and thus, where they outcrop together, must postdate gabbro mylonitisation. Since mylonites are comparatively rare in the WLFC, it is likely that they have accommodated only a small

componant of the total strike-slip offset. Instead, the majority of displacement appears to be confined to abundant serpentinite shear zones and brittle faults, described in the following sections below.

5.2.3 Serpentinite Shear Zones

Introduction

Serpentinite shear zones form the major displacement fractures in the WLFC. The serpentinite shear zones (here termed SSZs) are generally vertical, east-west striking, 10-200m wide and can be continuously traced for over 2km in the field, (Plate 5.8). From maps (Enclosure 1) the SSZs can be seen to form lineaments up to 8km long, that are commonly sigmoidal and bifurcate along strike. Internally, SSZs contain abundant phacoidal blocks, commonly chaotically orientated and consisting of dominantly mantle derived harzburgite and, more rarely, cumulate ultramafic, gabbroic and sheeted dyke material. The blocks are surrounded by a variable percentage of sheared, scaly cataclastic serpentinite with a crude, vertical foliation. SSZs also form the major boundary faults in the north and south of the WLFC where they separate the volcanic and subvolcanic lithologies of the Arakapas fault belt from the sheeted dykes and mantle peridotites of the plutonic complex, and the mantle sequence from the deformed Axis Sequence blocks at Venetou. Elsewhere in the WLFC, SSZs divide the plutonic core complex into relatively coherent, east-west elongate blocks.

In some places SSZs have been reactivated by vertical faulting and low angle thrusting. However, the presence of cross-cutting dykes, some of which have subsequently been deformed, indicates that the SSZs are synmagmatic, formed during the closing stages of Transform Sequence (T.S.) magmatism. The occurrence of phacoidal blocks of D_2 mylonite gabbro within SSZs [082530) further constrains the formation of the SSZs as D_3 events.

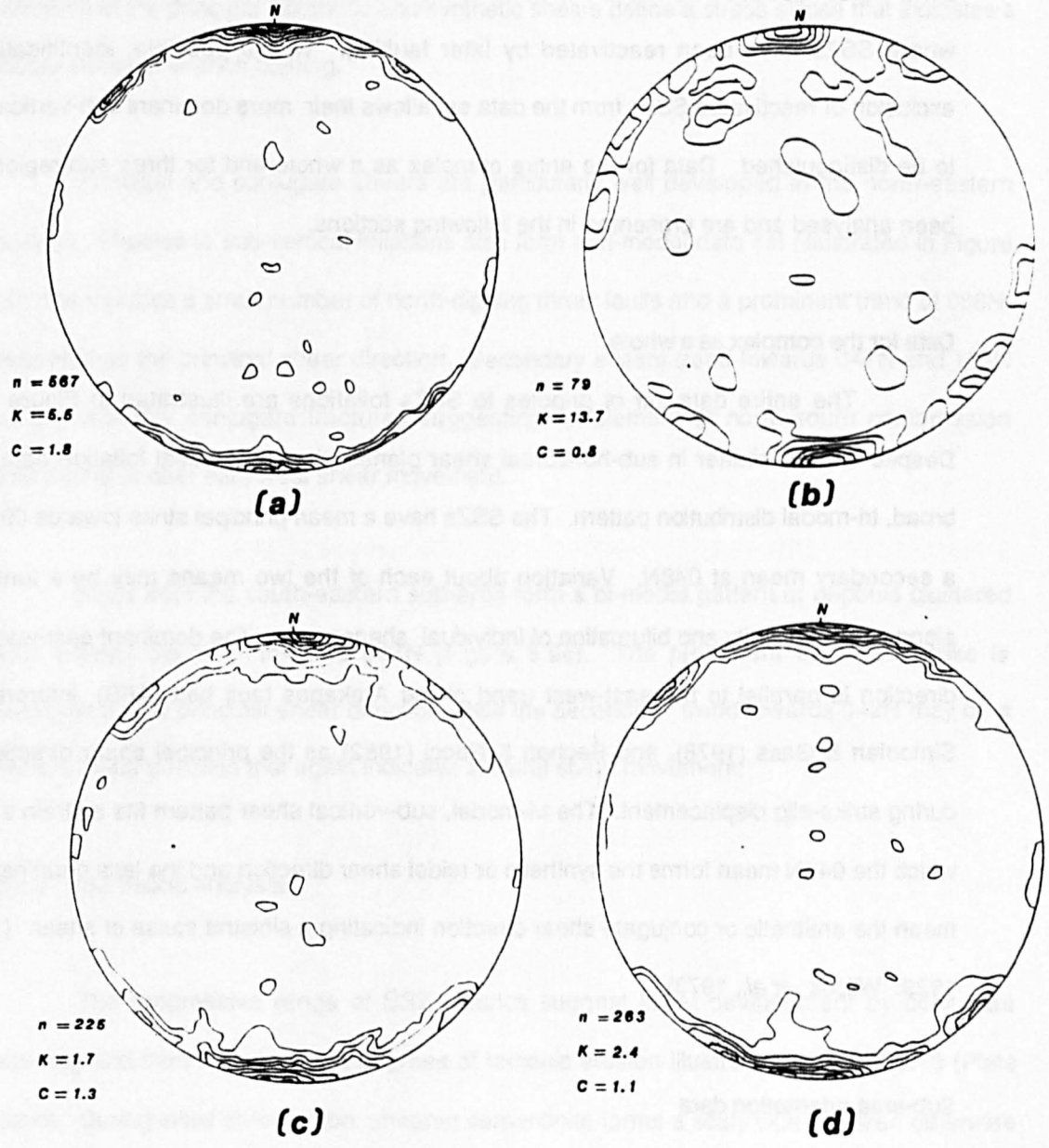

Figure 5.9 Lambert equal area lower hemisphere projection of serpentinite shear zones. **(a)** Data for the complex as a whole shows a distribution that suggests E - W principal and NNE - SSW synthetic shears. **(b)** Data for the western sub-area is dominated by an E - W principal shear direction. **(c)** Data for the northeast sub-area shows a distribution that suggests E - W principal shear, and NE - SW synthetic shear directions. **(d)** Data for the southeastern sub-area shows a similar distribution of principal and synthetic shears. The distributiion pattern of serpentinite shear zones in the WLFC consistantly indicates a sinistral sense of shear.

5.2.3.1 Orientation Data

Although serpentinite shear zone foliation is crude, it is generallly parallel to shear zone walls. Deviation from this orientation usually occurs around large entrained blocks and where SSZs have been reactivated by later faulting. Where possible, identification and exclusion of reactivated SSZs from the data set allows their more dominant sub-vertical trends to be distinguished. Data for the entire complex as a whole and for three sub-regions have been analysed and are presented in the following sections.

Data for the complex as a whole

The entire data set of pi-poles to SSZs foliations are illustrated in Figure 5.9a-d. Despite a large scatter in sub-horizontal shear planes, the sub-vertical foliation data form a broad, tri-modal distribution pattern. The SSZs have a mean principal strike towards 092N with a secondary mean at 048N. Variation about each of the two means may be a function of along-strike sinuosity and bifurcation of individual shear zones. The dominant east-west shear direction is parallel to the east-west trend of the Arakapas fault belt (AFB), interpreted by Simonian & Gass (1978), and Bechon & Rocci (1982) as the principal shear direction (σ_1) during strike-slip displacement. The tri-model, sub-vertical shear pattern fits a strain ellipse in which the 044N mean forms the synthetic or reidel shear direction and the less prominant125N mean the antithetic or conjugate shear direction indicating a sinistral sense of shear. (Riedel, 1929; Wilcox *et al.*, 1973).

Sub-area orientation data

Figure 5.9b illustrates 78 pi-poles to foliation planes from the western subarea. Although reactivation of SSZs by minor late thrusting is responsible for the sub-horizontal shear planes, the majority of SSZ strike data clearly indicate the mean principal, sub-vertical shear direction of 087N that is virtually coincident with the pi-pole mean plane orientation dipping at 87^{o} towards 188N. A dispersion towards the NE in sub-vertical SSZs forms a

tri-modal distribution which includes the east-west principal shear direction (σ_1) and 012N and 037N trending antithetic and synthetic shears respectively. Both the synthetic shears and those trending 128N form a conjugate set that suggest an element of transpression. The orientation of the principal antithetic and synthetic shears define a stress ellipse that indicates a sinistral sense of wrench faulting.

Principal and conjugate shears are particularly well developed in the north-eastern sub-area. Pi-poles to sub-vertical foliations also form a tri-modal data set (illustrated in Figure 5.9c) that includes a small number of north-dipping thrust faults and a prominent trend of 088N, interpreted as the principal shear direction. Secondary shears trend towards 047N and 138N and are probably conjugate fractures suggesting an element of north-south compression either during or after east-west shear movement.

SSZs from the south-eastern sub-area form a bi-modal pattern of pi-poles clustered about a mean dip of 7^{o} towards 003N (Figure 5.9c). The prominent east-west strike is interpreted as the principal shear direction while the secondary trend towards 042N may be a synthetic shear direction that again indicates sinistral shear movement.

5.2.3.2 SSZ Fabric analysis

The progressive range of SSZ fabrics suggest initial development by conjugate fracturing and then by increasing degrees of tectonic erosion illustrated in Figure 5.10 (Plate 5.9a-b). During initial deformation, sheared serpentinite forms a scaly skin between otherwise coherent blocks of partially serpentinised peridotite. The sheared serpentinite forms along *en-echelon* fractures separated by either 120^{o} or 80^{o}. The three-dimensional intersection of these fracture planes forms phacoidal blocks.with their long axes aligned east-west. With progressive shearing the *en-echelon* fractures widen and fill with sheared serpentinite forming anastomosing shear strands. This style of fabric is commonly developed in SSZ, which are, on

average, 20m wide. The phacoidal blocks are tectonically rounded, with a matrix of cataclastic serpentinite derived from crushed and eroded block corners. Blocks are generally aligned with their long axes parallel to shear zone walls and inclined at all angles. Fibrous antigorite-filled veins cutting both the matrix and the blocks resemble hydraulic fractures and are evidence of high pore fluid pressures during SSZ formation.

In their most extreme development, SSZs have more than 50% matrix totally surrounding isolated phacoidal and rounded blocks. Two styles of extreme SSZs are developed; a wide shear zone, up to 250 m across and a narrow shear zone, less than 50 m wide. In the former, a scaly serpentinite matrix with a crude foliation contains phacoidal blocks ranging in size from 10cm to 50m. Although the blocks are generally chaotically orientated, block long axes are orientated oblique to both the shear zone walls and matrix foliation (Figure 5.11). This can best be interpreted as anticlockwise rotation of the blocks during sinistral shearing. Where blocks have deviated more than 40^{o} from parallel with the matrix foliation, differential shear stress has disintegrated them into smaller phacoids orientated parallel to the matrix fabric.

Narrow, matrix-rich SSZs less than 50m wide contain a very sheared, pervasively foliated serpentinite matrix supporting small blocks, usually less than 0.5m in diameter, that are either strongly flattened or, if smaller than 5cm in diameter, rounded. All the blocks are orientated parallel to the vertical matrix foliation and shear zone walls [090542].

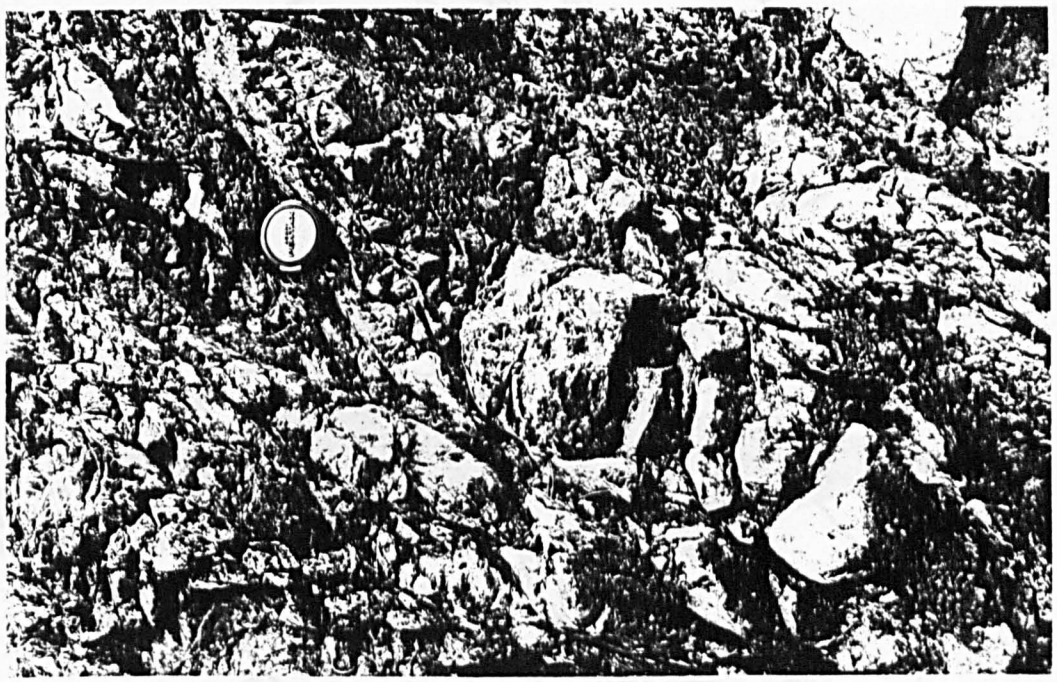

Plate 5.9a SSZ showing early development stage with narrow anastomosing shears dissecting fractured and slightly sheared blocks.

Plate 5.9b Mature development of an SSZ showing the formation of phacoidal blocks, vertically orientated and surrounded in a matrix of comminuted serpentinite.

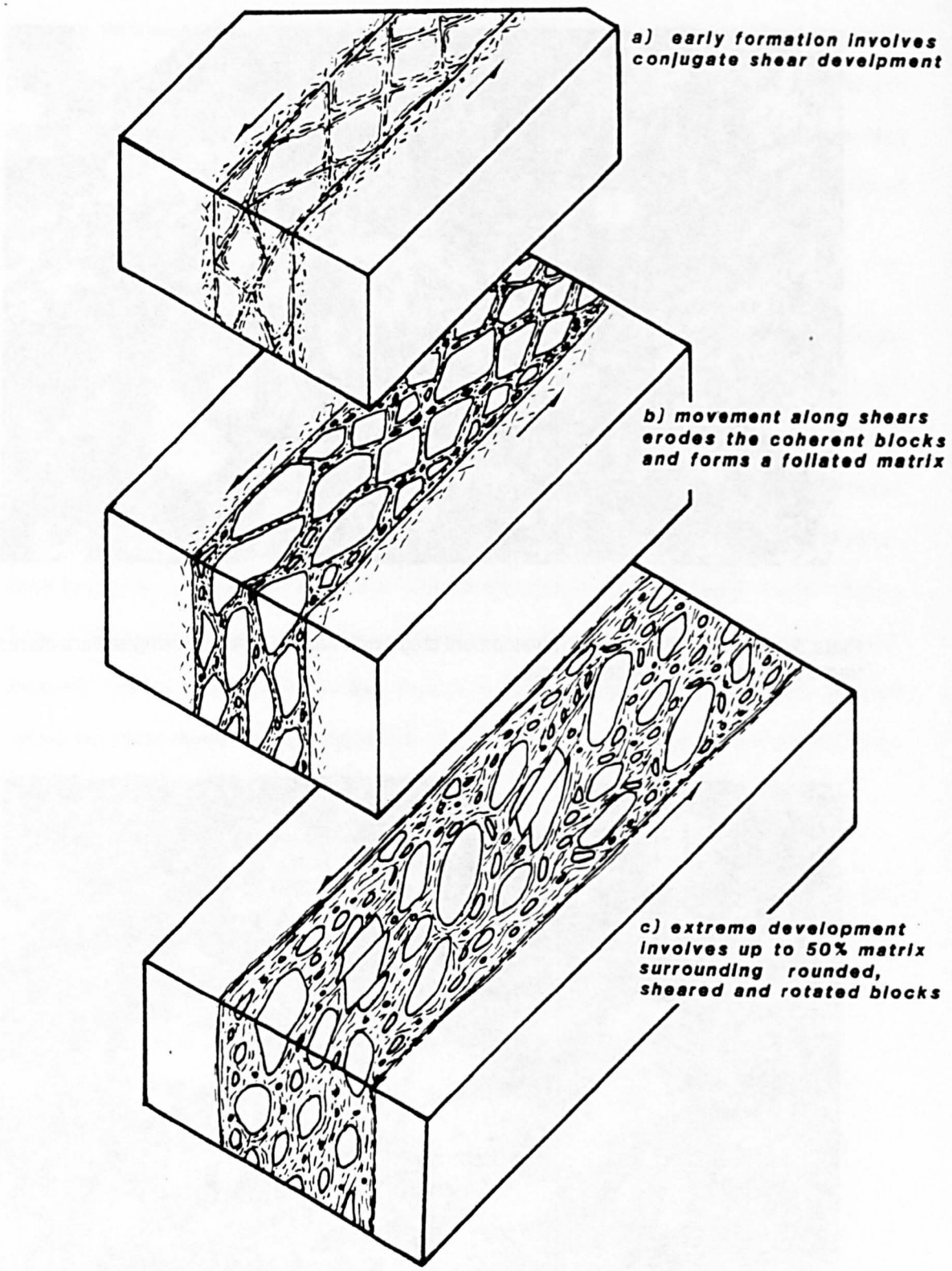

Figure 5.10 Schematic block diagram showing three successive stages in the development of SSZ fabrics. The SSZs are vertical and initially formed by shear and brittle faulting in partially serpentinised harzburgite from the Mantle Sequence. More extreme development of the SSZs includes their emplacment at high structural levels within the WLFC Axis Sequence.

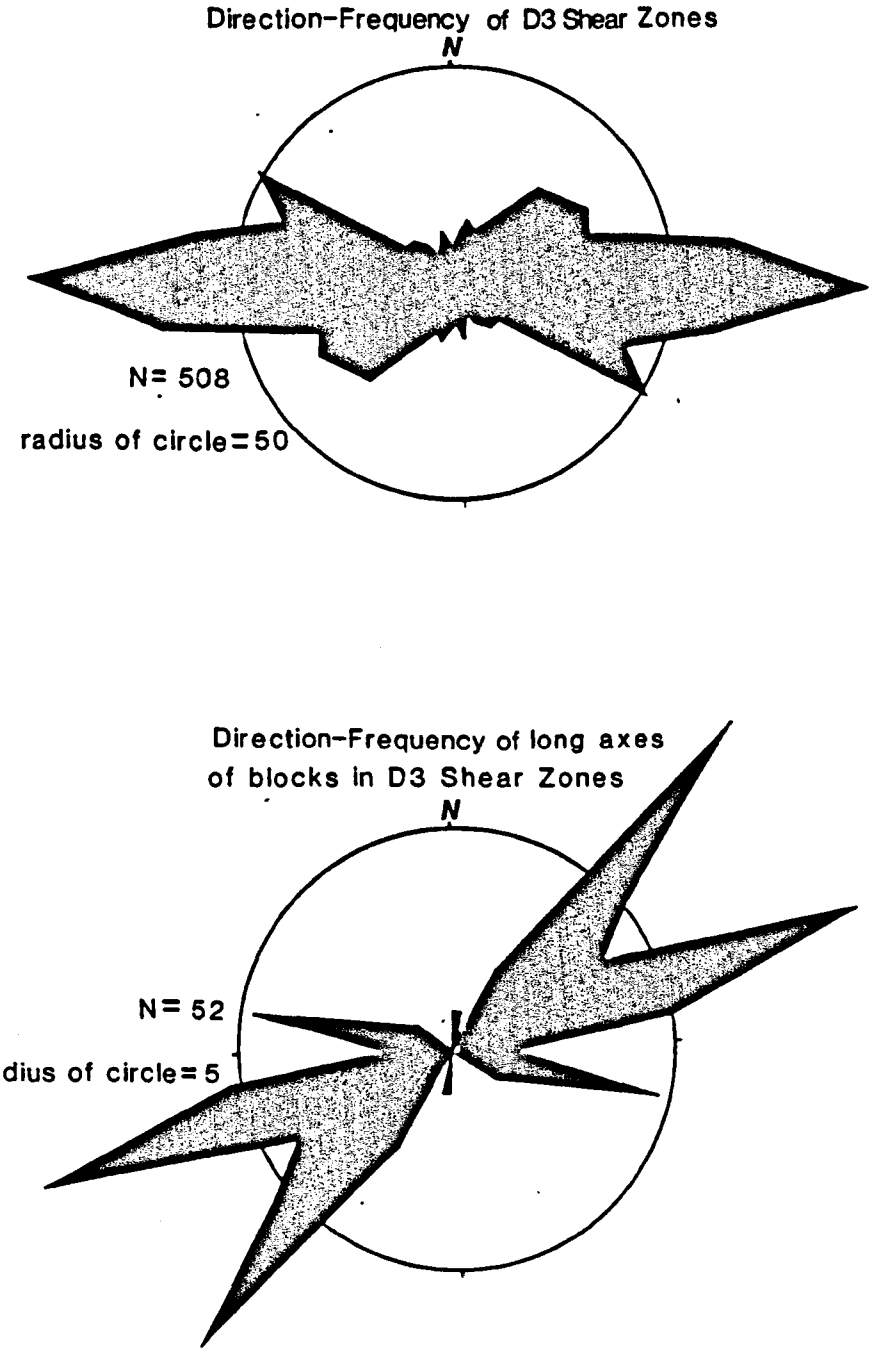

Figure 5.11 Cumulative direction v frequency diagrams for SSZs and long-axes of the largest blocks entrained within the SSZs, respectively. The block long-axes are oblique to the main SSZ trends suggesting anticlockwise rotation and sinistral shear vorticity (large blocks refer to inclusions greater than 4m in length).

5.2.3.3 Discussion

In the past many sheared serpentinites have been interpreted as sedimentary deposits (Bailey, 1964; Milovanovic *et. al.*, 1960; Moiseyer, 1969,1970; Lockwood, 1969,1970; Oakeshott 1968). Serpentinite protrusions on the sea-flooor are also common (Bonatti *et. al.*, 1974; Bonatti & Honnorez, 1971; Coleman, 1980) with tectonic emplacement processes only being speculated upon (Oakshott, 1968). Although Karson (1978) interprets a vertical, foliated and blocky serpentinite shear zone in the coastal complex of the Bay of Islands ophiolite, Newfoundland, as a sheared and serpentinised peridotite dyke, the closest approximation to the WLFC serpentinite shear zones have been described from the Mamonia complex, Cyprus, by Lapierre (1975) and in detail by Swarbrick (1980). Although Swarbrick interpreted the sheared serpentinites as hydrated mantle peridotite, mobilised at depth during transpressional strike-slip faulting, no attempt was made to ascribe a mechanism of vertical serpentinite emplacement. However, in the WLFC, mantle derived serpentinite has been protruded to high structural levels and (rarely) eroded onto the sea-floor (see Chapter 4). Based on thickness reconstructions of the WLFC Axis Sequence (A.S.), the sheared serpentinite rose almost 4km, while in an oceanic setting.

Buoyancy driven emplacement of serpentinite

In the absence of any single fault displacements sufficient to displace serpentinite to high structural levels, it is more probable that vertical protrusion involved a mechanism of density contrast between the sheared serpentinite and the associated WLFC Axis Sequence crustal units. The following model of emplacement involves relative buoyancy of serpentinite and initially assumes the following:-

i) serpentinite approximates to a viscous Newtonian fluid;

ii) the serpentinite is of constant density with depth (ie. down to about 11km)

iii) the serpentinite is confined to a conduit of finite width, with solid walls that impose hydrostatic pressure.

The objective of the following calculations is to establish whether the serpentinite in the SSZs could have been protruded on to the sea-floor by hydrostatic pressure imposed upon it from the overlying and surrounding Axis Sequence crustal units. This involves a mass-balance calculation between the total crustal sequence density P_T, the crustal thickness Z', the total serpentinite density P_Σ and the depth of the serpentinite column d (Figure 12). The formulae used are simple mass-balance equations in which the pressure at the base of the serpentinite column is compared to the overburden pressure at the base of the Axis Sequence. The difference between the two is expressed in terms of the level at which the serpentinite column will achieve equilibrium with the A.S., and the pressure with which the serpentinite will (if at all) be extruded on to the sea-floor.

The depth of the serpentinite column that is in isostatic equilibrium with the WLFC A.S. crustal units is given by:-

$$d = z' P_T / P_\Sigma \qquad \text{Equation 5.1}$$

where the average density of the crustal sequence P_T is given by:-

$$P_T = (P_{pl} \times a) + (P_{shd} \times b) + (P_{gb} \times c) + (P_{cum} \times d) \qquad \text{Equation 5.2}$$

where:-

P_{pl} is density of pillow lavas = 2.350g cm-3 (Vine, Unpub. data)

P_{shd} is density of sheeted dyke complex = 2.700 (Vine, *op. cit.*)

P_{gbh} is density of isotropic gabbros = 2.900 (Vine, *op. cit*)

P_{cgb} is density of layered cumulates = 3.000 (Shelton, 1984)

a is thickness of volcanic sequence; based on Kapillo section

b is thickness of sheeted dyke complex; based on Dherona block

c is thickness of isotropic gabbro + diorite; based on Venetou section

d is thickness of cumulates, based on Venetou section

P_Σ SSZs density (Vine & Smith, Unpub. data) taken as 2.600 and 2.630 g

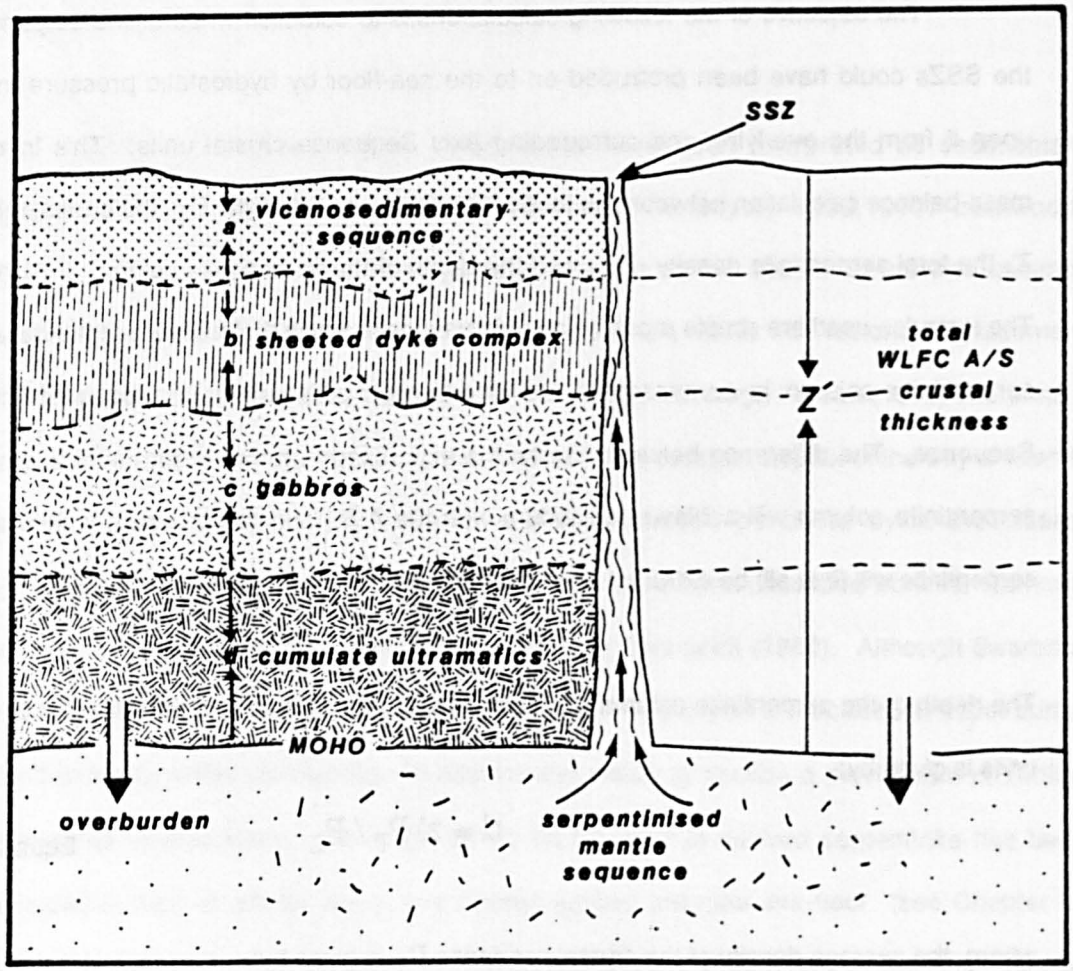

Figure 5.12 Schematic diagram showing a possible mechanism for the emplacement of SSZs to high structural levels. The model assumes a fluid behaviour for the serpentinite that is forced upward by the hydrostatic pressure imposed upon it from the overlying WLFC Axis Sequence crustal units. The figure notation refers to the relevant mass balance equations in the text.

From Equation 5.1 a range of dephs (d) of serpentinite columns can be found, depending on their density. On subtraction of d from Z' (the A.S. crustal thickness), a range in thickness (t) to which the sheared serpentinite will pond on the sea floor is given.

where:-

for P_{Σ} max. t = 86.3m

for P_{Σ} min. t = 14.3m

Although serpentinite may approach the behaviour of a highly viscous fluid (Bailey *et al.*, 1964), it is not Newtonian in that it can transmit shear stress and has an ultimate shear

strength. Experimental deformation of serpentinite (Rayleigh & Paterson, 1965) demonstrates decreasing shear strength with increasing temperature due to the increase in pore pressure during partial dehydration reactions to talc. Lockwood (1971) suggested a similar process of pore pressure 'lubrication' purely by the addition of water to shear zones. Assuming initial brittle shear and cataclasis of the serpentinised peridotite by fault displacement, any subsequent partial dehydration to talc and access of water will decrease the effective viscosity of the sheared serpentinite.

To calculate the extrusion pressure (P_{ex}) of the serpentinite, $P_{Z'}$ and P_{Σ}, the pressure at the base of the WLFC A.S. and serpentinite column respectively, must be evaluated.

base pressure of A.S.	$P_Z = P_T \times Z'$	= 983 bars
base pressure of the SSZ	$P_{\Sigma} = P_T \times Z'$	= 979.7 bars max or =961.1bars min.
The extrusion pressure	$P_{ex} = P_{Z'} - P_{\Sigma}$	= 3.32 bars min. or =21.78 bars max.

In either situation (P_{Σ} max. or min.), even a small viscous shear strength for serpentinite would inhibit extrusion onto the sea-floor. The limited amount of clastic serpentinised mantle peridotite, present only in intervolcanic breccias in the south of the WLFC (near Akrounda) would suggest that the SSZ serpentinites had a viscous shear strength in the range of the calculated extrusion pressure. This is consistent with the observed viscous shear strength of gravity-slide emplaced serpentinite flows both on land (Lockwood 1971; Dickenson, 1966; Moiseyer, 1970) in California and on oceanic ridges (Bonatti, 1976).

Conclusions

The dominance and orientation of SSZs as both principal east-west shear fractures and northeast - southwest trending synthetic shear fractures (Figure 5.13) illustrates a mean stress ellipse for the WLFC. Although the exact orientation and dimensions of the stress ellipse can not be accurately found its general orientation is consistent with those based on experimental work by Wilcox *et.al.* (1973) and indicates a sinistral sense of wrench faulting. The occasional presence of conjugate shear sets suggests that shear displacement was intermittently accompanied by both transtension and transpression. Progressive stages in SSZ matrix development from 10% to greater than 50% are the result of increasing shear both along and across serpentinite shear zones. Variation in orientation of phacoidal block long axes between horizontal and vertical indicate dip-slip while block long axes orientated horizontally and parallel to shear zone walls and matrix foliation indicate strike-slip movement. Fracturing and the resultant formation of phacoidal blocks and their subsequent rotation in a scaley serpentinite matrix indicates an increase in volume for the shear zone, and hence transtension across the principal east-west shear direction. Access of seawater to SSZs may have enhanced localised serpentinisation and increased pore fluid pressure, reducing the matrix serpentinite viscosity. Any increase in fluidity or decrease in density of sheared serpentinite would aid protrusion on to the sea-floor.

Although serpentinite at high structural levels within the A.S. is predominately of a harzburgite origin (and hence must have been emplaced vertically from below) it is posible that some serpentinite was derived from the cumulate ultramafics forming the base of the A.S. Where these later serpentinites form SSZs that cut A.S. cumulate ultramafics, many are probably *in situ* and have been formed directly from their wall rock by hydration and shear.

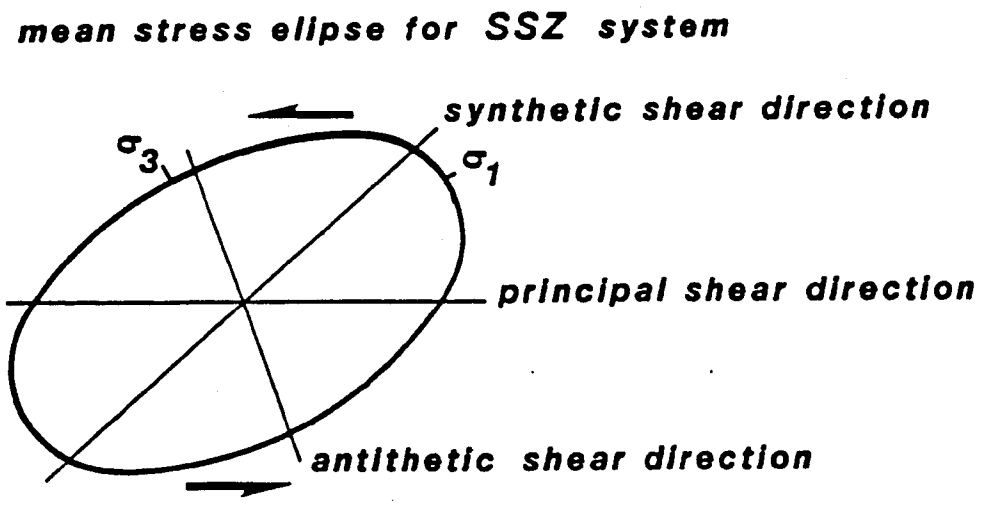

Figure 5.13 General stress ellipse constructed from the orientations of the SSZs and by a comparison with experimentaly produced strike-slip shear (Wilcox *et al.*, 1973). Although the precise orientation of the stress ellipse can not be known accurately, its general configuration with E - W principal, and NE - SW synthetic shear directions indicates a sinistral sense of shear.

5.2.4 Early Fault Structures

5.2.4.1 Minor faults

Abundant minor faults in the western Limassol Forest complex could not be followed for any significant distance along strike nor could they be stratigraphically dated with confidence. However, the presence of cross-cutting dykes or later, north-south faults allowed the older faults to be identified, and interpreted as early sea-floor structures. This initially tentative interpretation is supported by their average orientation that is similar to the east-west principal shear direction of the SSZs . Although their exposure is poor, detailed mapping of the faults allowed their cumulative lengths to be established reasonably accurately (Figure 5.14a). Comparison between this and a frequency $\underline{\vee}$ direction diagram (Figure 5.14b) illustrates major fault trends and identifies a significant structural fabric. Figure 5.14a illustrates a unimodal distribution centred about a vector mean strike of 097N. The coincidence between their average trend and direction of principal shear suggests east-west strike-slip shear.

Dispersion about the vector mean direction is probably due to lithospheric inhomogeneity producing sinuosity of the faults along strike.

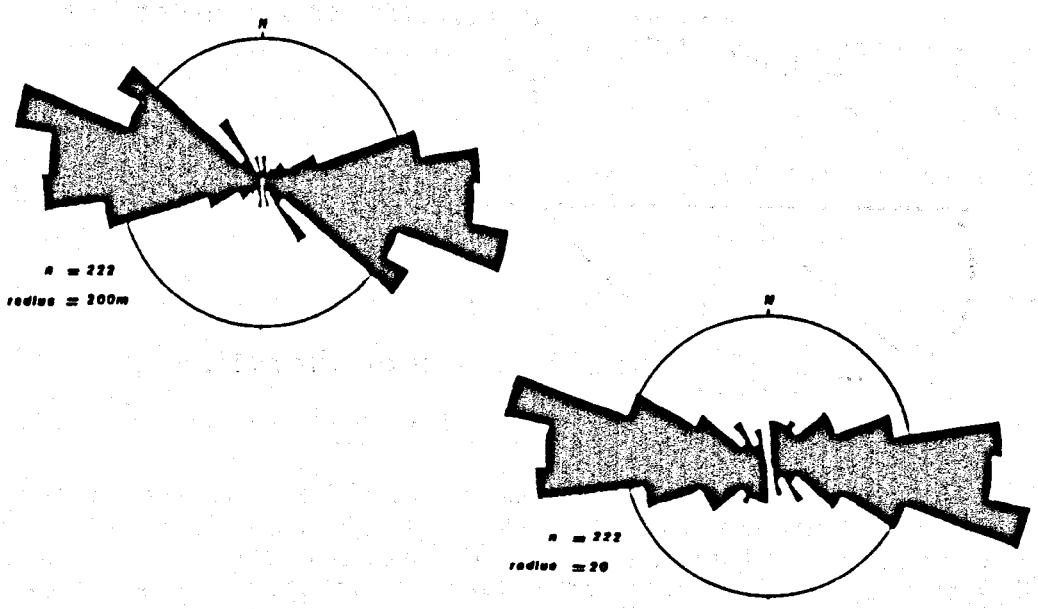

Figure 5.14 Cumulative length y direction and frequency y direction diagrams for 'early', oceanic faults systems cutting the WLFC. The pattern of faults is similar to that for the SSZs with a dominant E - W principal shear direction. The principal E - W trending faults are all of approximately the same length.

In comparison, the cumulate frequency y direction diagram (Figure 5.14b) also illustrates a unimodal distribution centred on a vector mean strike of 092N. The similarity in mean directions between this and Figure 5.14a indicates similar fault lengths with an average of 233m. This relatively short fracture length is, in part, a function of sampling. Larger, reactivated faults, have been treated separately in section 5.3.2.

5.2.4.2 Boundary faults

Boundary faults separate the WLFC from the main axial structural trend of the Arakapas fault belt in the north and define the beginning of the southern margin of the complex in the south. These faults are continuous shear zones, occasionally offset by small conjugate fractures. They can be traced over several kilometres in the field, allowing reasonable estimates of their overall length. In general, the orientation of these boundary faults is similar to

the east-west principal shear direction of the SSZs. This, combined with the disappearance of boundary faults beneath the Mesozoic and Tertiary sedimentary cover to the east and west, demonstrate that they were original oceanic features active during the formation of the WLFC.

Four major boundary fault sets are described in the following section. These fractures all come from the northern contact area between the WLFC and the Arakapas fault belt. The average trend and cumulative length of each fault has been calculated with individual fault segments plotted on cumulative length $\underline{v}$ direction diagrams (Figure 5.15a to Figure 5.15d). The resultant shear distribution patterns closely resemble those found experimentally for principal, synthetic and antithetic fracture development in sinistral shear regimes (Wilcox *et. al.*,1973). Reactivation of the boundary faults by reverse faulting results in anomalous NW-SE striking, northeasterly dipping trends. Such reactivation particularly affects boundary faults along the southern margin of the Limassol Forest complex, in the proximitty of the Yerasa fold belt.

Figure 5.15a shows a long, continuous fault system with individual segment lengths of about 500m. The distribution clearly defines a principal shear direction trending 092N, with conjugate shears at 050N and 140N that suggest occasional N-S compression across the complex. Figure 5.15b illustrates a system of shorter fault segments, each about 200 m in length. The distribution is bi-modal with the principal shear direction trending towards 097N and a synthetic shear direction of 025N.

The distribution of the fault segments also defines a principal shear direction of 090N and prominant synthetic shear set at 070N. The major boundary fault systems are offset by NE-SW trending faults forming a conjugate set with the larger ones. These faults are illustrated in Figure 5.15c where they have a prominant trend of 060N. This direction, when compared with the 0890N principal shear direction, is similar to the synthetic shear trends of Figures 5.15a-c.

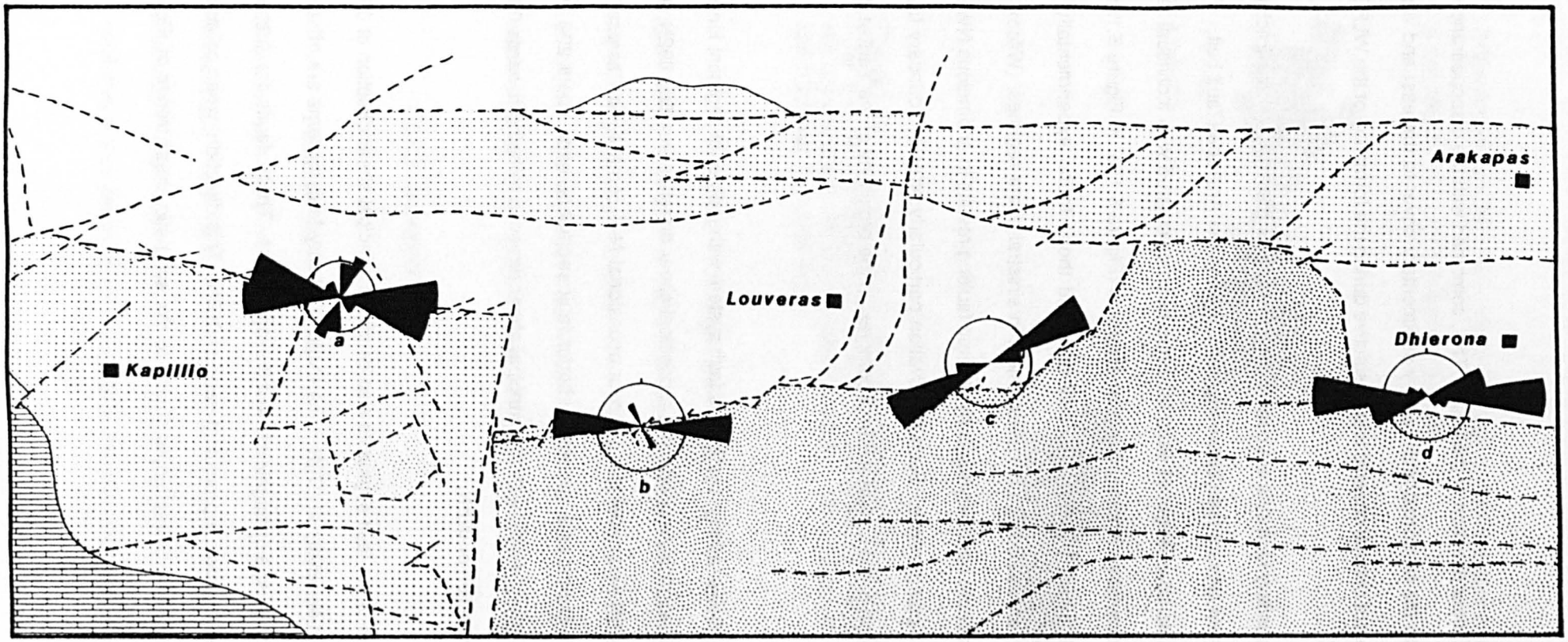

Figure 5.15 Structural map locating the positions and cumulative length y direction diagrams for the four boundary fault segments discussed in the text. Figure 5.15d illustrates another major fault system with segments 200 to 250 m long.

The difference in shear directions between the major boundary faults probably reflects stress variations in the WLFC lithosphere along its northern margin. These local variations in stress are probably the result of major sinuosity in the strike-slip boundary fault between the WLFC and the Arakapas fault belt.

5.2.5 The Structural Significance of Basic Dykes Cutting the WLFC

Introduction

The distribution and orientation of basic dykes cutting the plutonic core of the WLFC illustrate the tensional stress fields that were operative during its magmatic evolution. Cross-cutting relationships have revealed an intrusive stratigraphy involving early east-west striking dykes, cut by later 040N trending mafic and picritic varieties, all cut by sinuous, north-south striking, brownstone dykes. Spatial and temporal variations in dyke orientation, are examined by sub-dividing the WLFC into three arbitrary, structural domains and a further sub-division into mafic and picrite dykes emplaced into harzburgite, gabbro or serpentinite shear zones. Variation in the density of dyke swarms across the WLFC is assumed to be symmetrical and defines a crustal extension profile that predicts a minimum 9km width for the complex. Dyke strikes interpreted as perpendicular to σ_1, the principal axis of compression, are oblique to the principal east-west trending shear direction and indicate sinistral shear deformation.

5.2.5.1 Dykes cutting the mantle sequence

A dispersed bi-modal distribution of pi-poles to mafic dykes cutting harzburgite in the western sub-area is illustrated in Figure 5.16a. The bi-modal pattern is interpreted as two original dyke sets, the most prominant being vertical and striking towards 041N, whereas the

subsidiary set strikes 092N and varies in dip between vertical and sub-vertical, 66°SW, strike 123N. Southwest of Petro Mutti [012527] both dyke sets are present forming a conjugate pair in the vicinity of the Petro Mutti gabbro. A similar conjugate dyke set occurs at [068552], where isolated gabbro apophyses probably indicate the presence of the Kalithia gabbro pluton at depth. Dykes cutting T.S. gabbros form a well-defined pi-pole cluster (illustrated in Figure 5.16b) and have an average 83° dip, 050N strike. If these dykes are later than those described above, then they suggest a change in σ_1 to the NE-SW following gabbro emplacement.

In the north-eastern sub-area both the dykes cutting harzburgite and dykes cutting T.S. gabbros (illustrated in Figure 5.16c & d) have almost coincident mean dips of 86° SW, strike 049N and 82°SW, strike 052N, respectively. This common NE-SW trend approximates to the average orientation of the dykes cutting T.S. gabbros in the western sub-area. Despite being strongly clustered, both distributions have weak secondary concentrations of pi-poles to vertical dyke, striking 095N to115N respectively. In the vicinity of the Venetou area [065507], these essentially east-west trending dykes are often cut by and hence, pre-date, the dominant NE-SW dyke trend, where they are interpreted as intermittent intrusions parallel to the east-west principal shear direction.

In the southeastern sub-area basic dykes cutting harzburgite and T.S. gabbros form a tight cluster of pi-poles (Figures 5.16e and 5.16f). These dykes have a predominant mean dip of 81° NW, strike 044N and 86NW, strike 054N which is similar to the average orientation of dykes in the previous two sub-areas. Figure 5.16f also illustrates a subsidiary cluster of vertical east-west striking dykes which only cut T.S. gabbros. These 100N-115N trending dykes suggest north-south tension in the vicinity of the gabbros, possibly during the final stages of plutonic emplacement.

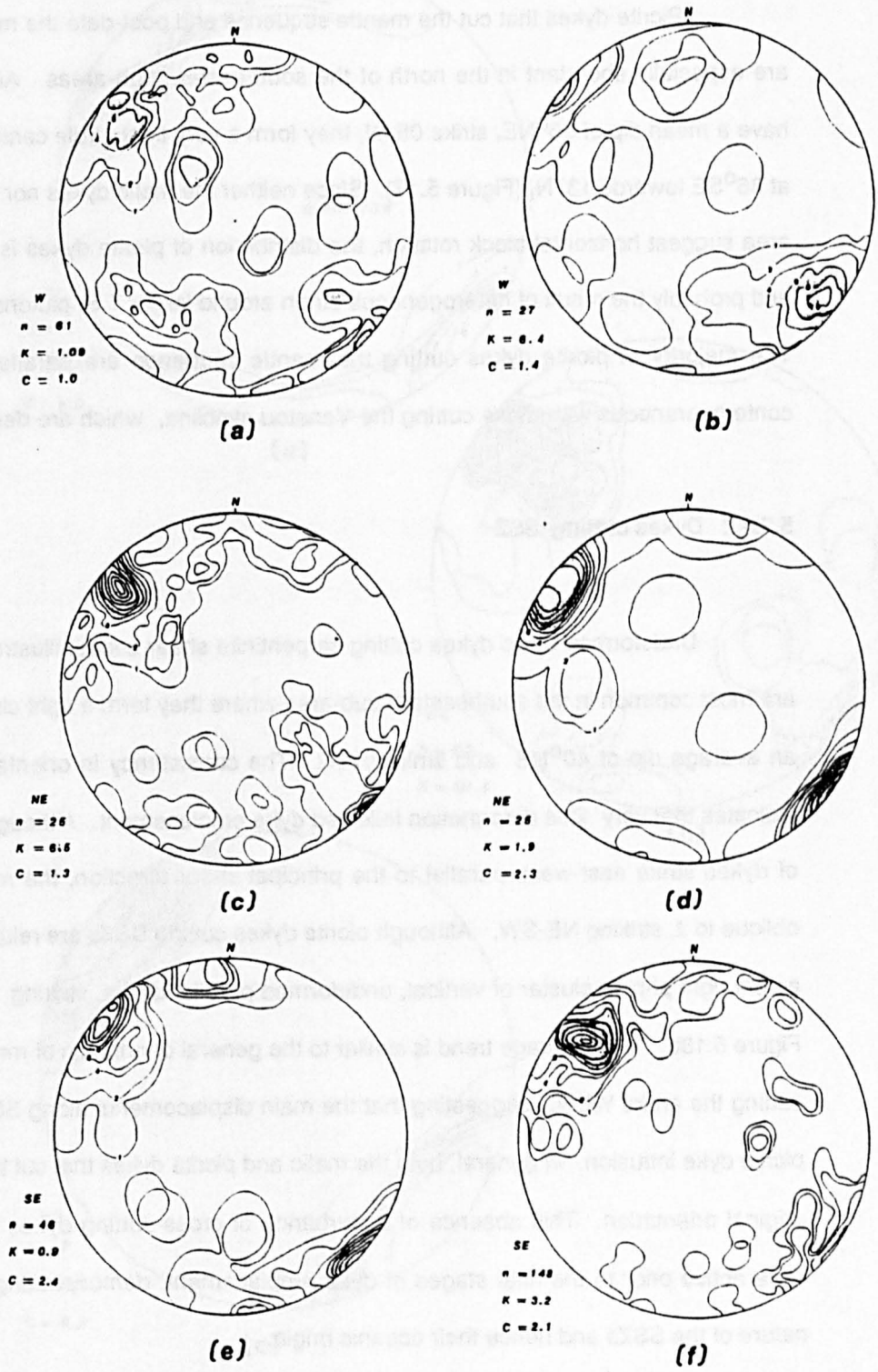

Figure 5.16 Lambart equal area lower hemisphere projections of pi-poles to mafic dykes. (a) distribution of pi-poles cutting Mantle Sequence, and (b) distribution of pi-poles to mafic dykes cutting T.S. gabbro, both from the western sub-area. (c) and (d), distributions of pi-poles to mafic dykes cutting Mantle Sequence and T.S. gabbro from the northeastern sub-area. (e) and (f), distributions of mafic dykes cutting Mantle Sequence and T.S. gabbro from the southern sub-area. All the dykes have a prominant mean NE - SW trend.

Picrite dykes that cut the mantle sequence and post-date the majority of mafic dykes are especially abundant in the north of the southeastern sub-areas. Although these dykes have a mean dip of 86°NE, strike 054N, they form a very tight girdle centred on a pole dipping at 86°SE towards 137N, (Figure 5.17). Since neither the mafic dykes nor fault structures in the area suggest horizontal block rotation, the distribution of picrite dykes is considered primary, and probably the result of heterogeneous strain around larger T.S. plutons.

The majority of picrite dykes cutting the mantle sequence are parallel to and considered contemporaneous with those cutting the Venetou syncline, which are described below.

5.2.5.2 Dykes cutting SSZ

Undeformed basic dykes cutting serpentinite shear zones, illustrated in Figure 5.18a, are most common in the southeastern sub-area where they form a tight cluster of pi-poles with an average dip of 40°NE and strike 079N. The consistency in orientation of these dykes indicates that very little deformation followed dyke emplacement. Although a small proportion of dykes strike east-west, parallel to the principal shear direction, the majority of dykes are oblique to it, striking NE-SW. Although picrite dykes cutting SSZs are relatively rare, they form a very tight pi-pole cluster of vertical, undeformed parallel dykes, striking 041N, illustrated on Figure 5.18b. Their average trend is similar to the general orientation of mafic and picrite dykes cutting the entire WLFC, suggesting that the main displacements along SSZ occurred prior to picrite dyke intrusion. In general, both the mafic and picrite dykes that cut the SSZs retain their original orientation. This absence of disturbance of cross-cutting dykes suggests the SSZs were active prior to the final stages of dyke emplacement, demonstrating the syn-magmatic nature of the SSZs and hence their oceanic origin.

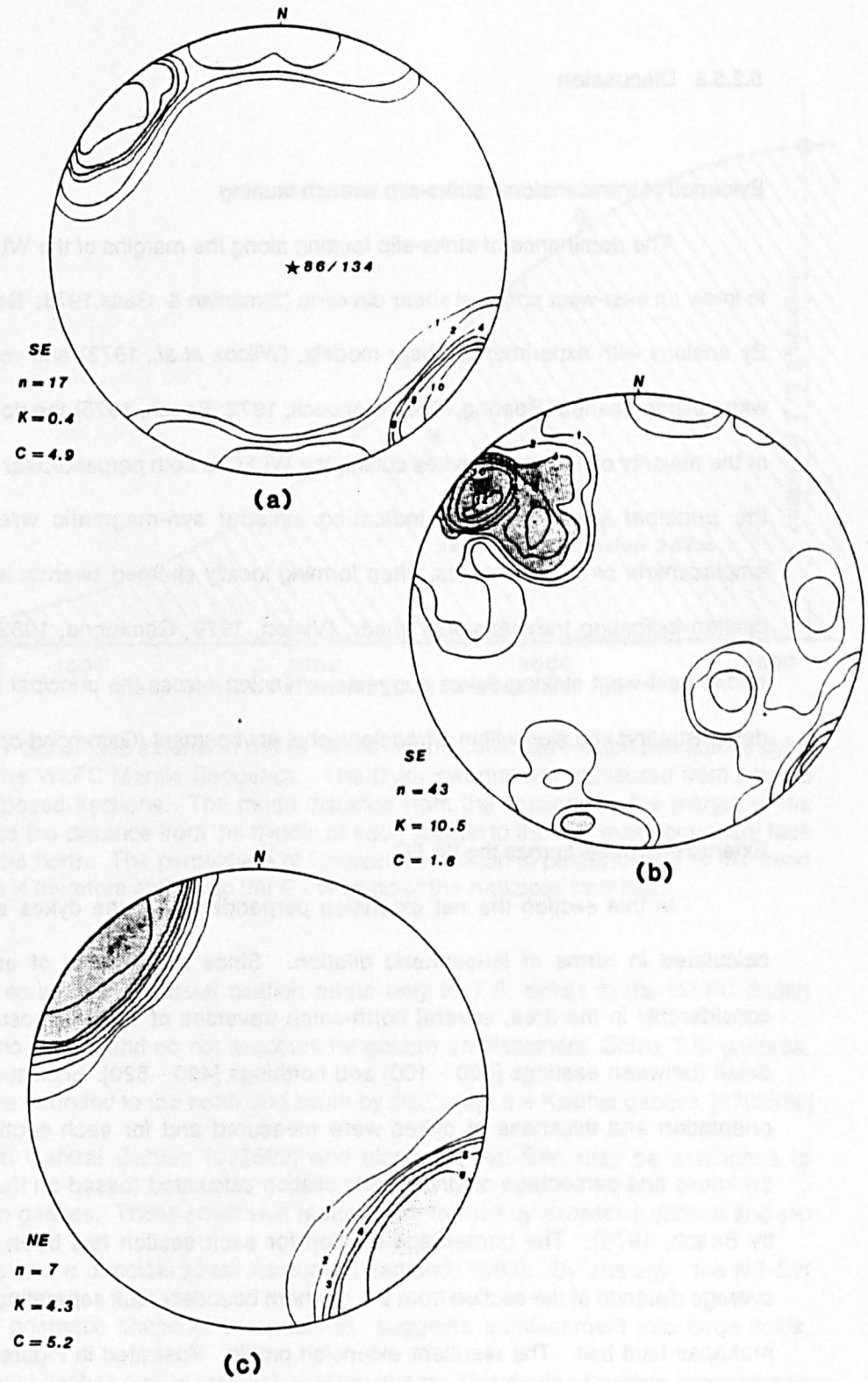

Figure 5.17 **(a)** Distribution of pi-poles to picrite dykes cutting the Mantle Sequence with a prominant E - W to NW - SW trend. **(b)** Distribution of mafic dykes cutting SSZs, the majority of dykes have a prominant NE - SW trend. **(c)** Distribution of picrite dykes cutting SSZs, also with a prominant NE - SW trend.

5.2.5.3 Discussion

Evidence of transtensional strike-slip wrench faulting

The dominance of strike-slip faulting along the margins of the WLFC has been shown to imply an east-west principal shear direction (Simonian & Gass,1978; Bechan & Rocci,1982). By analogy with experimental shear models, (Wilcox *et.al.*, 1973) and vein arrays associated with tension gashes (Roering,1968; Hancock, 1972; Beach, 1975) the dominant NE-SW trend of the majority of T.S. mafic dykes cutting the WLFC is both perpendicular to σ_1 and oblique to the principal shear direction indicating sinistral syn-magmatic wrench faulting. The emplacement of multiple dykes, often forming locally sheeted swarms is evidence of crustal dilation indicating transtensional shear, (Vialon, 1979; Gammond, 1983). The presence of earlier east-west striking dykes suggests extension across the principal shear direction, also demonstrating intrusion within a transtensional environment (Gammond *op. cit.*).

Extension profiles across the WLFC

In this section the net extension perpendicular to the dykes across the WLFC is calculated in terms of lithospheric dilation. Since the amount of exposed rock varies considerably in the area, several north-south traverses of 100% exposure were mapped in detail (between eastings [080 - 100] and northings [490 - 520], Enclosure 1). The number, orientation and thickness of dykes were measured and for each section their cumulative thickness and percentage of lithospheric dilation calculated (based on the technique outlined by Beach, 1975). The percentage dilation for each section has been plotted against the average distance of the section from the northern boundary fault separating the WLFC from the Arakapas fault belt. The resultant extension profile, illustrated in Figure 5.19, indicates the position of maximum dilation that if assumed to be symmetrical, gives a minimum width of the WLFC of 8.5km between boundary faults. Integration of the extension profile gives an estimate of the total lithospheric dilation perpendicular to the dykes of 774m or 9.1%.

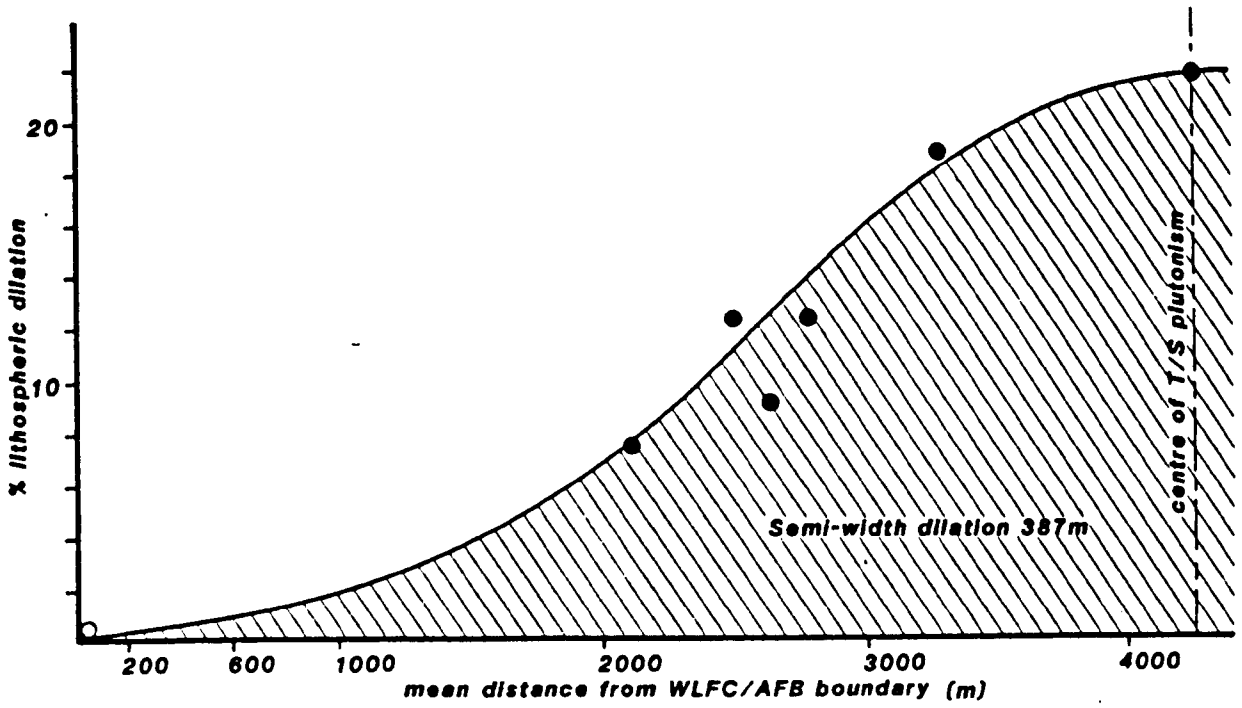

Figure 5.19 Schematic extension profile based on the cumulative extension across dyke swarms within the WLFC Mantle Sequence. The Dyke swarms are measured from several continuously exposed sections. The mean distance from the sections to the margin of the WLFC is taken as the distance from the middle of each section to the first major boundary fault immediately to the north. The percentage of lithospheric dilation is perpendicular to the trend of the dykes and is therefore oblique to the E - W trend of the Arakapas fault belt.

These estimates of crustal dilation relate only to T.S. dykes in the WLFC during transtensional movement and do not acccount for gabbro emplacement. Some T.S. gabbros, however, that are bounded to the north and south by SSZs (eg. the Kalithia gabbro [0705550] and the Eastern Central Gabbro [085522] and elongated NE-SW, may be analogous to prismatic tension gashes. These small vein features are formed by excessive dilation and slip across synthetic and a principal shear fractures (Gamond, 1983). By analogy, the NE-SW orientation and prismatic shape of the gabbros suggests emplacement into large scale, lithospheric tension gashes during regional, sinistral shear. This mode of gabbro emplacement is supported by the coincidence of the predicted maximum of lithospheric dilation and the main centre of gabbro intrusion. If the T.S. gabbros were emplaced into lithospheric tension gashes, then they contributed approximately 15% extra dilation in addition to the extension profile based on the dykes alone.

5.2.6 Syn-magmatic Regional Deformation

Introduction

A major problem in the identification of regional or large-scale deformation of ophiolite complexes is the lack of any reliable way-up criteria. Although interlava sediments may help, once below the volcanosedimentary pile there is very little palaeo-orientational control. Previous studies (Juteau *et. al.*, 1977; Girondeau & Nicolas,1981; Rothery, 1983) have resorted to structural analysis of the sheeted dyke complex. Such studies depend on the reliability of the *prima facae* assumption that the sheeted dykes were originally parallel and near vertical. Although simple models of oceanic accretionary processes support this assumption (Cann & Kidd,1977) evidence from the FAMOUS area and more subtle theoretical considerations of tectonic processes at ridge axis (Dewey & Kidd, 1977) suggest that there would be a regional tilt away from the ridge axes imposed on the oceanic lithosphere by cooling and crustal thickening with time. Also, extensional, graben structures with listric and antithetic faulting would further tilt large blocks of oceanic crust. Major thrust or fold tectonics would, however, be unlikely to occur at constructive ridge axes, which are generaly interpreted as essentially extensional environments.

Although the WLFC has suffered both syn-magmatic and post-magmatic regional deformation, post-magmatic deformation is dealt with in a later section. In this section, syn-magmatic regional deformation of two areas is examined in detail, the ophiolite complex having suffered large scale folding at an early stage during its sea-floor history.

The Venetou Syncline

The Venetou Syncline (between eastings [050 - 070] and northings [500 - 520], Enclosure 1) contains a coherent A.S. crustal section from the Moho to the sheeted dyke complex, that has been folded about a NW-SE trending synclinal axis and later intruded by multiple picrite dykes. The Venetou Syncline forms a block that is bounded to the west by a

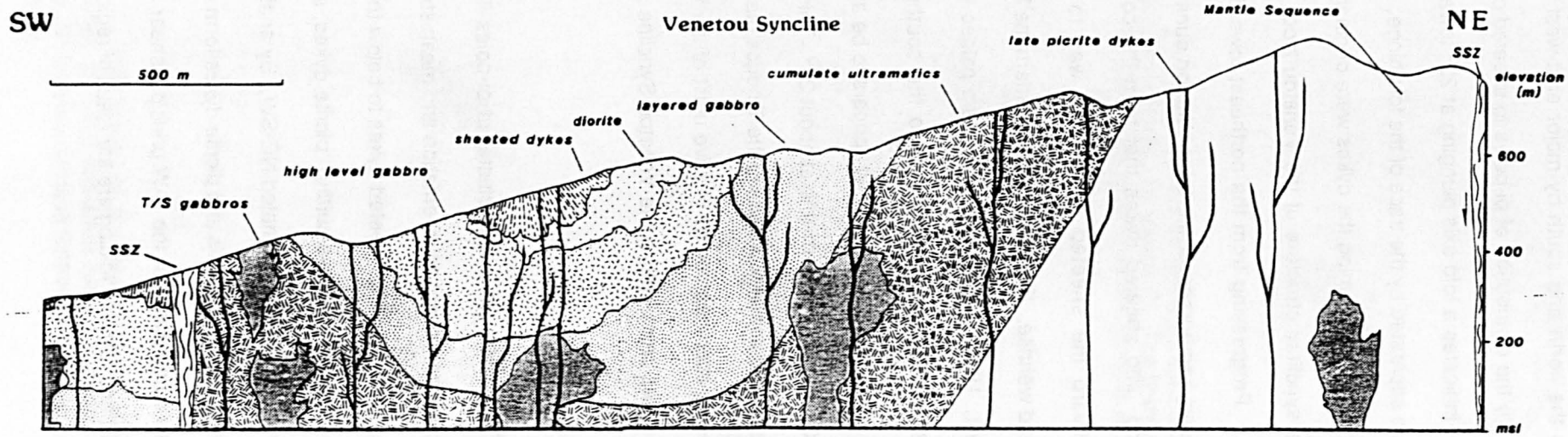

Figure 5.21 Structural cross-section of the Venetou area showing the overall synclinal structure.

major north-south fault and to the north and south by major east-west normal faults. The evidence of folding is two-fold: (i) the distribution of pi-poles to sheeted dykes is related by a small circle (Figure 5.20) that indicates a fold axis plunging at 23° towards 257N. The two resulting sheeted dyke trends are separated by the trace of the fold hinge. The fold is relatively open, having a closure angle of 108°. Assuming the dykes were originally vertical then their initial strike was 041N. (ii) the synclinal structure of the Venetou block is evident from the outcrop pattern (Enclosure 1). Progressing from the northeast towards the southwest, a sequence is seen from tectonised harzburgite at the base through dunite, wehrlite, gabbro, trondhjemite, leucogabbro and into sheeted dykes that form the core of the syncline. Continuing further southwestward the sheeted dykes give way to leucogabbro and trondhjemite, layered gabbro, and wehrlite. From the outcrop pattern the fold axis appears to trend towards the west northwest. Using the sheeted dykes as a palaeo-vertical, a structural cross-section has been constructed from the northeast to the southwest of the block, illustrated in Figure 5.21. From the cross-section, the fold appears to be asymmetric, with the northern limb dipping at about 60° and the southern limb at about 20°. This may be a result of an overall southwards tilt of the ophiolite complex including the Troodos masssif, or it may be a result of NE-SW compression being accompanied by relative uplift of the WLFC to the north. The presence of untilted picrite dykes cross-cutting the Venetou Syncline supports the latter interpretation.

Late cross-cutting picrite dykes form a tight cluster of pi-poles illustrated in Figure 5.22. On average the picrite dykes have a vertical orientation and mean strike of 038N. They occur throughout the Venetou Syncline from the sheeted dykes to below the Moho and in the mantle sequence. The presence of multiple cross-cutting picrite dykes, some of which are composite, suggest a tensional regime with σ_1 orientated NE-SW. By analogy with the basic T.S. dykes both the WNW trending Venetou fold axis and picrite dykes form a stress ellipse the oblique orientation of which, when compared with the E-W principal shear direction indicates that both picrite dyke emplacement and regional folding are the result of regional sinistral shear.

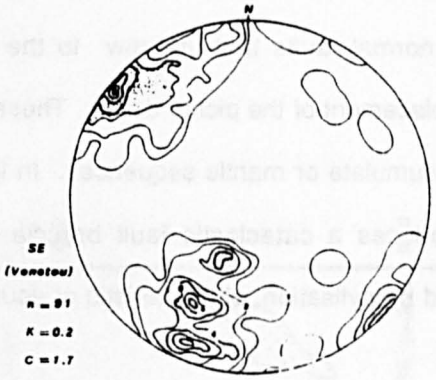

Figure 5.20 Diagram showing the bi-modal distribution of pi-poles to sheeted dykes in the Venetou area (see text and Enclosure 1). The bi-modal distribution is the result of folding of the Venetou area about a synclinal axis that plunges at 23° towards 257N.

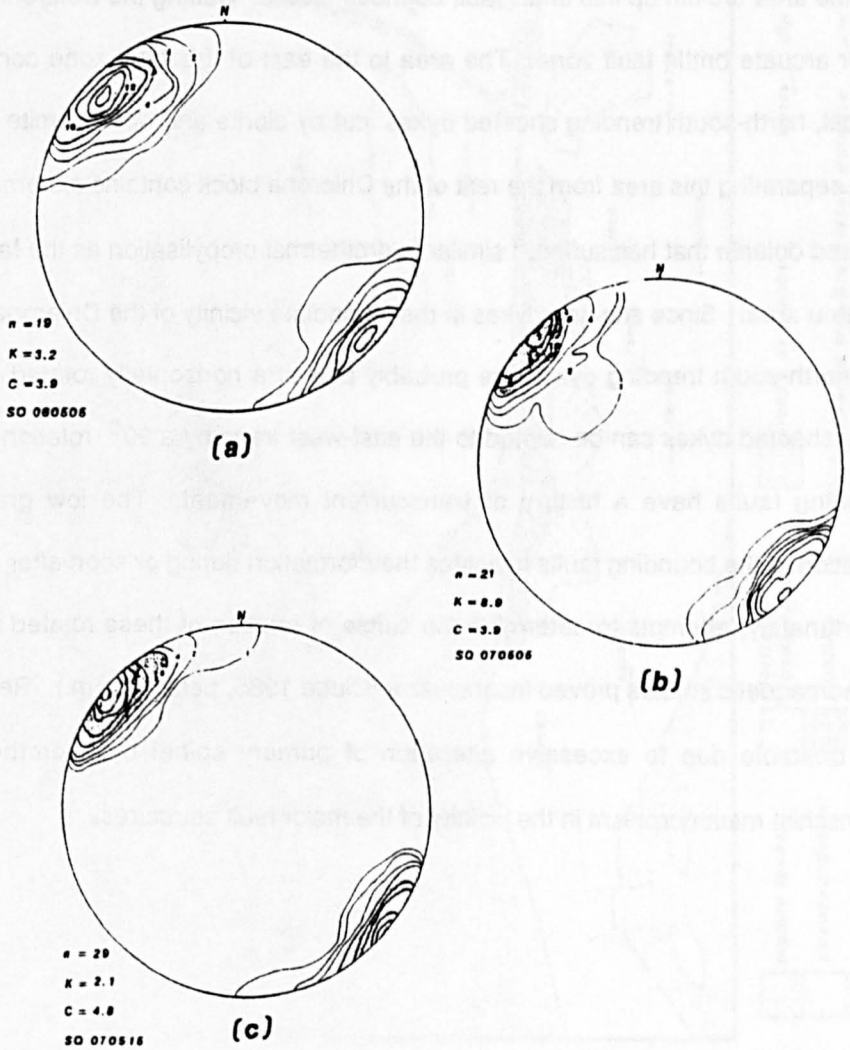

Figure 5.22 Distribution of pi-poles to picrite dykes that cut three sub-areas of the Venetuo syncline. All three sub-areas have a consistant NE - SW trend to the picrite dykes indicating that the Venetou syncline formed prior to picrite dyke emplacement, and was hence an oceanic event.

Major east-west normal faults that upthrow to the north followed folding of the Venetou Syncline and emplacement of the picrite dykes. These faults form serpentinite shear zones where they cut the cumulate or mantle sequences. In the gabbros and sheeted dyke complex, the faulting produces a cataclastic fault breccia that has suffered low grade hydrothermal oxidation and propylisation, characteristic of young sea-floor faulting (Sterns & Cann,1982).

The Dhierona block

From Figure 5.23, the outcrop pattern of the Dhierona block is seen to be complex with the area broken up into small fault bounded blocks. Cutting the Dhierona block in two is a major arcuate brittle fault zone. The area to the east of this fault zone consists of generally vertical, north-south trending sheeted dykes cut by diorite and trondhjemite bodies. The fault zone separating this area from the rest of the Dhierona block contains extremely brecciated and sheared dolerite that has suffered similar hydrothermal propylisation as the fault breccias in the Venetou area. Since sheeted dykes in the immediate vicinity of the Dhierona block trend E-W, the north-south trending dykes are probably part of a horizontally rotated block. If so, then these sheeted dykes can be related to the east-west trend by a 90^{o} rotation that suggests the bounding faults have a history of transcurrent movement. The low grade hydrothermal alteration of the bounding faults indicates their formation during or soon after magmatic activity. Unfortunately, attempts to determine the sense of rotation of these rotated sheeted dykes by palaeomagnetic studies proved inconclusive (Clube 1985, pers. comm.). Remnant magnetism was unstable due to excessive alteration of primary spinel by hydrothermal action and greenschist metamorphism in the vicinity of the major fault structures.

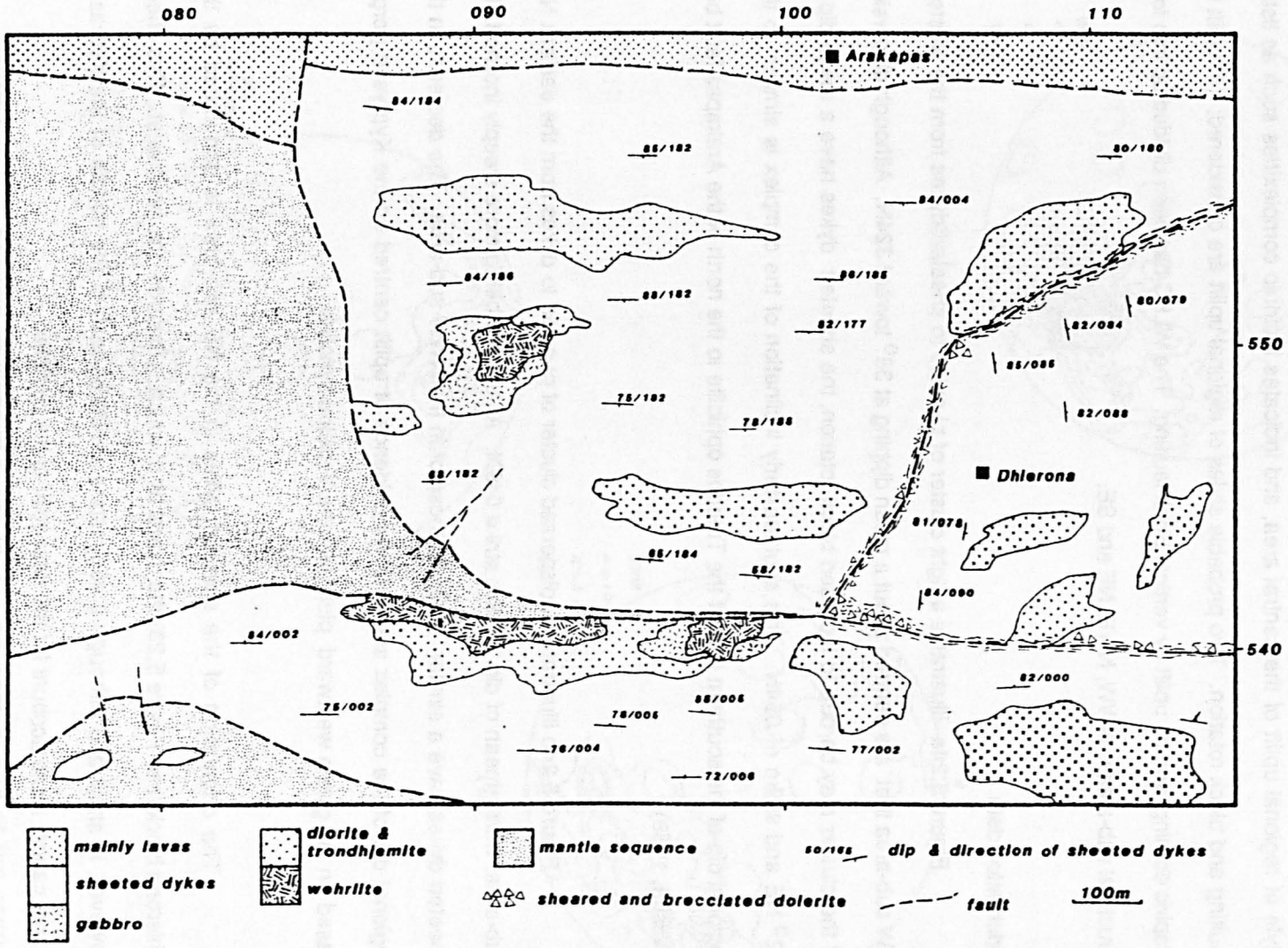

Figure 5.23 Structural map of the Dhierona block showing the position of the major fault structures and the orientation of the sheeted dykes.

5.2.7 Uplift Structures

Detailed study of the orientation of sheeted dykes around the WLFC illustrates the style of regional uplift of the central area, and indicates tectonic complexities such as listric faulting and block rotation. Two probable styles of regional uplift are considered; (i) uplift by diapiric doming, and (ii) uplift by vertical block faulting. The WLFC has been divided up into four structural sub-areas: NWW, NWE, NE and SE.

Orientation data

Figure 5.24a illustrates a tight cluster of pi-poles to sheeted dykes from the western NW sub-area that are centred about a mean dipping at 38^{o} toward 324N. Although dispersion of the cluster may be due to localised block rotation, the sheeted dykes have a mean dip of 52^{o} NE and strike of 054N. This southeasterly inclination of the complex is similar to the regional dip of the southern limb of the Troodos ophiolite to the north of the Arakapas fault belt (Wilson, 1958).

Figure 5.24b illustrates a dispersed cluster of pi-poles to dykes from the eastern NW sub-area, with a mean of dip 23^{o}SE, strike 049N. Apart from being more steeply inclined, the sheeted dykes have a similar strike to those of in the NWW sub-area. The decrease in the regional dip of the complex supports the evidence of uplift centred on the Kypryssa gorge, based on the gentle westward plunge of the Venetou syncline.

The orientation of the sheeted dykes in the NE sub-area is dominated by the Dhierona block (see Figure 5.23) the overal tilt of which is towards the southwest. This effect, however, is small and although it suggests a centre of uplift in the middle of the Kyprassa gorge, cannot alone account for the total uplift of the complex.

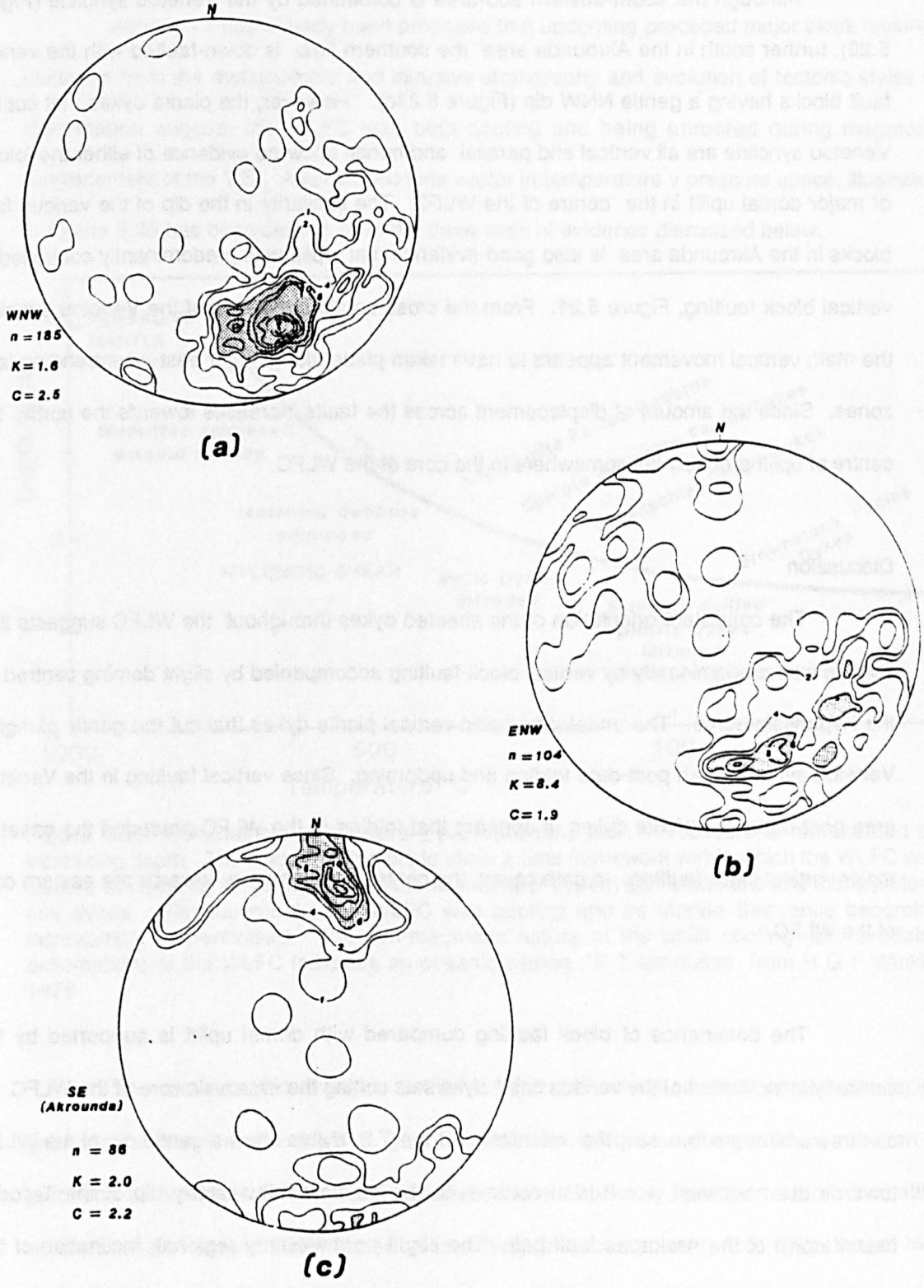

Figure 5.24 Pi-poles to sheeted dykes in: (a) the western part of the northwestern sub-area, (b) the eastern part of the northwestern sub-area and (c) the Akrounda area of the southeastern sub-area. Data for the norteastern sub-area are dominated by the rotated Dhierona block, and data for the rest of the southern area are dominated by the Venetou syncline.

Although the south-eastern sub-area is dominated by the Venetou syncline (Figure 5.20), further south in the Akrounda area the southern limb is down-faulted with the various fault blocks having a gentle NNW dip (Figure 5.24c). However, the picrite dykes that cut the Venetou syncline are all vertical and parallel and hence show no evidence of either the folding or major domal uplift in the centre of the WLFC. The similarity in the dip of the various fault blocks in the Akrounda area is also good evidence that uplift was predominantly controlled by vertical block faulting, Figure 5.21. From the cross-section and map of the Venetou syncline the main vertical movement appears to have taken place along major east-west trending fault zones. Since the amount of displacement across the faults increases towards the north, the centre of uplift probably lay somewhere in the core of the WLFC.

Discussion

The consistent orientation of the sheeted dykes throughout the WLFC suggests that uplifted was predominantly by vertical block faulting accompanied by slight doming centred on the Kyparissia gorge. The undeformed and vertical picrite dykes that cut the gently plunging Venetou syncline both post-date folding and updoming. Since vertical faulting in the Venetou area post-dates the picrite dykes, it appears that folding of the WLFC preceded the onset of major vertical block faulting. In both cases, the centre of upthrust lay towards the eastern core of the WLFC.

The dominance of block faulting compared with domal uplift is supported by the similarity in inclination of the various basic dyke sets cutting the ultramafic core of the WLFC. In all three arbitrary sub-areas, the orientation of the T.S. dykes show a gentle dip of the WLFC towards the northwest which is in contrast to the gentle southwesterly dip of the Troodos massif north of the Arakapas fault belt. The slight northwesterly regional inclination of the WLFC is probably the result of uplift and compressional deformation of the ophiolite during the Miocene.

Timing of Uplift

Although it has already been proposed that updoming preceded major block faulting, evidence from the metamorphic and intrusive stratigraphy and evolution of tectonic styles of deformation suggest the WLFC was both cooling and being unroofed during magmatic emplacement of the T.S.. A schematic time vector in temperature v pressure space, illustrated in Figure 5.25 has been derived from the three lines of evidence discussed below.

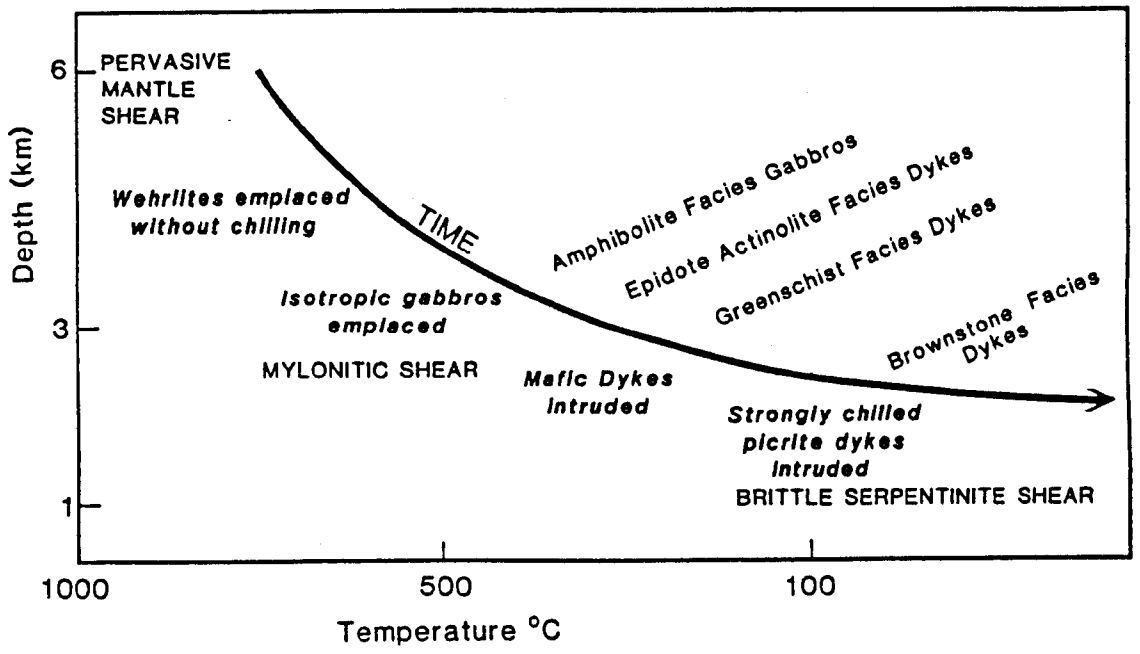

Figure 5.25 Schematic *temperature v pressure time path. Presssure is represented by increasing depth. The diagram attempts to show a time framework within which the WLFC was uplifted while being intruded first by plutonic and later hypabyssal ultramafic and mafic plutons and dykes. Simultaneously, the WLFC was cooling and its Mantle Sequence becoming increasingly serpentinised. The syn-magmatic nature of the uplift cooling (and probable exhumation) of the WLFC indicates an oceanic setting. *P T estimates from H G F Winkler 1976.

The metamorphic evolution of the WLFC initially involved lower amphibolite facies grade metamorphism of early T.S. gabbros. Metamorphic assemblages show reaction of pyroxene to brown hornblende and associated loss of primary igneous textures indicating temperatures of around 500°. Later cross-cutting gabbros and early T.S. dykes are of high greenschist metamorphic facies with metamorphic assemblages involving albite-epidote-actinolite and chlorite. Post-dating the majority of T.S. gabbros are abundant NE-SW trending mafic dykes mostly at lower greenschist grades. These dykes have

metamorphic assemblages that include chlorite after olivine, actinolite after clinopyroxene and intact orthopyroxene indicating temperatures of about 300°. The youngest T.S. dykes in the WLFC have suffered only intense propylisation (ie. brownstone metamorphic facies) characteristic of sea-floor alteration at or near 0°C (deWit & Stern, 1976). Since the T.S. plutonics and dykes were all emplaced at similar structural levels, their overall retrograde metamorphic history reflects cooling of the complex with time.

A history of uplift accompanying cooling is supported by the transition from ductile to brittle styles of deformation during the magmatic evolution of the WLFC. The first deformation event, D_1, produced a pervasive mantle foliation fabric at 1000-1200°C and 15-20 kbars. Later D_2 ductile mylonite zones were formed at about 800° C whereas the last sea-floor deformation, D_3, involved brittle serpentinite shear zones suggesting low confining pressures, high fluid pressures and temperatures below 400°C (Rayleigh & Paterson, 1965). The brittle behaviour of the SSZs suggest deformation occurred at depths down to 3km, below which serpentinite would have increasing plasticity (Rayleigh & Paterson, 1965). At temperatures above 400°C, serpentinite becomes increasingly unstable and dehydrates to talc and forsterite (Bowen & Tuttle, 1949).

Finally, a history of continuous cooling and exhumation of the WLFC is illustrated by the increasing presence of chilled intrusive contacts to T.S. plutons and dykes, emplaced into increasingly brittle Mantle Sequence peridotite. Marginal chill widths increase from zero during wehrlite emplacement to 3.5 cm at the time of mafic and picrite dyke intrusion, at the same structural level (see Chapter 3). The occurrence of both antigorite veins and dehydration-hydration reactions in the serpentinised mantle sequence, parallel to chilled NE-SW mafic and picrite dyke margins, are also evidence that serpentinisation accompanied cooling of the host mantle sequence. Uplift and unroofing of the WLFC during this time is further suggested by the change from pluton emplacement with highly irregular margins to hypabyssal intrusion of straight and parallel-sided mafic dykes. The final stage of emplacement

involved sinuous and vertically bifurcating, brownstone facies grade dykes suggesting almost hydrostatic stress conditions at shallow intrusive levels.

5.2.7.1 Uplift Processes

Although it could be a combination of both, in the following sections the two most probable uplift processes affecting the WLFC are considered:

(i) doming and folding with estimates of uplift based on the Venetou syncline and assuming all folding results in elevation and

(ii) isostatic uplift by serpentinisation and resultant bouyancy of the upper mantle.

However, before the amount of uplift can be estimated, the original thickness of the Axis Sequence must be reconstructed. This has been calculated as a minimum of 3.7km based on palinspastic reconstructions of sections from the Venetou syncline, the Dhierona block and the Kapillo area.

Axis Crustal Sequence Reconstruction

The WLFC contains a tectonically disrupted and thin A.S. Troodos type crust that consists of pelagic sediments and pillow lavas at the top, passing downward into sheeted dykes, isotropic gabbros, layered cumulates and finally through a palaeo-Moho into a mantle sequence of tectonised harzburgite and dunite (see Chapter 2). Crustal reconstruction can, therefore, only be made by combining measured separate sections through each lithostratigraphic unit. This assumes that the various crustal units in the sections measured are representative and have not suffered any tectonic change in thickness.

The thickness of the volcanosedimentary sequence is estimated from two sections that have been studied in detail in the Kapillo area and which are located in Enclosure 1. The upper volcanic group has an average dip of 75^{O}NE and outcrop width of ~1.05km giving a

calculated thickness of ~1.01km. The lower volcanic group dips at 62°SW and has an estimated thickness of 0.64km. From the outcrop in the Ayious Mamas area the thickness of the lava-sheeted dyke transition sequence has been calculated at ~0.52km.

Although not exposed in full, the thickness of the sheeted dyke complex has been estimated from the northern side of the Dhierona block. This area exposes a section from the base of the sheeted dykes in the core of the anticline to the base of the transition sequence just south of the main Arakapas fault belt boundary fault. The sheeted dyke complex dips at 30°N and has a (minimum) calculated thickness of 0.9km.

The plutonic sequence is exposed continuously from the base of the sheeted dykes to the Moho in the Venetou syncline. Thickness estimates are based on a section through the northern limb of the fold illustrated in Figure 5.21. The gabbro-granophyre unit has a calculated minimum thickness of ~0.26km, based on the orientation of the sheeted dykes to the south. The orientation of the cumulate unit is taken as an average between the dip of the overlying isotropic gabbro-granophyre unit and cumulate layering from just above the Moho, where it is assumed to be near horizontal (Smewing, 1981; Casey & Karson, 1981; Rothery 1983). From this and the ~0.43km outcrop width, the cumulate unit has a calculated thickness of ~0.41km. Similarly, the estimated dip of the cumulate wehrlite unit is 88°, giving a calculated thickness of ~0.47km. The overall reconstructed T.S. crustal section is only ~3.7km thick compared with the 5.8-9km calculated for the Troodos massif (Moores & Vine ,1971; Allen 1975).

Uplift by Folding

Extrapolation of the Venetou syncline northwards until it intersects the first major east-west, vertical fault, (Figure 5.26) gives a minimum uplift estimate of ~2.2km. Erosion of this uplifted section would expose the sheeted dykes down to ~0.57km from below the base of the volcanosedimentary sequence. This may explain why the majority of clasts in the intervolcanic

breccia deposits both in the north and south of the complex are of either volcanic or sheeted dyke origin.

The occurrence of layered ultramafic clasts, and more rarely, fragments of serpentinised, tectonised harzburgite in interlava breccia deposits in the Akrounda area indicate erosion to levels below the sheeted dyke complex. Based on the reconstructed thickness of the A.S. crustal section, exposure and erosion of the cumulate ultramafics would require a minimum further uplift of 1.03km.

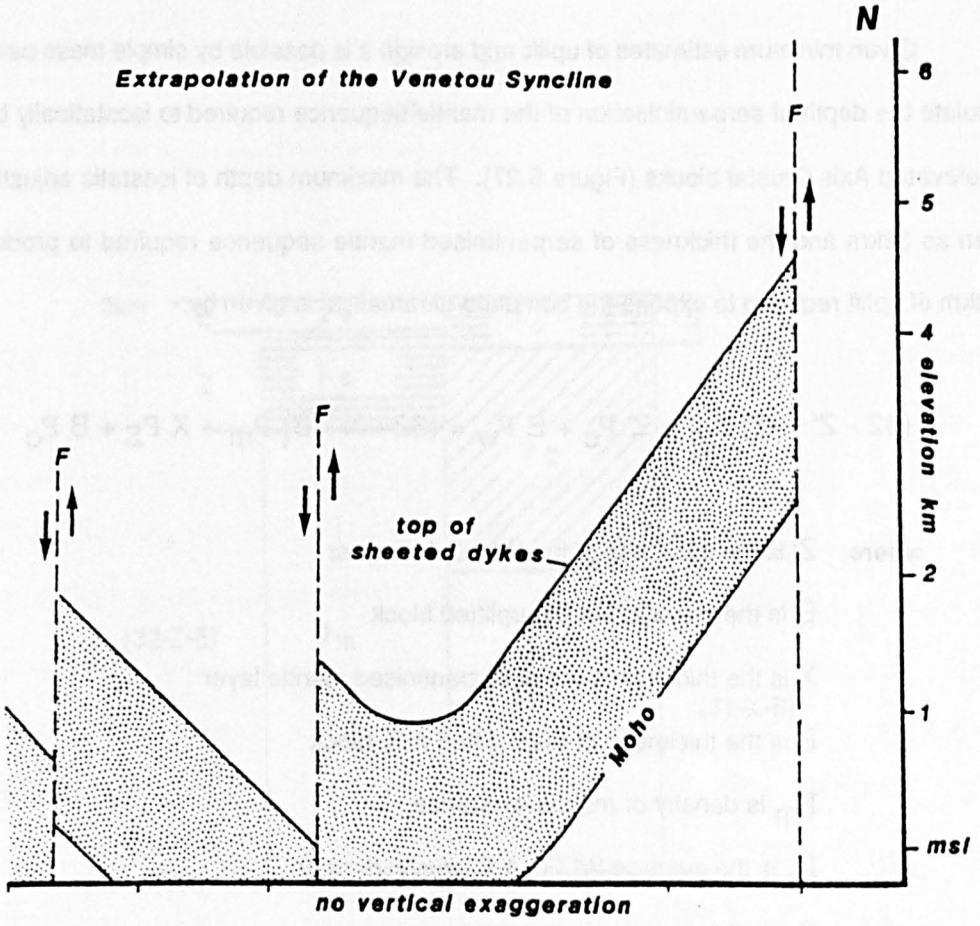

Figure 5.26 Hypothetical condition in which the Venetou syncline is extrapolated to the nearest major fault to the north. Assuming all the folding results in uplift this would result in elevation of the WLFC by about 2.2km.

Serpentinisation Driven Uplift

A more probable process considered to have driven block uplift is buoyancy due to volume expansion as a result of serpentinisation of the upper mantle. It is possible to reduce the density of the Mantle Sequence from 3.32 g cm^{-3} to 2.60 g cm^{-3} by hydration of the ferromagnesium phases, i.e.

$$MgSiO_3 + Mg_2SiO_4 + 2H_2O \Leftrightarrow Mg_3Si_2O_5(OH)_4$$

Enstatite Olivine Water Serpentine

where $\Delta V_{(solid)}$ for the reaction = $33.2cm^3$ ie. a 40% volume increase

Given minimum estimates of uplift and erosion it is possible by simple mass balance to calculate the depth of serpentinisation of the mantle sequence required to isostatically balance the elevated Axis Crustal blocks (Figure 5.27). The maximum depth of isostatic adjustment is taken as 32km and the thickness of serpentinised mantle sequence required to produce the 3.23km of uplift required to expose the cumulate ultramafics is given by:-

$$(32 - Z' - E)\,P_m + Z'\,P_c + E\,P_w = (32 - X - B)\,P_m + X\,P_\Sigma + B\,P_c$$

where Z' is the thickness of the WLFC A.S. crust

E is the elevation of the uplifted block

X is the thicknesss of the serpentinised mantle layer

B is the thickness of the uplifted A.S. block

P_m is density of mantle sequence

P_c is the average WLFC A.S. crustal density

P_w is the density of sea water

P_Σ is the density of serpentinised Mantle Sequence

This equation solves for X as :-

$$X = \frac{Z' (P_c - P_m) + E (P_w - P_m) + B (P_m - P_c)}{(P_\Sigma - P_m)}$$

Therefore a total uplift of the WLFC A.S. sufficient to expose the cumulate ultramafics and reach isostatic equilibrium would require a minimum of 4.6km of100% serpentinised mantle. However, it is more realistic to assume the degree of serpentinisation decreases with depth. An approximation of this effect involves the equivalent depth of partial serpentinisation to be twice that for 100% serpentinisation, i.e.

$$\sum_{100}^{1} x = 2x$$

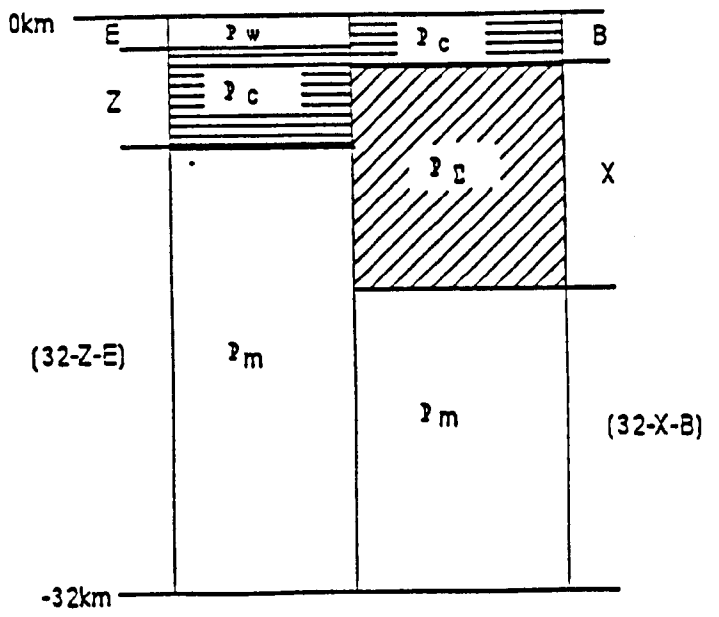

Figure 5.27 Bouyancy model for uplift of the core of the WLFC involving the elevation of an eroded (ie. unroofed) block supported by a layer of partially serpentinised mantle. The diagram shows the notation for the relative thicknesses and densities used in the mass balance calculations, refered to in the text. Bouyancy adjusted to an assumed maximum depth of 32km.

In the WLFC, the mantle sequence would need to be *partially* serpentinised to a depth of 8.12km below the Moho to maintain isostatic equilibrium. Given the estimated 3.7km thickness of the Axis Crustal Sequence, it is possible to derive a broad topographic profile across the WLFC between its northern and southern margins respectively. The profile is based on the isostatic equilibrium depth at which the sea-floor will reside, depending on the relative age and thickness of adjacent portions of oceanic lithosphere (Figure 5.28). The difference in seafloor level between the Troodos Massif and the WLFC is given by,

$$Q = (z - z') - h$$

where z is the thickness of the Troodos A.S.

z' is the thickness of the WLFC A.S.

h is the respective difference in depth of the Moho between the two areas and is given by;

$$h = (Z P_T - Z P_W) / (P_m - P_W)$$

where:-

$P_T = P_W$ and is the density of the Axis Sequences in the WLFC and Troodos massif respectively; other symbols are the same as in the previous equations.

Assuming a similar age for both the Troodos and WLFC A.S. crustal sections, the area south of the Arakapas fault belt would have formed a bathymetric depression, at least 1.6km deep, prior to the onset of uplift.

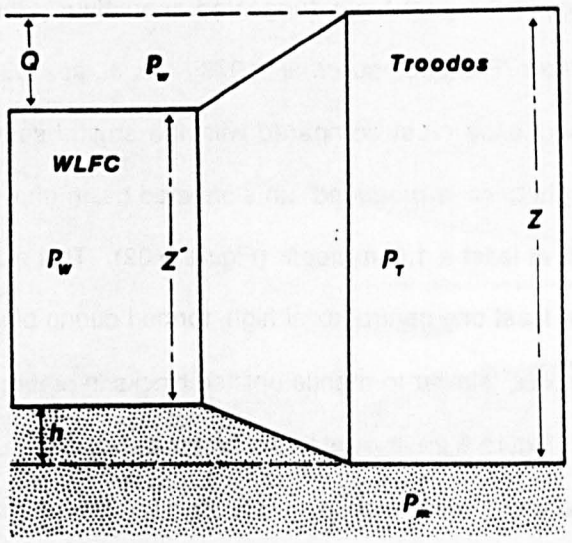

Figure 5.28 Effect of a thinned A.S. within the WLFC compared with that for the Troodos masssif on the topography of the TFFZ while in an oceanic setting. The diagram also shows the notation for the relative thicknesses and densities used in the mass balance calculation in the text.

Discussion

The absence of any ultramafic fragments in the breccia deposits in the north compared with the south of the WLFC may reflect both the palaeotopography and palaeoslope of the complex during its sea-floor history. The present outcrop position of the mantle sequence suggests that maximum uplift was localised along an east-west central axis. The distribution of ultramafic clasts suggests that whilst erosion levels were deepest towards the centre of the complex, transport of this material was dominantly southwards. This may be due to an overall southerly slope of the basin or to the presence of intervening troughs and highs towards the north of the complex, such as those identified by Simonian (1975), trapping and preventing the northward transport of centrally derived detritus. The early initiation of uplift of the WLFC block may explain its present isostatic equilibrium and hence the lack of any major gravity anomaly despite the extensive outcrop of 95-100% serpentinised harzburgite (Vine & Smith, *pers. comm.*; Gass & Masson-Smith, 1962)

Seismic studies in the past have suggested anomalously thin oceanic crust in the vicinity of transform offsets (Francheteau *et. al.*, 1976; Fox *et. al.*, 1980). In the case of the WLFC the thin Axis Sequence crust compared with the crustal sequence of the adjacent Troodos Massif is thought to have produced an elongated basin (that may have extended to both the east and west) at least a 1.6km deep (Figure 5.32). This elongated basin probably became bimodal with at least one central axial high, formed during block faulting and uplift of the ultramafic core complex, similar to mantle uplifted blocks in present day oceanic fracture zones (Bonatti, 1978). Figure 5.29 illustrates the tectonic evolution of the WLFC lithosphere during uplift and transtensional deformation. Following transcurrent shear during which the Arakapas fault belt was formed, extension across the WLFC disrupted the A.S. Serpentinisation of the Mantle Sequence beneath the core of the WLFC drove block uplift and faulting that produced an axial high. Transtension across the WLFC resulted in an extended and thinned oceanic lithosphere that was magmatically modified by T.S. intrusions and lavas.

5.3 Post - magmatic Deformation

The following sections deal with post-magmatic deformation that is interpreted as structures formed during the 'emergence' of the WLFC to its present position as part of the Troodos ophiolite complex.

5.3.1 Unroofing History

The WLFC reaches a a maximum elevation of 1200m. Although unroofing of the core of this complex may have reached a maximum depth of 3.23km during the Late Cretaceous, current erosion levels expose the mantle sequence down to an estimated depth of 800m below the petrological Moho (see Chapter 2). In addition to its uplift and erosion above sea level, the WLFC has also been elevated to a maximum of 440m above the floor of the Arakapas fault belt giving a total post Cretaceous uplift of 1.49km relative to the Troodos massif.

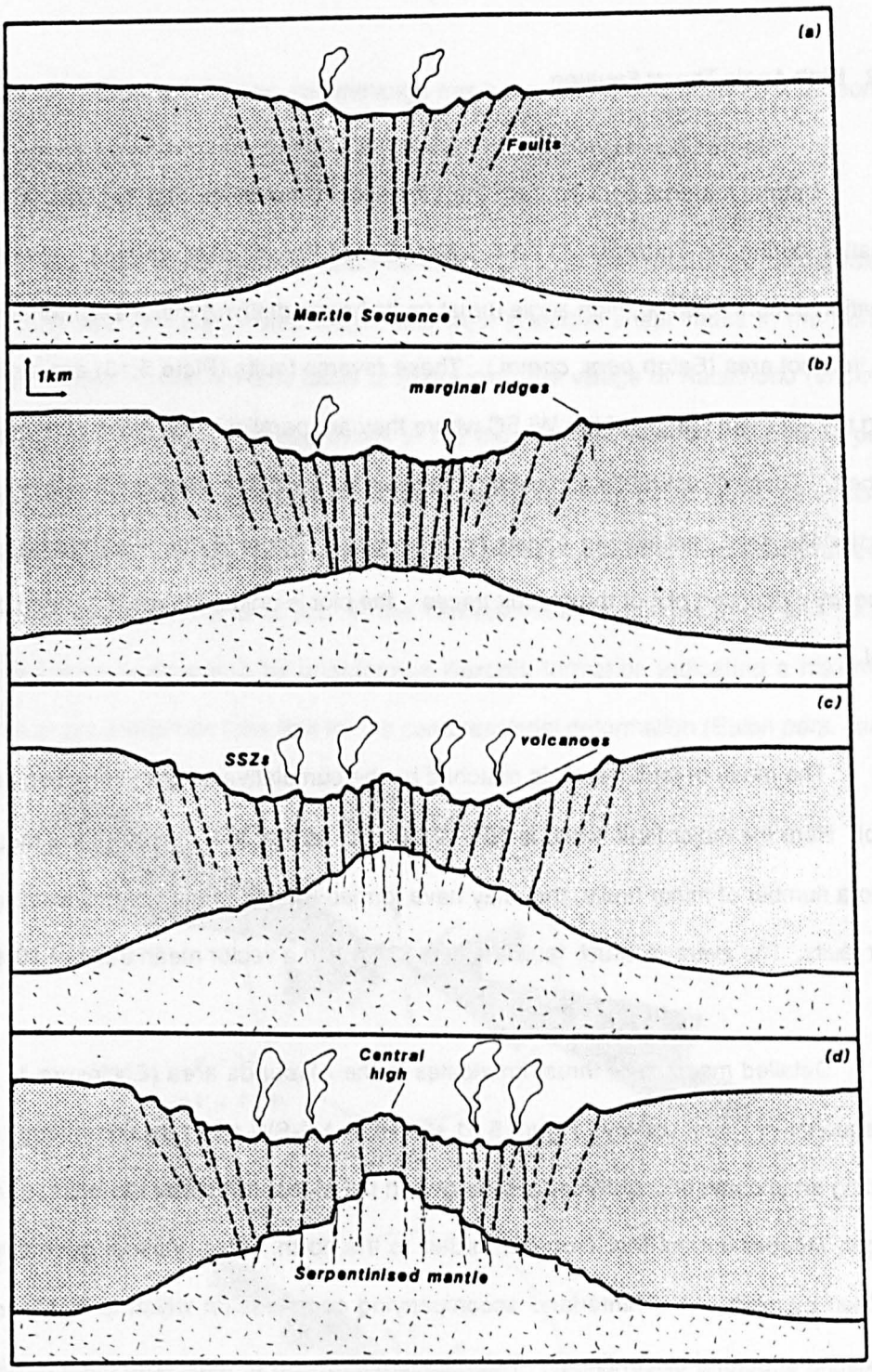

Figure 5.29 Schematic diagram showing the topographic profile development across the WLFC during its history of transform deformation. **(a)** The TFFZ is narrow with a relatively coherent and thin A.S. forming a 1.2km deep depression with small ridge features on the flank walls (eg. similar to those identified by Simonian, 1975). **(b)** An element of extension across the WLFC produces vertical block faulting, uplift and erosion. **(c)** Continued extension and bouyancy driven uplift produces a central axial high to the WLFC TFFZ. **(d)** The central axial high reaches a maximum elevation during which erosion exposes the cumulate ultramafics and the serpentinised mantle approaches isostatic equilibrium.

5.3.2 High Angle Thrust Faulting

Detrital material derived from the Limassol Forest block first appears in the Pakhna formation during the Tortonian, (11.3-6.5 Ma) (Simon Eaton, *pers. comm.*). Simultaneously, activation of north-dipping, high angle thrust faults began defining major sedimentary basins in the Limassol area (Eaton *pers. comm.*). These reverse faults (Plate 5.10) are also abundant along the southern margin of the WLFC where they are parallel to the NE-SW trending Yerasa fold belt. These thrust faults usually dip between 30^{o} and 55^{o} toward the northeast and are occasionally seen reactivating earlier normal faults. Figure 5.30a illustrates a cumulative frequency $\underline{v}$ direction plot of thrust fault traces. the plot is unimodal about a mean direction of 107N.

The mode of fault trends is matched by the cumulative length $\underline{v}$ direction plot (Figure 5.30b). Here the major fault trend is 100-120N. The scatter to the north of the mode may be due to a number of minor faults, that may have formed by reactivation of pre-existing principal shear faults. The average thrust fault length is 531m with a vector mean trend of 104N.

Detailed mapping of thrust imbricates in the Akrounda area (Enclosure 1) illustrates the sequence of thrust activity. Figure 5.31 shows an NE-SW cross section through this area, revealing an unconventional thrust geometry with the oldest thrusts at the base, truncated by younger, steeper thrusts that crop out further to the north. This unusual geometry may be explained by uplift of the hinterland accompanying compression which is localised along a pre-existing structural discontinuity. The resultant direction of maximum compression, σ_1, is inclined toward the northeast, producing steep (40^{o}- 50^{o}) thrusts with only a few hundred metres of throw. In the Apsiou area, overturning of pillow lavas (Plate 5.12) and thrusting of serpentinised mantle sequence has been aided by decollement along the Moni formation. This formation forms a sedimentary melange of exotic olistoliths entrained in a clay matrix.

In the vicinity of the sole thrust, the melange has been extensively sheared with reorientation of the olistoliths and development of a northeast dipping, pervasive cleavage.

Thrusts of a similar style and orientation cut both the southward facing folds of the Yerasa fold belt and reactivated major east-west principal shear faults in the north of the complex. These northern thrust faults crop out near the village of Kalakhorio (enclosure 1), and juxtapose brecciated sheeted dykes in the hanging wall against sheared serpentinised mantle sequence in the footwall (plate 5.12). If these northern thrust faults are of similar age, then this relationship suggests the mantle sequence was uplifted to high structural levels prior to Miocene compressional tectonics. In the Yermasoyia area both the thrust and Yerassa fold structures are transgressed by undeformed Koronia formation indicating a maximum Late Miocene to pre-Messinian time limit for the compressional deformation (Eaton *pers. comm.*).

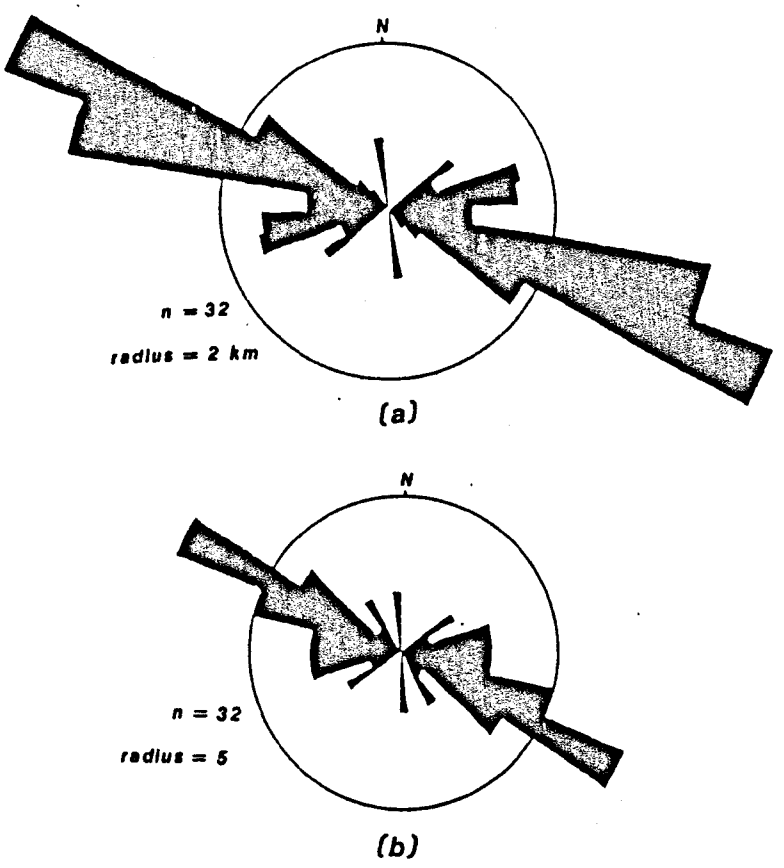

Figure 5.30 (a) & (b) Cumulative length $\underline{v}$ direction and cumulative frequency $\underline{v}$ direction diagrams, respectively, for high angle southwards transporting thrust faults from the southern margin of the WLFC with the sedimentary cover rocks to the south. The dominant 104N trend of the thrust faults is almost coincident with the axial trend of the Yerasa fold belt.

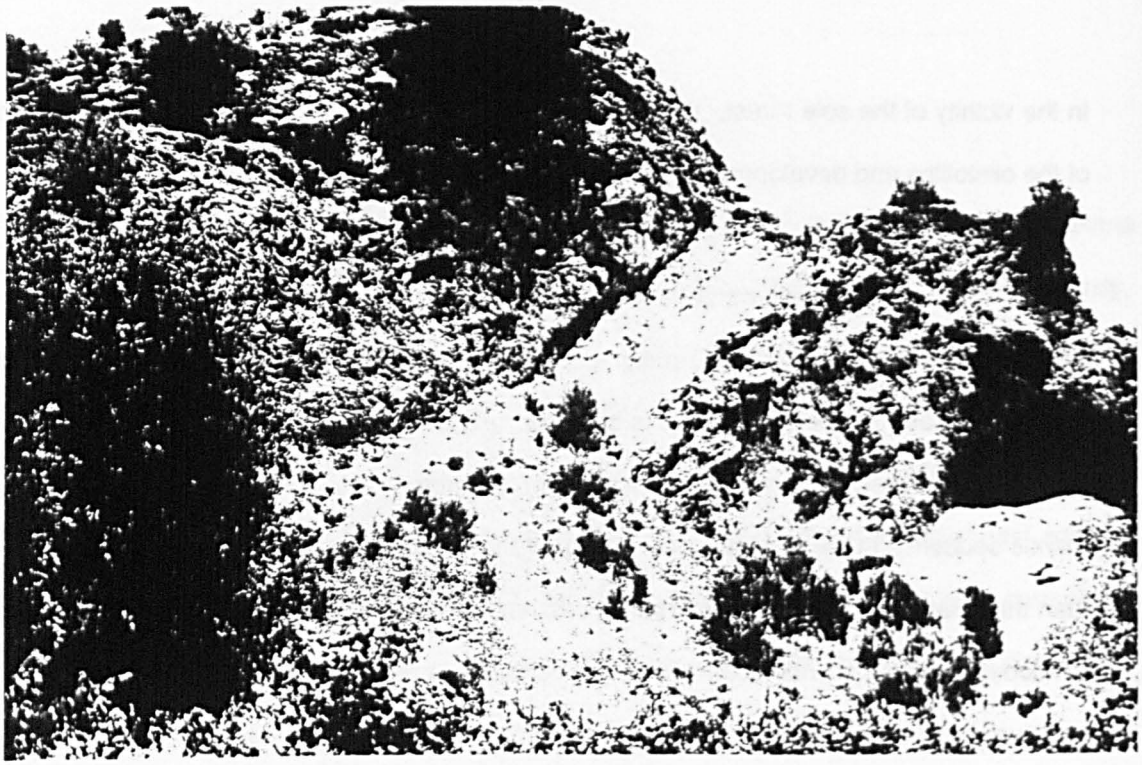

Plate 5.10 High angle thrust from the southern contact with the Lefkara chalks, near Apsiou. The sheeted dyke complex is brecciated (weathered brown) and thrust over brocken pillow lavas; the thrust gouge is a friable grey coloured cataclaysite.

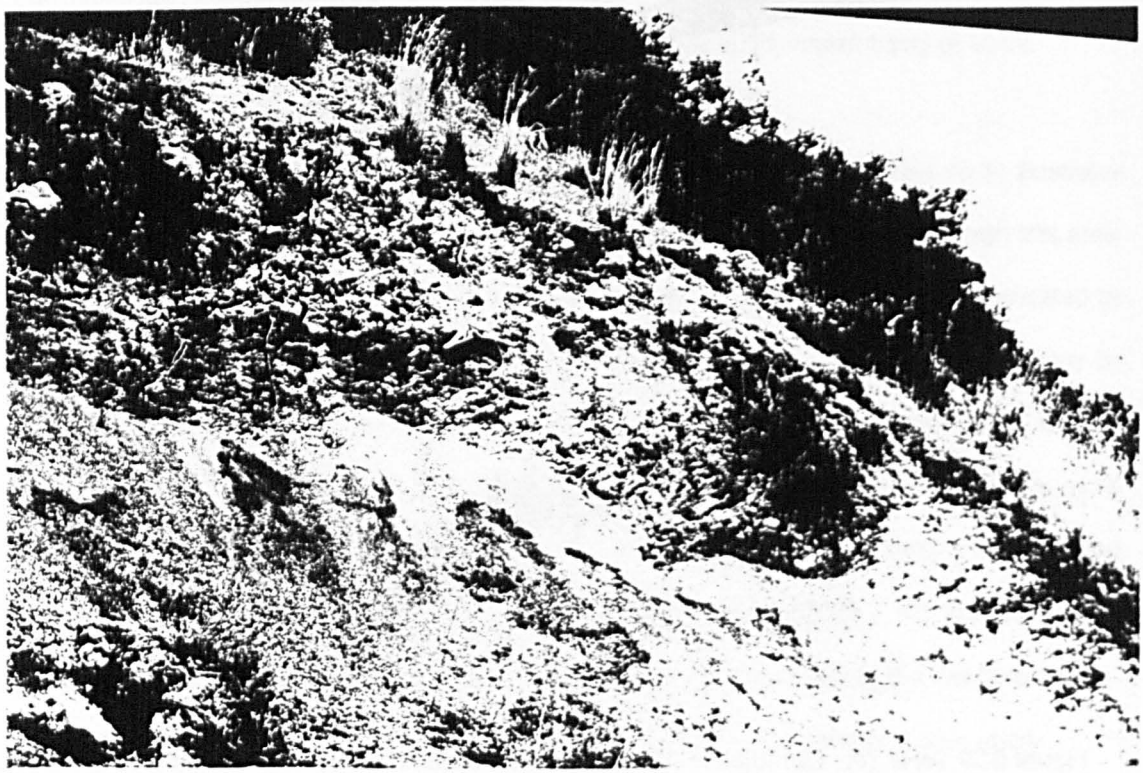

Plate 5.11 Overturned pillow lavas and Perapedhi Formation from Apsiou. The pillow lavas (brown) are inverted and now lie on umbers (dark brown) which in turn lie on ribbon cherts (pink)

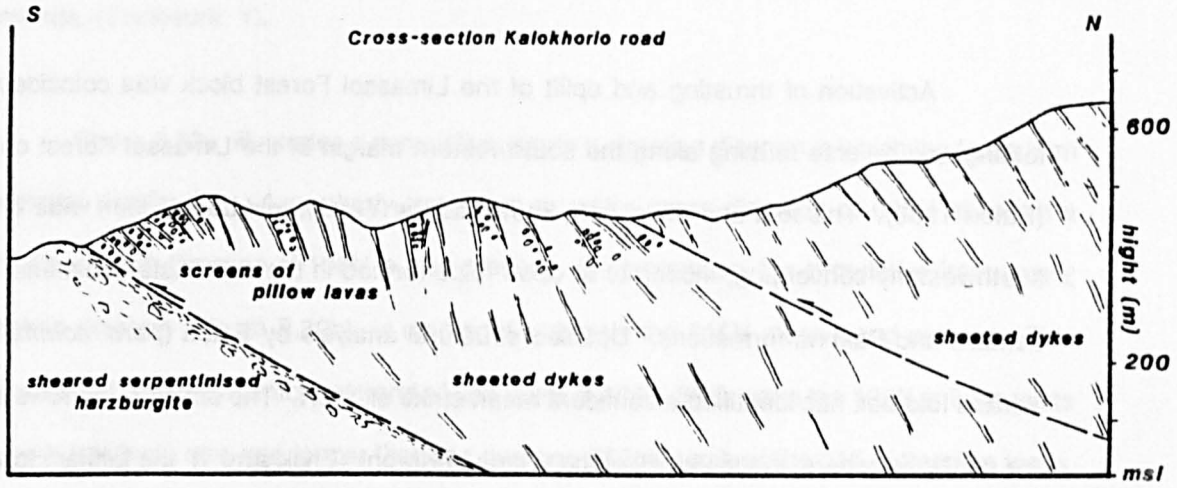

Figure 5.31(a) Structural cross-section of a high angle thrust that crosses the Kalakhorio - Limasol road and which throws a hanging wall of sheared sheeted dykes against a foot wall of sheared serpentinised Mantle Sequence harzburgite.

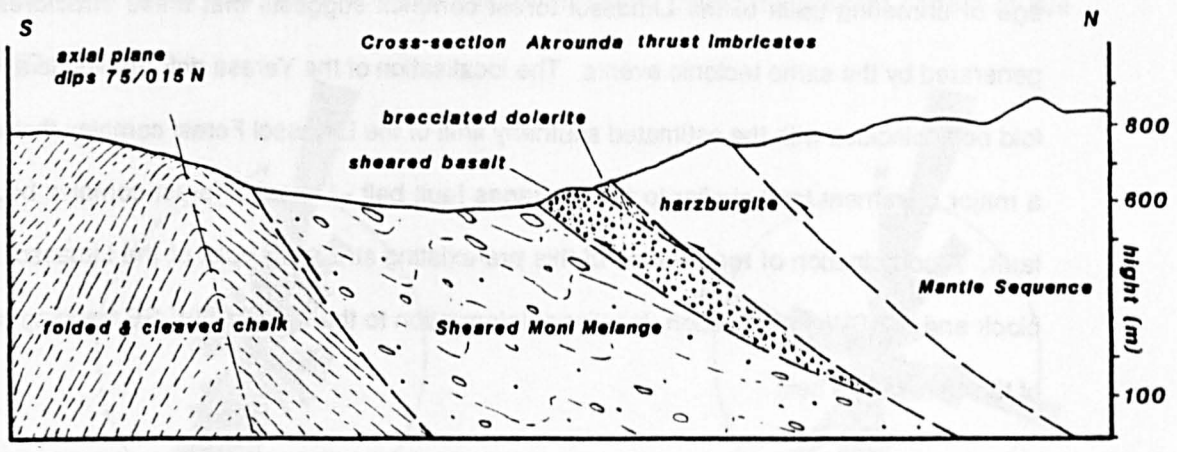

Figure 5.31(b) Structural cross-section through the high angle thrust imbricates in the Akrounda area. The thrust geometry is unusual in that the oldest thrusts are cut by younger ones suggesting compression was accompanied by an element of uplift in the hinterland.

5.3.3 The Yerasa Fold Belt

Activation of thrusting and uplift of the Limassol Forest block was coincident with folding and reverse faulting along the southwestern margin of the Limassol Forest complex (Eaton 1986). This fold and thrust belt, known as the Yerasa fold belt, is 5km wide and has southwesterly converging, moderate to open folds formed in the carbonate sediments of the Lefkara and Pakhna formations. Detailed structural analysis by Eaton (*pers. comm.*) of the Yerasa fold belt has identified a confident mean strike of 116N. The structure narrows toward the northwest where, in the vicinity of the village of Korphi, (Enclosure 1) the Lefkara formation is extensively sheared and develops a pervasive, vertical NE-SW trending cleavage. Further northwest the Yerasa fold belt gives way to major NW-SE faulting that continues into the basement of the Troodos Massif where it can not be traced.

Discussion

The similarity in the orientation of the Yerasa fold belt, high angle thrust faults and the age of unroofing uplift of the Limassol forest complex suggests that these structures were generated by the same tectonic events. The localisation of the Yerasa deformation to a narrow fold belt coincides with the estimated southerly limit of the Limassol Forest complex that locates a major basement fault similar to the Arakapas fault belt - Limassol forest complex boundary fault. A combination of reactivation of this pre-existing structure, uplift of the Limassol Forest block and NE-SW compression localised deformation to the narrow, NW-SE trending outcrop of the Yerasa fold belt.

5.3.4 Late Fault Structures

A system of late faults cut all other structures in the WLFC including the Miocene thrusts and Yerasa fold belt. These faults generally trend N-S and have a history of both oblique-slip and dip-slip, with both a component of dip-slip downthrow to the west and a

maximum of dextral movement 200 ± 50m centred around the southern thrust complex at Akrounda, (Enclosure 1).

Figure 5.32a illustrates a cumulative length y direction diagram in which the faults form a bimodal distribution. A northerly trend has a vector mean direction of 015N although a subsidiary mean direction of 108N is also present. In comparison, the cumulative frequency y direction diagram (Figure 5.32b) is unimodal with only the 015N mean trend present. This indicates that the major structural trend of late faults is NNW-SSE, while the 108N striking faults are both relatively rare and longer than the average 232m length of the 015 N trending faults. The 108N trend is almost parallel to the strike of late, high angle thrust faults and the Yerasa fold belt, suggesting tensional reactivation of earlier compressional structures.

The late faulting affects both the entire Troodos massif as well as the carbonate sedimentary cover to the south and hence can be considered regional in scale. However, an element of uplift centred on the Akrounda thrust imbricates and possibly some late displacement south may have localised this deformation, giving the present pattern of late faulting in this area.

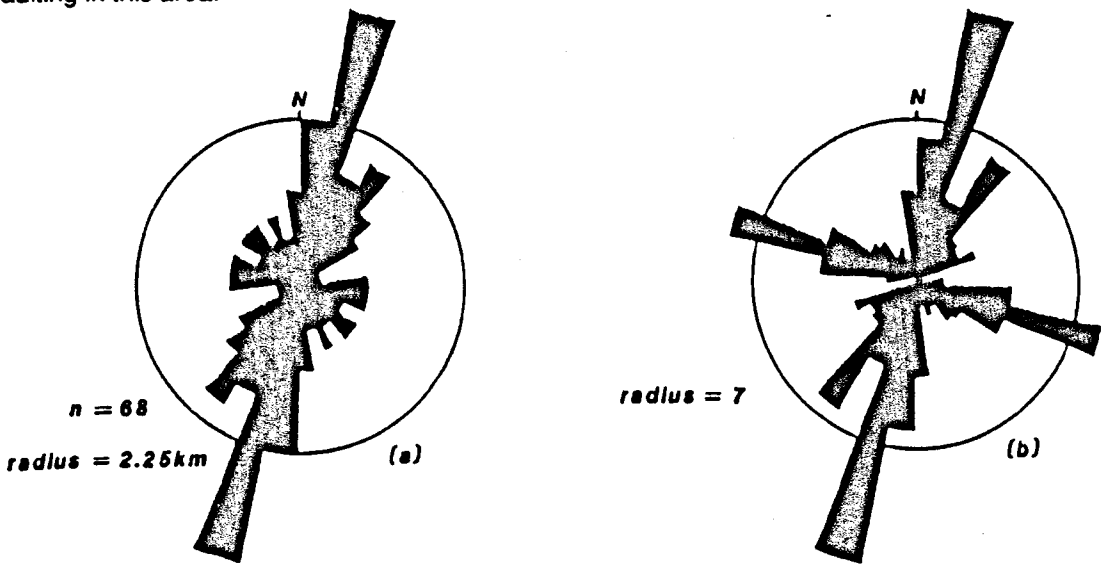

Figure 5.32 (a) & (b) Cumulative length y direction and cumulative frequency y direction of late faults that affect the WLFC. These faults cut all other structures and are prominant throughout the Troodos massif and sedimentary cover rocks to the south. The majority of faults trend 015N and are relatively short. A small number of large faults trend E-W and are probably reactivated high angle thrust faults.

5.4 Summary List of Conclusions

(i) The WLFC has a tectonic history involving syn-magmatic and later post-magmatic deformation

(ii) Mantle deformation fabrics resemble those of an oblique slow spreading ridge and suggest the coincidence of an upper mantle plume with a leaky transform fault zone.

(iii) Ductile shear zones and Serpentinite shear zones, indicate a sinistral sense of wrench faulting, localised the majority of strain in the WLFC and are both cut by T.S. mafic dykes and gabbros.

(iv) Early fault structures are parallel to the serpentinite shear zones and formed in a similar stress regime.

(v) Multiple T.S. basic dykes and picrite dykes are essentially parallel to both the serpentinite shear zones and the early faults.

(vi) The serpentinite shear zones, basic dykes and early fault structures define a stress ellipse indicating a sinistral sense of regional shear.

(vii) The syn-tectonic emplacement of both T.S. dykes and gabbros indicate up to 25% lithospheric dilation during regional sinistral transtensional shear.

(viii) The core of the WLFC was uplifted by vertical block faulting, with upthrust driven by an 8.12km thick layer of partially serpentinised upper mantle.

(ix) Compared with the 5-9 km thick A.S. crustal section for the Troodos massif, the WLFC has an A.S. that was only 3.7km thick, resulting in a 1.65km deep, E-W elongated, bathymetric basin with a central axial high that exposed the cumulate ultramafic sequence.

(x) Post-magmatic deformation involved a combination of further uplift of the WLFC block and N-S compression resulting in southerly closing folds and small scale, northerly dipping, high angle thrust faults.

CHAPTER 6

GEOCHEMISTRY

List of contents

6.1 Introduction

This Chapter is divided into three sections. The first part deals with the geochemistry and paragenesis of the WLFC plutonic rocks while the second and third parts deal with the geochemistry and petrogenesis of the WLFC basaltic dykes and lavas respectively. In each section, comparisons between the various plutonic and hyperbyssal and volcanic suites support the field evidence for two separate petrogenetic groups, the Transform Sequence (T.S.) and Axis Sequence (A.S.). It is shown that while there is geochemical continuity within the two groups, the WLFC T.S. and A.S. are not cogenetic and have been derived from different mantle sources. Initially, however, a discussion concerning major and trace element mobility during low to moderate grades of alteration and metamorphism is presented.

Major and trace element Mobility

Any process that changes the original mineralogy of a rock will mobilise the elements held within those particular, primary phases. In terms of bulk rock geochemistry it is important to know how far various elements travel during such processes; which particular elements are held within alteration products and therefore retain their original abundances, and which ones are liberated and mobilised by the alteration process. Before discussing individual element mobility, two points are considered: (i) since alteration effects are very heterogeneous, any consistent and strong correlation between elements most probably reflects original magmatic processes; (ii) all alteration processes up to amphibolite facies metamorphism involve hydration reactions, therefore Large Ion Lithophile (LIL) elements are more likely to be affected than High Field Strength Elements (HFSE).

Major Elements

The effects of alteration on major element geochemistry have been described by a number of authors (Moore, 1966; Hart, 1969; Matthews, 1971; Listsyna, 1968; Cann, 1969; Melson & Van Andel, 1966; Pearce & Cann,1973). For basalts altered up to greenschist facies (inclusive), only TiO_2 and Fe_2O_3/FeO are reliable. Basalts that are altered to sub-greenschist facies grades are reliable with respect to TiO_2 and Al_2O_3 and moderately reliable with respect to MgO, SiO_2, and FeO* (*as total Fe it is based on Fe_2O_3). Under all alteration conditions, CaO, Na_2O and K_2O are least reliable.

Trace elements

The most comprehensive study of trace element mobility during alteration or metamorphism involves the determination of ionic potential, Z/r, where Z is the ionic charge and r the ionic radius (Loughnan, 1969). This parameter is most effective in determining relative mobility in aqueous phases: elements with low (eg. less than 3), and very high (eg. greater than 12) ionic potentials are generally mobile, while those of intermediate ionic potentials are generally immobile. Of the mobile elements, LIL elements (eg. Sr, Rb, Ba, Th) are considered important in identifying subduction-zone related magmatism (Pearce, 1983), but are all very mobile in aqueous phases. The ionic potential parameter predicts relative immobility in aqueous phases (or alternatively, lithophile compatibility) for Ti, Zr, Y and Nb, which is in agreement with Pearce & Cann (1973) and Pearce & Norry (1979). Compatible trace elements (eg. the transition elements, Ni, V, Cr) are also considered to be immobile up to and including greenschist facies metamorphic grades (Pearce & Cann,1973; Pearce & Norry, 1979; Pearce, 1982).

Rare Earth Elements

The rare earth elements (REE), from La to Lu, show systematic variation in incompatibility in most basaltic fractionation and partial melting processes and are thus extremely useful in petrogenetic modelling. Studies of basalts that have been exposed to

sea-floor alteration, however, suggest selective mobilisation of the light rare earth elements (Ludden and Thompson 1979). Wood *et al*. (1976) and Hoffman *et al.* (1977) demonstrated similar LREE mobility, especially of La during low grade (zeolite facies) metamorphism. However, more recent work by Hajash (1984) indicates reliability of REE profiles in reflecting original magmatic ratios during hydrothermal metamorphism at 500-600^{o}C and 0.8 to 1 kb. These latest findings are also in agreement with Menzies *et al.* (1979) in which experimental evidence demonstrates REE immobility under hydrothermal conditions ranging from 150 to 350^{o}C (ie. up to moderate greenschist facies grades). Due to the apparent uncertainty in the literature, petrogenetic modelling of the WLFC basalts has only been attempted using REE determinations from fresh, glassy pillow lava cores. REE determinations from low grade metamorphic basaltic dykes are treated with caution and used only comparatively with other data.

6.2 Cumulate Geochemistry

The Plutonoic Group of the T.S. form plutons of gabbro and wehrlite. The gabbros are essentially isotropic, Cpx* - Plag* ± Ol* rocks, and rarely show any cumulate textures. In contrast, the wehrlites are Ol - Cpx cumulate rocks in which clinopyroxene oikocrysts enclose small, rounded olivines. The plutonic rocks of the A.S. consist of isotropic and layered gabbros, layered olivine gabbros and wehrlites. The gabbros occasionally show cumulate textures whereas the wehrlites are dominated by crystal accumulation*.

Data

Both the T.S. and A.S. plutonic rocks are plotted on major element covariation diagrams (Figure 6.1a - b and 6.2) in an attempt to identify any systematic differences between the two groups.

**The abbreviations used in this chapter are:- Ol = olivine, Opx = orthopyroxene, Cpx = clinopyroxene, Plag = plagioclase.*

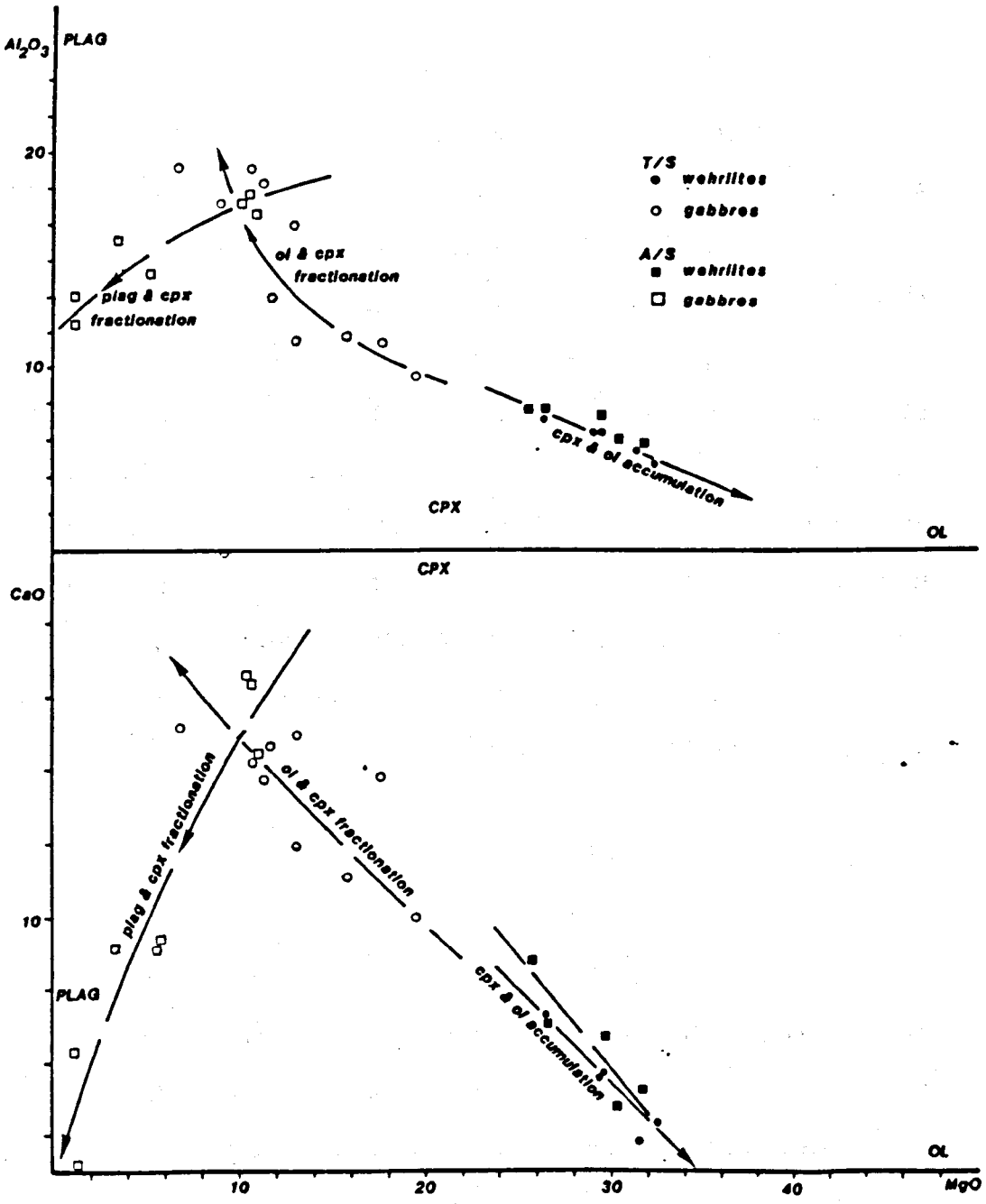

Figure 6.1a Al_2O_3 **v MgO** From the approximate positions of the major phase fields (Deer, Howe and Zeissman, 1969), both wehrlite groups appears to be dominated by olivine and clinopyroxene accumulation. In contrast, the T.S. gabbro evolution trend is controlled by variable amounts of olivine and clinopyroxene fractionation. The degree of olivine fractionation decreases with decreasing MgO, while clinopyroxene fractionation becomes dominant, causing the evolution trend to curve towards higher Al_2O_3 : MgO ratios. The A.S. gabbro evolution is, in contrast, a function of clinopyroxene and plagioclase extraction causing the fractionation trend to curve downward towards lower Al_2O_3 : MgO ratios values with decreasing MgO.

Figure 6.1b CaO v MgO Both the A.S. and T.S. gabbros and cumulate ultramafics form separate fields. Although both wehrlite groups form a trend that indicates olivine and clinopyroxene accumulation, the A.S. wehrlites are richer in CaO , relative to MgO, compared with the T.S. wehrlites. Similarly, the T.S. gabbro evolution trend is dominated by olivine and clinopyroxene fractionation, while the A.S. gabbros form a trend that is dominated by clinopyroxene and plagioclase fractionation.

Both groups of wehrlites form a trend that indicates olivine and clinopyroxene accumulation, consistent with their cumulate petrography. The A.S. wehrlites, however, have higher CaO and TiO_2, relative to MgO, compared with the T.S. wehrlites.

On all three covariation diagrams the T.S. gabbros form a fractionation trend away from olivine and pyroxene. Dispersion of the trends towards higher values of CaO and MgO may be due to slight clinopyroxene accumulation. In contrast, the A.S. gabbros form a fractionation trend that is dominated by clinopyroxene and plagioclase extraction. In general the T.S. gabbros have lower TiO_2, relative to MgO, compared with the A.S. gabbros.

Interpretation

Taken together, the two plutonic groups form an evolutionary suit in which the wehrlites form an accumulation trend towards olivine and pyroxene, and the gabbros form a low pressure fractionation trend involving olivine and clinopyroxene extraction, followed by clinopyroxene and plagioclase extraction. The inflection in the overall trend at 11 wt % MgO suggests the appearence of plagioclase on the liquidus. However, the differences in CaO and TiO_2, relative to MgO, between the two wehrlite groups can not be attributed to either crystal fractionation or accumulation and indicate crystal accumulation from different parental liquids.

This interpretation is supported by the geochemistry of the two gabbro groups. Although on all three variation diagrams the A.S. gabbros are more evolved than the T.S. gabbros, field evidence shows that the T.S. gabbros post date those of the A.S.. On this basis the A.S. gabbros can not be related to the T.S. by crystal fractionation, indicating evolution from separate parental liquids. The geochemistry of the A.S. suggests that it evolved from a parental liquid that was richer in CaO and TiO_2, relative to MgO, compared with the parental liquid from which the T.S. plutonic group evolved.

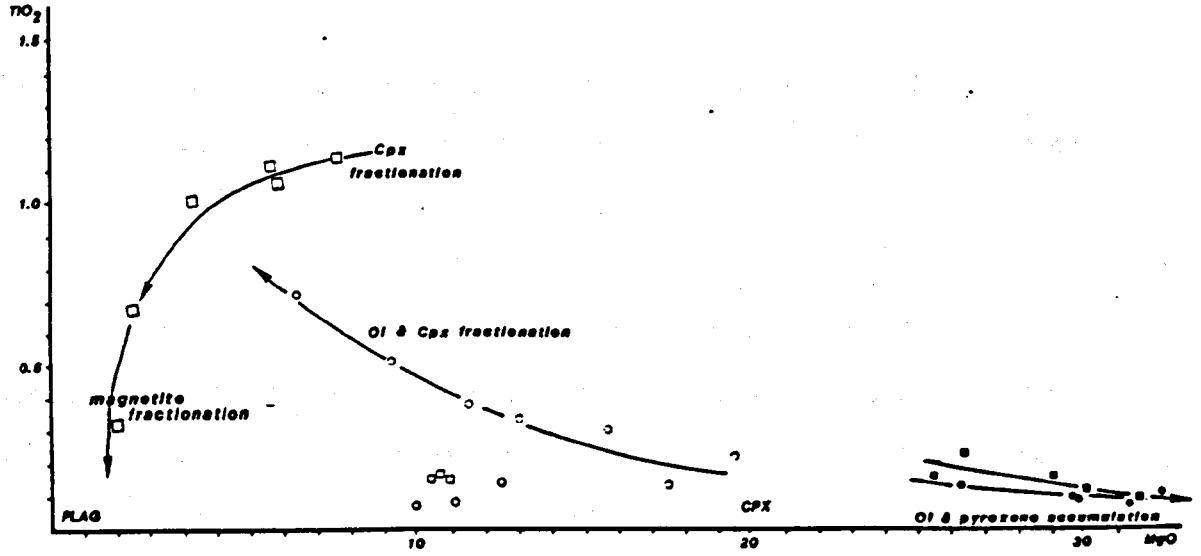

Figure 6.2 TiO_2 v Al_2O_3 The A.S. and T.S. gabbros and wehrlites form separate fields, the T.S. wehrlites having lower TiO_2 , relative to MgO, compared with those of the the A.S.. The T.S. and A.S. gabbros also have separate evolution trends, the former being dominated by olivine and clinopyroxene fractionation and the latter by clinopyroxene and titaniferous magnetite fractionation. The T.S. gabbro trend is concave and supports the evidence of increasing clinopyroxene fractionation with decreasing MgO. In contrast, the A.S. gabbro trend shows a rapid decrease in TiO_2 with decreasing MgO, indicative of titaniferous magnetite super saturation and extraction.

6.3 Geochemistry of Mafic Dykes and Lavas

The primary objective of this section is to describe the major and trace element fractionation of the A.S. and T.S. basalts, and attempt to relate them to source conditions during their generation. Three main questions are appraised: (i) how primative are the basaltic dykes and lavas, (ii) what is their paragenesis, and (iii) how do they compare with each other and the Troodos A.S.. The dykes and lavas are plotted on major and trace element co-variation diagrams that consistantly show two paragenetic evolution trends involving Ol -> Ol + pyroxene -> Cpx + Plag fractionation for the T.S., and Cpx + Plag fractionation for the A.S. respectively. Firstly, however, sample choice and classification are briefly described.

6.3.1 Sample choice

Mafic dykes and lavas crop out throughout the WLFC. The dykes belong to two petrographic groups, the T.S. and the A.S. The T.S. dykes are common in the Mantle Sequence and include picritic, olivine, pyroxene and a small number of plagioclase phyric varieties. The A.S. dykes form a sheeted dyke complex that is preserved as disrupted blocks around the periphery of the WLFC, and are variably metamorphosed to greenschist facies. Basaltic lavas form a volcanosedimentary sequence that crops out in the west and south of the WLFC. The lavas are generally pillowed and aphyric or olivine phyric and glasssy.

Mafic Dykes

In total, over 200 T.S. basaltic dykes were collected for geochemical analysis. Four petrological groups were identified:-

A, olivine phyric picrites with little or no groundmass plagioclase;

B, olivine and pyroxene phyric dykes with plagioclase in the groundmass;

C, olivine, pyroxene and plagioclase phyric varieties, and

D, pyroxene and plagioclase phyric types.

Three directional groups were identified; (1) 310-025N trending; (2) 025-075N trending and (3) 075-130N trending. The dykes were further subdivided on the basis of their host lithologies; (i) harzburgite, mantle sequence; (ii) T.S. intrusive wehrlites; (iii) T.S. gabbros; (iv) WLFC A.S. cumulates, gabbros and sheeted dykes, and (v) serpentinite shear zones (ssz). Compositional means and ranges for each group are given in Table 6.1. Brief petrographic descriptions and geochemical analyses are given in the appendices. The samples chosen for analysis were the freshest from each group. Relative alteration factors from 0 to 10 were determined on the proportion of secondary mineralisation of principal and groundmass phases. Generally, olivine and orthopyroxene are ubquitously altered while clinopyroxene is partly altered to actinolite. Plagioclase is variably altered from turbid to pervasively saussuritised.

Table 6.1 Range in compositions of various mafic dykes and lavas

	MAFIC DYKES						LAVAS		
Type	Picritic	A	B	C	D	Sheeted	Lower	Middle	Upper
major elements in wt %									
SiO_2	42-52	38-40	39-51	46-52	45-58	44-53	49-52	51-52	50-54
TiO_2	0.13-0.26	0.14-0.39	0.14-0.39	0.18-0.56	0.23-0.57	0.43-0.85	0.21-0.47	0.20-0.22	0.19-0.33
Al_2O_3	5.6-14.5	7-16	11-17	7-15	14-17	15-16	12-18	12-14	11-15
FeO*	8-9	7-12	7-10	7-9	7-9	7-9	7-8	7-8	7-8
MnO	0.12-0.38	0.14-0.17	0.15-0.20	0.10-0.17	0.13-0.18	0.05-0.11	0.12-0.38	0.15-0.17	0.13-0.17
MgO	10-31	10-21	7-16	7-13	5-13	7-12	9-15	11-12	10-13
CaO	5-13	7-9	11-16	10-13	9-16	7-14	5-10	10-11	10-11
Na_2O	0.4-1.7	0.2-0.3	0.0-1.4	0.4-4.1	0.1-4.7	1.0-5.0	0.4-0.9	0.6-1.0	0.6-3.4
K_2O	0.0-0.2	0.0-0.0	0.0-2.5	0.0-1.7	0.0-2.3	0.0-0.2	0.3-0.5	0.4-0.6	0.1-1.2
P_2O_5	0.02-0.09	0.00-0.00	0.00-0.08	0.00-0.04	0.00-0.08	0.00-0.01	0.00-0.03	0.03-0.04	0.03-0.04
trace elements in ppm									
Rb	1-6	2-3	2-13	0-8	2-8	1-3	6-14	13-14	2-24
Sr	2-232	2-132	3-120	56-450	10-390	44-145	79-188	117-276	51-515
Y	3-7	5-10	3-13	6-17	8-13	14-21	8-12	8	7-11
Zr	8-18	13-20	12-18	17-37	18-34	22-42	11-18	20-21	11-25
Nb	1-5	2-5	2-4	3-7	3-6	2-3	1-3	1-2	3-1
Pb	1-3	0-6	4-15	5-20	5-16	1-4	12-7	5-6	3-10
Th	0-2	0.5-0.9	0.5-1.2	0.5-0.9	1.0-2.1	12-3	0	0	0-3
Cr	630-2800	450-2308	45-1060	61-860	47-530	77-906	350-1060	943-1033	510-1137
Cu	14-88	12-194	73-106	8-106	3-190	6-370	111-140	113-124	40-120
Zn	32-60	44-66	50-80	21-52	26-63	33-230	69-72	69-82	9-72
Ga	6-12	8-12	8-12	10-14	12-14	1-50	8-12	8-12	8-12

* FeO calculated from Fe2O3

Major and trace elements were determined by E.D. XRF whole rock analyses with the exception of Cr, which was determined on a wave-length spectrometer XRF for greater accuracy.

Lavas

The choice of lavas was made on similar grounds to the mafic dykes: 55 lava samples were subdivided into three petrological groups; (i) aphyric lavas, (ii) olivine and orthopyroxene phyric lavas, and (iii) mafic, limburgite lavas. They were further subdivided stratigraphically into lower lavas, middle lavas and upper lavas. From these groups, only the freshest samples were taken for analysis. Pillow margins were avoided on the basis that there may have been ionic exchange between the lavas and seawater, especially of Ce, Sr, Rb and Na. The compositional ranges and means for the various lava groups are given in Table 6.1. Brief petrological descriptions and geochemical analyses are given in the appendices.

6.3.2 Major Element Geochemistry

Mafic Dykes

Due to the altered state of the mafic dykes, only five major element oxides (CaO, MgO, Na_2O, TiO_2 and Al_2O_3) show any magmatic trends (Figure 6.3). These trends show a pattern of magma evolution that is similar to the Plutonic Group, and that is consistant with the petrography of the mafic dykes. At values of MgO above 14 wt%, picrite and olivine + pyroxene phyric dykes form a trend towards a point that lies approximately half way between the compositions of the olivine and pyroxene phenocrysts (see appendix 4 for compositional analyses). This indicates olivine and pyroxene accumulation, in agreement with the petrography of the picrite and Ol + Opx + Cpx phyric dykes. Below 10 wt% MgO, the dykes form a trend that indicates Plag + Cpx crystal fractionation.

The T.S. and A.S. dykes are only distinguished in two major element oxide variation diagrams. In the TiO_2 v MgO plot (Figure 6.3), the A.S. form a separate group with higher TiO_2, relative to MgO, compared with the T.S. dykes. Similarly the A.S. dykes form a separate group with higher TiO_2 relative to Al_2O_3, compared with the T.S. (Figure 6.4).

Figure 6.3a Na_2O v MgO This diagram shows a dispersed, inverse relationship between MgO and Na_2O in which the overall evolution trend reflects a general change from olivine and pyroxene to clinopyroxene and plagioclase dominated fractionation for the T.S. and WLFC A.S. respectively. The picrite dykes lie on a line trending towards increasing olivine accumulation.

Figure 6.3b CaO v MgO Above 14 wt% MgO, the T.S. dykes, including the picritic varieties, are dominated by olivine and pyroxene accumulation. Bewtween 14 and 12wt% MgO the T.S. dykes form a trend that is dominated by olivine fractionation. Below 12 wt% MgO, clinopyroxene replaces olivine as the dominant fractionating phase and the evolution trend is dominated by clinopyroxene and plagioclase fractionation.

Figure 6.3c Al_2O_3 v MgO Between 14 and 10wt% MgO, the T.S. dykes are dominated by olivine and clinopyroxene fractionation. Between 10 and 5% MgO, both the T.S. and A.S. dykes follow an evolution trend dominated by clinopyroxene and plagioclase fractionation. The picritic dykes fall on a line trending towards olivine accumulation. Since both MgO and Al_2O_3 are considered immobile, the scatter in the correlation may be due to phenocryst phases forming non-liquid assemblages. This is supported by the petrographic evidence of phenocrystal and disequilibrium textured olivine and pyroxene in a large number of dykes.

Figure 6.3d TiO_2 v MgO The T.S. dykes form a dispersed trend, probably due to both the very low values of TiO_2 and and the presence of some cumulate phenocryst assemblages. Discrimation between the T.S. and A.S. mafic dykes is shown with the former having lower TiO_2 , relative to MgO, compared with the latter for similar MgO. This difference between the A.S. and T.S. basalt groups reflects differences in parental liquid compositions.

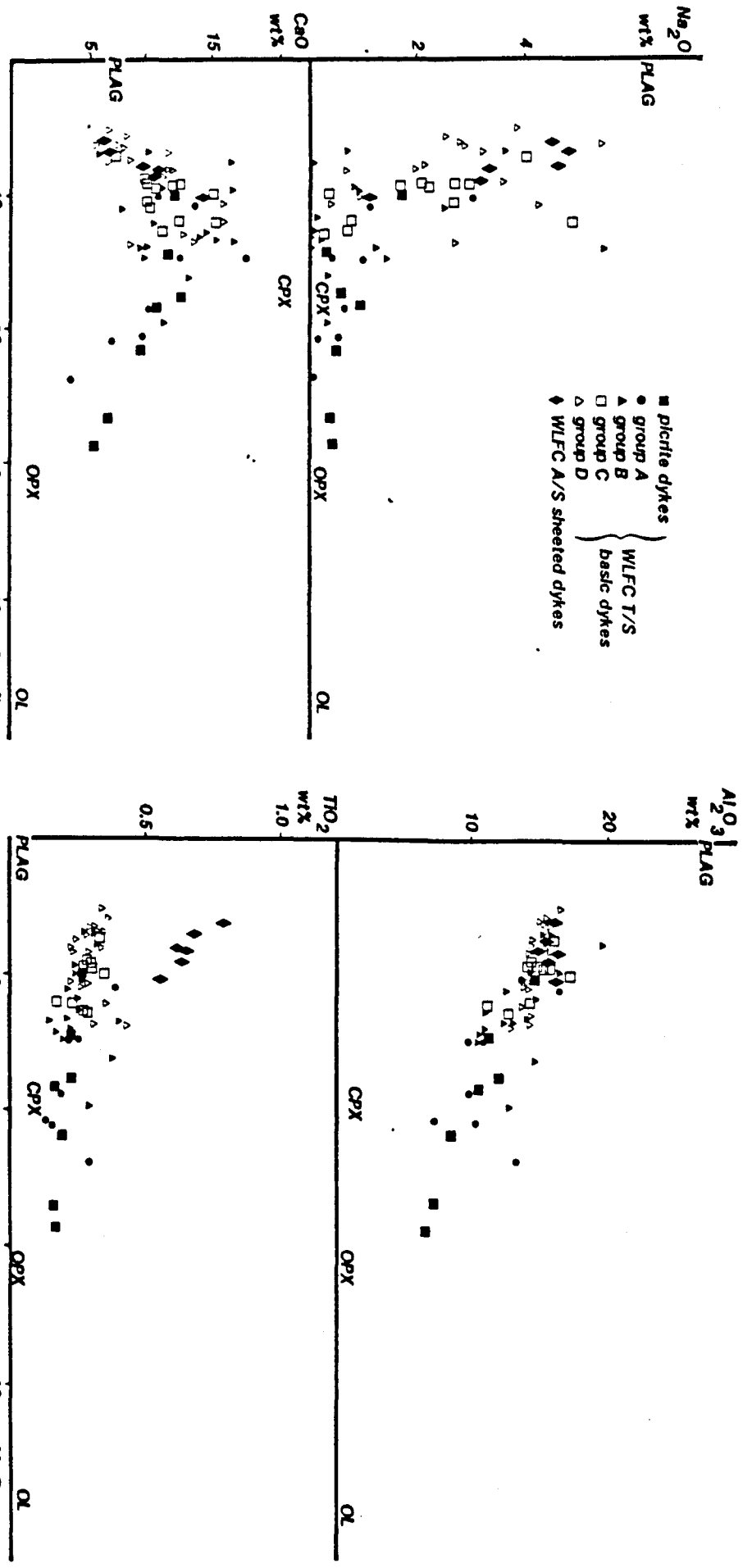
Na2O wt% PLAG
CaO wt% PLAG
Al2O3 wt% PLAG
TiO2 wt% PLAG
CPX
OPX
OL
MgO wt%
picrite dykes
group A
group B
group C
group D
WLFC A/S sheeted dykes
WLFC T/S basic dykes

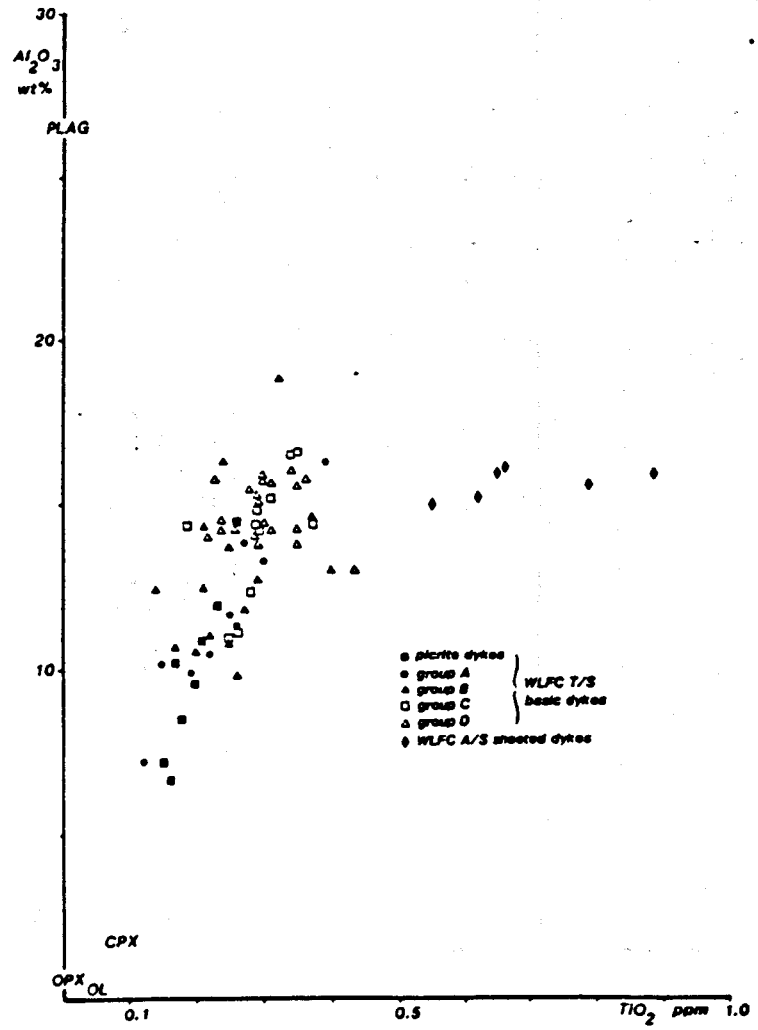

Figure 6.4 Al_2O_3 v TiO_2 This diagram also differentiates between the A.S. and T.S. mafic dykes . The T.S. dykes have an evolution trend that is dominated by olivine and pyroxene fractionation. Only those samples with TiO2 greater than 0.35% show any evidence of plagioclase extraction. In contrast, the A.S. dykes form a flat evolution trend with Al_2O_3 effectively buffered with respect to TiO_2, indicating approximately equal proportions of clinopyroxene and plagioclase fractionation.

Although in the latter case the A.S. trend may be explained in terms of plagioclase fractionation, the higher TiO_2, relative to MgO, can not be related to the T.S. dykes by crystal fractionation, and indicates evolution from a separate parental liquid.

Since magnetite fractionation only affects the most extremely evolved WLFC A.S. dykes, the bulk partition coefficient for Ti during fractionation of the dykes is very low and

approaches zero. Using the equation for Rayleigh crystal fractionation a minimum degree of fractionation can be calculated. For Rayleigh fractionation:-

$$\frac{C_L}{C_O} = F^{(D-1)}$$

where:- C_L = concentration in the residual liquid

C_O = concentration in the original liquid

F = fraction of liquid remaining

D = bulk distribution coefficient

Taking C_O to be the most primative 'liquid' composition in the T.S. suite (samples 43-CY83 or 150A-CY83) then the T.S. dykes have undergone at least 35% fractionation. Similarly, (starting from 1213A-CY4) the A.S. dykes have undergone at least 61% fractionation.

Basaltic Lavas

Major element variation of the WLFC lavas is small (Figure 6.5) compared with the mafic dykes. The lavas are primative with 14wt% MgO, 0.75 Mg/Mg + Fe (mole %) and 0.3 FeO*/MgO, indicating equilibrium with mantle olivine of Fo_{90-91} (Roeder & Emslie, 1970). Since the lavas show predominately quench textutes and are sparsely phyric, their composition represents a primative and primary liquid. Compared with the mafic dykes the lavas have low TiO_2, relative to MgO, indicating an affinity with the T.S.. Although the complete volcanic sequence was sampled and is represented in 6.4, there is no systematic stratigraphic variation in lava composition.

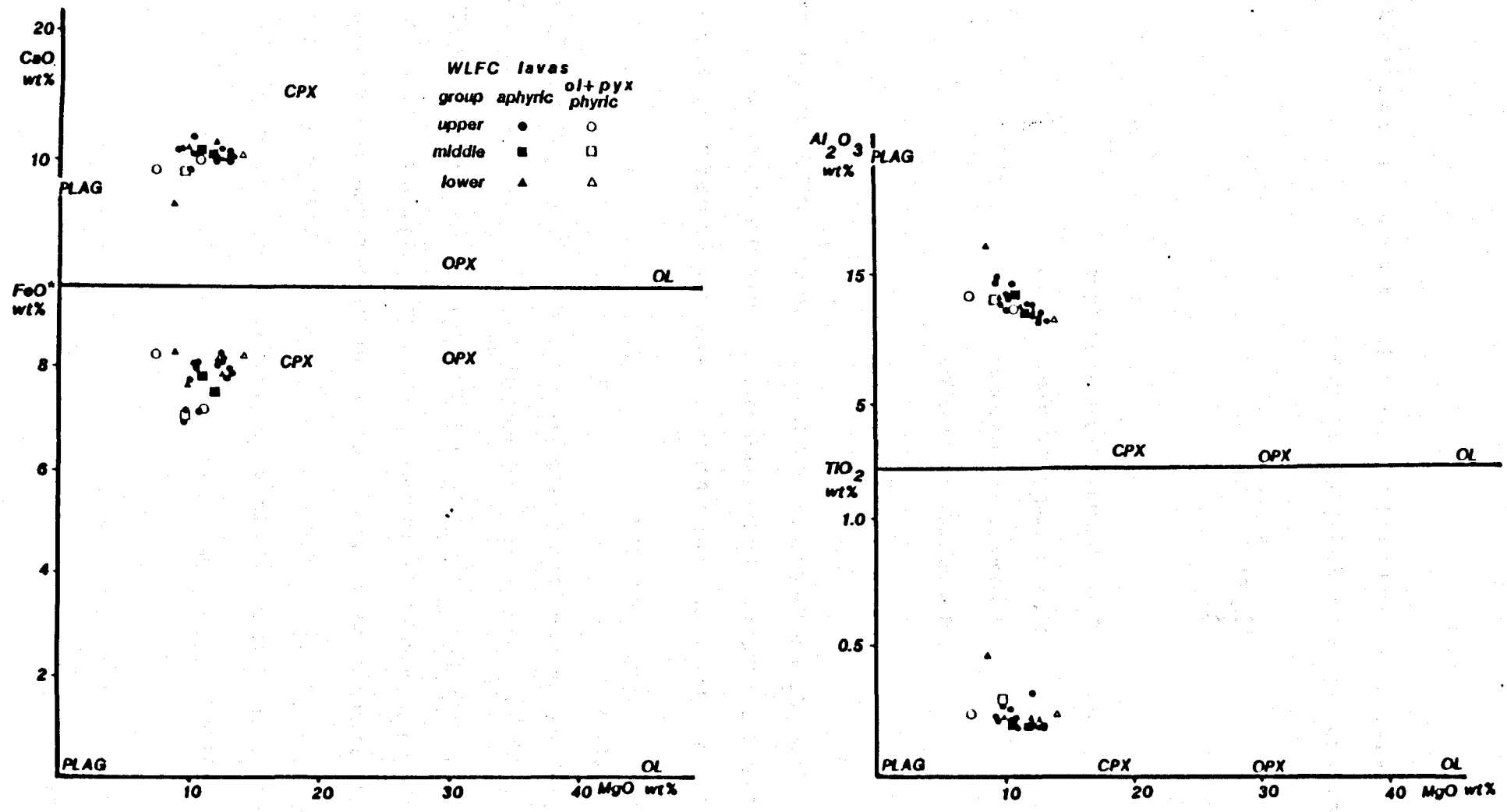

Figure 6.5 Major element covariation diagrams, for the basaltic lavas from the Kapillio area, show a narrow and primi tive range in composition. MgO is between 8.5% and 14% for most of the lavas. The Al_2O_3 suggests pyroxene and olivine fractionation and supports the petrographic evidence.

6.3.3 trace element Geochemistry

Due to the alteration of the mafic dykes, only those trace element considered immobile are used in this section. The trace elements found most useful are Ti, Cr, Ni, Zr, Y, and for the fresh, glassy lavas, Sr and Rb as well. Although Ti has been used as a major element oxide form in the preceding section, it is used here as a trace element.

Mafic Dykes

Both Cr and Ni are compatible in mafic phases and thus vary inversely with increasing, mafic crystal fractionation (Figure 6.6). The phase vectors have been constructed using the equation for Rayleigh fractionation at F = 0.8 (ie. 20% fractionation) and bulk distribution coefficients listed in Pearce (1980). In Figure 6.5 the dykes form a trend that is controlled by mafic phase accumulation and fractionation.

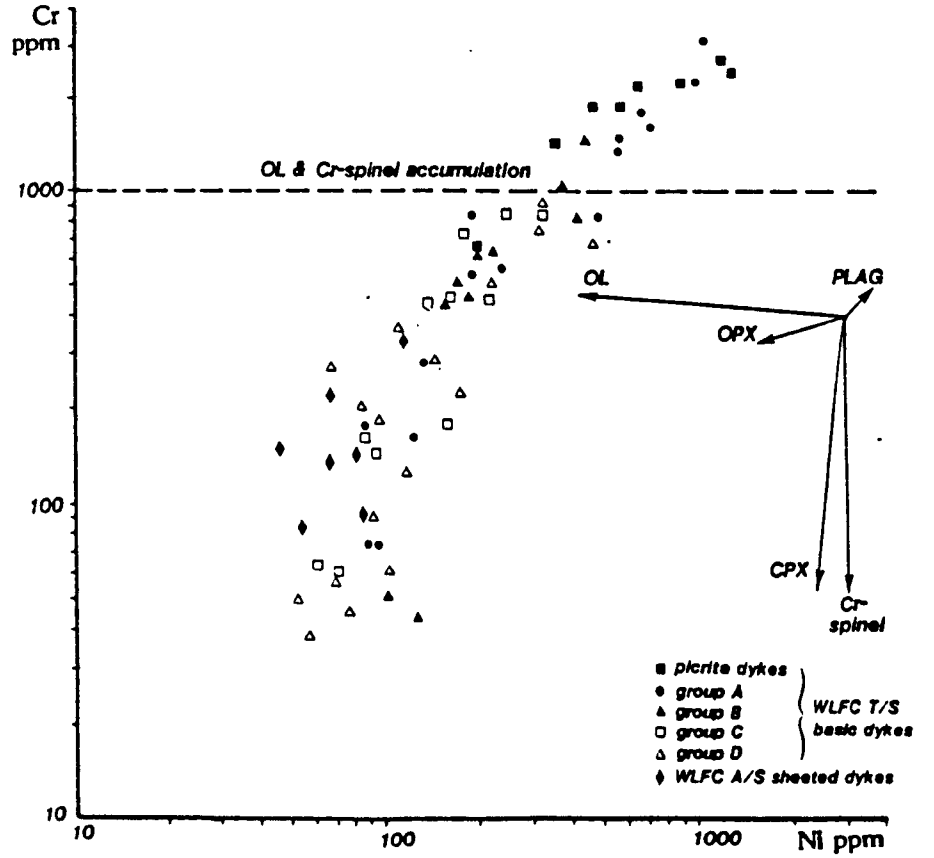

Figure 6.6 Cr v NI Trend for the T.S. dykes shows pyroxene abd olivine controlled fractionation in approximatly equal proportions. The picrite dykes are dominated by olivine and Cr-spinel accumulation.

Although the picrite dykes form a trend that appears to be dominated by olivine accumulation in terms of major element variations, in Figure 6.5 they form a trend that has significantly higher Cr, relative to Ni, than would be the case for olivine accumulation alone. This deviation is best explained in terms of chrome spinel accumulation accompanying olivine accumulation, and is consistant with the picrite petrography. Between 100 and 200 ppm Cr, the non-cumulate dykes form an evolution trend which, compared with the fractionation vectors for the major phases, indicates olivine and pyroxene dominated fractionation. Below 200 ppm Cr, the trend becomes steeper, indicating suggesting fractionation of plagioclase and clinopyroxene.

Although on most trace element covariation diagrams, the mafic dykes form a single continuous evolution suite, trace element variation with Ti discriminates between the A.S. and T.S. dyke groups. On a Ti v Cr covariation diagram (Figure 6.7), the mafic dykes form two distinct fields. The A.S. has higher Ti relative to Cr, compared with the T.S.. The T.S. dykes form an evolution trend that is subparallel to the Cr-axis, in which the picrite have Cr > 1000 ppm, indicating crystal accumulation, and the most evolved, Plag + Cpx phyric dykes have Cr < 50 pppm. Although the A.S. dykes form an evolution trend that is also subparallel to the Cr-axis, they range in composition from 950 ppm Cr to 80 ppm Cr, and have a higher abundance of Ti relative to Cr, compared with the T.S. dykes. Since the two dyke suites form subparallel trends, they can not be related by crystal fractionation and therefore indicate evolution from different primitive, parental liquid compositions. This indicates different sources or source conditions during the extraction of the two dyks suites.

Most mantle partial melting models for the genesis of oceanic magmas involve a spinel or plagioclase lherzolite in which a greater amount of plagioclase and clinpopyroxene contribute to the melt, compared with olivine or orthopyroxene (O'Hara, 1965; 1968; Myashiro, 1970; Menzies & Allen, 1974; Presnall *et al.*, 1979; Green *et al.*, 1979; Pearce, 1980). Since Ti is generally held in clinopyroxene, in such mantle melting models it is partitioned into the melt and thus removed from the mantle at a greater rate than Cr (ie. it behaves incompatibly).

Smaller degrees of partial melting form liquids that are relatively rich in Ti compared with Cr. In these mantle melting models, Ti is removed from the mantle at a faster rate than Cr. As a result, subsequent melts have less Ti available to Cr, and are thus depleated in Ti. Similarly the relative abundance of Ti is greatest at lower degrees of mantle partial melting and will become progressively diluted with higher degrees of melting.

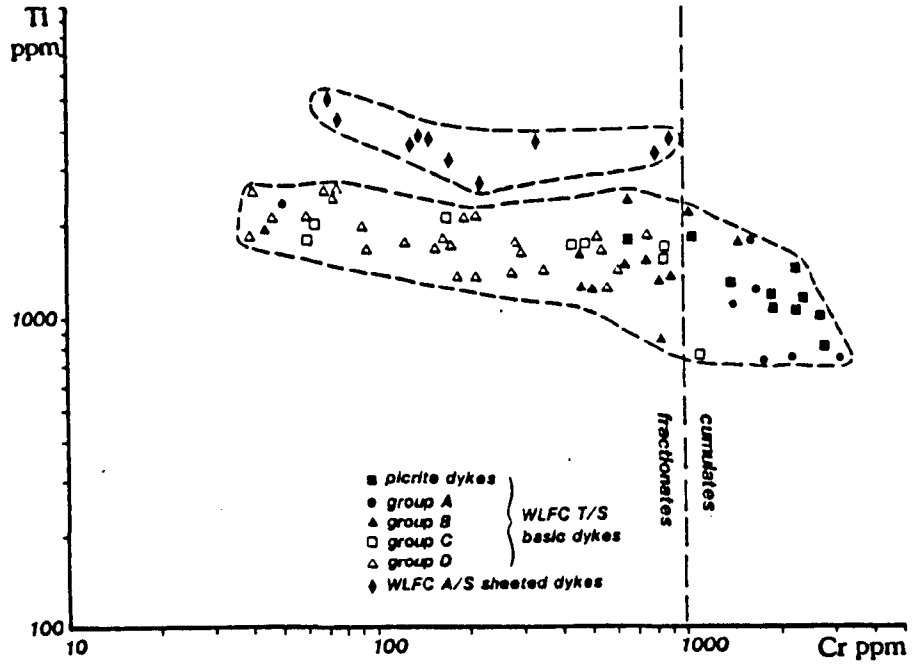

Figure 6.7 Ti v Cr There are two distinct suits, the WLFC A.S. from the T.S. Both suits follow near-parallel evolution trends but start at parental liquids with higher and lower Ti/Cr respectively, reflecting different source melting conditions. The picrite dykes coincide with the T.S. trend, consistant with their geological affixities. Discrimination between the WLFC A.S. and T.S. dykes has already been suggested from Figure 6.3d. Ti v Cr differentiates between fractionation suites and reflects parental liquid compositions. In principle, the more residual the mantle source, the lower the Ti/Cr of a subsequent melt. Higher degrees of partial melting of a mantle source has a similar effect. Fractionation in Ti v Cr space is both sub-horizontal and for different basaltic suites, approximately parallel.

The parallel evolution trends for the mafic dykes sugests either that the A.S. was derived from a lower degree of partial mantle melting compared with the T.S., or that the T.S. was derived from a mantle source that was already depleted in Ti relative to the source for the A.S. It is not, however, possible to distinguish between the two models on the basis of Ti v Cr alone.

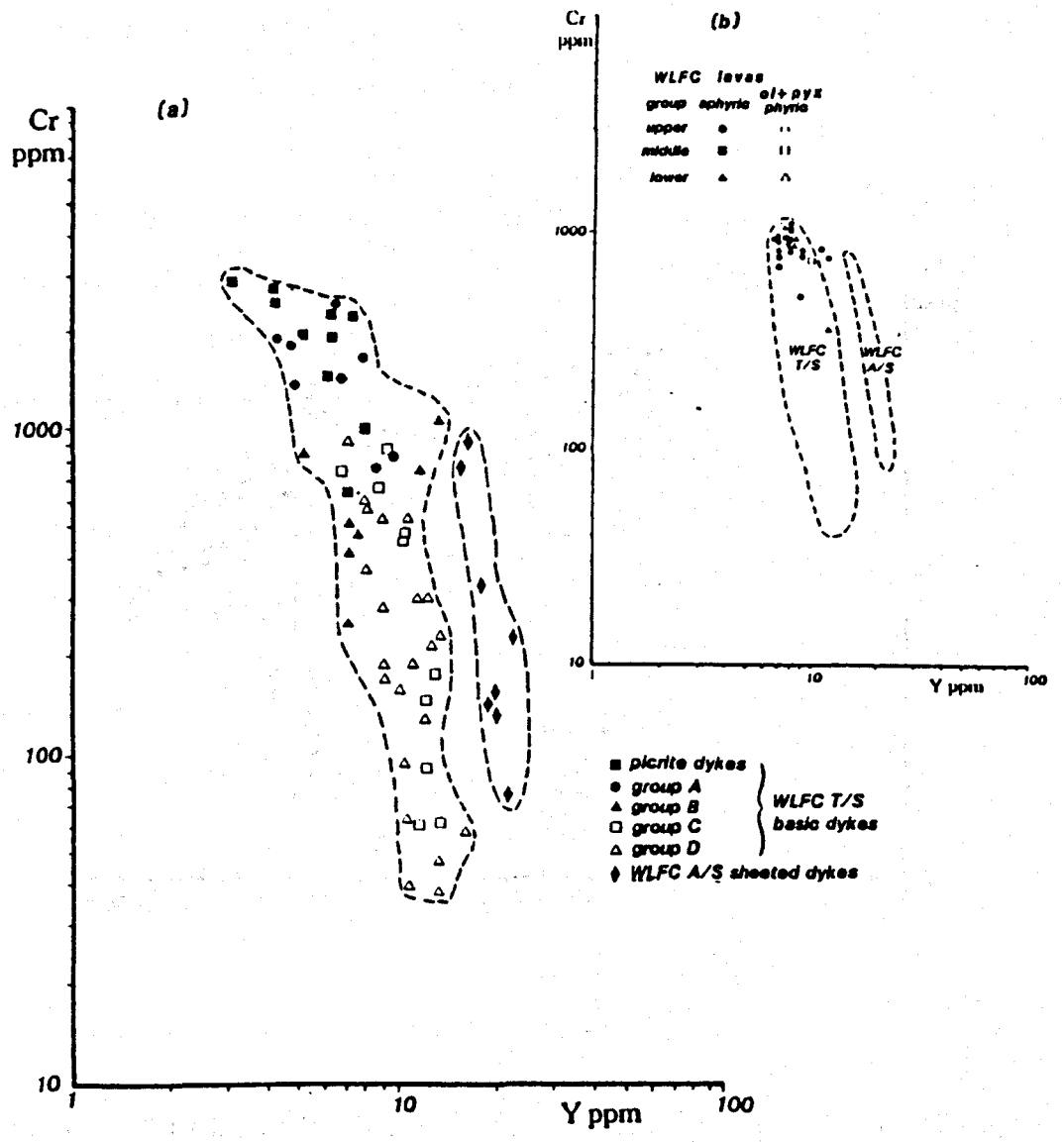

Figure 6.8 Cr v Y This covariation diagram discriminates between parental liquid compositions and genetically unrelated suites. Since Cr is compatible and Y incompatible in basaltic magmatic processes, different parental liquids will start from and evolve along fractionation paths that are approximately vertical and parallel (Pearce, 1980). (a) Both the T.S. lavas and dykes form coincident fractionation suites indicating cogenesis, while the WLFC A.S. forms a parallel suite but at lower Cr/Y for the same Cr values. Mean N-type MORB is plotted for reference (after Pearce, 1980). (b) The lavas fall within the T.S. dyke field suggesting cogenesis

Different basaltic source characteristics, such as those discussed above, are also revealed by Cr v Y covariation (Pearce, 1980). Figure 6.8a illustrates a Cr v Y covariation diagram in which the two mafic dyke groups form separate evolution trends that are subparallel but with different abundances of Y relative to Cr. Similar to the Ti v Cr diagram in which the incompatible element (Ti) is relatively depleted, the T.S. dykes also have lower Y (ie. also incompatible in basaltic phases) relative to Cr compared with the A.S. dykes. This supports the interpretation for a more depleted source or derivation from lower degrees of mantle partial melting for the T.S. compared with the A.S.. Plotted on Figure 6.8b are the lavas, which form a group that is coincident with the most primitive, non-cumulate T.S. dykes, suggesting that the lavas are cogenetic with the T.S. dykes.

Like Ti, Y is mainly held in oceanic asthenosphere in clinopyroxene. In the models for mantle partial melting refered to above, Y behaves incompatibly and is readily partitioned into the melt. As a result the mantle is rapidly depleted in y, such that the Cr : Y ratio of a melt varies with the degree of mantle partial melting and with successive melt extractions. The distinct, subparallel evolution trends for the mafic dykes supports the evidence that the two groups of dykes are derived from different parental liquids. The differences in Cr, relative to Y, between MORB the A.S. and the T.S. dykes, suggests derivation from a successively depleted mantle source, or from successively higher degrees of mantle partial melting. The coincidence between the lavas and the T.S. dykes suggests that the two groups are cogenetic.

Lavas

It has already been shown that the lavas have a narrow and primitive range of major element values. This is also reflected in their range of trace element compositions, with Ni values mostly of 200 to 400 ppm, and Cr values of about 1000 ppm. When compared with the mafic dykes on a Ti v Cr covariation diagram (Figure 6.9) the lavas form a tight group that is coincident with the most primitive, non-cumulate T.S. dykes.

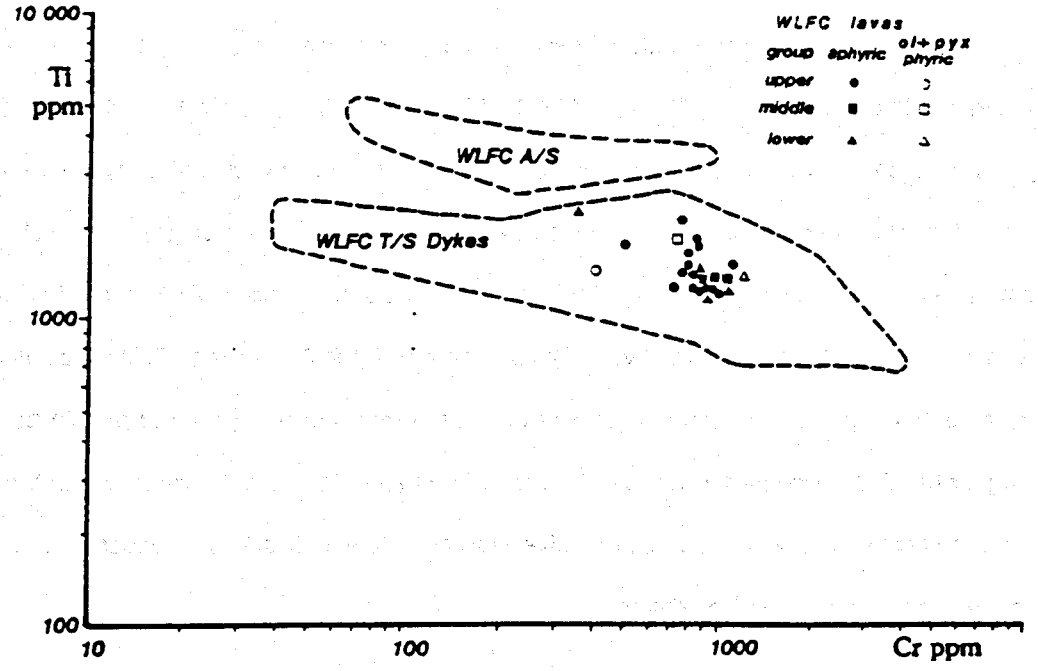

Figure 6.9 Ti v Cr During melting of a plagioclase lherzolite source, Ti behaves incompatibly while Cr is compatible, being partitioned in to residual orthopyroxene and Cr-spinel. As a result, cogenetic, primitive liquid, will have similar Ti : Cr ratios for the same Cr value. Differences in primitive Ti: Cr ratios indicate derivation from variable sources or source conditions. It is not possible to distinguish between high degrees of partial melting of a common source or melting of a source already depleated in basaltic componants, on the basis of Ti v Cr alone. In Figure 6.9 the T.S. lavas plot within the field defined by the T.S. dykes, and are coincident with the most primitive aphyric varieties. This indicates that both the T.S. dykes and lavas have a common parental liquid and are hence cogenetic. However, the WLFC A.S. dykes form a field with a high Ti : Cr ratio for similar Cr values, indicating derivation from a different parental liquid. The higher Ti : Cr ratio is due either to derivation from a less depleated source or from higher degrees of partial melting of a source common to both the T.S. and WLFC A.S.

The coincidence between the lavas and T.S. dykes supports the evidence that the two groups were derived from the same source.

Table 6.2 shows the mean compositions for the Troodos A.S., the Arakapas fault belt and WLFC lavas. The low Ti abundance in the WLFC lavas compared with the Troodos A.S. or MORB is reflected in low High Field Strength Element (HFSE) abundances (Zr, Y and Nb). The WLFC lavas have a very low abundance of both Zr and Y (Figure 6.10) compared with primitive N-Type MORB which has 90ppm Zr and 30ppm Y (Pearce, 1980). The lavas also have a Zr : Y ratio that varies from 1 to 3, and form a trend that ranges from 10 to 26ppm Zr and 7 to 12ppm

Y. Although both Zr and Y are HFSE that are incompatible in lherzolite mineralogy, Zr is slightly more incompatible than Y (Pearce & Norry, 1979, Pearce, 1980). As a result Zr : Y ratios vary inversely with increasing degrees of mantle partial melting and crystal fractionation. Only the presence of residual garnet, and to a lesser extent clinopyroxene, in the source region will preferentialy retain Y and hence lower Zr : Y ratios for subsequent melts. The large variation in the Zr : Y ratio for the lavas may be explained by residual garnet or amphibole in the source or by large variations in the degree of mantle partial melting.

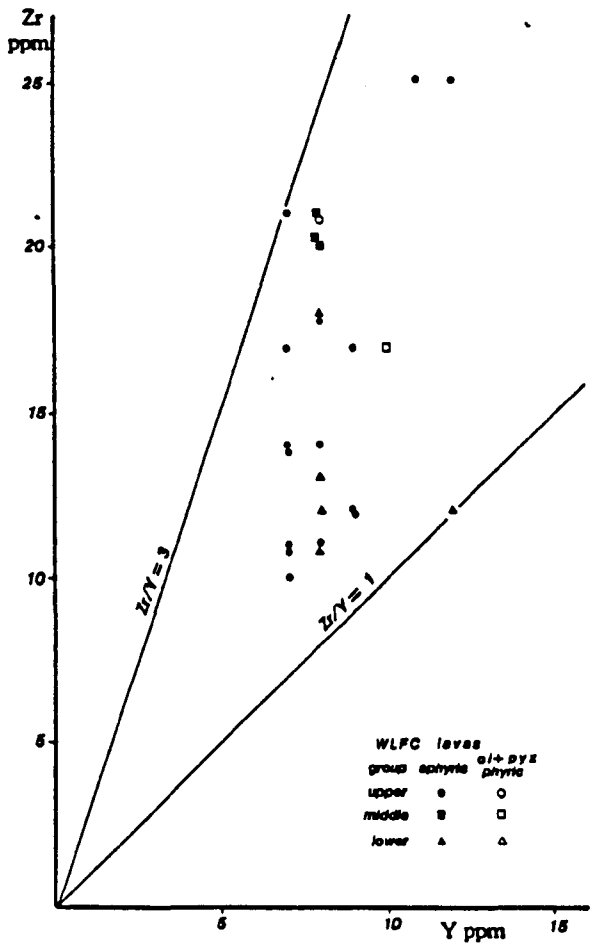

Figure 6.10 Zr v Y Both Zr and Y are high field strength elements (HFSE) that are immobile during alteration and moderate grades of metamorphism, and are extremely incompatible during basaltic fractionation. As a result, Zr/Y remains almost constant during fractionation and partial melting, of a spinel or plagioclase lherzolite source. Only the presence of residual garnet and to a lesser extent, clinopyroxene or amphibole in the source region will preferentially retain Y, and hence lower Zr/Y for subsequent melts. On Figure 6.11, the WLFC lavas have a very low abundance of both Zr and Y compared with N-type MORB

Such an interpretation, however, is not supported by the Rare Earth Element (REE) profiles for the lavas, which are all very similar, (ie. residual garnet will preferentially retain heavy REEs and large variations in the degree of mantle partial melting will greatly vary both the REE abundance and La : Yb ratio). This suggests that the variation in Zr : Y ratio may be due to Zr being enriched relative to Y and the other trace elements.

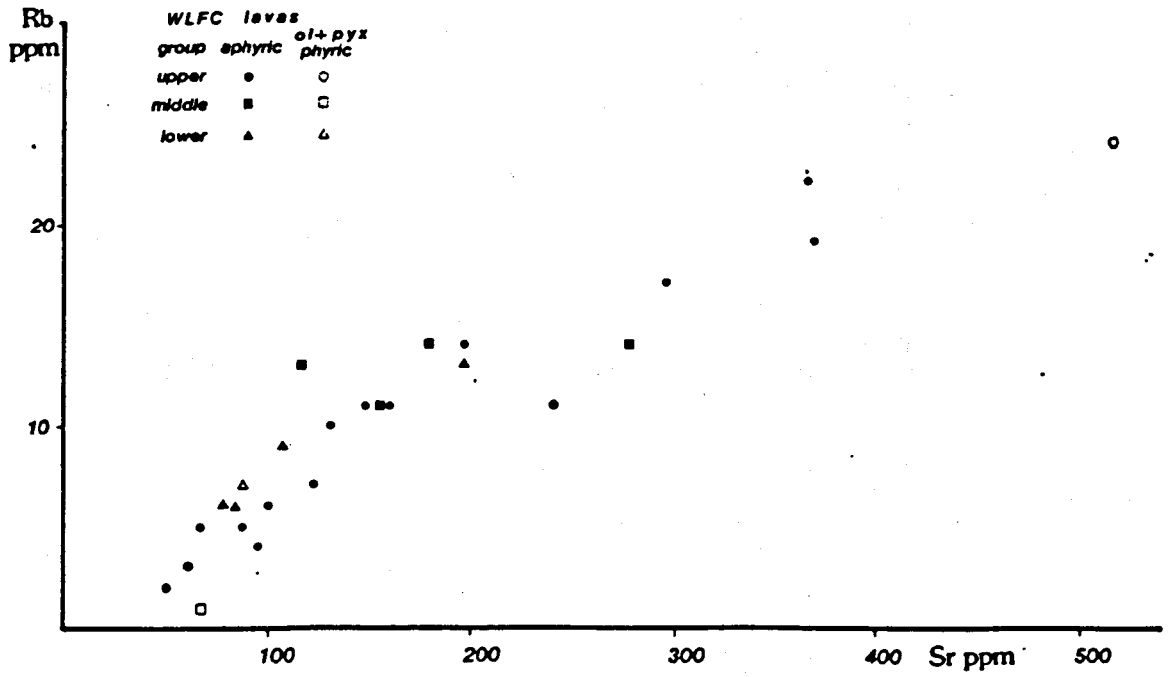

Figure 6.11 Rb v Sr When plotted against either incompatible or compatible trace elements, Rb and Sr do not show any coherent trends. Although Rb and Sr are very mobile during alteration, when plotted against one another (and K) both trace elements show strong positive correlations. Since such strong correlations probably reflect systematic processes and hence are unlikely to be the result of alteration (see text). Since Rb and Sr are decoupled from other major and trace elements, their variation within the WLFC lavas reflects independant LILE enrichment.

Although the HFS elements (Zr, Y & Nb) and Ti are depleted in the lavas, the LIL elements (Rb & Sr in particular) are not. Variation in both Rb and Sr shows an order of magnitude difference in their abundances (Figure 6.11), and is not consistent with the evidence that the lavas are primitive and have a narrow compositional range. When plotted against either incompatible or compatible trace elements, Rb and Sr do not show any coherent trends. Although Rb and Sr are very mobile during alteration, When plotted against one another (and K) both trace elements show strong positive correlations. Such strong correlations must reflect a systematic processes that is unlikely to be the result of alteration. The extreme variation of Rb and Sr within the WLFC lavas suggests that they are decoupled from the major and trace elements. The anomalously large variation in Sr and Rb, and their strong correlation with each other but not with the major and trace elements, suggests that they are added to,the lavas as part of a LIL element enrichment phase. This is supported by their strong correlation with K and the unusually high abundance of LIL elements compared with the other incompatible trace elements.

Table 6.2 Mean compositions for the AFB, AFB', Troodos A.S., N-Type MORB and the T.S. lavas, used in the normalised element diagrams refered to in the text.

Type	AFB basalt	AFB'	Troodos A.S.	N-Type MORB	T.S. basalts
Sr	155	138	88	120	148
K_2O	0.46	0.21	0.64	0.15	0.40
Rb	4	2.5	9	2	10
Th	0.19	0.22	0.22	0.20	0.28
Ta	0.16	0.17	0.13	0.18	0.08
Nb	1.8	2.5	–	3.5	2.1
La	–	–	–	3	1.4
Ce	1.17	1.12	4.9	9.0	2.4
Nd	0.77	0.42	5.4	7.7	1.2
P_2O_5	0.03	0.05	0.05	0.12	0.04
Zr	11	13	30	90	17
Hf	0.35	0.35	0.62	2.4	0.41
Sm	0.54	0.41	1.89	3.30	0.40
TiO_2	0.28	0.22	0.43	1.5	0.23
Y	6.4	4	14.7	30	8
Yb	1.24	1.15	–	3.4	1.1
Ni	234	296	275	250	319
Cr	580	946	697	500	941
Gd	1.00	0.77	2.87	–	–
Tb	0.20	0.17	0.55	–	0.20
Tm	0.22	0.21	0.38	–	0.25
Lu	0.14	0.21	0.43	–	0.20

Major element oxides are refered to in wt %.

Trace elements are refered to in ppm.

Major and trace elements were determined by E.D. XRF whole rock analyses with the exception of Cr, which was determined on a wave-length spectrometer XRF for greater accuracy. Rare earth element analysis were determined by instrumental neutron activation analysis. AFB is used in place of Arakapas fault belt; mean of six glassy lavas from Simonian (1975). AFB' is an average of the two most primative AFB lavas; from Simonian (1975). Troodos A.S.; mean of nine lavas and dykes; from Smewing (1975). N-Type MORB from Pearce (1980).

6.3.4 Rare Earth Element Geochemestry

Chondrite Rare Earth Element (REE) diagrams are plotted for both T.S. dykes and fresh glassy lavas. The REEs have been arranged in order of decreasing atomic weight. In general the light REEs (LREE) are less compatible than the heavy REEs (HREE) during mantle partial melting (of a spinel or plagioclase lherzolite source) or basaltic fractionation. As a result, REE profiles for basaltic systems become increasingly LREE depleted with succcessively larger degrees of partial melting and with successive melt extraction from a lherzolite mantle source.

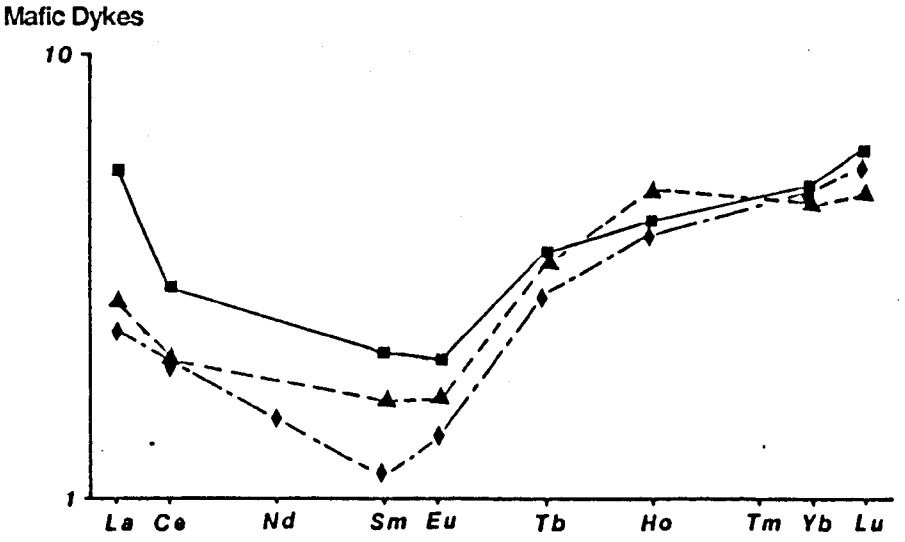

Figure 6.12 REE (dykes) Selected Rare Earth Element profiles for the mafic dykes, Chondrite normallised. The REE profiles are both depleated with respect to MORB and have a characteristic 'U'shape'.

Since the A.S. dykes are at upper greenschist facies and are not considered reliable for REE analysis, only T.S. dykes have been analysed. In general the T.S. mafic dykes have REE abundances that range from 3x to 10x chondrite. The REE profiles (Figure 6.12) have characteristic 'U' shaped REE patterns with increasing depletion of successively lighter REEs from Lu to Sm (ie. Yb/Sm < 1). From Sm to La the LREEs are successivly more abundant with Ce/Sm > 1. Overall the REE profiles are substatially lower in REE abundance than MORB which forms a flat pattern at 15x chondrite. Between Lu and Sm the successive depletion in LREEs

is consistent with the trace element evidence and indicates that the T.S. dykes were derived from either a high degree of mantle partial melting or an already depleted mantle source. Such LREE enriched REE profiles, however, can not be generated by partial melting of a spinel or plagioclase lherzolite source and suggests the addition of a strongly LREE component (Cameron *et al.*, 1983; Cameron, 1985; Hickey & Frey, 1982).

Lavas

REE profiles for the lavas (Figure 6.13) closely resembles those for the T.S. dykes. Absolute abundances are between 3 and 10x chondrite. The lavas have a similar pattern of successive REE depletion from Lu to Sm, with Ce/Sm < 1, and similar LREE enrichment from Sm to La , with La/Sm > 1. Differences in the absolute abundances between various lava flows may reflect variable amounts of crystal fractionation and/or degreees of mantle partial melting. The similarity between the REE patterns for both the WLFC T.S. lavas and dykes is evidence of their cogenetic nature.

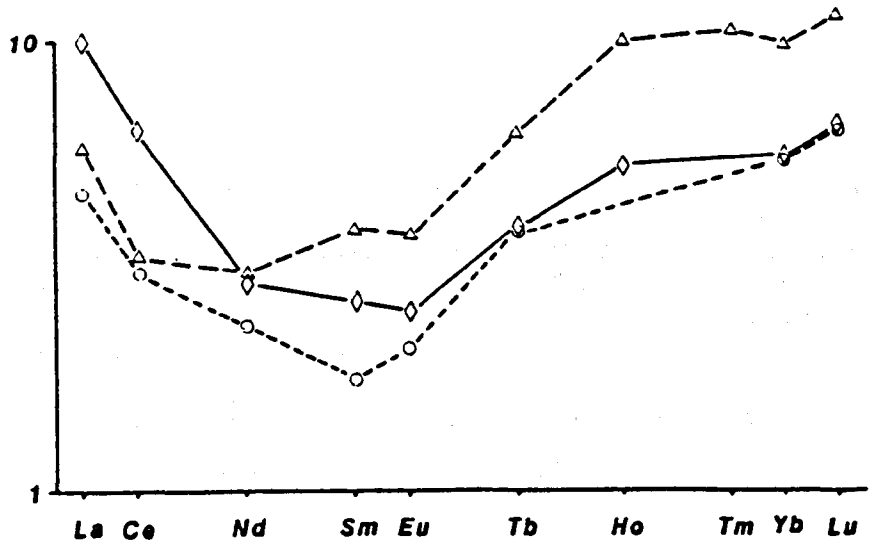

Figure 6.13 REE (lavas) Selected Rare Earth Element profiles for the basaltic lavas, Chondrite normallised. The REE profiles are similar in shape to those for the mafic dykes, but have slightly lower absolute abundances. They are both depleated with respect to MORB and have also have the characteristic 'U'shape'.

6.4 Discussion

In this section, the mafic dykes and lavas are compared with the Plutonic Sequence in an attempt to relate their geochemistry to a common source. The mafic dykes and lavas are also compared with those of the Troodos massif and the Arakapas fault belt.

6.4.1 Comparison Between the Dykes, Lavas and Plutonic Sequence.

It has already been shown that the Plutonic Group and the mafic dykes each contain two geochemically distinct suites, termed the A.S. and T.S. In both cases the A.S. is characterised by higher TiO_2 , relative to MgO (and in the case of the dykes, to Cr) compared with the T.S. and a fractionation path that is controlled by Cpx + Plag. In contrast, the T.S. in both cases forms a fractionation path that is dominated by olivine and pyroxene. The T.S. dykes are geochemically similar to the T.S. dykes and are both probably cogenetic. The primitive composition of the lavas suggests that they are the parental liquid to the T.S. dykes. This similarity in subdivision into an A.S. and a T.S. for both the Plutonic Sequence and the mafic dykes supports the field evidence for two magmatic groups.

6.4.2 Comparison Between the T.S., Arakapas fault belt and Troodos A.S. basalts.

Lavas from the Troodos A.S. (both uppper and lower lavas; Smewing, 1975) and the Arakapas fault belt (Simonion, 1975) are plotted on a Ti v Cr covariation diagram (Figure 6.14). The two groups of basalts form distinct fields in which the Troodos A.S. lavas have more Ti relative to Cr, compared with the Arakapas fault belt basalts. The position of the Troodos A.S. and Arakapas fault belt lavas is similar to the WLFC A.S. and T.S. mafic dykes and lavas respectively (Figure 6.9). This suggests that the Troodos A.S. and WLFC A.S. are genetically related. Similarly, the Arakapas fault belt and T.S. basalts also appear to be cogenetic.

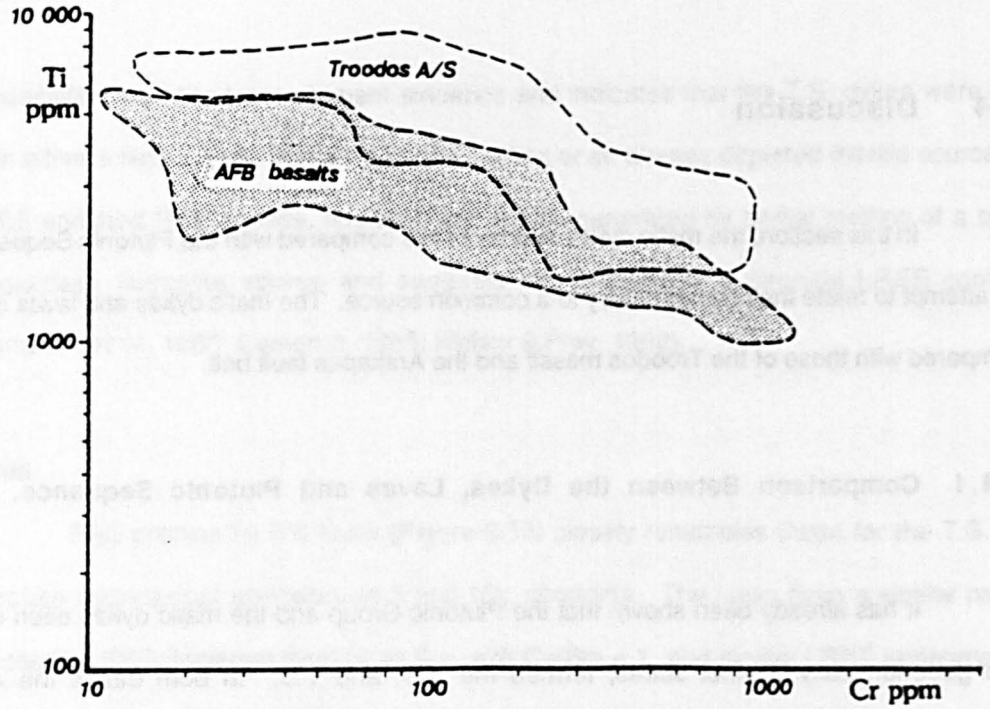

Figure 6.14 Tl v Cr The Arakapas fault belt and Troodos Axis Sequence basalts form two seperate and parallel fractionation suites. The positions of the twoe fields is similar to those for the WLFC A.S. and T.S. , respectively, and suggests a similar source.

On a normalised element diagram (Figure 6.15) the WLFC T.S. and Arakapas fault belt basalts are compared with the Trooodos A.S. basalts in an attempt to test their genetic relationships. In the normalised element diagram trace elements and selected REEs are arranged in order of decreasing incompatibility in basaltic mineralogy and decreasing mobility in vapour phases. The element abundaces are also nomalised to N-type MORB (Pearce, 1980; 1894; Hole *et al.*, 1984). Pearce (1980) and Pearce *et al.* (1984) interpret elemental abundances that are less than MORB as controlled by source depletion (ie. melt controlled), and elemental abundances in excess of MORB as enriched. Fractionation and differential partial melting of a source shifts the normalised element diagram profile vertically with respect to N-type MORB, but does not substantially change its shape, (Pearce, *op. cit.*). The data presented on the normalised element diagram consist of averages of nine Troodos A.S. lavas (Smewing, 1975), five glassy Arakapas fault belt lavas (Simonian, 1975) and six fresh lavas. The following sections compare the basalt normalised element diagram profiles for the T.S., the Arakapas fault belt and the Troodos A.S.

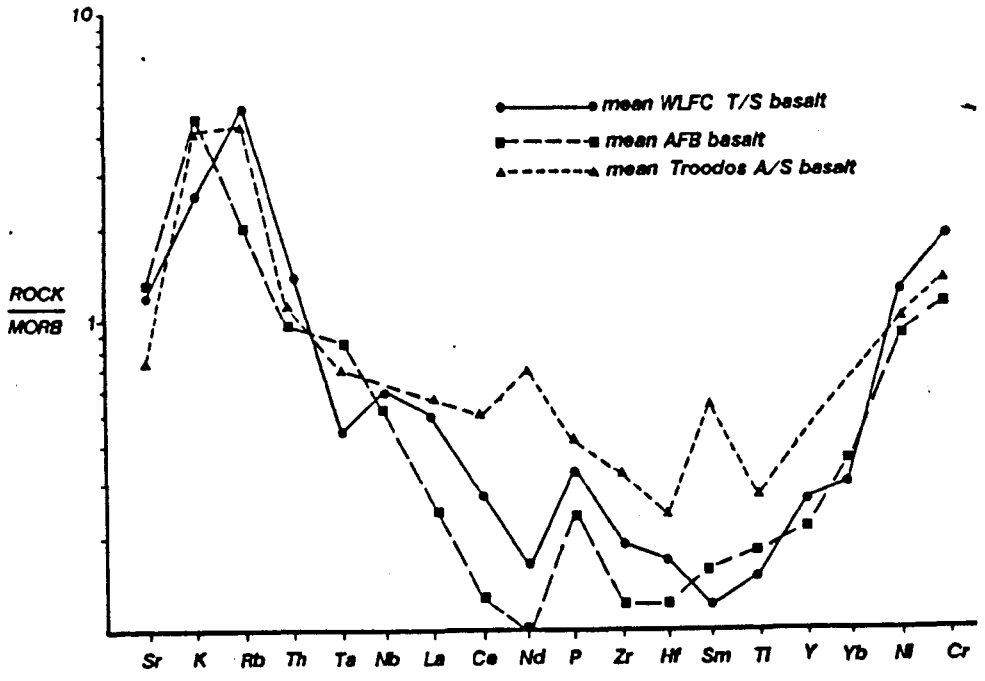

Figure 6.15 A normallised element diagram, normallised to N-Type MORB, for the WLFC lavas, Arakapas fault belt lavas (Simonian 1975) and the Troodos A.S basalts (Smewing 1975).

Compared with the Troodos A.S. basalts, the T.S. lavas are slightly richer in compatible transition elements (Ni, Cr) and poorer in HFSE (Y, Hf, Zr, Nb), TiO_2 and REE. This is consistent with the T.S. being derived from a more depleted source, compared with the Troodos A.S., or from a greater degree of partial mantle melting. In contrast to the Troodos A.S. the T.S. lavas have a positive P_2O_5 peak and a slight negative Ta anomaly. Both the T.S. and Troodos A.S. have similar amounts of LIL elements in excess of MORB, suggesting ubiquitous LIL element enrichment. The T.S. has lower a La : Yb ratio than the Troodos A.S., reflecting relative LREE enrichment in the former.

Transition element abundances in the T.S. are slightly higher than in the Arakapas fault belt basalts suggesting that the former are more primitive. The T.S. are also more depleted in TiO_2 and heavy to middle REE (Yb, Sm and Nd) relative to the Arakapas fault belt basalts. This may be accounted for by slight differences in the source regions (ie. heterogeneity in or partial melting), or it may reflect a larger degree of fractionation for the

Arakapas fault belt basalts compared with the T.S. lavas. In contrast to the Arakapas fault belt basalts, the T.S. lavas are slightly richer in high Zr, Hf and the middle to light REEs suggesting selective enrichment in these elements. While Ta in the T.S. forms a small negative anomaly, the Arakapas fault belt basalts show an opposite effect. Like the Troodos A.S., both the Arakapas fault belt and T.S. basalts have ubiquitous LIL element enrichment of approximately equal amounts.

The evidence that the Arakapas fault belt basalts and lavas are both depleted in incompatible elements relative to the Troodos A.S. and genetically related is supported by their REE profiles (Figure 6.16). Detailed comparison between the REE profiles for the Troodos A.S. and Arakapas fault belt basalts has already been made by Simonian (1975) and Simonian & Gass (1978). Compared with N-type MORB, which has a relatively flat REE profile at about 15 x chondrite, both the Troodos A.S. and Arakapas fault belt basalts have lower REE abundances and successively increasing degrees of LREE depletion between Sm and La. The successive depletion in REE, from N-type MORB to the Troodos A.S. and to the Arakapas fault belt basalts is in agreement with their trace element variation and supports the evidence of successively increasing degrees of mantle partial melting or derivation from an increasingly depleted source. Menzies and Allen (1974) suggested that the depletion in the Troodos A.S. compared with N-type MORB is due to derivation from a more depleted source than MORB mantle, and not larger degrees of partial melting. Simonian & Gass (1978), however, also suggested higher degrees of melting for the origin of the Arakapas fault belt basalts,compared with the Troodos A.S.

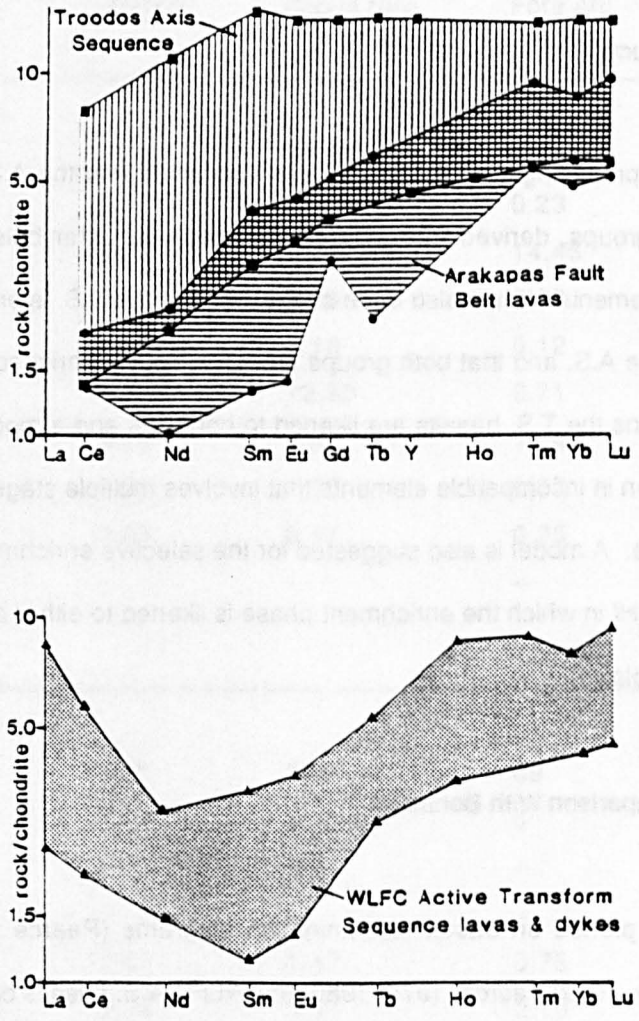

Figure 6.16 Chondrite normallised REE profiles for the Troodos, AFB and WLFC basalts. The AFB basalts *are* depleated relative to the Troodos A.S.; the WLFC and AFB basalts are similarly depleated but only the WLFC basalts are light REE enriched.

Compared with the Arakapas fault belt basalts the WLFC T.S. has both a similar Yb : Sm ratio and abundances of HREEs supporting the trace element evidence that both suites were derived from a similar source. As a result, the Arakapas fault belt basalts may represent a 'non-LREE enriched' end-member of a depleted basalt group that includes the T.S. lavas and dykes.

6.5 Basalt Petrogenesis

6.5.1 Introduction

In the preceding sections it has been suggested that the A.S. and T.S. basalts form two separate groups, derived from diferent sources, the latter being relatively depleted in incompatible elements. It has also been suggested that the T.S. is enriched in LREEs, Zr and Hf relative to the A.S. and that both groups are ubiquitiously enriched in LIL elements. In the following sections the T.S. basalts are likened to boninites and a model is suggested for their relative depletion in incompatible elements that involves multiple stages of melt extraction from a MORB source. A model is also suggested for the selective enrichment of the T.S. basalts in LREEs, Zr and Hf in which the enrichment phase is likened to either an ocean island basalt or an island arc tholeiite.

6.5.2 A Comparison With Boninites

When plotted on basalt discrimination diagrams (Pearce and Cann, 1971; 1973; Pearce & Norry, 1979; Pearce, 1975, 1980) the WLFC A.S. basalts coincide with the Troodos A.S. and fall within the field of island arc tholeiites (IAT). Many studies in the past have identified the Troodos A.S. basalts as being subduction-zone related, (Myashiro, 1975; Smewing *et al.*, 1975; Pearce, 1975, 1980; Cameron *et al.*,1980; Saunders *et al.*, 1980; Robinson *et al.*, 1983a and b; Schminke H-U *et al.*, 1983; McCulloch & Cameron, 1983; Rautenschlein, 1985). In contrast, the WLFC T.S. basalts lie outside the majority of basalt discriminant fields above.

Table 6.3 Mean T.S. lavas compared to representative boninite compositions.

Type	Bonin Islands Japan	Marianas Trench	Cape Vogel Papua New Guinea	Marianas Fore Arc region	WLFC lavas
major elements in wt %					
SiO_2	58.46	57.33	56.80	58.00	52.50
TiO_2	0.10	0.14	0.33	0.23	0.22
Al_2O_3	13.37	9.97	11.9	14.45	15.8
FeO*	8.27	9.06	7.10	8.03	7.60
MnO	0.12	0.13	0.16	0.12	0.15
MgO	9.36	15.19	12.60	6.71	12.12
CaO	8.11	5.86	7.89	10.47	10.82
Na_2O	1.59	1.59	1.05	1.87	0.44
K_2O	0.70	0.93	0.41	0.35	0.52
P_2O_5	–	–	–	–	0.03
trace elements in ppm					
Sr	97	107	339	89	163
Rb	12	15	8	8	10
Th	–	–	–	–	0.28
Ta	–	–	–	–	0.4
La	1.27	1.27	1.47	0.75	1.35
Ce	2.57	2.93	3.51	2.10	2.85
Nd	1.65	1.85	2.09	1.72	2.85
Zr	25	36	29	28	15
Hf	0.69	0.79	0.58	0.62	0.41
Sm	0.43	0.51	0.60	0.57	0.40
Y	5	5	7	7	8
Yb	0.59	0.60	0.81	0.74	1.09
Ni	140	258	154	–	266
Cr	538	1386	715	197	848
Tb	0.10	0.12	0.14	0.16	0.19
Lu	0.10	0.10	0.13	0.12	0.20

Boninite data are from Hickey & Frey (1982). Elemental analyses for the WLFC lavas are by Ed XRF except for Cr which was determined on a wavelength spectrometer, XRF.

Instead, the extremely low abundances of incompatible elements (Zr, Y, Nb & TiO_2) and the moderately high MgO content of the T.S. lavas is similar to boninites from Cape Vogel, Papua New Guiniea (Dallwitz *et al.*, 1966; 1968; Jenner, 1981) the Mariana trench wall (Dietrich *et al.*, 1978; Sharaskin & Dobretsou, 1979; Hawkins *et al.*, 1979) and the Mariana fore-arc region, DSDP site 458 (Meijer, 1980; Meijer *et al.*,1981). Table 6.3 gives an average composition of the T.S. lavas, where it is compared with a number of 'boninitic' compositions published by Hickey & Frey (1982).

The strongly incompatible element depleted nature of boninites is interpreted as hydrous partial melting of residual mantle peridotite at less than 10 kb (Hickey & Frey, 1982; Cameron *et al.*, 1979; Walker & Cameron, 1983; Cameron, 1983; 1985; Duncan & Green, 1980). The depleted geochemistry of the T.S. basalts agrees with above interpretation for boninite petrogenesis. Such a model, involving shallow mantle source melting, is supported by studies of ophiolitic mantle sequences. In both the Bay of Islands Ophiolite Complex, Newfoundland (Malpas, 1978) and in the Oman Ophiolite Complex (Browning, 1982), the residual mantle harzburgites grade downward into increasingly more fertile lherzolite. In the former example, the lower limit to the residual mantle harzburgite is located at about 10 km below the petrological Moho, (Malpas *op. cit.*). This implies the depth of mantle partial melting for the the genesis of boninites was as shallow as 13-14 km below the Moho (ie. between 5 and 7kb).

In their study of boninite petrogenesis Hickey and Frey (1982), Cameron *et al.*, (1983) and Cameron (1985) recognised both a ubiquitous LIL element enrichment and a variable LREE and Zr enrichment. In agreement with Pearce (1982 a and b) and Pearce *et al.* (1984), both Hickey and Frey (1982) and Cameron (1983) interpret LIL element enrichment as volatile release during oceanic slab subduction and subsequent metasomatism of the mantle wedge.

Although both Hickey and Frey (*op. cit.*) and Cameron (*op. cit.*) recognise a separate silicate melt related enrichment of LREE and Zr in some boninites the source for such a melt phase remains unknown.

6.5.3 Incremental Melting

In the following sections it is suggested that the A.S. and T.S. basalts represent two magmatic groups that were derived from a 12% melt, followed by a subsequent 10% melt, of an already depleted MORB source. Although there are a number of possible melting processes (Shaw, 1970) incremental batch melting is the most simple and has been used in the following calculations. The calculated degrees of partial melting are considered only relative to an assumed initial source, P_0. Mass balance calculations suggest that the final mantle residue following N-type MORB, A.S. and T.S. basalt extraction resembles an extremely depleted tectonised harzburgite.

It has already been suggested that the T.S. basalts were derived from a more depleted source or from a higher degree of partial melting compared with either the A.S. or N-type MORB. In the past, variations in oceanic mantle partial melting have been modelled in terms of Cr $\underline{v}$ Y covariation with melting curves for lherzolitic upper mantle calculated assuming phases enter the melt in the ratio of 3:1:4:4 for olivine, orthopyroxene, clinopyroxene and plagioclase respectively (Pearce, 1980; 1983) and using distribution coefficients listed in Pearce and Norry (1979) and Pearce (*op. cit.*). The positions of N-Type MORB (Bryan & Thompson, 1976; Fisk *et al.*, 1982; Pearce, 1980; 1983), the WLFC A.S. dykes and T.S. dykes and lavas are plotted on a Cr $\underline{v}$ Y covariation diagram (Figure 6.17). The position of the depleted MORB source, P_0, assumes melt extraction at an average of 20% . The position of C_3 chondrite is plotted for reference.

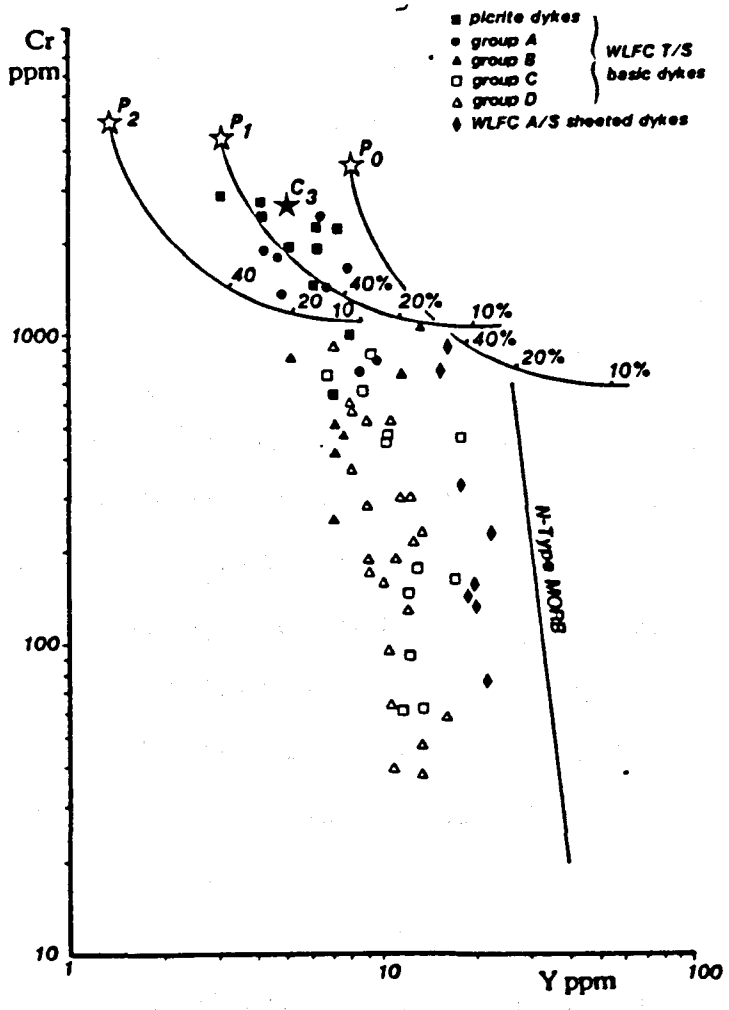

Figure 6.17 Cr v Y covariation diagram in which incrimental batch melt proportions are modelled. The positions of N-Type MORB and C3 chondrite are given for reference. Melt curves are based on those of Pearce (1980) and assumes the same phase ratios entering the melt in each case. The source P_0 referes to an assumed MORB source; P_1 is the residue folowing MORB extraction (at ~20% melting) and is taken as the source for the Troodos A.S.; P_2 is the residue, from P_1 following Troodos A.S. extraction (at ~12% melting) and is taken as the source for the T.S..

In Figure 6.16, the WLFC A.S. basalts intersect the incremental melting curve from P_0 between 45% and 50%, implying exceptionally hot, thermal conditions in the source region. The requirement of such an anomalous thermal condition has been used by Menzies and Allen (1975), Pearce (1980), Duncan and Green (1980) and Pearce *et al.* (1984) to argue in favour for a model of multiple melting for the genesis of similarly depleted magmas. Instead of using P_0, the position of the source for the WLFC A.S. is taken as the residue following MORB extraction.

Assuming similar phase melting ratios and conditions as above (Pearce *op. cit.*), the WLFC A.S. intersect the melt curve from the depleted source, P_1, at Ca12%. This value is in general agreement with the models of Menzies and Allen (1974) and Pearce (1980) and implies a cooler thermal regime than for the preceeding case.

Since the T.S. basalts do not intersect with the melt curve from P_0 they can not be generated from it. Instead, they intersect with the melt curve from P_1 between 50% and 55%. By applying a similar arguement as Menzies and Allen (1974), Pearce (1980), Duncan and Green (1980) and Pearce *et al.* (1984), P_2, which is the residue from P_1 following the extraction of the average A.S. basalt, is taken as the source for the T.S. basalts. The melt curve from P_2 interscts with the T.S. basalts at Ca 10% partial melting. In this case the lower degree of partial melting from P_2, compared with P_1, implies a cooler and perhaps more reasonable thermal regime.

It has often been argued that successive basalt extractions will rapidly deplete a lherzolite source in basaltic componants (especially CaO and Al_2O_3), thus making further basalt genesis impossible. In the following calculations, the source for the A.S. basalts is taken as an average of three tectonised plagioclase lherzolites from Troodos (Allen, 1975; Menzies & Allen, 1974). The composition of P_1 is given in Table 6.4. P_{2a} and P_{2b} are the various residues from P_1, following A.S. and T.S. extraction at 10% and 12% melting respectively, and are calculated by simple mass balance. Their compositions are also given in Table 6.4 along with the compositions of the primitive liquid end-members of the A.S. and T.S. basalts, termed here L_1 and L_2 respectively.

The residue composition from P_1 is :-

$$C_{P2} = \left(C_{P1} - C_{L1} F\right) \times \left(\frac{1}{1-F}\right)$$

where:- C_{P1} is the concentration in the source

C_{P2} is the concentration in the residue

C_{L1} is the concentration in the liquid extracted (ie the A.S. or T.S. basalts)

F is the melt fraction

Table 6.4 Calculated compositions of sources and residueas after A.S. and T.S. primitive basalt extraction.

Type	L_1	L_2	P_1	P_{2a}	P_{2b}	P_3
SiO_2	47.47	51.00	43.18	42.59	37.97	41.42
TiO_2	0.60	0.30	0.02	-0.06	-0.16	-0.10
Al_2O_3	17.17	13.50	3.67	1.83	-2.88	0.52
Cr_2O_3	0.14	0.14	0.65	0.72	0.99	0.78
FeO*	8.14	8.74	8.39	8.42	8.16	8.34
MnO	0.03	0.04	0.25	0.28	0.39	0.31
MgO	11.07	14.00	40.74	44.78	58.60	48.01
CaO	15.37	12.30	3.49	1.87	-2.38	0.71

L_1 and L_2 are primitive WLFC A.S. and T.S. basalts respectively and are averages from the most primitive sparsely phyric samples analysed. P_1 is an average of three Troodos plagioclase lherzolites, that are taken as the source for the Troodos A.S. by Menzies & Allen (1975), and used here as the source for the WLFC A.S.. P_{2a} and P_{2b} are the calculated residues following the bulk extraction of the WLFC A.S. at 12% meltig and the T.S. at 10% melting. P_3 is the calculated residue following the bulk extraction of the T.S. from P_{2a}.

Since the calculated composition of P_{2a} has an excess of major elements, it is possible to extract the A.S. from P_1 at 12% melting. The calculated composition of P_{2b}, however, has a deficit in CaO and Al_2O_3, indicating that the T.S. basalts can not be generated

from P_1 at the estimated 50% to 55% melting. This supports the suggestion made above that an anomalously hot thermal regime for the generation of the T.S. basalts is geologically unlikely. By taking P_{2a} as the source for the T.S. basalts and the estimated melt proportion of 10%, the composition of the calculated residue, P_3, is given in Table 6.4. The calculated composition of P_3 has an excess of major elements, supporting the suggestion that the depleted residue, P_{2a}, is the source for the T.S. basalts.

Although the above melting model is consistent for both the major and trace element abundances, TiO_2 is deficient in both P_{2a} and P_3. This apparent anomaly can be accounted for by the presence of 0.04% illmenite or 0.08% titaniferous magnetite in the initial source, P_1. Small amounts of titaniferous spinel are likely to result in TiO_2 being very heterogeneous, and make TiO_2 difficult to detemine on the basis of only the three plagioclase lherzolite samples available. The incremental batch melting model is further supported when P_3, the final residue, is compared to depleted tectonised harzburgite from Troodos (Table 6.5). The tectonised harzburgite is interpreted as refractory mantle material following extraction of the Troodos A.S. (Greenbaum, 1972; Menzies & Allen, 1974; Allen, 1975; Smewing *et al.*, 1975). The composition of P_0 is also in Table 6.5, where it compares favourably with suggested upper mantle compositions. The major element composition of P_0 has been calculated by adding 20% of primitive MORB (Bender *et al.*, 1978) to P_1. The composition of P_0 is calculated using the simple mass balance equation below:-

$$C_{Po} = \left(C_{P1} \times [1 - F]\right) + C_{L1} F$$

Where C_{Po} is the concentration in proposed MORB source

C_{P1} is the concentration in MORB source residue (ie. the Troodos plagioclase lherzolites).

C_{Lo} is the concentration in primitive liquid (ie. N-type MORB)

F is the melt fraction

The similarity between the calculated composition of P_0 and suggested upper mantle compositions supports the suggestion that P_1 is a residue following MORB extraction and that it is the source for the A.S. basalts (Menzies & Allen, 1975).

6.5.4 LREE, Hf and Zr Enrichment

Introduction

The T.S. basalts overall, REE depleted compared with the Troodos A.S. their REE profiles are 'U' shaped with La : Sm >1 Yb : Sm <1. It has also been suggeted that the T.S. basalts are Zr and Hf are enriched. In the following sections, an attempt is made to quantify the Zr and Hf enrichment and examine its relationship with the LREE enrichment.

Enrichment Factors

Since the only apparent difference between the Arakapas fault belt and T.S. basalts is the addition of a LREE, Zr and Hf enrichment phase to the latter, the Arakapas fault belt basalts are taken as a non-enriched end-member of the T.S. suite. The amount of this enrichment phase that has been added to the T.S. is quantified by subtracting the composition of the average primitive Arakapas fault belt basalt (termed here AFB') from an average of the T.S. lavas. From this method the enrichment phase has a $^*La_N : Sm_N = 4.2$ and a $Ce_N / Sm_N = 1.3$ (* the subscript 'N' refers to chondrite normalised values).

Figure 6.18 is a normalised element diagram, on which the mean of six primitive T.S. lavas are normalised to AFB'. Positive deviations from the normalising values are interpreted as enrichment, while negative deviations represent depletion relative to AFB'. The LREE enrichment that characterises the T.S. basalts is also associated with an enrichment in Y, Ti, Zr, Hf Rb, and Sr and slight depletion in Ta. The negative Ta anomaly can not be an 'added' component and suggests the formation of a phase retaining Ta, probably in the source region.

Table 6.5 Suggested upper mantle compositions compared with the compositions of the final calculated residue folowing incremental batch melting and the calculated N-Type MORB source, P_o.

Type	1	2	3	4	5	6	P_o	P_1	P_3	H
SiO_2	42.86	45.16	44.62	44.36	44.25	37.46	44.28	42.89	41.42	43.72
TiO_2	0.33	0.71	0.14	0.13	0.07	0.25	0.26	0.02	<0.01	0.01
Al_2O_3	6.99	3.54	3.66	3.59	3.25	4.48	5.80	3.64	0.52	0.47
Cr_2O_3	0.18	0.43	0.33	0.43	0.43	0.51	0.53	0.65	0.78	0.39
FeO*	9.29	8.45	8.17	9.00	7.88	8.83	8.62	8.31	8.34	8.19
MnO	0.14	0.14	0.13	0.18	0.11	0.15	0.18	0.18	–	0.15
NiO	0.20	0.20	0.27	0.27	0.26	0.37	0.21	0.25	0.31	0.27
MgO	35.07	37.45	38.98	38.51	39.50	43.50	35.62	40.48	48.01	45.99
CaO	4.37	3.08	3.31	3.31	3.25	3.95	4.46	3.47	0.71	0.77
Na_2O	0.45	0.57	0.26	0.11	0.23	0.46	0.21	0.06	<0.01	<0.01
K_2O	<0.01	0.13	<0.01	0.13	0.01	0.04	0.02	0.01	–	<0.01
Total	99.91	99.94	99.87	100.02	99.35	100.00	100.00	100.00	100.00	100.00

1 Kilbourne Hole (Carter, 1970)
2 Pyrolite (Ringwood, 1966)
3 Rhonda (Dickey, 1970)
4 Orthris, Greece (Menzies, 1974
5 Tarreyres, France (Hutchinson *et al.*, 1975)
6 Average of mantle nodules (Jagutz *et al.*, 1979)

Po Calculated N-Type MORB source
P_1 Average of three Troodos of plagioclase lherzolites (Allen, 1975)
P_3 Calculated residue after extraction of T.S.
H Average of eight tectonised harzburgites from Troodos (Allen, 1975)

The normalised element diagram profile for the T.S. basalts, above, suggests that Hf, Zr and Y are related to the LREE enrichment. On the basis of the procedure outlined by Cameron (1985), the propotion of LREE enrichment is estimated by calculating the abundance of Ce that has been added to AFB' to generate the degree of Ce enrichment observed. Figure 6.19 illustrates Zr, Hf and Hf/Yb covariation with Ce enrichment, E. All three covariation diagrams show a strong positive correlation demonstrating a close relationship between Zr, Hf and LREE enrichment processes.

Although there is no correlation between LIL element abundance and Zr, Hf and LREE enrichment, Figure 6.19 suggests an excess of LIL elements compared with the LIL element enrichment that effects the Arakapas fault belt, Troodos A.S. and T.S. basalts alike. This may be due to an extremely heterogeneous LIL element enrichment or to a LIL element component that is related to the LREE and Zr, Hf enrichment.

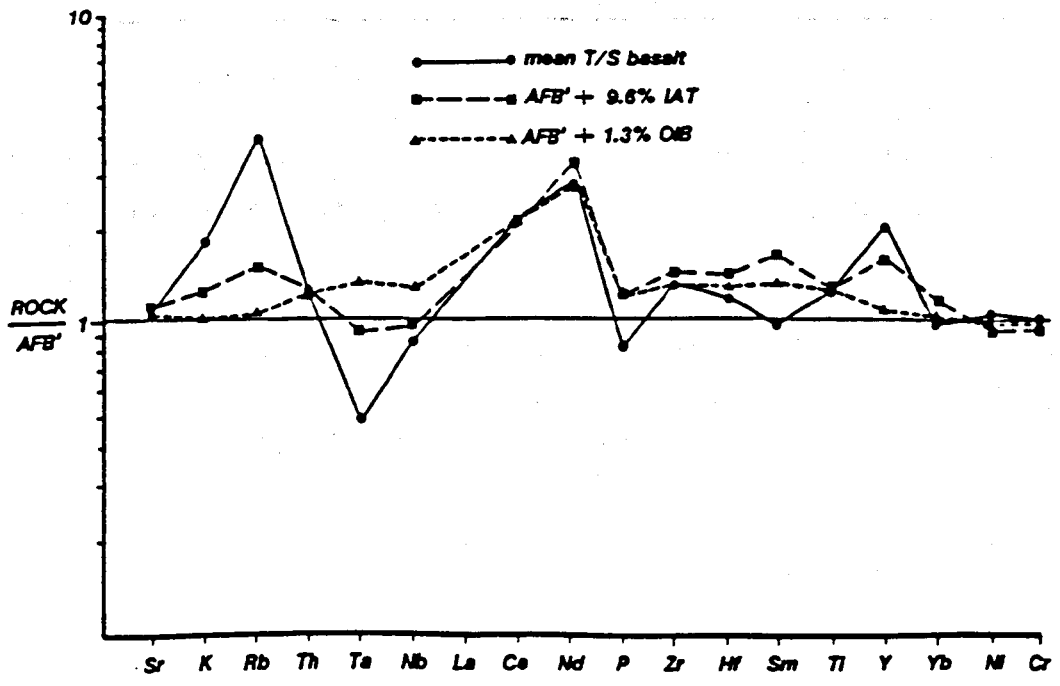

Figure 6.18 Multi-element diagram normallised to primatie Arakapas fault belt lava. The T.S basalt profile is closely matched by the bulk addition of 9.6% IAT or 1.3 % OIB to AFB'.

Nature of the LREE, Zr and Hf Enrichment Phase.

Although LIL elements and to a lesser extent, LREE are mobile in fluid phases, HFSE and HREE are most mobile in silicate melts (Pearce, 1975, 1982; Schneider & Eggler, 1986). Since the enrichment phase that effects the T.S. basalts carries LREE elements and selected HFS elements (Zr & Hf), it is most probably a silicate melt. In the multi-stage melting model described above, any enrichment in incompatible elements would have been removed at an early stage. Since the T.S .basalts are the last stage of melt extraction from an already depleted source, but are the only basalts to show this style of enrichment, this suggests that the enrichment was introduced after the extraction of the A.S. melt and prior to or during the generation of the T.S. melt. This suggests that the enrichment may have been in the form of a magma generated from a piece of mantle that was not involved in the formation of the A.S. or T.S.

The enriched phase that was added to a LREE depleted end-member (ie. the AFB') has already beeen calculated to have La / Sm = 4.2 (ie. strongly LREE enriched). In the following section an attempt is made to attribute this enrichment phase to a known basaltic melt. Two melts are considered, an ocean island basalt (OIB) and an island arc tholeiite (IAT).

A typical OIB (from La Palmas, Canary Islands, Pietz *pers. comm.*) has $La_N/Sm_N = 3.5$ and $La_N/Yb_N = 18$. Similarly, an average IAT (Hole *et al.*, 1984) has $La_N/Sm_N = 3.1$ and $La_N/Yb_N = 15$. Using the absolute values of Ce in both the IAT and OIB the amount needed of each, added to AFB' to produce the average observed Ce enrichment, has been calculated. This gives an absolute value of LREE enrichment as a proportion of either OIB or IAT.

$$\text{enrichment } E = \left(\frac{Ce - Ce^*}{Ce_E}\right)$$

where:- E is the proportion of enrichment phase present.

(Ce - Ce*) is the mean abundance of Ce added to AFB'.

Table 6.6 Compositions of OIB, IAT, primative T.S. basalt and OIB enriched and IAT enriched AFB' basalt.

Type	OIB	IAT	T.S. lava	E_1	E_2
Sr	818	293	148	147	153
K_2O	0.86	0.82	0.39	0.22	0.27
Rb	21	16	10	3	4
Th	4.40	0.89	0.28	0.27	0.28
Nb	57	1.5	2.1	3.2	2.4
La	47	6.6	1.4	_	_
Ce	102	13.8	2.4	2.4	2.4
Nd	56	10.9	1.2	1.14	1.43
P_2O_5	0.66	0.17	0.04	0.06	0.06
Zr	276	72	17	16	18
Hf	6.82	1.9	0.41	0.43	0.50
Sm	10.4	3.34	0.40	0.54	0.69
TiO_2	4.39	0.84	0.28	0.28	0.28
Y	31	27	8	4.3	6.2
Yb	2.22	2.76	1.1	1.16	1.30
Ni	52	8.7	319	293	268
Cr	49	8.1	941	934	856
Tb	1.35	0.68	0.20	0.32	0.19
Lu	0.34	0.45	0.20	0.23	0.22

OIB from La Palmas (Z. Palacz, *pers. comm.*)

IAT is an average Marianas IAT (Hole *et al.*, 1984)

E_1 is the calculated product followig bulk addition of 1.3% OIB

E_2 is the calculated product following bulk addition of 9.6% IAT

AFB' is given in Table 6.2

T.S. lava' average of six of the most primative sparsely phyric samples

Major elements are in wt %
Trace elements are in ppm

From the above equation, the average LREE enrichment in the T.S. basalts represents either 1.3% OIB or 9.6% IAT, added in bulk to AFB'. To test which candidate for the enrichment phase most closely resembles the actual enrichment, they have both been added in bulk to AFB' by simple mass balance.

concentration in the enriched basalt $C_1 = C_0 (1 - E) + C_E.E$

where:-

C_0 is the concentration in AFB'.

C_E is the concentration in the enrichment phase

C_1 is the concentration in enriched basalt

E is the proportion of enrichment phase added

In Figure 6.18, 9.6 % IAT and 1.3% OIB have been added to AFB' in an attempt reproduce the characteristic normalised element diagram profile of the T.S. basalt. The compositions of AFB', mean T.S. basalt, OIB, mean IAT and the calculated enriched basalts, are given with the results in Table 6.6. Although the model generated profiles do not exactly match the abundances of the observed, mean T.S. basalt profile, their relative shapes are similar. Since the IAT generated profile is closest in shape to the mean T.S. basalt, the T.S. basalts may be a mixture between a melt from a depleted mantle and 9.6% IAT.

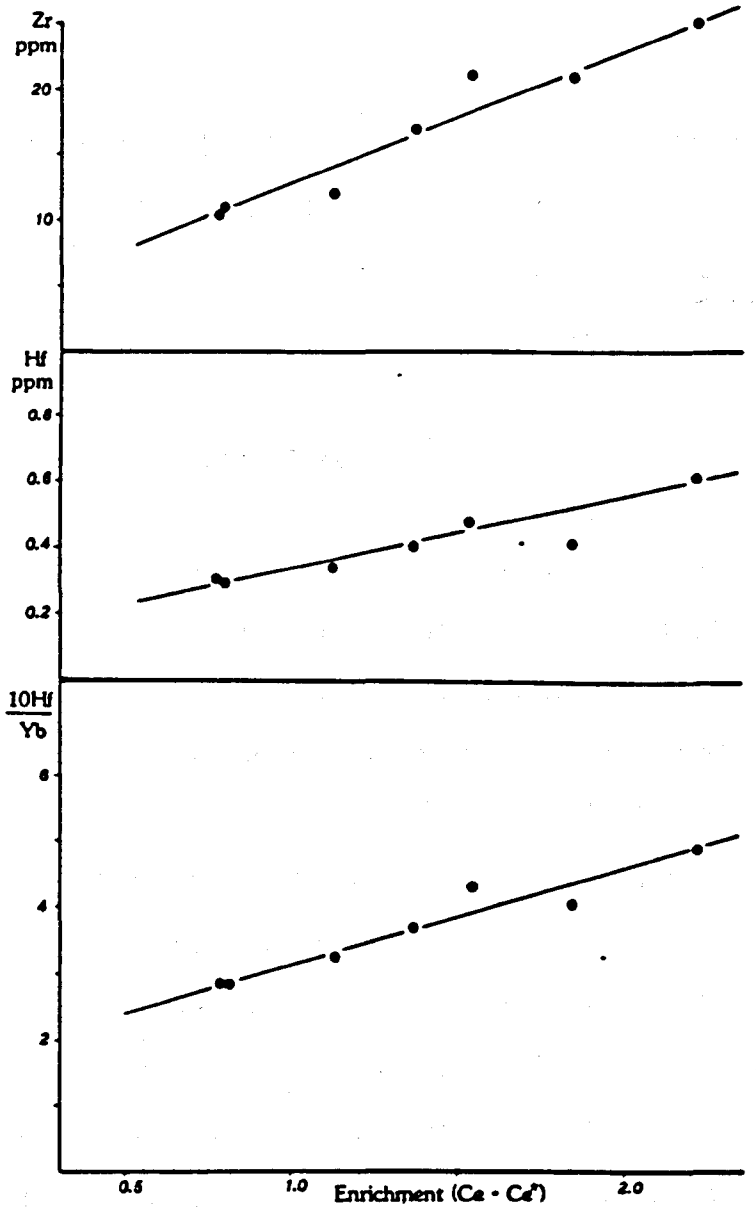

Figure 6.19 Plot ofZr, Hf and Hf/Yb against enrichment. The enrichment is relative to Ce, and is based on the difference between the actual Ce present compared with the calculated, pre-enrichment anount. The correlations indicate that the enridhment in Ce (ie. light REEs) was genetically related to the enrichment in HFSEs and suggest a silicate melt origin for the enrichment phase.

6.6 Comparison with Oceanic TFZ Magmatism

Although in the past TFFZs were considered zones of weakness (Turcotte 1974; Sykes, 1978 & Sandwell, 1985), there has been considerable controversy as to whether they are volcanically active. However, Vogt (1974) and Lourie (1986) presented convincing evidence that TFZ were vunerable to both intraplate seismic and volcanic activity. This was supported by the identification of alkalic basalts from several Mid-Atlantic Ridge transform

offsets including the Romanch Fracture Zone at 43°N, and St. Pauls Fracture Zone (Melson and Thompson, 1971; 1972; Melson *et al.*, 1972; Shabata *et al.* ,1979). However, not all the TFZs produce alkalic magmatism (Christie and Sinton, 1981; Sinton *et al.* ,1983). Instead, the Kane and Gibbs TFZs are characterised by tholeiitic magmatism that is only slightly enriched in incompatible elements relative to MgO, compared with N-type MORB (Bryan *et al.* ,1981, Compsie *et al.*, 1973). Systematic studies of the effects of TFZs on the geochemistry of adjacent spreading centres has been made by Bryan *et al.* (*op. cit.*), Bender *et al.* (1984), Bender (1984) and Langmuire & Bender (1984). These studies indicate a systematic increase in alkalinity towards a ridge-transform intersection. Although this effect is generally attributed to differences in high level fractionation, Langmuire & Bender (*op. cit.*) and Bender *et al.* (*op. cit.*) interpret this, the 'transform fault effect' as a result of increasingly lower degrees of partial melting of the mantle source as oceanic TFZs, are approached.

In contrast to the transform fault effect observed in modern oceanic basins, when compared with the Troodos A.S., the T.S. basalts show a reverse effect. Instead of being more alkalic than their spreading ridge counterparts, the T.S. basalts are less alkalic and more depleted in incompatible trace elements. Whereas basalts erupted within oceanic TFZs are generally more evolved (Bender *et al.*, 1984; Hekinian & Thompson, 1976; Schilling *et al.* 1983; Langmuir & Bender, 1984) the T.S. basalts have a very narrow and primitive compositional range and resemble primary, parental liquids. Although the transform fault effect has been interpreted as a result of decreasing degrees of partial melting, both basalts erupted within oceanic TFZs and their adjacent spreading centres are considered to have been derived from the same source (Langmuir & Bender, *op. cit.*; Bender *et al.*, *op. cit.*). However, this is in contrast with the T.S. basalts which are derived from a mantle source that has already had the adjacent Troodos A.S. extracted from it.

Structural and other evidence indicate that the T.S. magmatism occured within an oceanic transtensional and leaky TFZ, developed above an intra-oceanic subduction zone (Murton & Gass, 1986; Murton, 1986). The depleted geochemistry of the T.S. basalts indicates shallow melting of an already depleted source that has had the A.S. extracted from it. This high level mantle melting and primitive magmatism suggests rapid extension within the TFZ. Such rapid extension may be the result of the development of an extensional relay zone that laterally offsets a TFZ and dilates at the spreading rate of the adjacent ridges (Holecomb *et al.*, 1973).

6.7 List of Conclusions

(i) The WLFC hosts two genetically unrelated magmatic sequences, an early suite termed the Axis Sequence (A.S.) and a later suite termed the Transform Sequence (T.S.).

(v) The A.S. and T.S. were derived from a depleted source following 12% and 10% subsequent melting.

(xi) The T.S. (and Arakapas fault belt) lavas are similar to boninites.

(ix) The Troodos A.S., WLFC A.S. and T.S. all have ubiquitous LIL element enrichment.

(xii) The T.S. have beeen enriched by a LREE, Zr, & Hf phase that resembles an IAT

CHAPTER 7

Discussion and Conclusions

List of contents

7.1 Introduction

The complex igneous and tectonic structure of the Western Limassol forest complex (WLFC) is in contrast with the relatively simple layered oceanic crustal sequences of coherent ophiolite complexes (Penrose, 1972), that are believed to have been formed at constructive ridge axes (Gass, 1968; Moores & Vine, 1971; Cann, 1974). Similar anomalous and complex structures in other ophiolites have been interpreted as fossil transform fault zones : eg. the Coastal Complex, Newfoundland (Karson & Dewey, 1978); Antalya Complex, S. Turkey (Reuber, 1984); Bogotta Peninsula, Papua New Guinea. (Prinzhofer & Nicolas, 1980); The Fizh block of the Semail Nappe, Oman (Smewing 1980) and the Spontang Ophiolite of the Ladakh-Himalaya (Reuber, 1986) .

It has already been shown that the Arakapas fault belt, which separates the WLFC from the main Troodos complex, forms the northern wall to an E - W trending, fossil oceanic Transform Fault Zone (Simonian, 1975; Simonian & Gass 1978; Bechon & Rocci, 1984). The Limassol forest complex is probably part of the same transform domain (Simonian & Gass, *op. cit.*). In the following chapter the major features of present day transform fault zones are summarised and compared to the geology of the WLFC. Published theoretical models of transform fault zones are discussed and a comparison is made with the WLFC and other fossil examples. Three types of transform fault zones are distinguished. Finally, the geology of the WLFC is compared with its regional tectonic setting in the eastern Troodos massif and a model proposed to explain its structural and petrographical evolution in the wider tectonic framework of the eastern Mediterranean.

7.2 Present Day Oceanic Transform Fault Zones

There have been numerous studies of present day oceanic transform fault zones and fracture zones involving submersible observations (ARCYANA, 1975; Caytrough 1979; CYAMEX, 1981; Project FAMOUS, 1977 and 1978; OTTER, 1980) and more recently, high

resolution multibeam side scan sonar (eg. GLORIA, Somars *et al.*, 1978; Searle, 1986). As a result, the majority of present day oceanic transform fault zones are recognised as having some common morphological and structural features consistent with their being major, vertical strike-slip plate boundaries, juxtaposing younger and older oceanic lithosphere (Fox & Gallo, 1984; Searle, 1986).

Oceanic transform fault zones offset slow spreading ridge axis every 50 to 100 km (Fox *et al.*, 1969; Johnson & Vogt, 1973; Phillips & Fleming, 1978) and fast spreading ridge axis every 300-500 km (Mammerickx & Smith 1978; Fox & Gallo, 1984). They can be divided into two distinct tectonic regimes (Figure 7.1), an active transform domain that lies between and offsets two constructive ridge axes and which is dominated by strike-slip deformation (Wilson, 1965; Sykes, 1967), and the inactive transform fault segment, which seems to suffer only minor dip-slip faulting (DeLong *et al.*, 1979). To maintain consistency with the literature, the transform segment that contains the active transform domain is here termed the Transform Fault Zone (TFZ), and the inactive transform segment that has passed a ridge-transform intersection is termed the Fracture Zone (FZ). Strictly speaking, an active TFZ is a vertical strike-slip boundary between two oceanic lithospheric plates, whereas an inactive FZ is a fossil TFZ that has passed a terminal ridge-transform intersection and now locates the zone along which older and younger oceanic lithospheric plates are juxtaposed.

Although active TFZs usually form broad and linear bathymetric depressions several 10s of kilometres wide (Heezen *et al.*, 1964; Fox & Gallo, 1984) strike-slip deformation is generally restricted to a single, narrow fault, termed the Principal Transform Displacement Zone (PTDZ) (ARCYANA, 1975; OTTER, 1984). Lateral migration or sideways jumping from one PTDZ to another eventually produces a wide zone of pervasive deformation across the full width of the active transform domain. Occasionally TFZs may be 'tight', that is dominated by either strike-slip deformation and oblique compression or 'leaky' when extension and magmatic activity accompany strike-slip deformation.

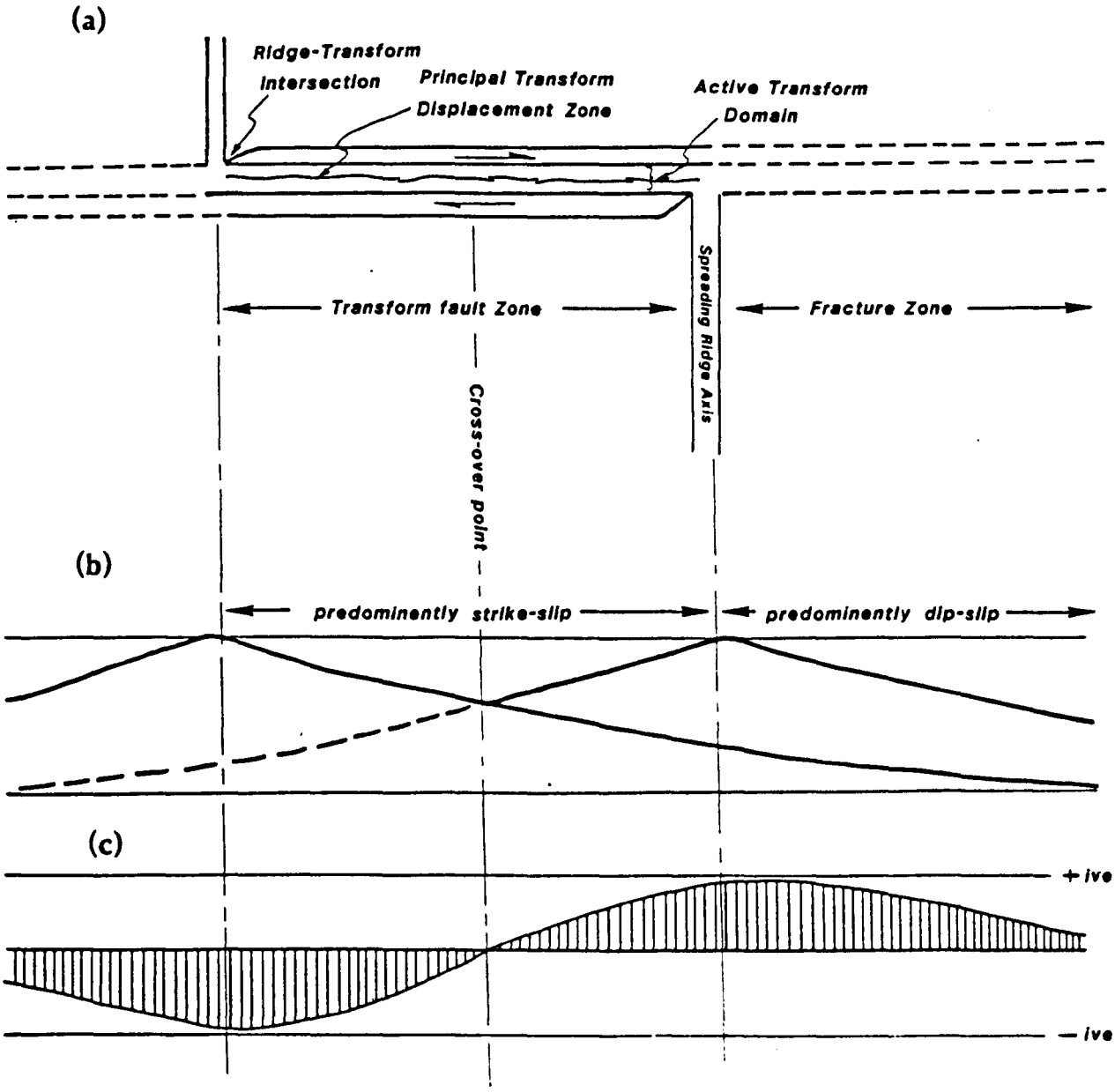

Figure 7.1 General features of present-day oceanic ridge-ridge transform fault zones (TFZs) (adapted from DeLong *et al.*, 1979). **(a)** Plan view of major transform features: between spreading axes the TFZ experiences mainly strike-slip faulting, with a minor element of dip-slip movement; this area is here termed the TFZ. Strike-slip movement within the TFZ is localised to a narrow fault strand, here termed the principal transform displacement zone (PTDZ), the lateral migration of which forms a pervasively tectonised zone here termed the active transform domain. Outside the ridge-ridge segment, the transform fault zone is relatively inactive tectonically and suffers mainly dip-slip faulting. To maintain consistency with the literature this segment is here termed the fracture zone. **(b)** Schematic cross-section showing the relative vertical height offset of the adjacent oceanic lithosphere across a TFZ. Height control is taken as a function of cooling and thickening of the lithosphere away from the spreading axes. **(c)** Due to the cooling-height phenomenon a TFZ experiences maximum strik-slip at the mid-way point; at the ridge-transform intersection movement is mainly dipsilp.

Slow and Intermediate Slipping TFZs

In general, slow and intermediate slipping (< 6 to 8 cm yr^{-1}) TFZs are characterised by a 1 to 3 km deep bathymetric valley, often with marginal and medial ridges (Figure 7.2a). Although these transform fault valleys may be up to 20 km wide (eg. the Oceanographer TFZ; OTTER, 1984; Menard & Chase, 1970) strike-slip displacement is restricted to a single fault, the principal transform displacement zone (PTDZ), that may laterally migrate to form anastomosing shear strands (Searle, 1986). Within the active transform domain, fault structures are dominated by principal shears that represent active and inactive PTDZs, and synthetic or reidal shears that are oblique to the principal shear direction and to the transform fault valley walls (Searle, 1986). The morphology and structure of present day slow and intermediate slipping ridge-transform intersections is dominated by a nodal basin deep that is developed at the end of the related constructive ridge axis and the basin is elongated in the direction of the opposite ridge-transform intersection (Figure 7.2a). The origin of these nodal basins is not clear, although their almost ubiquitous presence at slow and intermediate slipping ridge-transform intersections implies a common and characteristic plate tectonic control (Sleep & Biehler, 1970).

Fast Slipping TFZs

In contrast, fast slipping TFZs (> 8cm per year) such as the Quebrada - Gofar System and Garret TFZ at 12°S form wide TFZs within which small transform faults offset short oblique constructive margins (Lonsdale, 1978; Rea, 1981; Fox & Gallo, 1984). These fast slipping TFZs form a wide zone of ridges and troughs, parallel to the length of the zone, rather than a single transform fault valley (Figure 7.2b).

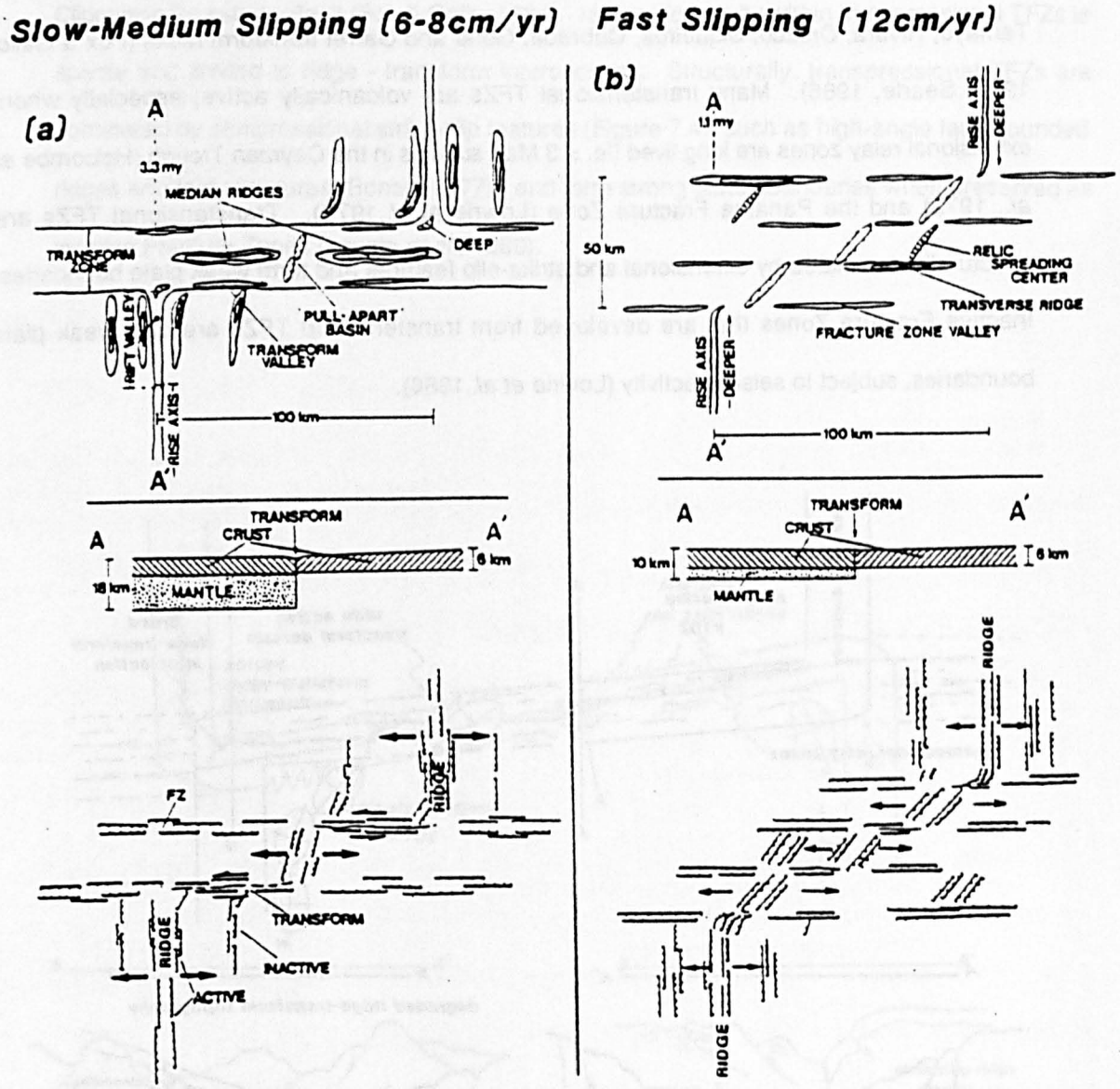

Figure 7.2 Contrast between slow and fast slipping TFZs: **(a)** Slow (and intermediate) slipping TFZs have narrow active transform domains with median and marginal ridges and pull-apart basins (ie. extensional relay zones). They are characterised by large age-height offsets and by deep basins at their ridge-transform intersections, termed in the literature and here, the nodal-deep. Spreading axes tend to swing into the TFZ forming a curved spreading fabric. **(b)** Fast-slipping TFZs are characterised by a broad active transform domain and a small age height offsets. The principal transform displacement zone is often off-set by short spreading ridges. (Diagrame after Fox & Gallo, 1984)

Transtensional TFZs

Transtensional oceanic TFZs are characterised by a broad transform trough containing a number of strike-slip strands forming an anastomosing PTDZ. The PDTZs are often offset by extensional relay zones (Figure 7.3). Present day examples include the Tamayo, Rivera, Orozco, Siqueiros, Qubrada, Gofar and Garret transform faults (Fox & Gallo, 1984; Searle, 1986). Many transtensional TFZs are volcanically active, especially where extensional relay zones are long lived (ie. > 3 Ma), such as in the Cayman Trough (Holcombe *et al.*, 1973) and the Panama Fracture Zone (Lowrie *et al.*,1979). Transtensional TFZs are structurally dominated by extensional and strike-slip features and form weak plate boundaries. Inactive Fracture Zones that are developed from transtensional TFZs are also weak plate boundaries, subject to seismic activity (Lowrie *et al.*,1986).

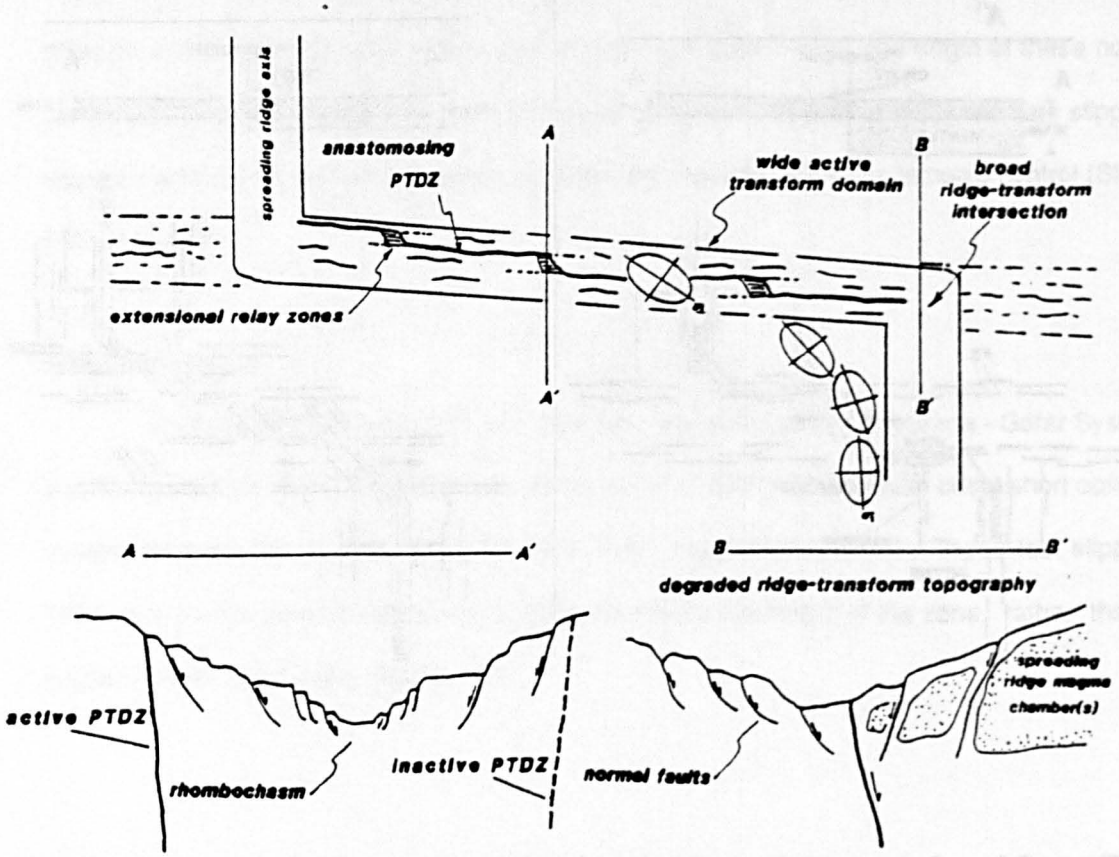

Figure 7.3 Schematic diagram of transtensional TFZs which are dominated by transtensional structures such as an anastomosing PTDZ, a wide active transform domain and pull-apart basins (rhombochasams). These TFZs are most likely to be magmatically active. The stress ellipse rotates almost 90^{0} into the TFZ.

Transpressional TFZs

In contrast, transpressional TFZs have a narrow transform trough containing a single, laterally stable PTDZ. This may be offset to form an oblique transverse ridge as in the Clipperton Transform Fault (Fox & Gallo, 1984). Magmatic activity within transpressional TFZs is sparse and limited to ridge - transform intersections. Structurally, transpressional TFZs are dominated by compressional strike-slip features (Figure 7.4), such as high-angle fault bounded ridges and fold structures (Bonatti 1977), and form strong plate boundaries when preserved as inactive Fracture Zones (Lowrie *et al.*, 1980).

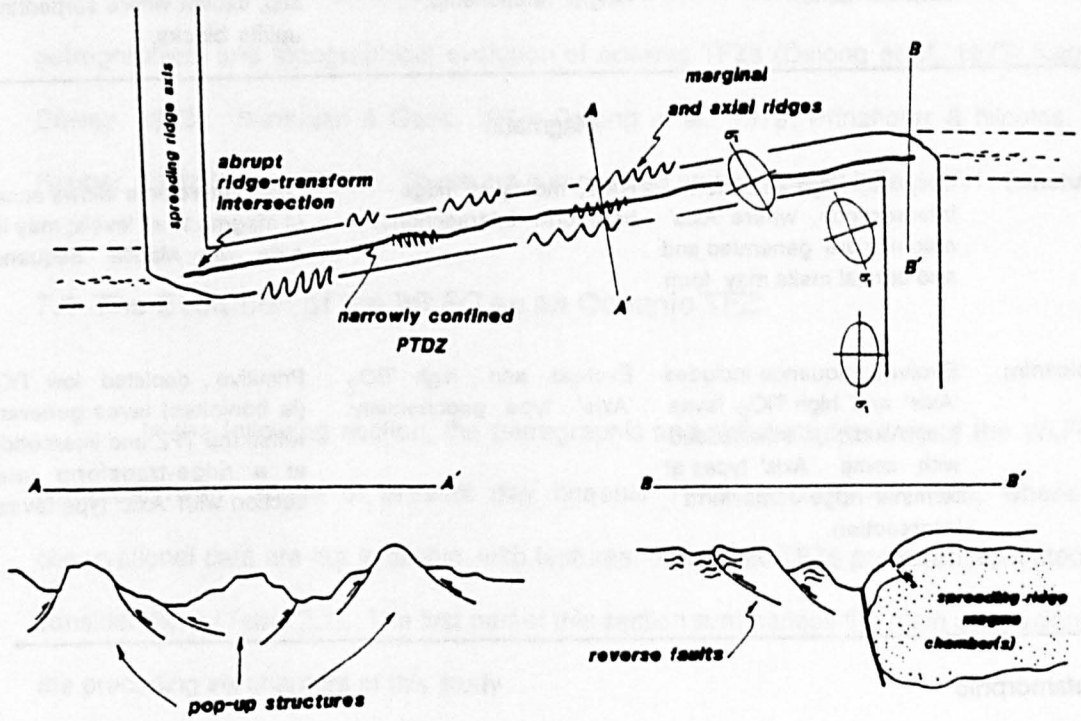

Figure 7.4 Schematic diagram of transpressional TFZs which are dominated by transpressional structures such as marginal and median ridges, high angle reverse faults and pop-up (flower structures) and fold structures. The stress ellipse rotates only slightly from the spreading ridge towards the TFZ. Blocks from the adjacent oceanic plates may rotate due to shear vorticity. Transpressional TFZs form narrow active transform domains with steep walls.

	Transpressional	Transcurrent	Transtensional
		Structural	
PTDZ:	More than one operative at any one time. Lateral stability forms narrow tectonised zone.	Only one operative at any time. Lateral migration forms broad tectonised zone.	Only one operative at any one time. Lateral jumps often form extensional relay zones and a broad tectonised zone.
Mylonites:	Broad zone, pervasively sheared, vertical fabric.	A few, anastomosing shear strands, vertical fabric.	Very scarce.
SSZs*:	Very scarce.	A few, mainly emplaced in to thermal contraction cracks.	Abundant, emplaced into extensional principal and synthetic shear zones.
Vertical Faulting:	Likely to be thrust or oblique high angle reverse faults.	Sense of off-set controlled by Sclater's (1973) age-height relationship.	Reactivation of strike-slip fault by age-height controlled dip-slip, except where serpentinite uplifts blocks.
		Magmatic	
Plutonic:	Only at ridge - transform intersections, where 'Axis' magmas are generated and and crustal melts may form.	Rare, mostly at ridge - transform intersections.	Dilational regime allows access of magma to all levels; may intrude the Mantle Sequence.
Volcanic:	Evolved sequence includes 'Axis' and high TiO_2 lavas (ie. Alkalic), interbedded with some 'Axis' types at terminal ridge - transform intersection.	Evolved and high TiO_2 'Axis' type geochemisty.	Primitive, depleted low TiO_2 (ie boninites) lavas generated within the TFZ and interbedded at a ridge-transform intersection with 'Axis' type lavas.
		Metamorphic	
TFZs	(1) For active TFZs, retrograde (ie. cooling) between initiating ridge - transform intersection and the mid-way point, then progressive (ie. increasing temperature) as the terminal ridge - transform intersection is approached.		
FZs	(2) For inactive Fracture Zone segments, dominantly prograde (ie. high temperature) formed during contact thermal effects at the terminal ridge - transform intersection.		

Table 7.1 Comparison and classification of features formed within various TFZs.

*SSZs abbreviated from serpentinite shear zones

Crustal Structure Adjacent to TFZs

It is now generally agreed that the curvature of ridge axes and ridge parallel normal faults, adjacent to the flanks of all types of TFZs, is the result of the progressive rotation of the stress ellipse under the increasing influence of shear stresses within the active transform domain (Crane, 1976; Searle & Loughton, 1977; Lonsdale, 1978; Fox and Gallo, 1984; Searle, 1986). This progressive reorientation of σ_3 from parallel to the spreading direction to subparallel to the PTDZ may also affect the trend of sheeted dykes.

7.3 Models for TFZ Evolution

A number of models have been presented in the literature to explain the structural, petrographical and topographical evolution of oceanic TFZs (Delong *et al.*, 1977; Karson & Dewey, 1978; Simonian & Gass, 1978; Delong *et al.*, 1979; Prinzhofer & Nicolas, 1978; Reuber, 1980; Karson 1986). These are summarised and compared inTable 7.1.

7.4 The Evolution of the WLFC as an Oceanic TFZ

In the following section, the petrographic and structural features of the WLFC are compared with those of present day oceanic TFZs (Section 7.2) and, where such observational data are not available, with features of oceanic TFZs predicted from theoretical considerations (Table 7.1). The first part of this section summarises the main conclusions from the preceding six chapters of this study.

7.4.1 Summary Interpretation of Evidence

Introduction or Regional Features

The evidence summarised above indicates that the WLFC was formed in a sinistrally shearing, transtensional TFZ. The presence within the WLFC of dismembered Axis Sequence crustal blocks, juxtaposed at different structural levels indicates tectonic slicing and incorporation into an active transform domain of fragments torn from the adjacent oceanic plates. The thin Axis Sequence in the WLFC, when compared with that for the Troodos Massif, is consistent with the evidence for thin oceanic crust within and adjacent to present day oceanic TFZs, (Fox *et al.*, 1980). The westard tilting and normal faulting of Axis Sequence blocks in the Louveras area suggests listric faulting in an extensional regime. Oceanic serpentinisation and uplift of an upper mantle blocks in the centre of the WLFC is similar to areas of present day regional oceanic lithospheric extension and sub-Moho access of sea-water (Bonatti, 1978).

Plutonic Activity

Transform Sequence plutons and dykes that were *syntectonically* emplaced into the disrupted Axis-Sequence and serpentinised Mantle Sequence indicate that the WLFC formed in the active domain of a transtensional and leaky oceanic TFZ. The prismatic, retort shape of some of the Transform Sequence gabbro outcrops and the predominantly NE-SW trend of the cross cutting dykes indicates emplacement during sinistral transtensional shear and is consistent with the orientation of faults, serpentinite shear zones and asymmetric matrix fabrics within ductile shear zones.

Volcanic Activity

The presence of a ~1km volcanic carapace consisting only of primitive Transform Sequence lavas interbedded with fault derived, breccia deposits indicates leaky TFZ magmatism. The NE-SW orientation of the Kapillio volcano-sedimentary basin is also consistent with a sinistral sense of transtensional, wrench faulting. Ultramafic clasts in some

breccia deposits indicates sea-floor exposure and erosion of deep structural levels including the Mantle Sequence. The presence of a volcanic stratigraphy that involves only T.S. lavas and not any derived at an oceanic constructive ridge axis suggests that the WLFC preserves the active domain of a TFZ rather than an inactive Fracture Zone that has passed a terminal ridge - transform intersection.

Geochemistry

Although both the Axis Sequence and Transform Sequence have subduction related geochemical components suggesting both were formed above a subduction zone, the Transform Sequence magmas are geochemically depleted. This is in contrast with most present day oceanic TFZs and witth the Axis Sequence lavas of the Troodos massif and implies melting of an already depleted upper mantle. This indicates an increased geothermal gradient and enhanced upper mantle melting conditions (Chapter 6) and suggests the T.S. magmatism was generated in a rapidly dilating, extensional environment. Such an environment within a TFZ is most commonly as an extensional relay zone, where extension can be at the full spreading rate of the adjacent oceanic ridges (eg. the Cayman Fracture Zone: Holcomb *et. al.*, 1973).

Structural Evolution

The orientation of E-W principal and NE-SW synthetic shears, that formed dilational strike-slip shear zones filled with serpentinite melange during Transform Sequence magmatism, define a stress ellipse that indicates deformation within a sinistral, transtensional, active transform domain. Serpentinite melanges, emplaced along fault systems parallel to the principal and synthetic shear directions, are the result of extensional strike-slip faults within an active transform domain. The relative paucity of mylonite zones compared with the abundance of dilational serpentinite shear zones also implies that the deformation was essentially transtensional.

Metamorphic History

The WLFC has a retrograde metamorphic history that, together with the intrusive stratigraphy of the Transform Sequence, indicates synmagmatic cooling and uplift of the complex while in an oceanic setting. This suggests that the complex preserves the active transform domain of a TFZ, rather than an inactive Fracture Zone segment that has passed a terminal ridge-transform intersection.

7.4.2 Summary

The WLFC has petrographic and structural characteristics similar to the active transform domain of present day intermediate to slow slipping transtensional TFZs. The formation of a 1.2 km deep, 8 to 10 km wide transform trough with abundant, anastomosing strike-slip strands (eg. serpentinite shear zones) that trend almost parallel to the inferred E-W palaeo-spreading direction for the Troodos massif indicates a probable transform origin for the WLFC. This is in agreement with the progressive change in strike of sheeted dykes in the southern Troodos massif, just north of the Arakapas fault belt reflecting a progressive rotation of the stress ellipse into the fossil TFZ, (Simonian & Gass, 1978). Patterns of oceanic fault and serpentinite shear zone trends in the WLFC are also similar to a pattern of principal and synthetic shears indicative of sinistral shear within present day oceanic TFZs. The emplacement and geochemistry of Transform Sequence magmas also suggests formation in a leaky extensional relay zone, within the active domain of a transtensional oceanic TFZ.

7.5 Comparison of the WLFC with other Postulated Ophiolitic TFZ

Other examples of ophiolitic TFZs are rare, the most complete descriptions being of the Coastal Complex, Newfoundland (Karson & Dewey, 1978) and the Antalya Complex, Turkey, (Reuber,1984). The main geological features of these complexes are summarised and compared with the WLFC (Table 7.2). The various transform features are interpreted in terms of different TFZ tectonics.

	WLFC	Newfoundland Coastal Complex	Antalya Complex Turkey
		Structural	
PTDZ:	Mostly anastomosing, vertical SSZs forming a 9 km wide transform tectonised zone. Virtually no mylonite shears. Sinistral shear pattern.	Confined to 0.5 to 1.5 km wide, sub-vertical zone of mylonite. Cuts mainly gabbro and cumulate ultramafic rocks. Has a dextral shear pattern.	Restricted to a 2km wide zone of anastomosing, mylonite shears that cut cumulate gabbro and the Mantle Sequence. Has a sinistral shear pattern.
Vertical Faulting:	Synmagmatic uplift of serpentinised Mantle Sequence as blocks forming bathymetric medial valley high. Upthrust low density serpentinite.	Synmagmatic and post-magmatic dip-slip. Interpreteted as thermal age height controlled.	Synmagmatic dip-slip, interpreteted as thermal age height controlled.
		Magmatic	
Plutonic:	Abundant syntectonic ultramafic and mafic plutons and dykes mainly cut the Mantle and Axis Sequences.	A few syntectonic dykes. Major emplacement of 0.8 km ultramafic dyke cuts the transform complex and separates it from the adjacent palaeo-oceanic plate.	A few syntectonic, coarse gabbroic dykes cut the Mantle Sequence.
Volcanic:	Primative, depleted, low TiO_2 glassy lavas interbedded with clastic sediments	Variably evolved, mainly alkalic, lavas.	None preserved.
		Metamorphic	
	Retrograde, cooling and uplift-unroofing history.	Prograde, contact thermal. Highest grades against the magmatic weld between the fossil oceanic plate and transform fault complexes.	Amphibolite facies, dynamothermal in mylonite zones, otherwise only cooling history.
		Tectonic Interpretation	
	Transtensional sinistral ridge - ridge leaky oceanic TFZ.	Transcurrent to transpressional dextral oceanic Fracture Zone that has passed a ridge - transform intersection.	Transpressional ridge - ridge sinistral TFZ.

Table 7.2 Summary, comparison and interpretation of features of the major palaeo-TFZs (after Karson & Dewey, 1978 and Reuber, 1985 repectively), including the WLFC.

7.6 Reconstruction of Ridge-Transform Geometry

7.6.1 Regional Geological Setting

Figure 7.5a illustrates the regional geology of the eastern Troodos massif and the major geological features used in a reconstruction of the ridge-transform geometry of the WLFC and Troodos massif during Late Cretaceous times. The tectonic interpretation and model is illustrated in Figure 7.5b, which in turn is based on a synthesis of the present study, on the geology of the Arakapas fault belt (Simonian,1975) and on present work to the west of the Arakapas fault belt (Gass & Xenophontos), in the eastern Limassol forest (MacLeod, *pers. comm.*) and on the eastern Troodos massif (Allerton, *in prep.*), all of which is briefly summarised below.

Arakapas Fault Belt

Simonian and Gass (1978) identified the Arakapas fault belt as a linear palaeo-bathymetric trough. Volcanic eruptions that were localised along the Arakapas fault belt are geochemically distinct from those of the Troodos massif, and are intercalated with abundant, coarse to medium grained, locally derived, clastic sediments. The thickness of the sediments generally increases towards the eastern end of the Arakapas fault belt where, in the vicinity of Lefkara (Layia and Kato Dhrys), there is a deep, sedimentary basin. Directly to the northwest of this deep basin, palaeo-medial-ridges, now represented by uplifted blocks of sheeted dyke complex, occur (Simonian, 1975). In the western end of the Arakapas fault belt, both the dominant E-W structural trend and palaeo-bathymetric trough become increasingly obscure until to the west of Perapedhi, the fault belt is no longer apparent (Simonian, 1975). Detailed mapping to the west at Perapedhi reveals a crustal sequence that is similar to that to the north of the Arakapas fault belt, consisting of a NE-SW trending sheeted dyke complex (Gass & Xenophontas, *pers. comm.*). The volcanic stratigraphy in this area consists of two groups of pillow lavas that are separated by a marked unconformity. The upper group is

geochemically intermediate between the Arakapas fault belt lavas and the Troodos Axis Sequence whereas the lower group is geochemicallly similar to the Troodos Axis Sequence (Gass & Xenophontos, *pers. comm.*). The dominant structural trend in this region consists of N-S trending normal faults that cross-cut earlier east-west trending structures (Gass *pers. comm.*).

Eastern Limassol Forest Complex

Compared with the essentially deep structural levels and relative abundance of T.S. plutons and dykes, exposed in the core of the WLFC, the eastern Limassol forest complex exposes mainly disrupted Axis Sequence blocks that are generally free of Transform Sequence plutonism (Panayiotou, 1977; MacLeod *pers. comm.*). The Axis Sequence blocks in the eastern Limassol forest complex have suffered extensional faulting across a major oceanic fault system that trends essentially NW-SE to WNW-ESE (MacLeod *pers. comm.*). Intercalated lavas and locally derived coarse clastic sediments (ie. termed infill deposits by Gass & Simonian, 1978) are only abundant in the south of the eastern Limassol forest complex, near Kalavasos (Adamides, 1980; MacLeod, *pers. comm.*).

Eastern Troodos

Recent work by Varga & Moores (1985) indicates the presence of three N-S trending, oceanic graben features that crop out in the northern part of the Troodos massif (Figure 7.5a). These grabens (termed the 'Solea graben', the 'Ayois Epiphanios' graben and the 'Larnaca graben') are interpreted by Varga & Moores (*op. cit.*) as palaeo-spreading ridges that with time became active successively eastwards. In contrast to this rather complex history of spreading axis evolution, a more obvious, N-S trending palaeo-spreading axis has been identified in the eastern part of the Troodos massif (Figure 7.5a), to the north of Lefkara (Allerton *in prep.*). On maps (Geol. Survey Dept. of Cyprus, regional sheet) this feature crops out as a N-S orientated graben, preserving upper pillow lavas in its centre and lower structural levels on its flanks.

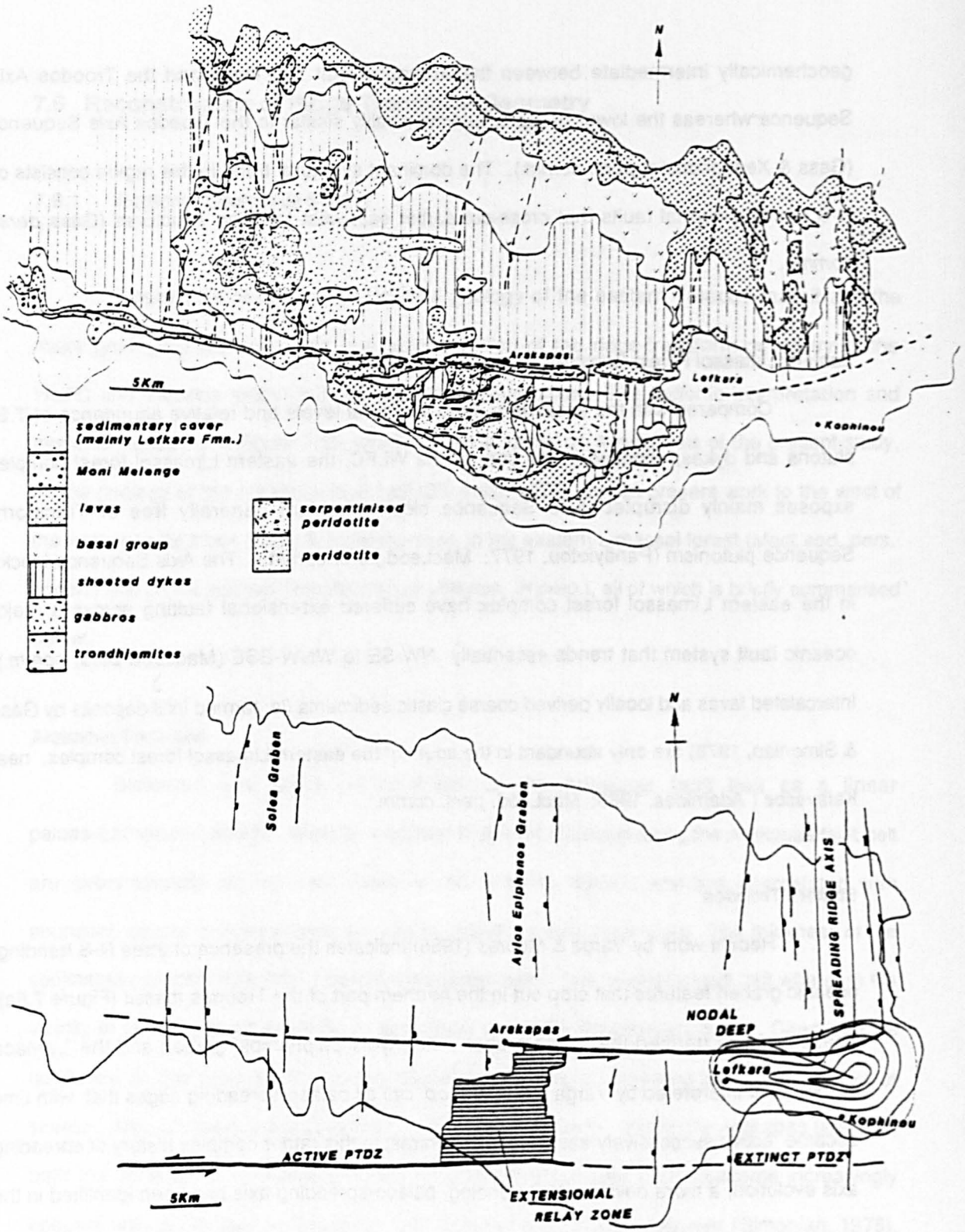

Figure 7.5 **(a)** Regional geology of the Troodos massif, including the Limassol forest complex, and **(b)** the tectonic interpretation of the southern Troodos TFZ showing the position of the Arakapas fault belt as a palaeo-PTDZ that was offset across an extensional relay zone, the WLFC. A deep sedimentary basin in the Lefkara-Kophinou area locates a possible ridge-transform intersction nodal-deep (with schematic isopachs). Possible palaeo-spreading ridges have been suggested for the north of the Troodos massif, the most probable being to the north of Kophinou (Allerton *pers. comm.*).

7.6.2 Tectonic Interpretation

In the following section it is proposed that the Limassol forest complex, Arakapas fault belt and the eastern Troodos graben preserve a fossil ridge-transform intersection and a fossil, sinistral transtensional TFZ containing an extensional relay zone (the WLFC) formed by lateral jumping to the south of the E-W trending Principal Transform Displacement Zone (ie. the PTDZ, preserved as the Arakapas fault belt).

The sinistral shear sense of the WLFC suggests that a spreading system that involved a dexturally offset ridge system. The progressively increasing thickness of infill sediments and lavas towards the eastern end of the Arakapas fault belt, where they form the edge of a deep basin to the west of Lefkara (at Layia and Kato Dhrys), may be part of a ridge-transform intersection nodal deep. The location of a palaeo-ridge to the north of Lefkara (Allerton *pers. comm.*) supports the interpretation that a fossil ridge-transform intersection may lie in the vicinity of Kophinou (Figure 7.5b). The unusually thick Lefkara chalk sequence at Lefkara (Pantazis, 1967) suggests that this nodal deep contiued as a bathymetric depression into the Lower Tertiary, after the ceasation of igneous activity.

It has been suggested in the preceeding six chapters that the WLFC is a segment of a fossil, leaky oceanic TFZ that suffered rapid dilation accompanied by syntectonic magmatism and disruption of an Axis Sequence crust. The difference in structural levels and T.S. magmatic activity between the WLFC and the eastern Limassol forest complex and the disappearence of the Arakapas fault belt to the west of Perapedhi, suggests that the WLFC is a fossil extensional relay zone that off set the PTDZ (ie. the Arakapas fault belt) to the south (Figure 7.5b). As a result of sinistral transform movement (Chapter 5) the eastern and western margins of the WLFC may have diverged, possably at the full spreading rate of the fossil spreading axes. This rapid extension across the WLFC may have initially formed a tear apart basin in which the Axis Sequence crust was disrupted. Serpentinisation and uplift of the Mantle Sequence in the centre of the WLFC (Chapter 5) suggests access of seawater to below

the Moho, probably through dilational fractures. The presence of low TiO_2 boninitic magmas, that are characteristic of the Transform Sequence (Chapter 6) also suggests rapid dilation across the WLFC (i.e. as an extensional relay zone) and subsequent shallow partial melting of the already depleted upper mantle by adiabatic decompression in the upper mantle.

The eastern flank of the WLFC extensional relay zone possibly crops out in the vicinity of the Kapryssa gorge, which has not been geologically mapped in detail. In the west of the WLFC a structurally complex zone, that trends NNW - SSE and crops out between Yerasa and Kalakhorio, is comprised of chaotically dismembered Axis Sequence crustal blocks. This structural zone separates the Mantle Sequence to the east from the essentially volcanoclastic sequence to the west, and may locate the western margin of the extensional relay zone. If the divergent margins of the extensional relay zone are located in these positions, then the WLFC has experienced ~15km of extension. The disappearance of the Arakapas fault belt to the west of Perapedhi suggests that the PTDZ was off set to the south by the WLFC extensional relay zone. The extensional faulting that overprints the the E - W t ectonic fabric, to the west of Perapedhi, also implies that a tensional stress existed across the WLFC.

At an intermediate slipping rate of 6cm yr^{-1} (ie. an intermediate spreading rate for the Troodos ridge; Moores *et al.*, 1984), the WLFC was an active extensional relay zone for ~0.25Ma. The complex was magmatically and structurally active during this relatively short period of time. This rapid extension and short-lived magmatic activity for the WLFC explains why only depleted upper mantle was melted producing the boninite geochemistry, characteristic of the T.S. lavas. Basalts from longer-lived extensional relay zones (1 to 3 Ma) have geochemistry that resembles MORB (Holecomb *et al.* 1973), suggesting upwelling and partial melting of more fertile mantle.

7.6.3 Geometry of Accetion and Relationship to Micro-plate Rotation

The transtensional, leaky evolution of the southern Troodos TFZ, and the opening of an extensional relay zone may indicate a change in relative plate motion during oceanic accretion and active transform movement in the Late Cretaceous. This is supported by palaeomagnetic studies (Mooores & Vine, 1971; Shelton & Gass, 1980) that indicate that the Troodos massif has rotated anticlockwise by Ca 90°, possibly iniating rotation in the Late Cretaceous, possibly during or soon after its formation (Clube *et. al.*, 1985). Although the margins of the Troodos micro-plate have not yet been identified, the onset of rotational tectonics in the Late Cretaceous was probably an effect of the plate tectonic geometry during the production of the Troodos oceanic lithosphere.

It has already been mentioned (Chapter 1) that the Troodos ophiolite is generally believed to have formed above an intra-oceanic subduction zone. The 'Tauric Arc' (Brunn, 1980) is a northerly inclined zone of major intermediate to deep earthquakes, 50km to the south of Cyprus, (Harrison, 1955; Gass & Mason-Smith, 1963), that was possibly an active subduction zone in the Late Cretaceous during the formation of the Troodos massif as oceanic lithosphere. As a result of the close proximitty of the subduction zone to the spreading axis that formed Troodos, Clube *et al.* (1985) suggest that the Cyprus microplate was rotated by frictional drag from the subducting plate; the tectonic setting is illustrated in Figure 7.6.

The sinistral shear sense of the WLFC (ie. the southern Troodos TFZ) is similar to the Antalya complex (Reuber, 1984). This implies a geometry of accretion that involved N - S spreading along E - W ridge axes, that were dextrally off set by short, N - S trending, sinistral TFZs. This is also in agreement with the geometry of accretion, proposed by Moores *et al.* (1984). Although the WLFC was a transtensional TFZ, the Antalya complex has predominantly transpressional features (Table 7.2). Since both fossil TFZs are of Late Cretaceous age and separated by only Ca. 80km, it seems probable that they were both part of the same spreading system.

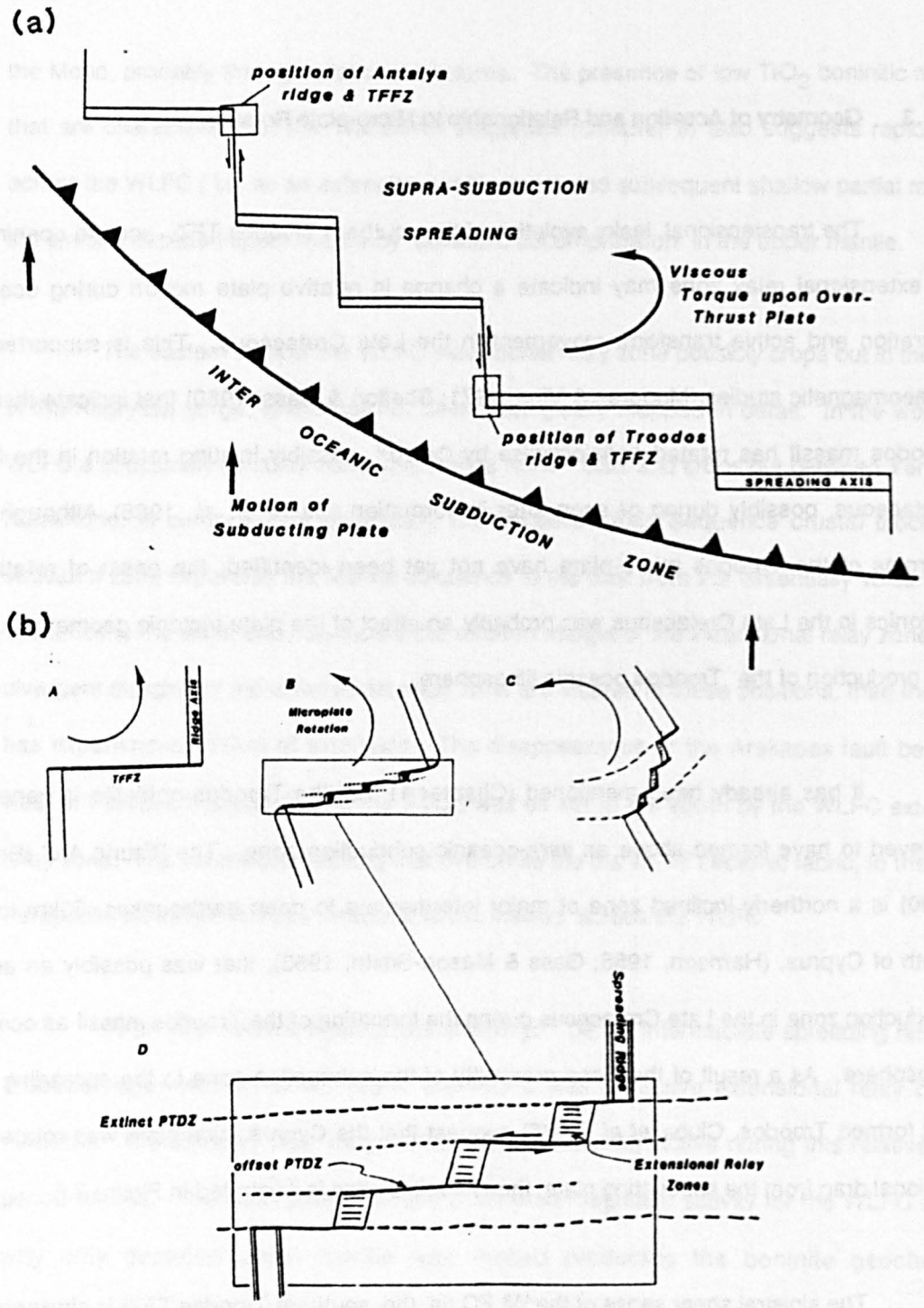

Figure 7.6 Tectonic interpretation for the formation of the WLFC and Troodos massif. **(a)** Supra-subduction spreading above a northerly inclined, oblique subduction zone in which the spreading axes are dextrally off-set by sinistral slipping TFZs. The oblique subduction imposes a viscous torque on the overlying oceanic lithosphere, resulting in the initiation of micro-plate rotation. The position of the pole for the rotation is broadly indicated, and results in oceanic transtension for the Troodos TFZ and oceanic transpression for the Antalya Complex TFZ. **(b)** Scematic evolution of the Troodos TFZ: **A** Initiation of viscous torque and micro-plate rotation of a ridge-ridge transcurrent TFZ (ie the Arakapas fault belt). **B** Micro-plate rotation results in a transtensional TFZ, with the development of an extensional relay zone (ie. the WLFC). **C** Micro-plate rotation accelerates and coincides with the ceasation of magmatism and spreading as the spreading axis moves away from its thermal source. **D** Detail of '**B** ' showing the development of extensional relay zones and off-set PTDZs.

Since only Troodos has suffered microplate rotation, there must be a tectonic discontinuity between the Antalya and Troodos ophiolite complexes. The difference in tectonic style, however, between the two fossil TFZs suggests that the pole of rotation was located to the north of the Troodos spreading system (Figure 7.6), causing a componant of E - W compression in the vicinity of the Antalya complex and E - W extension in the vicinity of the present day position of the Troodos complex .

7.6.4 Comparison with Present Day Spreading Systems

Extensional relay zones related to both changes in plate motion and microplate rotation, similar to that for the Troodos complex, occur in the vicinity of present day subduction zones. A lateral jump of a PTDZ and the subsequent formation of an extensional relay zone, occurs in the Cayman Trough (Holcombe *et al.*, 1973) and in the Panama Fracture Zone (Lowrie *et al.*, 1979). In the Caymen Trough, an E-W trending PTDZ is offset by a NNE-SSW trending, extensional relay zone across which there has been oceanic spreading for at least 12 Ma. The lateral jump of the PTDZ, opening of the extensional relay zone and bend in the Caymen Trough TFZ suggests a change in plate motion (Holcombe *et al.*, 1973). The lateral jump of the PTDZ in the Panama Fracture Zone and the subsequent formation of extensional relay zones, that were magmatically active for about 2 Ma, is also interpreted as a result of rapid changes in microplate motion in the vicinity of a subduction zone (Lowrie *et al.*,1979). Present day microplate rotation of about 90^{o} has occured in the eastern Pacific, where the Farallon microplate and spreading axis is undergoing pivotting subduction beneath the western North American continental margin. As a result, the Farallon microplate has transform plate boundaries that are both transtensional and transpressional and has a spreading axis that has been continuously reorientated, producing a 'fan-shaped' spreading fabric (Menard, 1977). Although the Farallon microplate is rotating, its present position as a subducting plate differs from the position of the Troodos microplate, which formed above an intra-oceanic subduction zone, immediately prior to or during the onset of microplate rotation. As such, although the Farallon plate approximates to the Troodos situation, it is not completely analagous.

7.7 List of Conclusions

(i) The WLFC has a structural, magmatic and metamorphic history that indicates formation in the active domain an E-W trending, leaky, sinistral, transtensional oceanic transform fault zone that was at least 10 km wide.

(ii) Oblique extension across the WLFC disrupted the thin Penrose type oceanic crust and allowed serpentinisation of the underlying upper mantle.

(iii) A block of serpentinised upper mantle was uplifted and, while cooling, was intruded by ultramafic and mafic plutons and dykes and in part, overlain by basalts of boninitic composition.

(iv) Oblique extension across the WLFC suggests a regional tectonic model in which the Arakapas fault belt formed the principal transform displacement zone to a sinistral oceanic TFZ, that was offset to the south by an extensional relay zone, now preserved as the WLFC.

(v) Dilation of the extensional relay zone resulted in lateral tension and subsequent pressure release and melting of the upper mantle. The resulting T.S. lavas have a boninitic geochemistry.

(vi) At intermediate slipping rates, the WLFC formed an extensional relay zone that was tectonically and magmatically active for ~0.25 Ma.

(vii) As a result of rapid changes in microplate motion, the southern Troodos TFZ became transtensional and its PTDZ was displaced to the south across the WLFC extensional relay zone.

(viii) Comparison between the tectonic styles of the WLFC and Antalya complex fossil TFZs, and the asumption that they belong to the same spreading system, suggests that the Troodos microplate pole of rotation was located immediately to the north of the present day position of Cyprus.

List of References

Allen, C.G. (1966). Summary of Microfaunas, Cyprus. Annual Report, Geol. Surv. Dept., Nicosia.

Allen, C.G. (1975). The petrology of a portion of the Troodos plutonic complex, Cyprus. Ph.D. thesis, Cambridge Univ., 315 pp.

ARCYANA, (1975). Transform fault and rift valley from bathysaphe and diving sources. Science,190, 108-116.

Bailey, E.H., Irwin, W.P. and Jones, D.L. (1964). Franciscan and related rocks and their significance in the geology of western California. Calif. Div. Mines, Geol. Bull., 183, 177pp.

Ballard, R.D. and Van Andel, T.H. (1977). Morphology and tectonics of the inner rift valey at lat 36°50'N on the Mid-Atlantic Ridge. Bull. geol. Soc. Am., 88, 507-530.

Baroz, F., Desmart, A. and Laplerre, H. (1975). Trois familes volcaniques pre-orogeniques à Chypre: comparison et discussion geotectonique. 3e Reun ann. Sci. Terre, Montpelier, 126.

Bartholomew, I.D. (1982). The primary structures and fabrics of the upper mantle and lower oceanic crust from ophiolite complexes. Ph.D. thesis, Open Univ., unpubl.

Beach, A. (1975). The geometry of en-echelon vein arrays. Tectonophysics, 28, 245-263.

Beach, A. (1980). Numerical models of hydraulic fracturing and the interpretaiton of syntectonic veins. J. Struc. Geol., 2, 425-438.

Bear, L.M. (1960). The Geology and Mineral Resources of the Agros-Apsiou Area - Cyprus. Geol. Surv. Dept., Cyprus, Mem. 7, pt. 1.

Bechon, F. and Rocci, G. (1982). Fault chronolgie in the Arakapas Belt and its effect on volcanic events. C.R. Acad. Sci. Paris, 294.

Bender, J.F., Langmuir, C.H. and Hanson, G.N. (1984). Petrogenesis of basalts glasses from the Gamago Region, East Pacific Rise. J. Petrol., 25, 213-254.

Berthé , D., Choukroune, P. and Jegouzo, P. (1979). Orthogneiss, mylonites and non-coaxial deformation of granites. The example of the South American Shear Zone. J. Struct. Geol., 1, 31-42.

Biju-Duval, B., Laplerre, H. and Letouzey, J. (1976). Is the Troodos Massif (Cyprus) allochthonous? Bull. Soc. geol. Fr., 18, 1347-1356.

Biju-Duval, B., Laplerre, H. and Letouzey, J. (1977). Reponse aux commentaires de Mm. J.H. Brunn et al. a propos de la note 'Is the Troodos Massif (Cyprus) allochthonous'. Cr. Somm. Soc. geol. Fr., 6, 346-348.

Bonatti, E. (1976). Mantle uplifted block in the western Indian Ocean. Science, 201, 249-251.

Bonatti, E. (1976). Serpentinite protrusions in the oceanic crust. Earth Planet. Sci. Letts., 32, 107-113.

Bonatti, E. and Honnorez, J. (1976). Sections of the Earth's Crust in the Equatorial Atlantic. J. Geophys. Res., 81, 4104-4116.

Bonatti, E. (1977). Vertical tectonism in oceanic fracture zones. Earth Planet Sci. Letts., 37, 369-379.

Bouchez, J.L., Lister, G.S. and Nicolas, A. (1980). Fabric asymmetry and shear sense in movement zones. Geologish Bundschau, 79, 401-410.

Boudier, F. and Coleman, R.G. (1981). Cross section through the peridotites in the Semail ophiolite, southeastern Oman Mountains. J. Geophys. Res., 86, 2573-2592.

Brocher, T.M., Karsan, J.A. and Collins, J.A. (1985). Seismic stratigraphy of the oceanic Moho based on ophiolite models. Geology, 13, 62-65.

Brown, M.A. (1980). Textural and geochemical evidence for the origin of some chromite deposits in the Oman ophiolite. In: 'Ophiolites' , Ed. *Panayiotou, A.*, Proc. Int. Ophio. Symp., Cyprus, 1979, 714-721.

Browning, P. (1982). The petrology, geochemistry and structure of the Plutonic rocks of the Oman ophiolite. PhD Thesis. Open University (unpub)

Browning, P. and Smewing, J.D. (1984). Processes in magma chambers beneath spreading axes: evidence from magmatic associations in the Oman ophiolite. J. geol. Soc. London, 138, 279-280.

Brunn, J.H., Argyriadis, I, Marcoux, J. and Ricou, L.E. (1977). Commaintaires sur la note 'Is the Troodos Massif allochthonous?' presentee par B. Biju-Duval, H. Lapierre et J. Letouzey. Discussion d'une origine nord ou sud-taurique. C.R. Sonn. Soc. geol. Fr., 6, 344-345.

Brunn, J.H. (1980). Ophiolites, origin of orogens and oceanisation. In: 'Ophiolites', Ed. *Panayiotou, A.*, Proc. Int. Ophio. Symp., Cyprus, 1979,169 - 171 .

Bryan, W.B. and Thompson, G. (1976). Basalts from DSDP Leg 37 and the FAMOUS area: compositional and petrogenetic comparisons. Can. J. Earth Sci., 14, 875-885.

Bryan, W.B. and Thompson, G., Luddon J.N. (1981a). Compositional variations in normal MORB from 22°N - 25°N mid-Atlantic ridge and Kane fracture zones. J. Geophys. Res. 86,11 815-836

Bryan, W.B. and Thompson, G., Luddon J.N. (1981b). Mid-Atlantic ridge and Kane fracture zone. J. Geophys. Res. 86,11 815-836

Bryan, W.B. (1983). Systematics of modal phenocrysts assemblages in submarine basalts: petrologic implications. Contrib. Mineral. Petrol., 83, 62-74.

Cameron, W.E., Nisbet, E.G. and Dietrich, U.J. (1979). Boninites, komatiites and ophiolitic basalts. Nature, 280, 550-553.

Cameron, W.E., Nisbet, E.G. and Dietrich, U.J. (1980). Petrographic dissimilarities between ophiolitic and ocean-floor basalts. In: 'Ophiolites', Ed. *Panayiotou, A.*, Proc. Int. Ophio. Symp., Cyprus, 1979, 182 - 192.

Cameron, W.E., McCulloch, M.T. and Walker, D.A. (1983). Boninite petrogenesis chemical and Nd-Sr isotopic constraints. Earth Planet. Sci. Letts., 65, 75-89.

Cameron, W.E. (1985). Petrology and origin of primative lavas from the Troodos ophiolite, Cyprus. Contrib. Mineral. Petrol., 89, 1-17.

Campsie J., Bailey J.C., Rasmussen M. & Ditterman F. (1973). Chemistry of tholeiites from the Reykjanes and Charlie Gibbs fracture zone. Nature Phys. Sci. 244 71-73

Cann, J.R. (1969). Spilites from the Carlsberg Ridge, Indian Ocean. J. Petrol., 10, 1-19.

Cann, J.R. (1974). A model for oceanic crustal structure developed. Geophys. J. R. astron. Soc., 39, 169-187.

Cann, J.R. (1979). Metamorphism in the ocean crust. In: Deep drilling results in the Atlantic Ocean: Ocean Crust. Eds. *Talwani, M., Harrison, C.G. and Hayes, D.E.*, A.G.U. Washington, D.C., 230-238.

Carter J.L. (1970). Mineralogy and chemistry of the Earth's upper Mantle based on the partial fusion - partial crystallisation model. Geol. Soc. Am. Bull., 81 2021-2034

Casey, J.F. and Karson, J.A. (1981). Magma chamber profiles from the Bay of Islands ophiolite complex. Nature, 292, 295-301.

Caytrough, (1979). Geological and geophysical investigations of the Mid-Cayman rise spreading centre: initial results and observations. In: Deep drilling results in the Atlantic Ocean: Ocean Crust, Eds. *Talwani, M., Harrison, C.G. and Hayes, D.E.*, A.G.U. Washington, D.C., 66-93.

Choukroune, P., Francheteau, J. and le Pichon, X. (1978). In situ structural observations along Transform Fault A in the Famous area, Mid Atlantic Ridge. Bull. geol. Soc. Am., 89, 1013-1029.

Christiansen, F.G. (1985). Deformation fabric and microstructures in ophiolitic chromites and host ultramafics, sultanate of Oman. Geol. Rund., 74/1, 61-76.

Christiansen, N.I. (1977). Ophiolites, seismic velocities and oceanic crustal structure. Tectonophysics, 47, 131-157.

Christie, D.M. & Sinton J.M. (1981) Evolution of abyssal lavas along propogating segments of the Galapagos spreading centre. Earth Planet Sci. Lett. 56 321-335

Clubb, T.M.M., Creer, K.M. and Robertson, A.H.F. (1985). Paleorotation of the Troodos microplate, Cyprus. Nature, 317, 522-525.

Collette, B.J. (1974). Thermal contraction joints in a spreading sea-floor as the origin at fracture zones. Nature, 251, 299-300.

Collette, B.J. (1986). Fracture zones in the North Atlantic: morphology and a model. J. geol. Soc. London, 143, 763-774.

Cowen, D.S. and Mansfield, C.F. (1970). Serpentinite flows on the Joaquin Ridge, Southern Coast Ranges, California. Bull. geol. Soc. Am., 81, 2615-2628.

Crane, K. (1976). The intersection of the Siqueiros transform fault and the east Pacific Rise. Geol. Mag., 21, 25-46.

Crane, K. and Ballard, R.D. (1981). Volcanics and structure of the FAMOUS Narrowgate rift: Evidence for cyclic evolution: AMAR 1. J. Geophys. Res., 86, 5112-5124.

CYAMEX Scientific Team and Pastoret, L. (1981). Submersible structural study of Tamayo Transform Fault, East Pacific Rise, 23°N (Project RITA). J. Geophys. Res., 4, 381-402.

Dalwitz, W.B., Green, D.H. & Thompson J.E. (1966). Clinoenstatite in a volcanic rock from Cape Vogel, Papua Vogel, Papua : a discussion. Proc. 23rd Int. Geol. Cong. Prague. 2, 229-242

Dalwitz, W.B. (1968). Chemical composition of clino enstatie-bearing volcanic rocks from Cape Vogel area, Papua: a discussion. In: Proc. 23rd Int. Congr. 2, 229-245.

DeLong, S.E., Dewey, J.F. and Fox, P.J. (1977). Displacement history of oceanic fracture zones. Geology, 5, 199-202.

DeLong, S.E., Dewey, J.F. and Fox, P.J. (1979). Topography and geologic evolution of fracture zones. J. geol. Soc. London, 136, 303-310.

Dewey, J.F., Pitman, W.C., Ryan, W.B.F. and Bonnin, J. (1973). Plate tectonics and the evolution of the Alpine System. Bull. geol. Soc. Am., 84, 3137-3180.

Dewey, J.F. (1975). Finite plate implications: some implications for the evolution of rock masses at plate margins. Am. J. Sci., 275-A, 260-284.

Dewey, J.F. and Kidd, W.S.F. (1977). Geometry of plate accretion. Bull. geol. Soc. Am., 88, 960-968.

de Wit, M.J. and Stern, R. (1976). A model for ocean-floor metamorphism, seismic layering and magnetism. Nature, 264, 615-619.

Dickey, J.S. Jr (1970). Partial fusion products in Alpine type peridotites, Serrania de la Rhonda and other examples. Min. Soc. Am. Spec. Paper 3 33-49

Dietrich, V., Emmermann, R. & Puchelt H. (1978). Geochemistry of basaltic and gabbroic rocks from the west Mariana Basin and the Mariana Trench. Earth Planet Sci. Lett. 39 127-144

Dietz, R.S. (1961). Continent and ocean basin evolution by spreading of the sea-floor. Nature, 190, 854-857.

Dixon, J.C. and Robertson, A.H.F. (1985). Introduction: Aspects of the geological evolution of the Eastern Mediterranean. In: The geological evolution of the Eastern Mediterranean, Eds. *Dixon, J.E. and Robertson, A.H.F.*, No. A, 1-73.

Dott, R.H. (1963). Dynamics of sub-aqueous gravity depositional processes. Bull. Am. Assoc. Petrol. Geol., 47, 104-120.

Dumont, J.F., Gutnic, M.,, Marcoux, J., Monod, O and Poisson, A. (1972). Les Trias Taurides occidentales (Turquie). Definition du bassin pamphylien: Un noveau domain à ophiolithes a la mange externe de la chaine tauriqu. A. at. Geol Ges., 123, 385-409.

Duncan, R.A. & Green, D.H. (1980). Role of Multistage melting in the formation of oceanic crust. Geology 8 22-26

Elsbacher, G.H. (1970). Deformation mechanisms of mylonite rocks and fractured granulites in Cobequid Mountains, Nova Scotia, Canada. Bull. geol. Soc. Am., 81, 2009-2020.

Fisher, R.A. (1953). Dispersion on a sphere. Proc. R. Soc. London, A217, 295-305.

Fisher, R.V. (1971). Features of coarse-grained, high concentration fluids and their deposits. J. Sediment. Petrol., 41, 916-927.

Fisk, M.R., Bence, A.E. & Schilling, J-G. (1982). Major element chemistry of Galapagos rift zone magmas and their phenocrysts. Earth Planet Sci. Lett. 61 171-189

Fox, P.J., Schreiber, E. Rawlett, H. and McCony, K. (1976). The geology of the Oceanographer Fracture Zone: A model for fracture zones. J. Geophys. Res., 81; 4117-4128.

Fox, P.J., Detrick, R.S. and Pundy, G.M. (1980). Evidence for crustal thinning near fracture zones: implications for ophiolites. In: 'Ophiolites', Ed. *Panayiotou, A.*, Proc. Int. Symp. Ophio., Cyprus, 1979, 161 - 168.

Fox, P.J. and Gallo, D.G. (1982). A mantle weld at ridge-transform intersections: implications for the development of oblique structures. Eos. Trans. Am. geophys. Union, 63, 486-498.

Fox, J.P. and Gallo, D.G. (1984). A tectonic model for ridge-transform-ridge plate boundaries: implications for the structure of oceanic lithosphere. Tectonophysics, 109, 205-242.

Fox, P.J., Moody, R.H., Karson, J.A., Bonatti, E., Crane, K., Kidd, W.S.F., Gallo, D.G., Stroup, J.B., Farnari, D.J., Elthan, D., Hamlyn, P., Casey, J.F., Needham, D. and Sartori, R. (1985). The geology of the Oceanographer Transform: The transform domain. In Press.

Francheteau, J., Choukroune, P., Hekinian, R., le Pichon, X. and Needham, D. (1976). Oceanic fracture zones do not provide deep sections into the crust. Can. J. Earth Sci., 13, 1223-1235.

Frey, F.A., Green, D.H. and Roy, S.D. (1979). Integrated models of basalt petrogenesis. J. Petrol., 19, 463-513.

Fuji, T. and Kushiro, I. (1977). Melting relations and viscosity of an abyssal tholeiite. Carnegie Inst. Washington Yearbook, 76, 461-465.

Gamond, J.F. (1983). Displacement features associated with fault zones: a comparison between observed examples and experimental models. J. Struct. Geol., 5, 33-45.

Garnett, J.A. (1973). A mechanism for the development of en-echelon gashes in kink zones. Tectonophysics, 23, 129-138.

Gass, I.G. (1960). The geology and mineral resources of the Dali area. Cyprus Geol. Surv. Dept. Mem., 4, 116.

Gass, I.G. and Masson-Smith, D. (1963). The geology and gravity anomalies of the Troodos Massif, Cyprus. Philos. Trans. R. Soc.London, A255, 414-467.

Gass, I.G. (1968). Is the Troodos Massif of Cyprus a fragment of Mesozoic ocean floor? Nature, 20, 39-42.

Gass, I.G. and Smewing, J.D. (1973). Intrusion, extrusion and metamorphism at constructive ridge margins: evidence from the Troodos Massif, Cyprus. Nature, 242, 26-29.

Gass, I.G. (1980). The Troodos Massif: its role in the unravelling of the ophiolite problem and its significance in the understanding of constructive plate margin processes. In: 'Ophiolites', Ed. *Panayiotou, A.*, Proc. Int. Ophio Symp., Cyprus, 1979, 23 - 35.

Gass, I.G. and Smewing, J.D. (1981). Ophiolites: obducted oceanic lithosphere. In: The Oceanic Lithosphere. Ed. *Emiliani, C.* The Sea, Vol. 7, Wiley Interscience. pp356

Gass, I.G. (1982). Ophiolites. Scientific American, 247, 121-131.

George, R.P.J. (1975). The internal structure of the Troodos ultramafic complex, Cyprus. Ph.D. Thesis, State Univ., New York, 196 pp.

Ghosh, S.K. and Ramberg, H. (1976). Reorientation of inclusions by combination of pure shear and simple shear. Tectonophysics, 34, 1-70.

Girardeau, J. and Nicolas, A. (1981). The structures of two ophiolite massifs, Bay-of-Islands, Newfoundland: a model for the oceanic crust and upper mantle. Tectonophysics, 77, 1-34.

Goode, A.D.T. (1976). Small scale primary cumulus igneous layering in the Kalka Layered Intrusion, Giles Complex, Australia. J. Petrol., 17, 379-397.

Goud, M.R. and Karson, J.A. (1985). Tectonics at short-offset, slow-slipping transform zones in the Famous Area, Mid-Atlantic Ridge. Preprint.

Green, D.H., Hibberson, W.O. and Jaques, A.L. (1979). Petrogenesis of mid ocean ridge basalts. In: The Earth: its origin, structure and evolution, Ed. *McElhinney, M.W.* Academic Press, London, 265-290.

Greenbaum, D. (1972). Magmatic processes at oceanic ridges: evidence from the Troodos Massif, Cyprus. Nature, 238, 18-21.

Hajash, A. Jr. (1984). Rare Earth Element abundances and distribution patterns in hydrothermally altered basalts: experimental results. Contrib. Mineral. Petrol., 85, 409-412.

Hampton, M.A. (1972). The role of subaqueous debris flows in generating turbittity currents. J. sediment.Petrol. 42, 775-793.

Hancock, P.L. (1972). The analysis of en-echelon veins. Geol. Mag., 109, 269-276.

Harrison, J.C. (1955). An interpretation of the gravity anomalies in the eastern Mediterranean. Philos. Trans. R.Soc. London, A248, 283-296.

Hart R. (1979) Chemical exchange between sea water and deep ocean basalts. Earth Planet Sci. Lett. 9 269-279

Hawkins, J.W. Jr. (1976). Petrology of back-arc basins and island arcs: their possible role in the origin of ophiolites.

Hawkins, J.W. Jr., Bloomer S., Evans, C. & Melchoir, J (1979). Maraina arc-trench system: petrology of inner trench wall. EOS Trans. Am. Geophys. Un. 60 968p

Hekinian R., & Thompson G. (1976). Comparative geochemistry of volcanics from rift valleys, transforms and aseismic ridges. Contrib. Mineral. Petrol. 57 145-162

Hérbert, R., Dibeau, D. and Hekinian, R. (1983). Ultramafic and mafic rocks from the Garret Transform Fault near 13°30'S on the East Pacific Rise: Igneous petrology. Earth Planet. Sci. Letts., 65, 107-125.

Heezen, B.C., Bunce, E.T. and Tharp, M. (1964). Chain and Romanch fracture zones. Deep-Sea Res., 11, 11-18.

Helwig, J. (1970). Slump folds and early structures, northeastern Newfoundland, Appalachians. J. Geol., 78, 172-187.

Heirtzler, J.R. and Van Andel, T.H. (1977). Project FAMOUS: Its origin, programs and setting. Bull. geol. Soc. Am., 88, 481-487.

Henson, F.R.S., Browne, R.V. and McGinty, (1949). A synopsis of the stratigraphy and geological history of Cyprus. Q. J. geol. Soc. London, 105, 1- 41.

Hess, H.H. (1960). The stillwater igneous complex. Mem. geol. Soc. Am., 80, 130-146.

Hess, H.H. (1962). History of ocean basins. In: Petrologic Studies, Geol Soc. Am., 599-620.

Hickey, R.L. and Frey, F.A. (1982). Geochemical characteristics of boninite series volcanics: implications for their source. Geochim. Cosmochim. Acta, 46, 2099-2115.

Holcombe, T.L., Vogt, P.R., Mattews, J.E. and Murchison, R.R. (1973). Evidence for sea-floor spreading in the Caymen Trough. Earth Planet. Sci. Lett., 20, 357-371.

Hole, M.J., Saunders, A.D., Marriner, G.F. and Tarney, J. (1984). Subduction of pelagic sediments: implications for the origin of Ce-anomalous basalts from the Marianas Islands. J. geol. Soc. London, 141, 453-472.

Huppert, H.E. and Sparks, R.S.J. (1980). Restrictions on the compositions of mid-ocean ridge basalts: a fluid dynamical investigation. Nature, 286, 46-48.

Hynes, A. (1974). Notes on the petrography of some ophiolites, Onthris Mountains, Greece. Contrib. Mineral. Petrol., 46, 233-239.

International Crustal Research Drilling Group (1984). Are Troodos deposits an East Pacific analog? Geotimes, 12-14.

Jagoutz, E., Palme, H., Hidegard Baddenhausen, Blum, K., Cendales, M., Gerlind, D., Spettel, B, Lorenz, V. and Wanke, H. (1979). The abundances of major, minor and trace elements in the Earth's mantle as derived from primitive ultramafic nodules. Proc. 10th Lunar. Planet. Sci. Conf., 2031-2030.

Jenner, G.A. (1981) Geochemistry of high Mg andesites from Cape Vogel, Papua New Guinea. Chem. Geol. 33 307-332

Johnon G. L. & Vogt P.R. (1973). Mid-Atlantic Ridge from 47^{o} ro 51^{0}N. Geol. Soc./ Am. Bull. 84 3443-3462

Juteau, T. (1970). Petrogenèse des ophiolites des nappes d'Antalya, leur laison avec une phase d'expansion oceanique active au Trias supérieur. Sci. Terre, 15, 265-306.

Juteau, T. (1975). Les ophiolites des nappes d'Antalya (Taurides occidentales, Turquie). Petrologie d'un fragment de l'ancienne croûte océanique Tethysienne. Mem. Sci. Terre, Nancy, 32, 692-721.

Juteau, T., Nicolas, A., Dubessy, J., Fruchard, J.C. and Bouchez, J.L. (1977). Structural relationships in the Antalya ophiolite complex, Turkey: possible model for an oceanic ridge. Bull. geol. Soc. Am., 88, 1740-1748.

Juteau, T. and Whitechurch, H. (1980). The magmatic cumulates of Antalya (Turkey): evidence of multiple intrusions in ophiolitic magma chambers. In: 'Ophiolites', Ed. *Panayiotou, A.*, Proc. Int. Oph. Symp, Cyprus, 337-391.

Karson, J. and Dewey, J.F. (1978). Coastal complex, western Newfoundland: an early Ordovician oceanic fracture zone. Bull. geol. Soc. Am., 89, 1037-1049.

Karson, J.A. (1983). Variations in structure and petrology in the coastal complex, Newfoundland: the anatomy of an oceanic fracture zone. J. geol. Soc. London.

Karson, J.A., Elthon, D.L. and DeLong, S. (1983). Ultramafic intrusions in the Lewis Hills Massif, Bay of Islands Ophiolite Complex, Newfoundland: implications for igneous processes of oceanic fracture zones. Bull. geol. Soc. Am., 94, 15-29.

Karson, J.A. and Fox, P.J. (1985). Geological and geophysical investigations of the Mid-Cayman spreading center. Seismic velocity measurements and implications for the constitution of layer 3. In Press

Karson, J.A. (1986). Lithosphere age, depth and structural complications resulting from migrating transform faults. J. geol. Soc. London, 143, 785-788.

Kidd, R.G.W. and Cann, J.R. (1974). Chilling statistics indicate an ocean floor spreading origin for the Troodos Complex, Cyprus. Earth Planet. Sci. Lett., 24, 151-155.

Kidd, R.G.W. (1977). A model for the formation of the upper oceanic crust. Geophys. J. R. astron. Soc., 50, 149-183.

Kushiro, I. (1972). Effects of water on the composition of magmas formed at high pressures. J. Petrol., 13, 311-

Langmuir, C.H. and Bender, F.J. (1984). The geochemistry of oceanicbasalts in the vicinity of transform faults: observations and implications. Earth Planet. Sci. Lett., 69, 107-127.

Laplerre, H. and Rocci, S. (1967). Le Massif de Kellaki (Chypre), 1-c tude petrographique et structural. Sci. Terre. Nancy., 12, 145-181.

Laplerre, H. (1968). Nouvelles observation sur la serie sedimentaire de Mamonia (Chypre). C.R. Acad. Sc. Paris., D267, 32-35.

Laplerre, H. and Parrot, J.F. (1972). Identite geologique des regions de Paphos (Chypre) et du Baer-Bassit (Syrie). C.R. Seances Acad. Sci. Paris, 274, 1999-2002.

Laplerre, H. (1975). Les formations sedimentaires et eruptives des nappes de Mamonia et leures relation s avec le Massif du Troodos (Chypre occidentale). Mem. Soc. Geol. France, 123, 1-132.

Laplerre, H. and Rocci, G. (1976). Le volcanisme du sud-ouest de Chypre et la probleme de l'ouverture des region Tethysiennes au Trias. Tectonphysics, 30, 299-313.

Lister, G.S. and Williams, P.F. (1979). Fabric development in shear zones: theoretical controls and observed phenomena. J. Struct. Geol., 1, 283-297.

Lister, G.S. and Price, G.P. (1978). Fabric development in a quartz-feldspar mylonite. Tectonophysics, 49, 37-78.

Lockwood, J.P. (1960). Sedimentary emplacement of serpentinite and related ultramafic rocks. (Abstract). Geol. Soc. Am. Spec. Pub., 121, 178-179.

Lockwood, J.P. (1970). Sedimentary serpentinites from the Guajina Peninsula, Colombia. Geol. Soc. Am. Mem., 130, 162pp.

Lockwood, J.P. (1971). Sedimentary and gravity-slide emplacement of serpentinite. Bull. geol. Soc. Am., 82, 919-936.

Lonsdale, P. (1978). Near-bottom reconnaissance of a fast-slipping transform fault zone at the pacific-Nazca Plate boundary. J. Geol., 6, 451-472.

Louden, K.E. and Forsyth, D.W., (1976). Thermal conduction across fracture zones and the gravitational effects. J. Geophys. Res., 81, 4869-4874.

Lowrie, A. (1978). Buried trench south of the Gulf of Panama. Geology, 6, 434-436.

Lowrie, A., Aitken, T., Grim, P., McRaney, L. (1979). Fossil spreading centre and faults within the Panama Fracture Zone. Marine Geophysical Research, 4, 153-166.

Lowrie, A., Smoot, C. and Batiza, R. (1986). Are oceanic fracture zones locked and strong or weak? New evidence for volcanic activity and weakness. Geology, 14, 242-245.

Ludden, J.N. and Thompson, G. (1979). An evaluation of the behaviour of the rare earth elements during weathering of sea-floor basalt. Earth Planet. Sci. Lett., 43, 85-92.

Macdonald, A.H. and Fyfe, W.A. (1984). Rate of serpentinization in sea-floor environments. Tectonophysics, 116, 123-135.

Malpas, J.M. (1978). Magma generation in the upper mantle, field evidence from ophiolite suites and application to the genaration of oceanic lithosphere. Phil. Trans. Rojal Soc. London Ser. A. 288 527-546

Maltman, A.J. (1978). Serpentine textures in Angelsey, North Wales, United Kingdom. Bull. geol. Soc. Amer., 89, 972-980.

Mammerickx, Y. and Smith, S.M. (1978). Maps, charts ser-MC-26, at the Geol. Soc. Am., Boulder, Colorado.

Mantis, M. (1971). Paleontological evidence defining the age of the Troodos Pillow Lava Series in Cyprus. Kypriakos Logos III, 15-16, 202-208.

Matthews, D.H. (1971) Weathered basalts from Swallow Bank, an abyssal hill in the NE Atlantic. Phlos. Trans. Royal. Soc. (london) ser A. 268 551-571

McBirney, A.R. and Noyes, R.M. (1979). Crystallisation and layering of the Skaergaard intrustion. J. Petrol., 20, 487-554.

McCulluch, M.T. and Cameron, W.E. (1983). Nd-Sr isotopic study of primative lavas from the Troodos ophiolite, Cyprus: evidence for a subduction-related setting. Geology, 11, 727-731.

McKenzie, D.P. (1972). Active tectonics of the Mediterranean region. Geophys. J.R. astron. Soc., 30, 109-185.

Meijer, A. (1980). Primitive arc volcanism and a boninite series: examples from the western Pacific island arcs. In The Tectonic and Geologic Evolution of Southeast Asian Seas and Islands. D.E. Haynes (ed) Am. Geophys. Un. Mem. N^{O} 23 269-282

Meijer, A., Anthony, E.& Reagan, M. (1981). Petrology of volcanic rocks from the fore-arc sites. Initial Reports DSDP 60 709-730

Melosh, H.J. (1983). Acoustic fluidisation. Am. Jour. Sci., 71, 158-164.

Melson, W.G. & Van Andel Tj. H.(1966) Metamorphism in the Mid-Atlantic Ridge 22^{O} latitude. Mar. Geol. 4 165-186

Melson, W.G., Hart S.R. & Thompson G. (1971). Petrology of a transform zone and adjacent ridge segments. Philos. Trans. Royal. Soc. London. 268 423-441

Melson, W.G., Hart S.R. & Thompson G. (1972). St Paul's rocks, equatorial Atlantic; petrogenesis, radiometric ages and implications on seafloor spreading. Geol. Soc. Am. Mem. 132 241-272

Menard, H.W. and Atwater, T. (1969). Original fracture zone topography. Nature, 222, 1037-1040.

Menard, H.W. and Chase, T.E. (1970). Fracture zones. In: " The Sea". *A. E. Maxwell (Ed.)* Wiley Interscience. New York, 4, 321-443.

Menard, H.W. (1977). Fragmentation of the Farallon Plate by pivoting subduction. Journal of Geology, 86, 99-110.

Menzies, M.A. (1974). Petrogenesis of the Makrirraki ultramafic complex. PhD Thesis at the Open University (unpub.)

Menzies, M.A. and Allen, C.R. (1974). Plagioclase lherzolite-residual mantle relationships within two eastern Mediterranean ophiolites. Contrib. Mineral. Petrol., 45, 195-213.

Menzies, M.A . & Segfried W. Jr. & Blanchard D. (1979) Rare earth elements and trace element geochemistry from metabasalts from the Point Sal ophiolite, California. Earth Planet Sci. Lett. 37 203-213

Middleton, G.V. and Hampton, M.A. (1976). Subaqueous sediment transport and deposition by sediment gravity flows. In: "Marine sediment transport and environmental management", *Stanley, D.D. and Swift, D.J.P. (Eds).* 197-218. Wiley , New York 368p.

Middleton, G.V. and Southard, J.B. (1984). Mechanics of sediment transport, In: Lecture Notes for short coarse Nos. 3, Eastern Section, the Society of Economic Paleontologists and Mineralogists, U.S.A.

Milovanovic, Bramislav and Karamata-Stevan (1960). Uber den diapirismus serpentinischer Massen. Internat. Geol. Cong. 21st. Copenhagen. 18, 409-417.

Mitra, G. (1979). Ductile deformation zones in Blue Ridge basement rocks and estimation of finite strain. Bull. geol. Soc. Am. pt.1, 90, 935-951.

Miyashiro, A., Shido, F. and Ewing, M. (1970). Crystallisation and differentation in Abyssal Tholeiites and gabbros for mid-oceanic ridges. Earth Planet. Sci. Lett., 7, 361-365.

Miyashiro, A. (1973). The Troodos ophiolitic complex was probably formed in an island arc. Earth Planet. Sci. Lett., 19, 218-224.

Moiseyeu, A.M. (1970). Late serpentinite movements in the California Coast Ranges: new evidence and its implications. Bull. geol. Soc. Am., 81, 1721-1732.

Moores, E.M. and Vine, F.J. (1971). The Troodos Massif, Cyprus and other ophiolites as oceanic crust: evaluation and implications. Phil. Trans. R. Soc. London, 268, 443-466.

Moores, E.M., Robinson, P.T., Malpas, J. and Xenophantos, C. (1984). The tectonic setting for the evaluation of the Troodos Complex, Cyprus. Geology, 12, 500-503.

Murase, T. and McBirney, A.R. (1973). Properties of some common igneous rocks and their melts at high temperatures. Bull. geol. Soc. Am., 84, 3563-3592.

Murton, B.J. and Gass, I.G. (1986). Western Limassol Forest Complex, Cyprus. Part of an Upper Cretaceous leaky transform fault. Geology, 14, 255-258.

Mysen, B. and Boettcher, A.C. (1975a). Melting of hydrous mantle: In. Phase relations of natural peridotites at high pressures and temperatures with controlled activities, of water, carbon dioxide and hydrogen. J. Petrol., 16, 520-548.

Naylor, M.A. (1983). Statistics of slide blocks. J. Struct. Geol., 5, 627-628.

Neary, C.R. and Brown, M.A. (1979). Chromites from Al Ayes complex, Saudi Arabia and the Semail Complex, Oman. In; Evolution and Mineralisation of the Arabian Shield, (ed) Al-Shanti, A.M.S. I.A.G. Bull., 2, 193-205.

Needham, H.D. and Francheteau, J. (1974). Some characteristics of the rift valley in the Atlantic Ocean near 36° 48' north. Earth Planet. Sci. Lett., 22, 29-43.

Nicholas, A. and Poirer, J.P. (1976). Crystalline plasticity and solid state flow in metamorphic rocks, in: Wiley, New York, 444p.

Nicholas, A., Boudier, F. and Bouchez, J.C. (1980). Interpretation of peridotite structures from ophiolitic and oceanic environments. Am. J. Sci., 280A, 192-210.

Nicholas, A. and Le Pichon, X. (1980). Thrusting of young lithosphere in subduction zones with special references to structures in ophiolitic peridotites. Earth Planet. Sci. Lett., 46, 397-406.

Nicholas, A. and Violette, J.F. (1982). Mantle flow at oceanic spreading centres: models derived from ophiolites. Tectonophysics, 81, 319-339.

Oakeshott, G.B. (1968). Diapiric structures in Diablo Range, California. Bull. Am. Assoc. Petrol. Geol., 8, 228-243.

OTTER, Scientific Team (1980). The Oceanographer transform: Morphotetctonic character of a ridge-transform intervention. Eos. Trans. Am. Geophys. Union., 61, 1105-1132.

OTTER, Scientific Team (1984). The geology of the Oceanographer transform: The Transform Domain. Mar. Geophys. Res., 7, 86-112.

O'Hara, M.J. (1965). Primary magmas and the origin of basalts. Scott. J. Geol., 1, 19-40.

O'Hara, M.J. (1968). Are any ocean floor basalts primary magmas? Nature, 220, 683-686.

Ozkaya, I. (1982). Origin and tectonic setting os some melange units in Turkey. J. Geol., 90, 269-278.

Pallister, J.S. and Hopson, C.A. (1981). Semail ophiolite plutonic suite: field relations, phase variation, cryptic variation and layering and a model of a spreading ridge magma chamber. J. Geophys. Res., 86, 2593-2644.

Pallister, J.S. and Gregory, R.T. (1983). Composition of the Samail Ocean Crust. Geology, 11, 638-642.

Panayiotiou, A. (1977). The geology and geochemistry of the Limassol Forest Plutonic Complex and the associated Cu-Ni-Co-Fe sulphide and chromite deposits, Cyprus. Ph.D. Thesis Dept, Geol. New Brunswick, Univ. Canada.

Pantzis Th. G. (1967). The geolgy and mineral resources of the Pharmakas-Kalavasos area. Memoirs of the Geological Survey Dept. Cyprus N^{O} 8, 187p

Parsons, B. and Sclater, J.G (1977). An analysis of the variation of ocean floor bathymetry and heat flow with age. J. Geophys. Res., 82, 803-827.

Parson, L.M. and Searle, R.C. (1986). Strike-slip fault styles in slow-slipping oceanic transform faults, evidence from GLORIA surveys of Atlantis and Rornarch fracture zones. J. geol. Soc. London, 143, 757-781.

Pearce, J.A. and Cann, J.R. (1973). Tectonic setting of basic volcanic rocks determined using trace element analyses. Earth Planet. Sci. Lett., 19, 290-300.

Pearce, J.A. (1976). Statistical analysis of major element patterns in Basalts. J. Petrol.,17, 15-43.

Pearce, J.A. (1975). Basalt geochemistry used to investigate post tectonic environments on Cyprus. Tectonophysics, 25, 41-67.

Pearce, J.A. & Norry, M.J. (1979). Petrogenetic implications of Ti, Zr, and Nb variations in volcanic rocks. Contrib. Mineral. Petrol. 69 33-47

Pearce, J.A. (1980). Genesis and eruptive environment of lavas from Tethyan ophiolites. In: 'Ophiolites', Ed. *Panayiotou, A.*, Proc. Int. Ophio. Symp., Cyprus, 1979

Pearce, J.A. (1980). REE values for various OIB etc. from lead isotope study of young volcanic rocks from mid-ocean ridges, ocean islands and island arcs. Phil. Trans. R. Soc. Lond., A297, 409-445.

Pearce, J.A. (1982). Trace element characteristics of lavas from destructive plate boundaries. In: Andesites. Thorpe, E.S. (ed) 525-548 Wiley , New York, 678p.

Pearce, J.A. (1983). Role of the sub-continental lithosphere in magma genesis of active continental margins. In: Continental basalts and mantle xenoliths, Hawkesworth, C.J. and Norry, M.J. (eds). Shiva, 267p.

Pearce, J.A., Lippard, S.J. and Roberts, S. (1984). Characteristics and tectonic significance of supra-subduction zone (s.s.z) ophiolites. In: Marginal basin geology, Kokellar and Howells (eds). Spec. Publ. Geol. Soc. London, 16, 77-94.

Penrose (1972). Penrose field conference on ophiolites. Geotimes, 17, 24-25.

Penrose (1982). Significance and petrogenesis of mylonitic rocks. Geology, 10, 227-230.

Phillips, J.D. & Fleming H.S. (1978). Multi-beam sonar study of the mid-Atlantuic rift valley 36^{o}-37^{o}N FAMOUS. Geol. Soc. Am. MC-19

Presnal, D.C., Dixon, J.R., O'Donnell, T.H. and Dixon, S.A. (1979). Generation of mid-ocean ridge tholeiite. J. Petrol., 20, 3-35.

Prinzhofer, A. and Nicolas, A. (1980). The Bagota Peninsula, New Caledonia: A possible oceanic transform fault. J. Geol., 88, 387-398.

Raleigh, C.B. and Paterson, M.S. (1965). Experimental deformation of serpentinite and its tectonic implications. J. Geophys. Res. ,70, 16, 3965-3985.

Ramberg, I.B., Gray, D.F. and Raynolds, R.G.H. (1977). Tectonic evolution of the FAMOUS area of the mid-Atlantic ridge, lat. 30° 50' to 37° 20' N. Bull. geol. Soc. Am. 88, 507-530.

Ramsay, J.G. and Graham, R.H. (1970). Strain variation in shear belts. Can. J. of Earth Sci., 7, 786-813.

Ramsay, J.G. (1980). Shear zone geometry: a review. J Struct.Geol., 2, 83-99.

Rea, D.K. (1981) Tectonics of the Nazca-Pacific divergent plate boundary. In L.D. Kulm, J. Drymond, E.J. Dash & D.M. Hussong (eds), Nazca plate: crustal formation and Andean convergence. Geol. Soc. Am. Mem., 154 27-62

Rauterschlien, M., Jenner, G.A., Hertogen, J., Hofmann, A.W., Kerrich, R., Schmincke, H.U. and White, W.M. (1985). Isotopic and trace element composition of volcanic glasses from the Akaki Canyon, Cyprus: Implications for the origin of the Troodos ophiolite. Earth Planet. Sci. Lett., 75, 369-383.

Reuber, I., Whitechurch, H. and Caron, J.M. (1982). Setting of gabbro dikelets in an ophiolite complex (Antalya, Turkey) by hydraulic fracturing: downward injection of residual liquids. Nature, 296, 141-143.

Reuber, I. (1985). Mylonitic ductile shear zones within tectonites and cumulates as evidence for an oceanic transform fault in the Antalya ophiolite, S.W. Turkey. In: Dixon, J.E. and Robertson, A.H.F. (eds), The geological evolution of the Eastern Mediterranean, Special Publication of the Geology Society, No.17.

Reuber, I. (1986). Geometry of accretion and oceanic thrusting of the Spongtang ophiolite, Ladakh-Himalaya. Nature, 321, 592-596.

Richand, M.J. and Dixon, C.K. (1983). Stress configurations in conjugate quartz veins. J. Struct. Geol., 5, 573-578.

Ricou, L.E., Argyriadis, I. and Marcoux, J. (1985). L'axe calcaire du Tourus un alignement de fenetres arob-africaines sous des nappes radiolaritiques, ophiolitiques el metamorphiques. Bull. Soc. Geol. Fr., 17, 1024-1044.

Riedel, W. (1929). Zur mechanik geologischen Brucherscheinungen. Zentralbl. Mineral. Geol. Palaeontol. 1929b, 354-368.

Ringwood A.E. (1966). Chemical evolution of ther terrestrial planets. Geochim. Cosmochim. Acta. 30 326-339

Robertson, A.H.F. and Hudson, J.D. (1974). Pelagic sediments in the Cretaceous and Tertiary history of the Troodos Massif, Cyprus. Spec. Publ. No.1, International Association of sedimentologists, Hsu, K.J. and Jenkyns, H.C. (eds).

Robertson, A.H.F. (1977). The Moni melange, Cyprus; an olistostrome formed at a destructive plate margin. J. geol. Soc. Lond., 133, 447-461.

Robertson, A.H.F. and Woodcock, N.H. (1980). Tectonic setting of the Troodos Massif in the eastern Mediterranean. In: 'Ophiolites', Ed. *Panayiotou, A.*, Proc. Int. Symp. Ophio., Cyprus, 1979, 36-49.

Robinson, P.T., O'Hearn, T. and Schminke, H.U. (1983). Volcanic glass compositions of the Troodos ophiolite, Cyprus. Geology, 1, 400-404.

Roeder, P.L. and Emslie, R.F. (1970). Olivine-liquid equilibrium. Contrib. Mineral .Petrol., 29, 275-289.

Roering, C. (1968). The geometrical significance of natural en-echelon crack arrays. Tectonophysics, 5, 107-123.

Rollinson, H.R. and Roberst, C.R. (1986). Ratio correlations and major element mobility in altered basalts. Contrib. Mineral. Petrol., 93, 89-97.

Rothery, D.A. (1983). The base of the sheeted dyke complex, Oman ophiolite: implications for magma chamber configuration of oceanic spreading axes. J. geol. Soc. Lond, 140, 287-296.

Sandwell, D., & Schubert G., (1982). Lithosphere flexure at fracture zones. Journal Geophys. Res. 87 4657-4667

Saunders A.D., Tarney, J., Marsh N.G. & WSood D.A. (1980). Ophiolites as ocean crust: a geochemical approach. In: 'Ophiolites', Ed. *Panayiotou, A.*, Proc. Int. Symp. Ophio., Cyprus, 1979, 122-134

Sharaskin, A.Y., Dobretsov, N.L. (1980). Marianites: the clinoenstatite bearing pillow lavas associated with ohioloites of the Marana Island Arc. In: 'Ophiolites', Ed. *Panayiotou, A.*, Proc. Int. Symp. Ophio., Cyprus, 1979, 166-175

Schminke, H-U., Rautenschein, M., Robinson, P.T., Mehegan, J.M. (1983). Troodos extrusive series of Cyprus: a comparison with oceanic crust. Geology, 11, 405-409.

Sclater, J.G., Karig, D., Lawver, L.A. and Louder, K. (1976). Heat flow, depth and crustal thickness of the marginal basins of the South Philipine Sea. J.Geophys. Res., 81,2, 309-318.

Searle, D.L. and Panayiotou, A. (1980). Structural implications in the evolution of the Troodos massif, Cyprus. In: 'Ophiolites', Ed. *Panayiotou, A.*, Proc. Int. Symp. Ophio., Cyprus, 1979, 50-60.

Searle, R.C. and Laughton, A.S. (1977). Sonar studies of the mid-Atlantic ridge and Kurchatou fracture zone. J. Geophys. Res., 82, 5313-5328.

Searle, R.C. (1979). Side-scan sonar studies of North Atlantic fracture zones. J. geol. Soc. Lond., 136, 283-292.

Searle, R.C. (1983). Multiple closely spaced transform faults in fast-slipping fracture zones. Geology, 11, 607-610.

Searle, R.C. (1986). GLORIA investigations of oceanic fracture zones: a comparative study of the transform fault zone. J. geol. Soc. Lond., 143, 743-756.

Schneider, M.E. and Eggler, D.H. (1986). Fluids in equilibrium with peridotite minerals: implications for mantle metasomatism. Geochem. Cosmochim. Acta., 50, 711-724.

Schilling J.G., Zajac M., Evans R., Johnston T., White W., Devine J.D. & Kingsley R. (1983). Petrologic and geochemical variations along mid-Atlantic ridges from 29° N to 73°N. Am. J. Sci. 510-586

Shaw, D.M. (1970). Trace element fractionation during anatexis. Geochem. Cosmochim. Acta, 34, 237-243.

Shaw, H.R. (1969). Rheology of basalt in the melting stage. J. Petrol., 10, 510-569.

Shaw, H.R. (1972). Viscosities of magmatic silicate liquids: an empirical method of prediction. Am. J. Sci., 272, 870-893.

Shelley, R.C., Shearman, D.J., Sutton, J. and Watson, J.V. (1963). Some underwater disturbances in the Torridonian of Skye and Raasay. Geol. Mag., 100, 224-243.

Shelton, A.W. and Gass, I.G. (1980). Rotation of Cyprus microplate. In: 'Ophiolites', Ed. *Panayiotou, A.*, Proc. Int. Symp. Ophio., Cyprus, 1979, 61-65.

Shelton, A.W. (1984). Geophysical studies on the northern Oman ophiolite. Ph.D. Thesis (unpubl. Open University, U.K.)

Shibata, T., Thompson G. & Frey F.A., (1979). Tholeiitic and alkali basaltes from the mid-Atlantic ridge at 43°N. Contrib. Mineral. Petrol. 70 127-141

Sinton J.M., Wilson D.J., Christie D.M., Hey R.N. & Delaneyt J.R. (1983). Petrologic consequenses of rift propogation at oceanic spreadfing ridges. Earth Planet Sci. Lett. 62 193-207

Sleep, N.H. and Blehler, S. (1970). Topography and tectonics of the intersections of fracture zones with central rifts. J. Geophys. Res., 75, 2748-2752.

Sleep, N.H. (1984). Tapping of magmas from ubiquitous mantle heterogeneities: An alternative to mantle plumes? J. Geophys. Res., 89, B12, 10,029-10,041.

Sibson, R.H. (1977). Fault rocks and fault mechanisms. J. geol. Soc. Lond., 133, 191-213.

Simonian, K.O. (1975). The geology of the Arakapas fault belt area, Troodos Massif, Cyprus. Ph.D. Thesis, Open University, U.K.

Simonian, K.O. and Gass, I.G. (1978). Arakapas fault belt, Cyprus: a fossil transform belt. Bull. geol. Soc. Am., 89, 1220-1230.

Simpson, C. and Schmid, S.M. (1983). Evaluation of criteria to deduce the sense of movement in sheared rocks. Bull. geol. Soc. Am., 94, 1281-1288.

Smewing, J.D. (1975). Metamorphism of the Troodos Massif, Cyprus. PhD Thesis Open University (unpub.)

Smewing, J.D., Simonian, K.O. and Gass, I.G. (1975). Metabasalts from the Troodos massif, Cyprus: genetic implications deduced from petrography and trace element geochemistry. Contr. Miner. Petr., 51, 49-64.

Smewing, J.D. (1980). An Upper Cretaceous ridge-transform intersection in the Oman Ophiolite. In: 'Ophiolites', Ed. *Panayiotou, A.*, Proc. Int. Symp. Ophio., Cyprus, 1979, 407-415.

Smewing, J.D. (1981). Mixing characteristics and compositional differences in mantle-derived melts beneath spreading axes: evidence from cyclically layered rocks in the ophiolite of North Oman. J. Geophys. Res., 86, 2645-2659.

Smith, A.G. (1971). Alpine deformation and the oceanic areas of the Tethys, Mediterranean and Atlantic. Bull. geol. Soc. Am., 82, 2039-2070.

Somers M.L., Carson R.M., Revie J.A., Edge R.H., Barrow B & Andrews A.G. (1978) GLORIA II - an improved long range side-scan sonar. In Proc. of the IEEE/IERE sub-conference of offshore instrumentation and communications. BPS London (pub) j16-j24

Sparks, R.S.J. and Pinkerton, H. (1978). The effect of degassing on the rhealogy of basaltic lava. Nature, 276, 384-385.

Sparks, R.S.J., Meyer, P. and Sigurdsson, H. (1980). Density variation amongst mid-ocean ridge basalts: implications for magma mixing and the scarcity of primative lavas. Earth Planet. Sci. Lett., 46, 419-430.

Spray, J.G. and Roddick, J.F. (1981). Evidence for Upper Cretaceous transform fault metamorphism in West Cyprus. Earth Planet. Sci. Lett., 55, 273-291.

Starkey, J. (1977). The contouring of orientation data represented in spherical projection. Can. Jour. Earth Sci., 14, 268-272.

Steinmann, G. (1927). Die ophiolithischen zones in deri Mediterranean ketengebirge. In 14th Inter. Geol. Cong. Madrid, 2, 638-667.

Sterns, M.R. and Cann, J.R. (1982). A model of hydrothermal circulation in fault zones of mid-ocean ridge crests. Geophys. J.R. astron. Soc., 71, 225-240.

Stroup, J.B. and Fox, P.J. (1981). Geologic investigations in the Cayman Trough: evidence for thin oceanic crust along the mid-Cayman Rise. J. of Geol., 89, 395-420.

Swarbrick, R.E. (1980). The Mamonia complex of S.W. Cyprus: a Mesozoic continental margin and its relationship to the Troodos complex. In: 'Ophiolites', Ed. *Panayiotou, A.*, Proc. Int. Symp. Ophio., Cyprus, 1979, 86-92.

Sykes, L.R. (1967). Mechanisms of earthquakes and nature of faulting on the mid-Atlantic ridge. J. Geophys. Res., 72, 2131-2153.

Sykes, L.R. (1978). Intraplate seismicity reactivation of pre-existing zones of weakness, alkaline magmatism and other tectonism post dating continental Fragmentation. Review of Geophisics and Space Physics, 16 621-688

Tapponnier, P. and Francheteau, J. (1978). Necking of the lithosphere and the mechanics of slowly accreting plate boundaries. J. Geophys. Res., 83, 3955-3970.

Taylor, G.R. and McLennon, M. (1981). The composition and evolution of the continental crust: rare earth element evidence from sedimentary rocks. Phil. Trans. R. Soc. Lond., A301, 381-399.

Tchalenko, J.S. (1970). Similarities between shearzones of different magnitudes. Bull. geol. Soc. Am., 81, 1625-1640.

Thompson, G. and Melson, W.G. (1972). The petrology of oceanic crust across fracture zones in the Atlantic ocean. Evidence of a new kind of sea-floor spreading. Jour. of Geol. Soc. Lond., 80, 526-538.

Tullis, J., Snoke, A.W., Todd, V.R. (1983). Significance and petrogenesis of ryolitic rocks - Penrose Field Conference Report.

Turcotte, . (1974). Are transform faults thermal contraction cracks? Journal of Geophys. Res. 79 2573-2577

Varga, R.J. and Moores, E. M. (1985). Spreading structure of the Troodos ophiolite, Cyprus. Geology, 13, 846-850.

Varne, R., Gee, R.D. and Quilty, P.J. (1969). Maquarie Island and the cause of marine magnetic anomalies. Science, 166, 230-233.

Vine, F.J. and Matthews, D.H. (1963). Magnetic anomalies over oceanic ridges. Nature, 199, 947-949.

Vine, F.J., Poster, C.K. and Gass, I.G. (1973). Aeromagnetic survey of the Troodos igneous massif, Cyprus. Nature Phys. Sci., 244, 34-38.

Violon, P. (1979). Les deformations continues - discontinuea des roches anisotropes. Eclog. Geol. Helv., 72, 531-549.

Vogt, P.R. and Johnson, G.L. (1975). Transform faults and longitudinal flow below the mid-oceanic ridge. Jour. Geophysical. Res., 80, 1399-1428.

Vogt, P.R. (1976). Plumes, subaxial pipe flow, and topography along the mid-oceanic ridge. Earth Planet. Sci. Lett., 29, 309-325.

Wager, L.R. and Deer, W.A. (1939). Geological investigations in East Greenland. Pt III. The Petrology of the Skaergaard intrusion Kangerdlugssuaq, East Greenland. Medd. Om. Gronland, 105, 1-352.

Wager, L.R. and Brown, G.M. (1968). Layered igneous rocks. Oliver and Boyd (pub). 588pp.

Walker, D.A. and Cameron, W.E. (1983). Boninite primary magmas: evidence from the Cape Vogel Peninsula. P.N.G. Contrib. Miner. Petrol., 83, 150-158.

Walker, D.A. (1980). Modern and ancient submarine fans: reply. Bull. Am. Assoc. Petrol. Geol., 64, 1101-1108.

Walker, D.A. (1984). Turbidites and associated coarse clastic deposits. In: Facies models, 2nd edition. Walker R.G. (ed). Geol. Assoc. Canada, (pub).

Watson, G.S. (1965). Equatorial distributions on a sphere. Biometrika, 52, 193-201.

Watson, G.S. (1966). The statistics of orientation data. J. Geol., 74, 786-797.

White, S.H., Burrows, S.E., Shaw, N.D. and Humphreys, F.J. (1980). On mylonites in ductile shear zones. J. Struct. Geol., 2, 175-187.

Whitechurch, W., Juteau, T. and Montignt, R. (1985). Role of the eastern Mediterranean ophiolites (Turkey, Syria, Cyprus) in the history of the Neo-Tethys. In: Dixon, J.E. and Robertson, A.H.F. (eds), The geological evolution of the eastern Mediterranean. Spec. Publ. of the Geol. Soc., 17.

Whitmarsh, R.B. and Laughton, A.S. (1975). The fault pattern of a slow-spreading ridge near a fracture zone. Nature, 258, 505-507.

Wilcox, R.E., Harding, T.P. and Seely, D.R. (1973). Basic wrench tectonics. Bull. Am. Assoc. Petrol. Geol., 57, 74-96.

Wilson, J.T. (1965). A new class of faults and their bearing on continental drift. Nature, 207, 343-347.

Wilson, R.A.M. (1959). The geology of the Xeros-Troodos area Cyprus. Geol. Surv. Mem., 1, 135.

Wong, H.K., Zarudzki, E.F.K., Phillips, J.D. and Giermann, G.K.F. (1971). Some geophysical profiles in the Eastern Mediterranean. Bull. geol. Soc Am., 82, 81-100.

Wood, D.A. (1971). A variably veined suboceanic upper mantl-genetic significance for mid-ocean ridge basalts from geochemical evidence. Geology, 7, 499-503.

Wood, D. A., I. L. Gibson & Thompson R. N. (1976). Elemental mobility during zeolite facies metamorphism of the Tertiary basalts of the eastern Iceland. Contributions Mineral. Petrol. 55 241-248

Woodcock, N.H. (1977). Specification of fabric shapes using an eigen value method. Bull. geol. Soc. Am., 88, 1231-1236.

Woodside, J. and Bowin, C. (1970). Gravity anomalies and inferred crustal structure in the eastern Mediterranean Sea. J. geol. Soc. Lond., 81, 1107-1122.